Master's thesis

NTNU
Norwegian University of Science and Technology
Faculty of Natural Sciences
Department of Physics

Martine Dyring Hansen

Spin-Orbit Enhanced Josephson Effect

Master's thesis in Applied Physics and Mathematics
Supervisor: Professor Jacob Linder
June 2021

NTNU
Norwegian University of
Science and Technology

Martine Dyring Hansen

Spin-Orbit Enhanced Josephson Effect

Master's thesis in Applied Physics and Mathematics
Supervisor: Professor Jacob Linder
June 2021

Norwegian University of Science and Technology
Faculty of Natural Sciences
Department of Physics

ABSTRACT

This thesis will investigate the supercurrent across a Josephson junction comprised of two conventional s-wave superconductors separated by a heavy metal with Rashba spin-orbit coupling. The results demonstrate that the supercurrent responds to both the strength and orientation of the spin-orbit coupling. Furthermore, the behavior of the current magnitude is understood through an interplay between the scattering- and spin-orbit potential.

A scattering potential will provide a Fermi vector mismatch at the interface between a superconductor and a heavy metal. However, it is possible to make the effective barrier disappear by using spin-orbit coupling. The spin-orbit coupling will couple the spin of the electron to its momentum. Therefore, the energy bands will undergo a momentum-dependent Zeeman-splitting, and the Fermi surface of the heavy metal will displace into two co-centered surfaces. By tuning the magnitude of the spin-orbit, we can make the Fermi surface of the superconductor coincide with one of those to the heavy metal. When they are coincided, it will remove any Fermi vector mismatch which acts as an effective barrier. With this underlying physics, we predict that the supercurrent can be made larger in magnitude in the presence of spin-orbit coupling compared to its critical value without spin-orbit coupling. These observations are in stark contrast to a magnetic Josephson junction where the magnetization always suppresses the supercurrent compared to the case without magnetization.

In addition, a current flowing along a given direction is determined primarily by the electrons with momentum in the same direction. Consequently, the supercurrent will increase when these electrons experience an absent barrier at the interface between the superconductor and the heavy metal. Thus, when the spin-orbit coupling is oriented parallel to the interface compared to a perpendicular orientation, the spin-orbit coupling provides a larger supercurrent. This behavior differs from a magnetic Josephson junction where the supercurrent is invariant to changes in the magnetization direction.

SAMMENDRAG

Denne masteravhandlingen vil undersøke superstrømmen gjennom en Josephson-kontakt bestående av to konvensjonelle superledere adskilt av et tungmetall med Rashba spinn-bane kobling. Vi demonstrerer hvordan superstrømmen gjennom en slik kontakt er følsom for både retningen og styrken til spinn-bane koblingen i tungmetallet. Den fysiske oppførselen til superstrømmen er forklart ved et samspill mellom spredningspotensialet og spinn-bane koblingen ved grensesjiktet mellom materialene.

Dersom det er et spredningspotensial ved grensesjiktet mellom en superleder og et tungmetall, vil dette potensialet føre til en uoverensstemmelse av Fermi-vektorene mellom de to materialene. Vi har vist hvordan det er mulig å gjenopprette symmetrien mellom Fermi-vektorene ved å introdusere en spinn-bane kobling. Spinn-bane koblingen vil kombinere elektronenes spinn og impuls, slik at energibåndene gjennomgår en impulsavhenging Zeeman-splitting. Følgelig vil Fermi overflaten til tungmetallet dele seg i to overflater med invertert spinn-symmetri. Styrken til spinn-bane koblingen vil avgjøre i hvor stor grad denne Zeeman-splittingen finner sted, og åpner dermed muligheten for å justere en av de nye Fermi-overflatene til å sammenfalle med superlederens Fermi-flate. Ved å oprette symmetri mellom materialenes Fermi-overflater vil uoverensstemmelsene av Fermi-vektorene, som effektivt fungerer som en barriere for partikler som vil transmittere over grensesjiktet, ikke lenger finne sted. Med utgangpunkt i denne fysikken kan man predikere en superstrøm som er sterkere i denne kontakten sammenlignet med en kontakt uten spinn-bane kobling. Disse observasjonene er i sterk kontrast til lignende forsking på ferromagnetiske Josephson-kontakter hvor superstrømmen alltid svekkes av det magnetiske feltet.

Videre har vi gjort rede for hvilken retning av spinn-bane koblingen som påvirker superstrømmen mest. Med et oppsett som undersøker superstrøm i en gitt retning, vil superstrømmen naturlig avhenge sterkt av partikler med impuls i samme retning. Det er derfor essensielt at disse elektronene ikke opplever en barriere ved grensesjiktet for å transmittere lettere over kontakten. Dermed vil en spinn-bane kobling orientert parallelt med grensesjiktet gi mulighet for sterkere superstrøm sammenlignet med en vinkelrett orientering. En slik oppførsel er ulik en ferromagnetisk Josephson-kontakter hvor superstrømmen er uavhengig av mangetfeltets retning.

PREFACE

This master thesis has been written as an integral part of a Master of Science in Applied Physics and Mathematics at the Norwegian University of Science and Technology (NTNU). It was written during the spring semester of 2021, after a precursory work undertaken in the preceding semester. The work was supervised by Professor Jacob Linder at the Center for Quantum Spintronics (QuSpin).

I want to express my gratitude towards my supervisor Professor Jacob Linder who has provided excellent guidance, insight, and feedback throughout the entire process. Through several discussions, he has inspired me with his passion for physics. I am genuinely grateful for the valuable follow-up he has given me, and for making this project possible. I truly appreciate his availability and accommodating approach to counseling me with the physics behind the theoretical models, as well as writing this thesis itself.

I am grateful to Oda Bygdnes, Tora Bjørkmann Vikhaug, Marit Schei Olsen, and Margaret Doyle for reading the manuscript and providing helpful comments.

To all my classmates at Applied Physics and Mathematics, thank you for making the last five years unforgettable. I have made friends for life! In addition, I especially want to mention my fellow student Vemund Falch with whom I have shared a reading room this final year. Your support has made a massive impact on me. The Covid-19 pandemic turned my student everyday life upside-down, but the friendly company of you at school has been essential to finish this master-year. I have had the privilege of asking you questions at all times, and you have always provided me with your knowledge and invaluable help. I am grateful for all our valuable conversations — both academic but perhaps, more importantly, those which where not.

Last but not least, thank you to my parents, Jan Ove Hansen and Lara Ann Dyring, for always believing in me. Finally, I want to end this preface by expressing my love for my siblings Aleksander Dyring Hansen, Camilla Dyring Hansen, and Natalie Dyring Hansen.

Martine Dyring Hansen
Trondheim, Norway
June 2021

CONTENTS

ABBREVIATIONS

ABS	Andreev bound state
BCS	Bardeen-Cooper-Schrieffer
BdG	Bogoliubov-de Gennes
BTK	Blonder-Tinkham-Klapwijk
F	ferromagnet
HM	heavy normal-metal with Rashba spin-orbit coupling
NC	normal-metal (without spin-orbit coupling)
SC	superconductor

1

INTRODUCTION

Spintronics, or spin electronics, is a field of research that is quickly growing. The research topic studies the manipulation and active control of the spin degrees of freedom in solid-state systems [1]. Rather than dealing with their charge, spintronics deals with the spin properties of electrons. Spintronics has the potential to substitute the classical charge-based computer processor device resulting in greater energy efficiency and more time-efficient performance [1][2]. The application of spintronics in technology has already started. For instance, there are some hard drive heads that are based on the giant magnetoresistance effect [3][4][5]. However, two main challenges regarding the further development of spintronics devices are manifested [6]. First, the Joule heating leads to high energy loss and, in the most extreme cases, it can melt the sample. Second, there is a short decay length of the spin currents due to spin-flip scattering. One can solve these two problems by placing the material with a spin effect next to a superconductor. A proximity effect will then occur [7][8][9][10][11][12], where some of the Cooper pairs in the superconductor will leak into the normal state material. As a result, the proximity material gets superconducting properties [13][14][15]. The corresponding supercurrent will experience zero resistance, which will decrease the Joule heating problem significantly.

Combining spintronics with superconductors provides several interesting research questions. For example, how can the superconducting properties enhance the effect of the spintronics? A key topic in this research is how conventional Cooper pairs with singlet symmetry are converted to triplets. In a simplified picture, the new Cooper pairs can be treated as spinful bosons with spin $S = 1$. Previous experiments have shown that one can produce Cooper pairs with triplet symmetry by introducing a nonhomogeneous magnetic exchange field. It can be achieved by using either one ferromagnet with a spatial varying exchange field, or utilize two or more ferromagnetic elements with noncollinear exchange fields [13][16][17]. Additionally, it can be produced equal projection Cooper pairs through a time-varying exchange field [18]. Furthermore, in recent years it has been proposed that an intrinsic spin-orbit coupling can generate these equal spin-projection states [19].

Moreover, these equal spin-projection triplets can align themselves with the exchange field of a ferromagnet and receive a much longer decay length than for states with zero-projection [14][20]. From this, the Josephson junction with

two superconductors incorporating a series of ferromagnets can carry supercurrents over a much longer distance compared to a homogeneous ferromagnet. As mentioned, it has been proposed that spin-orbit coupling can generate spin-triplet states [19][21][22][23], which can be found, for instance, in heavy metals [24][25][26]. An interesting question is, what occurs if we replace the nonhomogeneous ferromagnet with a heavy metal with spin-orbit coupling? Will it then be possible to achieve a similar effect of a long-range supercurrent without any magnetic fields? If so, this could have markedly important implications for further spintronics applications. These questions provide the primary motivation for this thesis: To what extent can we control the supercurrent using the magnitude and direction of the spin-orbit coupling?

1.1 HISTORICAL BACKGROUND

Already at the beginning of the 19^{th} century, Oersted, Ampére, and Faraday did a pioneering work in order to understand magnetism [27]. Oersted started in 1820 to demonstrate how electric current induces magnetic fields. Not far behind, Ampére calculated the mathematical expression for the magnetic force due to two electrical current elements. Faraday discovered a more complete connection between magnetism and electric current as he showed how a varying magnetic field gives rise to an induced electric field. About 100 years later (1964), the phenomenon was explained classically by Maxwell in his equations which related the magnetic fields to electric currents [28]. However, the emergence of quantum mechanics in the 1920s found that a complete description of magnetism could not be sufficient covered by a classical formalism. The detection of an intrinsic angular momentum carried by electrons was indicated through the famous Stern-Gerlach experiment in 1925 [29]. Today, this is commonly known as the spin of the electron. About the same time, the Pauli exclusion principle (1925) was formulated [30]. A few years later (1928), Heisenberg combined the Pauli exclusions principle with the electron-electron Coulomb repulsion. He then realized that the phenomenon of spin is responsible for the high-temperature magnetic order in some materials [31]. As a result, a quantum mechanical formulation is required to provide a complete description of magnetism.

Superconductivity is a field within solid state physics that has attracted much interest over the past decades. In modern condensed matter physics, this is considered one of the largest research topics. Additionally, the presence of fundamental physics and its value in technological applications in the fields of medicine, space technology, and ultra-sensitive sensors make superconductivity a highly valuable research topic.

More than 100 years ago, the Dutch physicist Kamerlinght Onnes observed how the electrical resistance of cryogenic mercury vanished for a DC current at 4.2K [32]. For the next 22 years, one thought that the characteristics of superconductivity only depended on temperature. The two physicists, Meissner and Ochsenfeld, proved this wrong in 1933 when they demonstrated how the superconducting state was characterized by, in addition to temperature, the phenomenon of diamagnetism [33]. In other words, superconductors expel magnetism perfectly from their bulk regardless of how the state was reached [34]. In 1950, Ginzburg and Landau formulated a macroscopic theory of superconductivity, which today is known as the Ginzburg-Landau theory [35]. Seven years later, in 1957, Bardeen, Cooper, and Schrieffer published a microscopic quantum mechanical model of superconductivity [36]. This microscopic model is today known as the BCS theory and applies to conventional superconductors at a temperature sufficiently close to 0K [37]. In the following years, Bogoliubov (1958) and de Gennes (1964) formulated the BCS framework, today know as the BdG equations [38][8]. The BdG formalism is a matrix formulation equivalent to the BCS Hamiltonian. An advantage of this formulation is that it enables problem-solving numerically on a computer by diagonalizing the involved matrices. A numerical solution is helpful since the broken translational symmetry of hybrid systems makes an analytical solution challenging.

Previous research has also detected high-temperature superconductivity. For instance, Bednorz and Müller (1986) observed the superconductivity of perovskite-type copper oxide at 35K [39][40]. This discovery was the beginning of a new era of superconductivity research. No more than a year later, yet another material with high-temperature superconductivity was detected at 93K [41]. Since then, even more materials that are high-temperature superconductors have been explored. Still, the ambition of room-temperature superconductivity is not yet achieved [42]. Even though it is more than 50 years since the BCS theory describing conventional superconductors was published, there exists no widely accepted theory for unconventional high-temperature superconductors [43].

1.2 SCOPE OF THE THESIS

The main objective of this academic year was to establish the theoretical framework which enabled us to, analytically and numerically, investigate a modified Josephson junction by incorporating a heavy metal with Rashba spin-orbit coupling. In particular, we have explored the supported supercurrent across the modified junction from the developed framework and explained how the spin-orbit coupling affects the supercurrent.

The academic year was divided into two parts: A specialization project studying the fundamental physics of superconductors, ferromagnets, and spin-orbit coupled materials, followed by a research project ending in this thesis. The first project provided familiarity with the technical framework for describing such structures. More concrete, we used second quantization applied on lattice models and the Bogolioubov-de Gennes method. In addition, a numerical program capable of reproducing results from previous research was developed. This thesis is based on this numerical framework. Therefore, chapter 5, as well as appendix A.1 and A.2, were mostly produced during the first project [44]. Additionally, chapter 1 is a modified version of the same chapter from the project. The remaining chapters have been created as part of this thesis.

The structure of this thesis is as follows: We start by presenting the fundamental physics behind superconductors, which is the main focus of chapter 2. Chapter 3 describes the concepts of ferromagnetism and spin-orbit coupling. These two properties incorporated in a Josephson junction will affect the flow of charges across the junction. Thus, chapter 4 is used to discuss the spin-dependent supercurrent in the presence of ferromagnetism or spin-orbit coupling.

We have investigated a Josephson junction incorporating a heavy metal with Rashba spin-orbit coupling through two different frameworks. First, the numerical framework is developed in chapter 5, which describes a tight-binding lattice following the BdG formalism. This chapter shows how the Hamiltonian gives the eigenvectors along with the energies of the system. It also covers numerical aspects which has to be considered while obtaining a self-consistent solution. Chapter 6 describes the analytical framework where we investigate a superconductor/superconductor Josephson junction with Rashba spin-orbit coupling imposed to the boundary. The main focus of this chapter is the development of this BTK-like model. The supercurrent, calculated from the numerical and analytical models, are presented in chapter 7. An interpretation providing the physical understanding is made in chapter 8. Finally, we end this thesis by a summary and outlook in chapter 9.

1.3 UNITS AND USEFUL IDENTITIES

For brevity of notation, the following have been used:

$\hat{v}$	Unit vectors and operators are written with a hat
$\boldsymbol{\nu}$	Vectors are written in a bold font
$\delta_{i,j}$	The Kronecker-delta function
$\delta(x)$	The Dirac-delta function
$\langle i,j\rangle$	Used in sums to denote that i and j only runs over nearest neighbours
$\sum_k$	Equivalent to $\sum_{k\in 1BZ}$ where 1BZ stands for 1st Brillouin zone
$[\hat{A},\hat{B}]$	Commutator of two operators $\hat{A}$ and $\hat{B}$, $[\hat{A},\hat{B}]=\hat{A}\hat{B}-\hat{B}\hat{A}$
$\{\hat{A},\hat{B}\}$	Anticommutator of two opertators $\hat{A}$ and $\hat{B}$, $\{\hat{A},\hat{B}\}=\hat{A}\hat{B}+\hat{B}\hat{A}$
∂_n	The partial derivative, $\partial_n \equiv \partial/\partial n$

To avoid confusion with subscripts, we drop "," (comma) after equations.

Pauli matrices spanning spin space are defined as

$$\sigma_x \equiv \begin{pmatrix} 0 & 1 \\ 1 & 0 \end{pmatrix}, \quad \sigma_y \equiv \begin{pmatrix} 0 & -i \\ i & 0 \end{pmatrix}, \quad \sigma_z \equiv \begin{pmatrix} 1 & 0 \\ 0 & -1 \end{pmatrix}, \tag{1}$$

where the vector of the Pauli matrices is defined as $\boldsymbol{\sigma} \equiv \sigma_x\hat{x} + \sigma_y\hat{y} + \sigma_z\hat{z}$, and $\{\hat{x},\hat{y},\hat{z}\}$ are the Cartesian unit vector.

Pauli matrices spanning Nambu (particle-hole) space are defined as

$$\tau_1 \equiv \begin{pmatrix} 0 & 1 \\ 1 & 0 \end{pmatrix}, \quad \tau_2 \equiv \begin{pmatrix} 0 & -i \\ i & 0 \end{pmatrix}, \quad \tau_3 \equiv \begin{pmatrix} 1 & 0 \\ 0 & -1 \end{pmatrix}. \tag{2}$$

The identity matrices for spin- and Nambu space are respectively

$$\sigma_0 \equiv \begin{pmatrix} 1 & 0 \\ 0 & 1 \end{pmatrix}, \quad \tau_0 \equiv \begin{pmatrix} 1 & 0 \\ 0 & 1 \end{pmatrix}. \tag{3}$$

In the text, we use the Pauli matrices in both spin- and Nambu space to construct 4×4 matrices. This is done by the Kronecker product denoted as $\tau_i \otimes \sigma_j \equiv \hat{\tau}_i\hat{\sigma}_j$ where $i = \{0,1,2,3\}$ and $j = \{x,y,z\}$. Note the Kronecker product notation by the use of hat-symbol $\hat{\tau}_i\hat{\sigma}_j$ to not be confused with the matrix multiplications $\tau_i\sigma_j$ which gives a 2×2 matrix.

E.g.

$$\hat{\tau}_1\hat{\sigma}_0 = \begin{pmatrix} 0 & 0 & 1 & 0 \\ 0 & 0 & 0 & 1 \\ 1 & 0 & 0 & 0 \\ 0 & 1 & 0 & 0 \end{pmatrix} \quad \text{and} \quad \tau_1\sigma_0 = \begin{pmatrix} 0 & 1 \\ 1 & 0 \end{pmatrix}. \tag{4}$$

In the numerical framework, we will use a lattice model with periodic structure as illustrated in two dimensions in Figure 1a.

A lattice spacing $a = 1$ between nearest neighbours is used. We will consider three-dimensional cubic lattices of size $N_x \times N_y \times N_z$ and a one-dimensional lattice of size N_x. The symbol N refers to the size of the lattice, i.e. the number of atoms in the specified direction, as shown in Figure 1b. In this thesis, we will only model layers with interface normal along the x-direction.

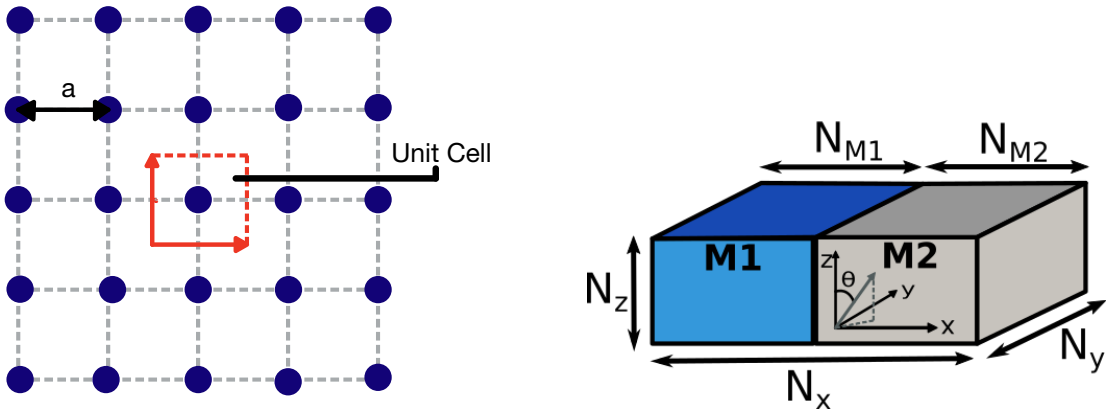

(a) (b)

Figure 1: Illustration of the lattice model. In the left panel, we can observe how the lattice is periodic with a lattice spacing a, and the unit cell marked by the red lines. The right panel illustrates an example of a system build up by two materials, *e.g.* M1 next to M2 in the x-direction.

1.3.1 *The second quantization formalism*

In this thesis, we will use the so-called second quantization formalism to utilize the Hamiltonian suitable for the numerical framework [45] [46]. In the first quantization formalism, one uses wave functions to describe the respective system. This formalism utilizes probability functions to localize the particles in space and time. Thus, there is *one* wave function for each particle. For a many-particle state, it is more convenient to define the system given the number of particles in each single-particle state. This is the basis of the second quantization formalism. We express it by ket-vectors of the occupation number, *i.e.*

$$|n_1, n_2, n_3, \dots\rangle \tag{5}$$

where $n_i (i = 1, 2, 3, \dots)$ is the occupation of the single particle state i. It is then natural to introduce the creation and annihilation operators to create or annihilate particles. Fermions have anti-symmetric many-particle states, which is reflected in the anti-commutation relation of fermionic creation and annihilation operators,

$$\{\hat{c}_\mu^\dagger, \hat{c}_\nu\} = \delta_{\mu,\nu} \tag{6}$$

for fermions in state μ and ν. For bosons, we get the following commutator due to the symmetric exchange of single-particle coordinates,

$$[\hat{b}_\mu^\dagger, \hat{b}_\nu] = \delta_{\mu,\nu} \tag{7}$$

for bosons in state μ and ν. According to the Pauli exclusion principle, the eigenvalues of the fermonic number operator $\hat{n}_\mu = \hat{c}_\mu^\dagger \hat{c}_\mu$ have only two possible values, $\{0, 1\}$. On the other hand, bosons do not have any restriction on the maximal occupation number and $\hat{n}_\mu = \hat{b}_\mu^\dagger \hat{b}_\mu$ can take all non-negative integers.

Let us take a look at the second quantization analogy to the single- and two-particle operator, which in first quantization formalism depends on the coordinates of the particles. For a single-particle operator $\hat{C}$ we obtain a transform as

$$\begin{aligned} &\sum_i \hat{C}(x_i) \to \sum_{\mu\nu} \langle\mu|\, \hat{C}\, |\nu\rangle\, \hat{c}_\mu^\dagger \hat{c}_\nu \\ &\text{where } \langle\mu|\, \hat{C}\, |\nu\rangle = \int \phi_\mu^*(x) \hat{C}(x) \phi_\nu(x) dx. \end{aligned} \tag{8}$$

Here, ϕ_μ is the wave function in first quantization formalism. We can interpret the part of creation and annihilation operators $\hat{c}_\mu^\dagger \hat{c}_\nu$ as an attempt to transfer a fermion from state ν to state μ, and the bra-ket $\langle\mu|\, \hat{C}\, |\nu\rangle$ as the probability for this transition to take place.

For a two-particle operator $\hat{B}$, the transform is

$$\begin{aligned} &\sum_{i,j\neq i} \hat{B}(x_i, x_j) \rightarrow \sum_{\mu\nu,\gamma,\lambda} \langle \mu, \nu | \hat{B} | \gamma, \lambda \rangle \, \hat{c}_\mu^\dagger \hat{c}_\nu^\dagger \hat{c}_\lambda \hat{c}_\gamma \\ &\text{where } \langle \mu, \nu | \hat{B} | \gamma, \lambda \rangle = \iint \phi_\mu^*(x) \phi_\nu^*(x') \hat{B}(x, x') \phi_\gamma(x) \phi_\lambda(x') dx dx'. \end{aligned} \tag{9}$$

Equivalent to the single-particle case, one can interpret the creation and annihilation operators $\hat{c}_\mu^\dagger \hat{c}_\nu^\dagger \hat{c}_\lambda \hat{c}_\gamma$ as the part which attempts to transfer two fermions from state γ and λ to state μ and ν, and the bra-ket $\langle \mu, \nu | \hat{B} | \gamma, \lambda \rangle$ as the probability for this transition to occur.

2

SUPERCONDUCTIVITY

Superconductors are materials that exhibit zero electrical resistance below a critical temperature [47][48][32]. When cooled below a critical temperature, the superconductor will expel the magnetic flux from an external magnetic field out of its body [33][49]. This phenomenon is called the Meissner effect, and the superconductor exhibits perfect diamagnetism. However, in the presence of a large magnetic field, the superconductivity will be destroyed, and the superconductor goes into a normal state [36][50][51].

2.1 BCS THEORY

A microscopic interpretation of a superconductor was invented by J. Bardeen, L. N. Cooper, and R. Schrieffer (BCS), known today as BCS theory [36][52][53]. The key ingredient in BCS theory is an attractive electron-electron interaction that gives rise to a so-called Cooper pair. A Cooper pair is a bound state consisting of two electrons with opposite spin and momentum. To form such a Cooper pair we require a well-defined Fermi surface.

2.1.1 *The creation of one Cooper pair*

Before we investigate the creation of Cooper pairs in a many-body system, let us begin by understanding the creation of one Cooper pair. Therefore, study a simple quantum mechanics problem of two electrons interacting through an attractive potential $V(\mathbf{r}_1 - \mathbf{r}_2)$. Describe the problem with a relative position displacement $\mathbf{r} = \mathbf{r}_1 - \mathbf{r}_2$ and introduce the center-of-mass position $\mathbf{R} = \frac{1}{2}(\mathbf{r}_1 + \mathbf{r}_2)$. The Schrödinger equation is then given by,

$$\left[-\frac{\hbar^2 \nabla^2_{\mathbf{R}}}{2m^*} - \frac{\hbar^2 \nabla^2_{\mathbf{r}}}{2\mu} + V(\mathbf{r}) \right] \Psi(\mathbf{r}, \mathbf{R}) = E\Psi(\mathbf{r}, \mathbf{R}) \tag{10}$$

where $m^* = 2m$ is the total mass, $\mu = m/2$ is the reduced mass, E is the energy and $\Psi(\mathbf{r}, \mathbf{R})$ represent the wave-function of the system. Notice how the attractive potential $V(\mathbf{r})$ is independent of the center-of-mass coordinate $\mathbf{R}$. We can therefore seek a solution of the form $\Psi(\mathbf{r}, \mathbf{R}) = \psi(\mathbf{r}) e^{i\mathbf{K}\cdot\mathbf{R}}$ where $\mathbf{K}$ is the momentum

vector of the center-of-mass position $\mathbf{R}$. The eigenvalue problem in Eq. (10) will then reduce to

$$\left[-\frac{\hbar^2\nabla_r^2}{2\mu}+V(\mathbf{r})\right]\psi(\mathbf{r})=\tilde{E}\psi(\mathbf{r}) \tag{11}$$

where we have defined $\tilde{E}=E-\frac{\hbar^2k^2}{2m^*}$. In order to minimize the energy E for a given eigenvalue $\tilde{E}$, we require $\mathbf{K}\to 0$, *i.e.* for the momentum of the center-of-mass to vanish and the energy reduces as $E=\tilde{E}$. In this minimized energy case, the two involved electrons have opposite momentum. Taking a closer look at the resulting wave function, we can observe the spatial part to decide the symmetry of the electrons' spins in order to fulfill the anti-symmetric property of the total wave function. An even wave-function where $\psi(\mathbf{r})=\psi(-\mathbf{r})$ will force the spins to form a singlet state, while an odd symmetry of the wave functions, $\psi(\mathbf{r})=-\psi(-\mathbf{r})$, will create a triplet state. We discuss the singlet and triplet state in more detail in Appendix A.2.

At this point, we have minimized the energy by choosing $\mathbf{K}=0$, which gives $\tilde{E}=E$. Now, perform a Fourier transform on Eq. (10) given as

$$\psi(\mathbf{r})=\int d^3r\psi(\mathbf{r})e^{-i\mathbf{k}\cdot\mathbf{r}}. \tag{12}$$

The result yields,

$$\begin{aligned}
&\frac{\hbar^2k^2}{2\mu}\psi(\mathbf{r})+\int d^3rV(\mathbf{r})\psi(\mathbf{r})e^{-i\mathbf{k}\cdot\mathbf{r}}=E\psi(\mathbf{r})\\
&\int\frac{d^3q}{(2\pi)^3}V(\mathbf{q})\int d^3r\psi(\mathbf{r})e^{-i(\mathbf{k}-\mathbf{q})\cdot\mathbf{r}}=\left(E-\frac{\hbar^2k^2}{m}\right)\psi(\mathbf{r})\\
&\qquad\int\frac{d^3k'}{(2\pi)^3}V(\mathbf{k}-\mathbf{k}')\psi(\mathbf{k}')=\left(E-2\varepsilon_{\mathbf{k}}\right)\psi(\mathbf{k})
\end{aligned} \tag{13}$$

where we have substituted $\mathbf{q}=\mathbf{k}-\mathbf{k}'$ and introduced the free electron energy $\varepsilon_{\mathbf{k}}=\frac{\hbar^2k^2}{2m}$. In a bound state, the two involved electrons have a total energy smaller than for two independent electrons, *i.e.* $E<2\varepsilon_{\mathbf{k}}$. We therefore introduce a new wave-function

$$\Delta(\mathbf{k})=\left(E-2\varepsilon\mathbf{k}\right)\psi(\mathbf{k}) \tag{14}$$

which gives the Schrödinger equation the new form

$$\Delta(\mathbf{k})=-\int\frac{d^3k'}{(2\pi)^3}\frac{V(\mathbf{k}-\mathbf{k}')}{2\varepsilon_{\mathbf{k}'}-E}\Delta(\mathbf{k}'). \tag{15}$$

To continue this exercise, we will need to use a finding we will derive in the many-body system investigated in the next section. In particular, only electrons

near the Fermi surface will be affected by the attractive electron-electron interaction. To resemble such behavior, we will set the attractive potential $V(\mathbf{k}-\mathbf{k}') = -V_0$ for the unoccupied states above Fermi energy ε_F. That is for $\varepsilon_{\mathbf{k}'} - \varepsilon_F < \hbar\omega_D$ and $\varepsilon_{\mathbf{k}} - \varepsilon_F < \hbar\omega_D$, and zero otherwise. We will later show that the property $\Delta(\mathbf{k})$ is independent of $\mathbf{k}$, seeking a solution with constant $\Delta(\mathbf{k}) = \Delta$. Note how this solution will provides an even spatial wave-function, $\psi(\mathbf{r}) = \psi(-\mathbf{r})$. Thus, the two involved electrons have to create a singlet state with anti-parallel spin symmetry.

Since we are studying a system of two electrons, the density of states per spin is

$$\rho(\varepsilon) = \frac{m^{3/2}}{\sqrt{2}\hbar^3\pi^2}\sqrt{\varepsilon} \tag{16}$$

and we obtain

$$\Delta = V_0\Delta \int_{\varepsilon}^{\varepsilon+\omega_D} \frac{\rho(\varepsilon)}{2\varepsilon - E}\, d\varepsilon\,. \tag{17}$$

The property ω_D represents the Debye frequency where $\hbar\omega_D \ll \varepsilon_F$. Therefore, approximate the density of states within the region $\varepsilon_F < \varepsilon < \varepsilon_F + \omega_D$ to equal the density of states at Fermi level where $\varepsilon = \varepsilon_F$. The previous equation then reduces to

$$\frac{2}{V_0\rho(\varepsilon_F)} = \ln\Big(\frac{2\varepsilon_F - E + 2\omega_D}{2\varepsilon_F - E}\Big). \tag{18}$$

Consider the limit of $V_0\rho(\varepsilon_F) \ll 1$, and observe how this limit requires $2\varepsilon_F - E \ll 1$. Thus, the approximation $2\varepsilon_F - E + 2\omega_D \simeq 2\omega_D$ is reasonable. The binding energy between the two bound electrons are defined by the energy difference from a free energy state,

$$\begin{aligned} E_b &\equiv 2\varepsilon_F - E \\ &= 2\omega_D e^{-\frac{2}{V_0\rho(\varepsilon_F)}}. \end{aligned} \tag{19}$$

The resulting expression for the binding energy shows that a bound state is established regardless of the magnitude of the attractive potential V_0. In other words, the bound state is formed as long as the attractive potential is present. We call this bound state a Cooper pair and is fundamentally different from a free electron case where the attractive potential has a lower threshold to create a bound state. A fundamental property of the unique behavior of a Cooper pair to be established is the existence of a well-defined Fermi surface, which separates the occupied and unoccupied states.

We can calculate the threshold in a free electron case by starting out from Eq. (15), and consider an attractive potential $V(\mathbf{k}-\mathbf{k}') = -V_0$ for all electronic states where $\varepsilon_{\mathbf{k}} < \hbar\omega_D$ and $\varepsilon_{\mathbf{k}'} < \hbar\omega_D$, and zero otherwise.

2.1.2 *BSC state - creating Cooper pairs in a many-body system*

This section will consider the BCS state with a mean-field theory applied on a many-body system. To investigate the origin of superconductivity, we will start from the effective Hamiltonian given as

$$H = \sum_{k,\sigma} \xi_k \hat{c}^\dagger_{k\sigma} \hat{c}_{k\sigma} + \frac{1}{N} \sum_{kk'} V_{kk'} \hat{c}^\dagger_{k\uparrow} \hat{c}^\dagger_{-k\downarrow} \hat{c}_{-k'\downarrow} \hat{c}_{k'\uparrow} \tag{20}$$

where the creation operator $\hat{c}^\dagger_{k\sigma}$ creates an electron with spin σ and momentum $\mathbf{k}$, and $\xi_k = \varepsilon_k - \mu$ defines the energy relative to the chemical potential. Note how the second term describes the destruction of a pair of electrons with opposite spin and momentum, and the subsequent creation of another two paired electrons. From the definition, these paired electrons, with opposite spin and momentum, are Cooper pairs because they interact with an attractive force of magnitude $V_{kk'}$.

The sum runs over all $\mathbf{k}$ values in the bound energy band. With extremely many ways of choosing the $N/2$ states of pair occupancy, it will be hopeless to determine all the terms in the sum. BCS theory argued that a mean-field approximation would be a good approach with many particles involved. We will therefore perform a mean-field approximation to the quadratic term of the Hamiltonian in Eq. (20),

$$\langle \hat{c}^\dagger_{k\uparrow} \hat{c}^\dagger_{-k\downarrow} \hat{c}_{-k'\downarrow} \hat{c}_{k'\uparrow} \rangle \simeq \langle \hat{c}^\dagger_{k\uparrow} \hat{c}^\dagger_{-k\downarrow} \rangle \hat{c}_{-k'\downarrow} \hat{c}_{k'\uparrow} + \hat{c}^\dagger_{k\uparrow} \hat{c}^\dagger_{-k\downarrow} \langle \hat{c}_{-k'\downarrow} \hat{c}_{k'\uparrow} \rangle - \langle \hat{c}^\dagger_{k\uparrow} \hat{c}^\dagger_{-k\downarrow} \rangle \langle \hat{c}_{-k'\downarrow} \hat{c}_{k'\uparrow} \rangle. \tag{21}$$

The mean value $\langle \hat{c}^\dagger_{k\uparrow} \hat{c}^\dagger_{-k\downarrow} \rangle$ corresponds to the creation of one Cooper pair in the superconducting state. Let us use this term to introduce a quantity called the gap function given as

$$\Delta_k = -\frac{1}{N} \sum_{k'} V_{kk'} \langle \hat{c}^\dagger_{k\uparrow} \hat{c}^\dagger_{-k\downarrow} \rangle. \tag{22}$$

We will later comment on why we call this quantity a gap. After substituting this new quantity into the Hamiltonian, we obtain

$$H = \sum_{k,\sigma} \xi_k \hat{c}^\dagger_{k\sigma} \hat{c}_{k\sigma} - \frac{1}{N} \sum_{k} \left(\Delta_k \hat{c}^\dagger_{k\uparrow} \hat{c}^\dagger_{-k\downarrow} + \Delta^*_k \hat{c}_{-k\downarrow} \hat{c}_{k\uparrow} \right) + \sum_k \Delta_k \langle \hat{c}^\dagger_{k\uparrow} \hat{c}^\dagger_{-k\downarrow} \rangle. \tag{23}$$

In order to solve the modified Hamiltonian, we introduce a set of new fermonic operators $\gamma_{k\sigma}$ and coefficients u_k, $v_{k\sigma}$ through a so-called Bogoliubov transformation defined as [38]

$$\begin{aligned} c_{k\uparrow} &= u^*_k \gamma_{k\uparrow} + v_k \gamma^\dagger_{-k\downarrow} \\ c^\dagger_{-k\downarrow} &= u_k \gamma^\dagger_{-k\downarrow} + v^*_k \gamma_{k\uparrow}. \end{aligned} \tag{24}$$

Requiring the fermionic commutation relations to be fulfilled, the normalization condition yields $|u_k|^2 + |v_k|^2 = 1$. The different terms of the effective Hamiltonian will then transform as

$$\begin{aligned}
\sum_{k,\sigma} \xi_k \hat{c}^\dagger_{k\sigma}\hat{c}_{k\sigma} &= \sum_k \xi_k \left[\hat{c}^\dagger_{k\uparrow}\hat{c}_{k\uparrow} + \hat{c}^\dagger_{k\downarrow}\hat{c}_{k\downarrow}\right] \\
&= \sum_k \xi_k \left[\left(|u_k|^2 - |v_k|^2\right)\left(\gamma^\dagger_{k\uparrow}\gamma_{k\uparrow} - \gamma^\dagger_{-k\downarrow}\gamma_{-k\downarrow}\right) + 2|v_k|^2 + 2u_k v_k \gamma^\dagger_{k\uparrow}\gamma^\dagger_{-k\downarrow} + 2u_k^* v_k^* \gamma_{-k\downarrow}\gamma_{k\uparrow}\right] \\
-\sum_k \left(\Delta_k \hat{c}^\dagger_{k\uparrow}\hat{c}^\dagger_{-k\downarrow} + \Delta_k^* \hat{c}_{-k\downarrow}\hat{c}_{k\uparrow}\right) &= \sum_k \left[\left(\Delta_k u_k v_k^* + \Delta_k^* u_k^* v_k\right)\left(\gamma^\dagger_{k\uparrow}\gamma_{k\uparrow} - \gamma^\dagger_{-k\downarrow}\gamma_{-k\downarrow}\right) - \left(\Delta_k u_k v_k^* + \Delta_k^* u_k^* v_k\right)\right] \\
&\quad - \sum_k \left[\left(\Delta_k u_k^2 - \Delta_k^* v_k^2\right)\gamma^\dagger_{k\uparrow}\gamma^\dagger_{-k\downarrow} + \left(\Delta_k^* (u_k^*)^2 - \Delta_k (v_k^*)^2\right)\gamma_{-k\downarrow}\gamma_{k\uparrow}\right]
\end{aligned} \tag{25}$$

such that the total effective Hamiltonian reads

$$\begin{aligned}
H = &\sum_k \left[2\xi_k 2|v_k|^2 - \Delta_k u_k v_k^* - \Delta_k^* u_k^* v_k + \Delta_k \langle \hat{c}^\dagger_{k\uparrow}\hat{c}^\dagger_{-k\downarrow}\rangle\right] \\
&+ \sum_k \left[\xi_k\left(|u_k|^2 - |v_k|^2\right) + \Delta_k u_k v_k^* + \Delta_k^* u_k^* v_k\right]\left(\gamma^\dagger_{k\uparrow}\gamma_{k\uparrow} - \gamma^\dagger_{-k\downarrow}\gamma_{-k\downarrow}\right) \\
&+ \sum_k \left[2\xi_k u_k v_k - \Delta_k u_k^2 + \Delta_k^* v_k^2\right]\left(\gamma^\dagger_{k\uparrow}\gamma^\dagger_{-k\downarrow}\right) + \text{h.c.}
\end{aligned} \tag{26}$$

Here, h.c. denotes the hermitian conjugate. We wish to diagonalize the Hamiltonian. To do so, we need to find the coefficients u_k, v_k that make the last sum disappear. The choice is determined by setting the last sum to zero. The following quadratic equation must then be fulfilled:

$$2\xi_k u_k v_k - \Delta_k u_k^2 + \Delta_k^* v_k^2 = 0. \tag{27}$$

Solving the previous equation for the ratio v_k/u_k gives

$$\frac{u_k}{v_k} = \frac{\sqrt{\xi_k^2 + |\Delta_k|^2} - \xi_k}{\Delta_k^*} \tag{28}$$

where we chose the positive root to ensure that the energy of the BCS state is a minimum and not a maximum. Notice that the numerator is real, stating that the phase of the gap function Δ_k is equal to the relative phase of v_k and u_k. For further calculations, we can choose the phase of u_k to zero. As a result, the phase of Δ_k and v_k are being equal.

By inserting the normalization condition $|u_k|^2 + |v_k|^2 = 1$ to the previous equation, we can solve for the coefficients u_k, v_k which is found to be

$$\begin{aligned}
|u_k|^2 &= \frac{1}{2}\left(1 + \frac{\xi_k}{\sqrt{\xi_k^2 + |\Delta_k|^2}}\right) \\
|v_k|^2 &= \frac{1}{2}\left(1 - \frac{\xi_k}{\sqrt{\xi_k^2 + |\Delta_k|^2}}\right).
\end{aligned} \tag{29}$$

Substituting the relations of v_k, u_k into the effective Hamiltonian, we get

$$H = \sum_{k\sigma} E_k \gamma^\dagger_{k\sigma}\gamma_{k\sigma} + \sum_k \left(\xi_k - E_k + \Delta_k \langle c^\dagger_{k\uparrow} c^\dagger_{-k\downarrow}\rangle\right). \tag{30}$$

Notice that the last sum is a constant. Hence, it determines the BCS ground state. The first term determines the increased energy of the fermions above the ground state. This term is denoted in terms of the number operator $\gamma^\dagger_{k\sigma}\gamma_{k\sigma}$, thus the operator $\gamma_{k\sigma}$ represent the elementary quasi-particle excitation of the system with the excitation energy E_k. It is now clear why we call the quantity Δ_k the gap function. From the previous equation, we can observe that the superconductor has a gap in the energy spectrum at Fermi level ($\xi_k = 0$) of size $|\Delta_k|$.

The operators $\gamma_{k\sigma}$ are usually called Bogoliubons and is a mixture of electrons and holes. We can determine their relations by rewrite Eq. (24) as

$$\begin{aligned} \gamma_{k\uparrow} &= u_k c_{k\uparrow} - v_k c^\dagger_{-k\downarrow} \\ \gamma^\dagger_{-k\downarrow} &= u^*_k c^\dagger_{-k\downarrow} 0 v^*_k c_{k\uparrow}. \end{aligned} \tag{31}$$

The behavior of u_k and v_k are determined by Eq. (29). For $\Delta_k \to 0$, we have for energies above Fermi level ($\xi_k > 0$), $u_k \to 1$ and $v_k \to 0$, while for energies below Fermi level ($\xi_k < 0$), $u_k \to 0$ and $v_k \to 1$. Consequently, in the normal state where $\Delta_k \to 0$, a Bogoliubon excitation corresponds to creating an electron above Fermi level and simultaneous destroying an electron (creating a hole) below Fermi level with opposite spin and momentum. On the other hand, in the superconducting state, $\Delta_k \neq 0$, a Bogoliubon excitation becomes a superposition of both a hole and an electron state.

From this exploration, we can write the BCS ground state wave-function in terms of the vacuum of Bogoliubons,

$$\gamma_{k\sigma} |\Psi_{BCS}\rangle = 0. \tag{32}$$

Substitute the electron operator, to write this wave-function in terms of the vacuum of electrons, $|0\rangle$, we get

$$u_k c_{k\uparrow} |\Psi_{BCS}\rangle = v_k c^\dagger_{-k\downarrow} |\Psi_{BCS}\rangle . \tag{33}$$

Replace the BCS wave-function with an arbitrary combination of Cooper pairs, $|\Psi_{BCS}\rangle = A \prod_q e^{\alpha_q c^\dagger_{q\uparrow} c^\dagger_{-q\downarrow}} |0\rangle$, where A is a normalization constant and the function α_q is to be determinant. Pay attention to how the operator $c_{k\uparrow}$ commutes with all terms inside the product except the one where $q = k$. To evaluate this operation, use the commutation relation of $[A, BC] = \{A, B\}C - B\{A, C\}$ and find that

$$\left[c_{k\uparrow}, \alpha_k c^\dagger_{k\uparrow} c^\dagger_{-k\downarrow}\right] = \alpha_k \left\{c_{k\uparrow}, c^\dagger_{k\uparrow}\right\} c^\dagger_{-k\downarrow} = \alpha_k c^\dagger_{-k\downarrow}. \tag{34}$$

Consequently,

$$\begin{aligned} c_{k\uparrow}\alpha_k c^\dagger_{k\uparrow}c^\dagger_{-k\downarrow}\left|0\right\rangle &= \alpha_k c^\dagger_{-k\downarrow}\left|0\right\rangle \\ c_{k\uparrow}\left(\alpha_k c^\dagger_{k\uparrow}c^\dagger_{-k\downarrow}\right)^2\left|0\right\rangle &= 2\left(\alpha_k c^\dagger_{k\uparrow}c^\dagger_{-k\downarrow}\right)\alpha_k c^\dagger_{-k\downarrow}\left|0\right\rangle \\ &\vdots \\ c_{k\uparrow}\left(\alpha_k c^\dagger_{k\uparrow}c^\dagger_{-k\downarrow}\right)^n\left|0\right\rangle &= n\left(\alpha_k c^\dagger_{k\uparrow}c^\dagger_{-k\downarrow}\right)^{n-1}\alpha_k c^\dagger_{-k\downarrow}\left|0\right\rangle \end{aligned} \tag{35}$$

thereby

$$\begin{aligned} c_{k\uparrow}e^{\alpha_k c^\dagger_{k\uparrow}c^\dagger_{-k\downarrow}}\left|0\right\rangle &= \sum_{n=1}^{\infty}\frac{c_{k\uparrow}\alpha_k c^\dagger_{k\uparrow}c^\dagger_{-k\downarrow}}{n!}\left|0\right\rangle \\ &= \alpha_k\sum_{n=1}^{\infty}\frac{\left(\alpha_k c^\dagger_{k\uparrow}c^\dagger_{-k\downarrow}\right)^{n-1}}{(n-1)!}c^\dagger_{-k\downarrow}\left|0\right\rangle \\ &= \alpha_k c^\dagger_{-k\downarrow}\sum_{n=0}^{\infty}\frac{\left(\alpha_k c^\dagger_{k\uparrow}c^\dagger_{-k\downarrow}\right)^{n}}{(n)!}\left|0\right\rangle \\ &= \alpha_k c^\dagger_{-k\downarrow}e^{\alpha_k c^\dagger_{k\uparrow}c^\dagger_{-k\downarrow}}\left|0\right\rangle \end{aligned} \tag{36}$$

where we have used $\left[c^\dagger_\mu, c^\dagger_\nu\right] = 0$. Inserting the result into Eq. (33) gives

$$u_k\alpha_k c^\dagger_{-k\downarrow}\left|\Psi_{BCS}\right\rangle = v_k c^\dagger_{-k\downarrow}\left|\Psi_{BCS}\right\rangle. \tag{37}$$

The previous equation implies that $\alpha_k = v_k/u_k$. Taking advantage of the Pauli exclusion principle giving $\left(c^\dagger_{k\uparrow}c^\dagger_{-k\downarrow}\right)^n = 0$ for $n > 0$, the expression for the BCS wave-function is reduced to

$$\left|\Psi_{BCS}\right\rangle = A\prod_k e^{\alpha_k c^\dagger_{k\uparrow}c^\dagger_{-k\downarrow}}\left|0\right\rangle = A\prod_k\left(1+\frac{v_k}{u_k}c^\dagger_{k\uparrow}c^\dagger_{-k\downarrow}\right)\left|0\right\rangle. \tag{38}$$

To evaluate the normalization constant A, notice that

$$\begin{aligned} \left\langle 0\right|\left(u^*_k + v^*_k c_{k\uparrow}c_{-k\downarrow}\right)\left(u_k + v_k c^\dagger_{k\uparrow}c^\dagger_{-k\downarrow}\right)\left|0\right\rangle &= \left\langle 0\right|\left(|u_k|^2 + |v_k|^2 c_{k\uparrow}c^\dagger_{k\uparrow}c_{-k\downarrow}c^\dagger_{-k\downarrow}\right)\left|0\right\rangle \\ &= \left\langle 0\right|\left(|u_k|^2 + |v_k|^2\left(1-c^\dagger_{k\uparrow}c_{k\uparrow}\right)\left(1-c^\dagger_{-k\downarrow}c_{-k\downarrow}\right)\right)\left|0\right\rangle \\ &= \left\langle 0\right|\left(|u_k|^2 + |v_k|^2\right)\left|0\right\rangle. \end{aligned} \tag{39}$$

Finally, the normalized result for the BCS wave-function given as

$$\left|\Psi_{BCS}\right\rangle = \prod_k\left(u_k + v_k c^\dagger_{k\uparrow}c^\dagger_{-k\downarrow}\right)\left|0\right\rangle \tag{40}$$

which implies that the identity $|v_k|^2$ gives the probability of a pair state of electrons with opposite spin and momentum being occupied. Recall from Eq. (29) that

$$|v_k|^2 = \frac{1}{2}\Big(1 - \frac{\xi_k}{\sqrt{\xi_k^2 + |\Delta_k|^2}}\Big). \tag{41}$$

Hence, the value of $|v_k|^2$ is greatest when ξ_k is small. Since $\xi_k \equiv \varepsilon_k - \mu$, a small value of ξ_k implies an energy close to Fermi surface. Consequently, a Cooper pair is most likely to exist for electrons with $|\mathbf{k}| = k_F$.

By introducing the Bogoliubov transformation, we can determine the gap function Δ_k in Eq. (22). The Bogoliubons are all independent of each other and follows the Fermi-Dirac distribution with an energy dispersion of E_k given as

$$\langle \gamma_{k\uparrow}^\dagger \gamma_{k\uparrow} \rangle = \langle \gamma_{-k\downarrow}^\dagger \gamma_{-k\downarrow} \rangle = \frac{1}{e^{\beta E_k} + 1}. \tag{42}$$

Thus, the gap equation yields

$$\Delta_k = -\frac{1}{N} \sum_{k'} \frac{V_{kk'}\Delta_{k'}}{2E_{k'}} \tanh\Big(\frac{E_{k'}}{2k_B T}\Big). \tag{43}$$

Furthermore, let us investigate for which attractive potential, $V_{kk'}$, we obtain a non-zero gap. Assume a constant attractive potential $V_{kk'} = -V_0$ for electrons around the Fermi energy, $|\xi_k|, |\xi_{,1}| < \hbar\omega_D$. It corresponds to a shell of thickness $\hbar\omega_D$ around the Fermi energy. With a potential independent of the momenta of the involved particles, we look for a gap function which is also independent of the momenta, $\Delta_k = \Delta$. An isotopic gap like this one is called an s-wave gap, and the gap equation reduces to

$$1 = \frac{V_0}{N} \sum_{k<k_D} \frac{1}{2E_k} \tanh\Big(\frac{E_k}{2k_B T}\Big). \tag{44}$$

Similar to the exercises with only two electrons, we introduce the density of states per spin, $\rho(\varepsilon)$, and get

$$1 = V_0 \int_{-\hbar\omega_D}^{\hbar\omega_D} \frac{\rho(\varepsilon)}{2\sqrt{\varepsilon^2 + \Delta^2}} \tanh\Big(\frac{\sqrt{\varepsilon^2 + \Delta^2}}{2k_B T}\Big)\, d\varepsilon\,. \tag{45}$$

To approximate the density of states to its value at the Fermi level, we use the fact that $\hbar\omega_D \ll \mu$ and get

$$1 = V_0 \rho_F \int_0^{\hbar\omega_D} \frac{1}{2\sqrt{\varepsilon^2 + \Delta^2}} \tanh\Big(\frac{\sqrt{\varepsilon^2 + \Delta^2}}{2k_B T}\Big)\, d\varepsilon\,. \tag{46}$$

This equation evaluates the gap function at a given temperature. The maximal value is obtained when $T = 0$, since $\tanh(x \to \infty) \to 1$. This temperature provides

$$\begin{aligned} 1 &= V_0 \rho_F \int_0^{\hbar\omega_D} \frac{1}{\sqrt{\varepsilon^2 + \Delta_0^2}} \, d\varepsilon \\ \frac{1}{V_0 \rho_F} &= \operatorname{arcsinh}\left(\frac{\hbar\omega_D}{\Delta_0}\right) \end{aligned} \tag{47}$$

where we have defined the gap at zero temperature as $\Delta_0 \equiv \Delta(T = 0)$. Experimentally, the gap Δ_0 is usually of the order a few meV for conventional superconductors, whereas $\hbar\omega_D$ is of an order hundred times greater. As a result, we can approximate the $\arcsin(x)$ for large arguments,

$$\begin{aligned} \frac{1}{V_0 \rho_F} &= \ln\left(\frac{2\hbar\omega_D}{\Delta_0}\right) \\ \Delta_0 &= 2\hbar\omega_D e^{-\frac{1}{V_0 \rho_F}}. \end{aligned} \tag{48}$$

At this point, we can conclude with the same conclusion as for the two electrons-exercise: A gap in the energy spectrum occurs as long as the attractive electron-electron interaction is non-zero, regardless of its strength. This shows that the Fermi liquid state is unstable towards the creation of the BCS superconducting state.

2.2 THE BOGOLIUBOV-DE GENNES EQUATIONS

The Bogoliubov-de Gennes (BdG) equations are a generalization of the BCS formalism that facilitate the treat of non-uniform superconductors.

We can derive the BdG equations by writing the real-space Hamiltonian in terms of field operators [51]. The definition of field operators are [45]

$$\begin{aligned}\hat{\psi}_{\uparrow}(\mathbf{r}) &= \sum_{n}\left[u_{n,\uparrow}(\mathbf{r})\gamma_n - v^{*}_{n,\uparrow}(\mathbf{r})\gamma^{\dagger}_n\right]\\ \hat{\psi}_{\downarrow}(\mathbf{r}) &= \sum_{n}\left[u_{n,\downarrow}(\mathbf{r})\gamma_n + v^{*}_{n,\downarrow}(\mathbf{r})\gamma^{\dagger}_n\right]\end{aligned} \tag{49}$$

where the coefficients $u_{n,\sigma}(\mathbf{r})$ and $v_{n,\sigma}(\mathbf{r})$ are to be considered as the real space functions of electrons and holes in the state (n,σ), respectively. The BCS Hamiltonian in terms of field operators reads

$$\hat{H} = \sum_{\sigma}\int d^3r\hat{\psi}^{\dagger}_{\sigma}(\mathbf{r})H_t\hat{\psi}_{\sigma}(\mathbf{r}) + \int d^3r\left\{\Delta^{*}(\mathbf{r})\hat{\psi}_{\downarrow}(\mathbf{r})\hat{\psi}_{\uparrow}(\mathbf{r}) + \Delta(\mathbf{r})\hat{\psi}^{\dagger}_{\uparrow}(\mathbf{r})\hat{\psi}^{\dagger}_{\downarrow}(\mathbf{r})\right\} \tag{50}$$

where the superconducting gap is given by

$$\Delta(\mathbf{r}) = U\langle\hat{\psi}_{\uparrow}(\mathbf{r})\hat{\psi}_{\downarrow}(\mathbf{r})\rangle. \tag{51}$$

We will now derive an equivalent expression for the Hamiltonian defined in Eq. (50). In order to do so, consider the commutator

$$\left[H, \hat{\psi}_{\sigma}(\mathbf{r})\right]. \tag{52}$$

The key is to evaluate this commutator in two separate ways, equating the two results and obtaining the BdG equations. It is a set of matrix equations equivalent to the Schrödinger equations, which makes them suited for finding the energy eigenvalues and eigenstates of a system.

To evaluate the commutator in Eq.(52), use the anticommutation relations of fermonic field operators, $\{\hat{\psi}_{\alpha}, \hat{\psi}^{\dagger}_{\beta}\} = \delta_{\alpha,\beta}$, to achieve the relations

$$\begin{aligned}\left[\int d^3r'\hat{\psi}^{\dagger}_{\sigma'}(\mathbf{r}')\hat{\psi}_{\sigma'}(\mathbf{r}'), \hat{\psi}^{\dagger}_{\sigma}(\mathbf{r})\right] &= \hat{\psi}^{\dagger}_{\sigma'}(\mathbf{r})\delta_{\sigma',\sigma}\\ \left[\int d^3r'\hat{\psi}^{\dagger}_{\sigma'}(\mathbf{r}')\hat{\psi}_{\sigma'}(\mathbf{r}'), \hat{\psi}_{\sigma}(\mathbf{r})\right] &= -\hat{\psi}_{\sigma'}(\mathbf{r})\delta_{\sigma',\sigma}\\ \left[\int d^3r'\hat{\psi}_{\sigma'}(\mathbf{r}')\hat{\psi}_{\sigma''}(\mathbf{r}'), \hat{\psi}^{\dagger}_{\sigma}(\mathbf{r})\right] &= \hat{\psi}_{\sigma'}(\mathbf{r})\delta_{\sigma'',\sigma} - \hat{\psi}_{\sigma''}(\mathbf{r})\delta_{\sigma',\sigma}\\ \left[\int d^3r'\hat{\psi}^{\dagger}_{\sigma'}(\mathbf{r}')\hat{\psi}^{\dagger}_{\sigma''}(\mathbf{r}'), \hat{\psi}_{\sigma}(\mathbf{r})\right] &= \hat{\psi}^{\dagger}_{\sigma'}(\mathbf{r})\delta_{\sigma'',\sigma} - \hat{\psi}^{\dagger}_{\sigma''}(\mathbf{r})\delta_{\sigma',\sigma}.\end{aligned} \tag{53}$$

By inserting Eq.(53) into Eq.(52) we get

$$\begin{aligned}\left[H,\hat{\psi}_\uparrow(\mathbf{r})\right] &= -H_t\hat{\psi}_\uparrow(\mathbf{r}) - \Delta(\mathbf{r})\hat{\psi}^\dagger_\downarrow(\mathbf{r})\\ \left[H,\hat{\psi}_\downarrow(\mathbf{r})\right] &= -H_t\hat{\psi}_\downarrow(\mathbf{r}) + \Delta(\mathbf{r})\hat{\psi}^\dagger_\uparrow(\mathbf{r}).\end{aligned} \tag{54}$$

Finally, perform the Bogoliubov transformation of the field operators

$$\begin{aligned}\left[H,\hat{\psi}_\uparrow(\mathbf{r})\right] &= \sum_n \left[\Big(-H_t u_{n,\uparrow}(\mathbf{r}) - \Delta_n(\mathbf{r})v_{n,\downarrow}(\mathbf{r})\Big)\gamma_n - \Big(-H_t v^*_{n,\uparrow}(\mathbf{r}) + \Delta_n(\mathbf{r})u^*_{n,\downarrow}(\mathbf{r})\Big)\gamma^\dagger_n\right]\\ \left[H,\hat{\psi}_\downarrow(\mathbf{r})\right] &= \sum_n \left[\Big(-H_t u_{n,\downarrow}(\mathbf{r}) - \Delta_n(\mathbf{r})v_{n,\uparrow}(\mathbf{r})\Big)\gamma_n + \Big(-H_t v^*_{n,\downarrow}(\mathbf{r}) + \Delta_n(\mathbf{r})u^*_{n,\uparrow}(\mathbf{r})\Big)\gamma^\dagger_n\right].\end{aligned} \tag{55}$$

This is the first step in order to obtain the BdG equations.

Let us now evaluate the commutator in Eq. (52) in a different manner. We know that the field operators diagonalize the Hamiltonian by definition. Thus, we can insert the Bogoliubov transformations of the operators directly into the Hamiltonian before we compute the commutator. Use the anticommutation relations of the $\gamma_{n,\sigma}$-operators and get

$$\begin{aligned}\left[H,\gamma_{n,\sigma}\right] &= -E_{n,\sigma}\gamma_{n,\sigma}\\ \left[H,\gamma^\dagger_{n,\sigma}\right] &= E_{n,\sigma}\gamma^\dagger_{n,\sigma}.\end{aligned} \tag{56}$$

Now, if we calculate the commutator in Eq.(52) we obtain

$$\begin{aligned}\left[H,\hat{\psi}_\uparrow(\mathbf{r})\right] &= \sum_n \left[-u_{n,\uparrow}(\mathbf{r})E_n\gamma_n - v^*_{n,\uparrow}(\mathbf{r})E_n\gamma^\dagger_n\right]\\ \left[H,\hat{\psi}_\downarrow(\mathbf{r})\right] &= \sum_n \left[-u_{n,\downarrow}(\mathbf{r})E_n\gamma_n + v^*_{n,\downarrow}(\mathbf{r})E_n\gamma^\dagger_n\right].\end{aligned} \tag{57}$$

Combining the result of the commutator in Eq. (55) and (57), we receive a set of equations. These equations are commonly known as the BdG equations and reads

$$\begin{aligned} H_t u_{n,\uparrow}(\mathbf{r}) + \Delta_n(\mathbf{r})v_{n,\downarrow}(\mathbf{r}) &= E_n u_{n,\uparrow}(\mathbf{r})\\ H_t u_{n,\downarrow}(\mathbf{r}) + \Delta_n(\mathbf{r})v_{n,\uparrow}(\mathbf{r}) &= E_n u_{n,\downarrow}(\mathbf{r})\\ -H^*_t v_{n,\uparrow}(\mathbf{r}) + \Delta^*_n(\mathbf{r})u_{n,\downarrow}(\mathbf{r}) &= E_n v_{n,\uparrow}(\mathbf{r})\\ -H^*_t v_{n,\downarrow}(\mathbf{r}) + \Delta^*_n(\mathbf{r})u_{n,\uparrow}(\mathbf{r}) &= E_n v_{n,\downarrow}(\mathbf{r})\end{aligned} \tag{58}$$

which in matrix form yields

$$\begin{pmatrix} H_t & 0 & 0 & \Delta \\ 0 & H_t & -\Delta & 0 \\ 0 & -\Delta^* & -H^*_t & 0 \\ \Delta^* & 0 & 0 & -H^*_t \end{pmatrix} \begin{pmatrix} u_{n,\uparrow}(\mathbf{r}) \\ u_{n,\downarrow}(\mathbf{r}) \\ v_{n,\uparrow}(\mathbf{r}) \\ v_{n,\downarrow}(\mathbf{r}) \end{pmatrix} = E_n \begin{pmatrix} u_{n,\uparrow}(\mathbf{r}) \\ u_{n,\downarrow}(\mathbf{r}) \\ v_{n,\uparrow}(\mathbf{r}) \\ v_{n,\downarrow}(\mathbf{r}) \end{pmatrix}. \tag{59}$$

2.3 ANDREEV REFLECTIONS

An Andreev reflection is a quantum mechanical phenomenon that may occur at the interface of a superconductor (SC) and a normal state metal (NC) [54]. The reflection is the fundamental process behind the proximity effect, and all phenomena related to it [12][55][56]. To obtain electron-electron interactions in the normal region, which is necessary to create superconducting correlations, we need the correlations to leak from the superconductor into the normal metal [7][8][9][10][11][12]. It is Andreev reflections that produce this leakage, where Cooper pairs in the superconductor, with close proximity, diffuses into the normal metal. As a result, the normal metal will then obtain superconducting properties [13][14][15]. The length of this superconducting region, inside the normal metal, exceeds the superconducting coherence length. It depends on various properties like temperature and the presence of impurities, tunnel barriers, or boundaries.

Since an Andreev reflection gives a normal metal superconducting properties, the reflection depends on the order parameter of the superconducting material by nature. Recall the derivation of the Cooper pairs and the superconducting gap in section 2.1, showing that electrons around the Fermi level might interact and cause a gap in the energy spectrum surrounding $E = 0$. This gap makes it impossible for an electron to find an available state if its energy is less than the gap, $E < \Delta$. Nevertheless, the electron can interact with another electron and create a Cooper pair, which can penetrate the superconductor and give rise to a supercurrent.

Look at an NC/SC bilayer. For an incoming electron towards the interface on the NC side, there are four possible processes. This is illustrated in Fig. 2. Notice how these four processes change the parallel $(v_{\parallel})$ and the perpendicular $(v_{\perp})$ part of the group velocity relative to the interface. The four processes are:

- specular reflection : $v_{\parallel} \to v_{\parallel}$, $v_{\perp} \to -v_{\perp}$
- Andreev reflection : $v_{\parallel} \to -v_{\parallel}$, $v_{\perp} \to -v_{\perp}$
- transmission as an electron : $v_{\parallel} \to v_{\parallel}$, $v_{\perp} \to v_{\perp}$
- transmission as a hole : $v_{\parallel} \to -v_{\parallel}$, $v_{\perp} \to v_{\perp}$

Suppose the energy of the incoming electron is greater than the superconducting gap, $E > \Delta$. In that case, the electron can either reflect as an electron (specular reflection) or transfer into the superconductor as a quasiparticle. On the other hand, if the energy of the incoming electron is less than the gap, $E < \Delta$, there are no available states in the superconductor that the electron can inhabit. There are only existing Cooper below the energy gap. As a result, the electron can-

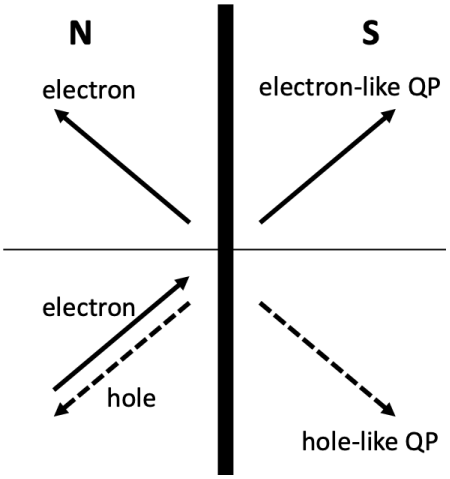

Figure 2: Scheme of the scattering processes that takes place at the interface of an NC/SC bilayer. An incoming electron inside the normal region can Andreev reflect as a hole, normal reflect as an electron, transmit as an electron-like quasiparticle, or transmit as an hole-like quasiparticle.

not penetrate the superconductor alone. In 1964, the Russian physicist Andreev demonstrated how an electron with $E < \Delta$ can reflect as a hole [54]. In detail, the incoming electron may interact with an electron close to the interface and penetrate the superconducting gap as a Cooper pair [57]. The interaction will leave a quasiparticle hole in the normal metal. This sequence is what we call an Andreev reflection and is illustrated in Figure 3. Since there are no free electrons in the superconductor at $E < \Delta$, the incoming electron with momentum k has to form a Cooper pair with an electron on the normal side of the interface. The process conserves charge, momentum, energy, and spin. Thus, the reflected hole has momentum k, since a Cooper pair is created by two electrons with opposite momenta. Consequently, the reflected hole will travel away from the interface. Conservation of energy gives that the incoming electron with energy E, relative to the chemical potential of the superconductor, will interact with another electron with energy $-E$, such that the generated hole has energy E [57].

An incoming hole can also Andreev reflect. In that event, it reflects into an electron. The Andreev reflection will then split a Cooper pair in the superconductor and transfer both electrons across the interface. Finally, one of the electrons will cancel the hole while the other starts traveling away from the interface.

It is important to note that an Andreev reflection gives rise to a phase coherence between the hole and the electron. For an incoming electron with energy equal to the Fermi energy, $E = 0$, the reflected hole must mirror the energy $E = 0$. The resulting correlation will have a center-of-mass momentum equal to zero. Thus, in theory, the superconducting correlation can be carried infinitely far into the normal metal. However, in the presence of *e.g.* magnetic impurities, these will ruin the superconducting correlations in the normal metal after they reach the

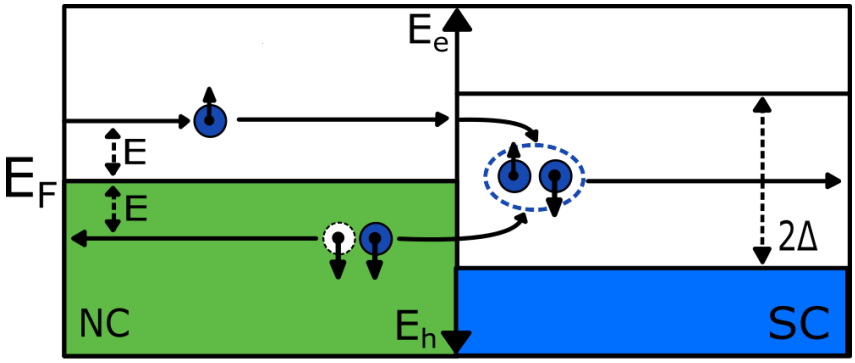

Figure 3: Illustration of Andreev reflection. An incoming spin-up electron (dark blue) with energy $E_F + E$, where $E < \Delta$, can interact with an electron with spin-down at energy $E_F - E$. Together, they can penetrate the superconductor and create a Cooper pair. The spin-down electron leaves a spin-down hole (white) with energy $E_F - E$. By conservation of momentum, the hole will travel away from the interface. In the figure, the axes of the electron energy E_e and the hole energy E_h are oppositely directed.

spin-flip relaxation length [58]. In the opposite case, when the incoming electron has energy that differs from the Fermi energy, the reflected hole will have a mismatch in the momentum [59]. As a consequence, the correlation between the electron and the hole will eventually be lost.

2.4 JOSEPHSON EFFECT

The previous section demonstrated how electrons could Andreev reflect into holes at the interface of a superconductor/normal-metal (SC/NC) bilayer. This section outlines how this phenomenon affects the current across a superconductor/normal-metal/superconductor (SC/NC/SC) trilayer. As shown in section 2.1, the superconducting gap is determined by the absolute value of Δ. However, Δ is a complex parameter that can fluctuate within the complex plane without changing the physical energy gap, *i.e.* $\Delta = |\Delta|e^{-i\phi}$. Recall that the gap is produced by the creation of Cooper pairs consisting of electrons around the Fermi level. Moreover, the phase of the superconducting gap is produced by the phase of the Cooper pairs. In the ground state, the superconductor wants to minimize its energy. Consequently, the ground state is obtained when all Cooper pairs in the bulk superconductor have equal phases. We will refer to this phase of the Cooper pairs, in the bulk ground state superconductor, as the superconducting phase.

The superconducting ground state can be interrupted by forcing the superconductor to interact with other materials. In a system with two superconductors next to each other (SC/SC), the superconductors could have an equal energy gap of $|\Delta|$. However, it does not imply that their phase will coincide. A system with two or more superconductors coupled with a weak link is called a Josephson junction [50]. A Josephson junction is simply a series connection of a superconductor, a non-superconducting material, and a superconductor. By sending a current through the junction, the phase of the two sandwiched superconductors will adapt to the applied current. Consequently, it can appear a dissipationless current which is what we call a supercurrent.

The zero-voltage supercurrent was first predicted by Josephson in 1962 [60]. He calculated the flow of charges between two superconductors separated by a thin barrier to be

$$I_s = I_c \sin(\Delta\phi). \tag{60}$$

Here, $\Delta\phi$ is the phase difference between the two superconducting electrodes, and the critical current I_c is the maximal supercurrent supported by the junction. The tunneling effect for an electron to move through a barrier, even if its kinetic energy is lower than the barrier potential, was already confirmed experimentally the year after [61]. Josephson also suggested how a phase difference would evolve over time if a voltage difference, V, was maintained across the junction,

$$\frac{d(\Delta\phi)}{dt} = \frac{2eV}{\hbar}. \tag{61}$$

Such a phase-voltage relation will provide an alternating current with frequency $\nu = 2eV\hbar$ and amplitude I_c. These two predictions are today known as DC

and AC Josephson effect and have been fully confirmed by a huge amount of experiments [50]. In this thesis, only the DC Josephson effect will be studied as a consequence of an applied current.

We can reproduce Josephson's results by considering an SC/SC junction. For this, we utilize a treatment invented by Feynman [62]. Assume that the two superconducting states can be described by a single wave function due to a collective state of the bosonic Cooper pairs. The wave functions of the two superconductors are coupled as

$$i\hbar\frac{d\psi_L}{dt} = eV_a\psi_L + K\psi_R, \qquad i\hbar\frac{d\psi_R}{dt} = -eV_a\psi_R + K\psi_L \tag{62}$$

where K describes the barrier potential that separates the two superconductors, and V_a is the applied current across the junction. An applied voltage of V_a will increase the energy to a pair of electrons (of charge $2e$) by $2V_a$ in the left superconductor relative to a pair in the right one. Assume the wave functions to be given as $\psi_{L(R)} = \sqrt{\rho_{L(R)}}e^{i\phi_{L(R)}}$ where ρ and ϕ are the density of Cooper pairs and the superconducting phase, respectively. By considering the real and imaginary part of Eq. (62), we end up with a set of four equations. Considering the imaginary part, we get

$$\frac{d\rho_L}{dt} = -\frac{d\rho_R}{dt} = \frac{2K}{\hbar}\sqrt{\rho_L\rho_R}\sin(\phi_L - \phi_R) = I_1 \sin\Delta\phi \tag{63}$$

where we have defined $\Delta\phi = \phi_L - \phi_R$. The previous equation determine the current across the junction without any voltage applied. This is the DC Josephson effect. Be aware that the expression explicit states that we require a phase difference to achieve zero-voltage current.

The AC voltage is derived by looking at the real part of Eq. (62) which gives

$$\begin{aligned} \frac{d\Delta\phi}{dt} &= \frac{d\phi_L}{dt} - \frac{d\phi_R}{dt} = \frac{2eV_a}{\hbar} \\ \Delta\phi &= \Delta\phi_0 + \omega_J t \end{aligned} \tag{64}$$

where $\Delta\phi_0$ is a constant term and $\omega_J = \frac{2eV_a}{\hbar}$ is the Josephson frequency. This AC Josephson effect is rising from an applied voltage which causes a phase difference that increases at a linear rate with time. The result is sinusoidal oscillations in the supercurrent.

The zero-voltage supercurrent is driven by the transport of electrons between the two superconductors. Unlike a normal electric current, the transferred electrons are Cooper pairs instead of free electrons. The exchange of Cooper pairs is possible through the Andreev reflections of electrons and holes. In relation to this, we will provide a short explanation of the transport of Cooper pairs: An incoming electron, inside the normal conductor and towards the right superconductor, can interact with another electron and penetrate the superconductor

as a Cooper pair. Effectively, the process creates a Cooper pair in the right superconductor. The reflected hole will propagate away from the superconductor inside the normal metal. It may reflect in a similar manner when it reaches the left superconductor. Effectively the hole has destroyed a Cooper pair in the left superconductor. A procedure like this can continue back and forth between the two superconductors and effectively transport Cooper pairs. This process will happen in both directions, and depending on the phase difference, there might be a net current [60][61][63]. The Josephson effect is illustrated in Figure 4.

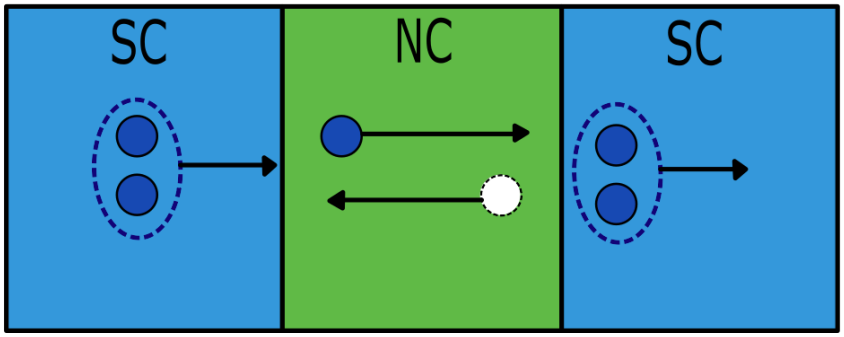

Figure 4: Illustration of the Josephson effect, where a Cooper pair is effectively transferred from the left superconductor to the right superconductor. The process is driven by electrons and holes that are Andreev reflected back and forth in the normal conductor.

In general, any arbitrary current-phase relation can be developed as a Fourier series of sines and cosines since the phases are periodic. We can therefore assume all current-phase relations to follow

$$I(\Delta\phi) = \sum_{n=1}^{\infty} \Big(A_n \sin(n\Delta\phi) + B_n \cos(n\Delta\phi) \Big). \tag{65}$$

Many junctions have a symmetrical geometry that demands the current to be reversed when the superconducting phase is inverted. For these types of junctions, as every junction investigated in this thesis, we have

$$I(\Delta\phi) = -I(-\Delta\phi). \tag{66}$$

It follows that $\Delta\phi = 0$ must provide zero current. Thus, $B_n = 0$ for all n to make the cosines disappear. The resulting current is then a series of sines, where we can recognize a general expression including higher-order terms given as

$$I(\Delta\phi) = I_1 \sin(\Delta\phi) + I_2 \sin(2\Delta\phi) + I_3 \sin(3\Delta\phi) + \cdots + I_n \sin(n\Delta\phi). \tag{67}$$

The higher-order terms connect to electrons and holes which bounce back and forth repeatedly, so-called higher harmonics.

Later in this thesis, we will show that the supercurrent depends on various parameters, and not only the superconducting phase. Among others, the thickness

of the normal metal is of great importance due to the superconducting decay length. The Cooper pairs, that leak from the superconductor into the normal metal, have a coherent phase relation. In other words, the Andreev reflected electrons, which travel through the normal conductor, would carry information about the superconducting phase. An ideal theoretical situation provides the phase information to be carried infinitely far into the normal region within the zero-temperature limit. However, at finite temperature, the phase information will eventually be lost within the phase-relaxation length due to scattering [8][64][65][66], or by spin-flip relaxation in the presence of magnetic impurities [58].

2.5 BLONDER TINKHAM AND KLAPWIJK (BTK) FORMALISM

In 1982, Blonder, Tinkham and Klapwijk (BTK) used the BdG-equations to study the nature of supercurrent arising in a normal-metal/superconductor (NC/SC) bilayer [57]. At this point in time, the idea of Andreev reflection was already suggested, but BTK introduced a new formalism which today is the most used and cited one. The trio investigated an NC/SC interface with a flat surface. The superconducting side was characterized by the mass m_{SC}, the Fermi energy $E_{F,SC}$ measured from the bottom of the conduction band, and the order parameter Δ, which was assumed to be constant inside the superconductor. The NC side was characterized by the mass m_{NC} and the Fermi energy $E_{F,NC}$ measured from the bottom of the conduction band. The model assumed perfect quadratic dispersion relations in both layers and no band effects beyond the effective mass. The transport through the interface was affected by a scattering potential modeled by a delta-function barrier potential H. The formalism considered particles moving perpendicular to the interface, chosen to be along the x-axis.

The scattering theory of the transport across the interface was developed by investigating an incoming electron particle on the NC side. It was then possible to calculate the transmissions and reflections probability amplitudes for the energetically allowed processes. BTK constructed the wave function on each side of the interface by combining the incoming electron state and the possible reflected states in the normal metal, and the possible transmitted states in the superconductor. Finally, to fulfill continuity, BTK demanded some boundary conditions: (i) a continuous wave function and (ii) a discontinuity in the derivative of the spatial wave function determined by the strength of the barrier potential.

Before we adapt the BTK formalism to our system in chapter 6, a description of the BTK formalism is needed. Consider a particle traveling on the normal side of an NC/SC bilayer. Recall the four different processes that may occur when the electron reaches the interface: the electron can undergo a reflection (as an electron or a hole) or a transmission (as an electron-like or a hole-like quasiparticle). This is illustrated by BTK in an energy scheme shown in Fig. 5. If the incoming electron has an energy below the gap, it cannot transfer into the superconductor alone. For the electron to drain off into the superconductor, the electron has to coherent reflect into a hole and transfer a charge of $-2e$ across the interface, namely through an Andreev reflection. Such a process cannot be calculated through a lower order description by the tunneling Hamiltonian to an NC/SC bilayer, making the BTK formalism very useful.

While studying Andreev reflections through the BTK formalism, we can interpret the transport of $-2e$ across the interface as the transport of a Cooper pair into the superconductor's ground state. The opposite reflection, where a hole reflects into an electron, can be described equally by removing one Cooper pair

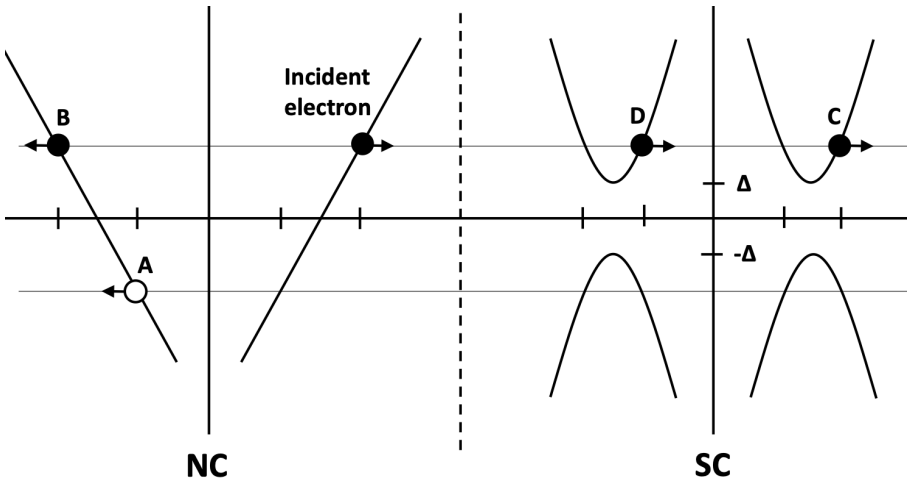

Figure 5: Diagram of energy vs. momentum at NC/SC interface. Black circles denote electrons, and white circles indicate holes, and the arrows point in the direction of the group velocity. The figure illustrated the four different outcomes of an incident electron. It can reflect as a hole (A), reflect as an electron (B), transmit as an electron-like quasiparticle (C) and transmit as a hole-like quasiparticle (D). Reproduced from ref. [57]

out of the superconducting ground state. As illustrated earlier, when electrons and holes are Andreev reflected back and forth in a Josephson junction, it can promote a transport of charges across the junction. The transport can take place even though the particles' energy is too low to be transmitted into the superconductors as quasiparticles. We refer to these bound states that transfer Cooper pairs as Andreev bound states (ABS), which can be calculated with the BTK formalism.

Furthermore, utilize the BTK formalism to calculate the Andreev reflection. Let us do so on a NC/SC bilayer. Starting from the conventional version of the BdG-equations as in Ref. [67] we arrive at

$$\begin{aligned} i\hbar\frac{\partial f}{\partial t} &= -\left[\frac{\hbar^2\nabla^2}{2m}+\mu\right]f(x,t)-\Delta(x)g(x,t)\\ i\hbar\frac{\partial g}{\partial t} &= \left[\frac{\hbar^2\nabla^2}{2m}+\mu\right]g(x,t)-\Delta(x)f(x,t). \end{aligned} \tag{68}$$

The steady state solution of these two equations takes the form [67],

$$\begin{aligned} f(x,t) &= ue^{ik^{\pm}x}e^{-Et/\hbar}\\ g(x,t) &= ve^{ik^{\pm}x}e^{-Et/\hbar}\\ &\text{where } \hbar k^{\pm} = \sqrt{2m}\left(\mu\pm\sqrt{E^2-\Delta^s}\right)^{\frac{1}{2}}. \end{aligned} \tag{69}$$

Function f is identified as the electron wave and g is the hole wave function. We can obtain this identification of f and g by generalizing to a normal state, *i.e.* $\Delta(x) = 0$ [67]. Moreover, from BCS theory [36], we have that E, u, and v are

$$\begin{aligned} E^2 &= \left(\frac{\hbar^2 k^2}{2m} - \mu\right)^2 + \Delta^2 \\ u^2 &= \frac{1}{2}\left[1 \pm \frac{\sqrt{E^2 - \Delta^2}}{E}\right] \\ v^2 &= \frac{1}{2}\left[1 \mp \frac{\sqrt{E^2 - \Delta^2}}{E}\right] \end{aligned} \tag{70}$$

with $\pm$ sign correlated with $\hbar k^{\pm} = \sqrt{2m}\left(\mu \pm \sqrt{E^2 - \Delta^s}\right)^{\frac{1}{2}}$.

We want to look at the behavior of a normal electron as it hits the NC/SC boundary. Combining Eq. (69) and Eq. (70), we observe that the incoming electron has the wave function given by

$$\psi_{inc} = \begin{bmatrix} 1 \\ 0 \end{bmatrix} e^{iq^+ x}, \tag{71}$$

where $\hbar q^+ = \sqrt{2m}\sqrt{\mu + E}$.

We find the reflected hole wave function as

$$\psi_{ref} = a \begin{bmatrix} 0 \\ 1 \end{bmatrix} e^{iq^- x}, \tag{72}$$

where $\hbar q^- = \sqrt{2m}\sqrt{\mu - E}$.

and the transmitted wave is

$$\psi_{tran} = b \begin{bmatrix} u \\ v \end{bmatrix} e^{ik^+ x}, \tag{73}$$

where k^+ is defined as in Eq. (69). By requiring a matching amplitude at the boundary, we find that the reflection coefficient, $A(E) = aa^*$ is

$$A(E) = \begin{cases} 1 & |E| < \Delta, \\ \frac{u^2}{v^2} = \frac{|E| - \sqrt{E^2 - \Delta^2}}{|E| - \sqrt{E^2 + \Delta^2}} & |E| \geqslant \Delta. \end{cases} \tag{74}$$

The transmission coefficient is then $T(E) = bb^* = 1 - A(E)$.

We can interpret from Eq. (74) that if the energy of the incoming electron is less than the gap, the electron will be reflected completely as a hole through an Andreev reflection [54][67]. In other words, the flow of current is carried exclusively by Andreev reflections. For energies greater than the gap, there are partial Andreev reflections. However, note how this calculation is done by assuming no

barrier at the interface. Junctions with a non-zero barrier effect at the interface will be investigated later in this thesis.

In chapter 6, we will utilize the BTK formalism to calculate the ABS across our system. Therefore, let us do a short description of the procedure. Start by constructing the wave function of the system of interest. For instance, a superconductor/ normal-metal/superconductor trilayer where the wave functions inside the normal metal describe electrons and holes propagating in both directions, while the wave functions inside the superconductor describe quasiparticles. Together with the boundary conditions, all these wave functions create a system with unknown coefficients. The coefficients represent the weight of the various eigenstates. At this point, we do not solve for the coefficients. Instead, require the system to be solvable, and achieve an equation for the allowed energies of the system; the ABS.

3

SPIN-DEPENDENT INTERACTIONS

3.1 SPIN-ORBIT COUPLING

Spin-orbit coupling is, as the name indicates, a coupling between the particle's spin and momentum. The phenomenon manifests itself in lifting the degeneracy of the energy levels of one electron [68]. In other words, an electron moving in an external electric field feels an effective magnetic field without the need for an applied one. The coupling has the following understanding: An electron with momentum $\mathbf{p}$ will experience a Lorentz force perpendicular to its motion

$$\mathbf{F} = -e\mathbf{p} \times \mathbf{B}/m \tag{75}$$

while moving across a magnetic field $\mathbf{B}$. The electron will then possess a Zeeman energy of $\mu_B \boldsymbol{\sigma} \cdot \mathbf{B}$ where $\boldsymbol{\sigma}$ is the vector of Pauli matrices, μ_B is the Bohr magnetron, and e and m are, respectively, the charge and mass of the electron. This force is analogous to when an electron moves across an electric field which causes an effective magnetic field in its rest-frame as

$$\mathbf{B}_{\text{eff}} \sim \mathbf{E} \times \frac{\mathbf{p}}{mc^2} \tag{76}$$

where c is the speed of light. A field like the one described previously will produce a momentum dependent Zeeman energy of

$$H_{SO} \sim \mu_B \Big(\mathbf{E} \times \mathbf{p} \Big) \cdot \boldsymbol{\sigma}/mc^2 \tag{77}$$

known as the spin-orbit coupling.

We can derive the existence of the coupling in a similar fashion as done in Ref. [69]. Look at an electron orbiting around in a crystal of nucleons. The electron's rest frame will observe the nucleons circulating around itself with velocity $\boldsymbol{v}$. As a result, the electron will feel an effective magnetic field given by

$$\mathbf{B} = \frac{\boldsymbol{v}}{c} \times \mathbf{E} \tag{78}$$

where $\mathbf{E}$ is the electric field of the nucleons, and c is the speed of light. The magnetic momentum of the electron $\boldsymbol{\mu}$ is related to its spin angular momentum $\mathbf{S}$ as

$$\boldsymbol{\mu} = \frac{eg}{2mc}\mathbf{S} \tag{79}$$

where the g-factor is taken to be $g = 2$. We can now write the equation of motion for the spin angular momentum in the electron's rest frame like

$$\left(\frac{dS}{dt}\right)_{\text{restframe}} = \mu \times B' \tag{80}$$

where we have defined $B' = \gamma\left(B - \frac{v}{c} \times E\right)$ as the magnetic field in the electron's rest frame. Keep in mind that B and E are the magnetic and electric field of the nucleons, respectively. Assuming $v \ll c$ such that we can neglect terms of order $\frac{v^2}{c^2}$, Eq. (80) reads

$$\left(\frac{dS}{dt}\right)_{\text{restframe}} = \mu \times \left(B - \frac{v}{c} \times E\right). \tag{81}$$

This equation of motion for the spin angular momentum is equivalent to an energy provided by an coupling with the spin of the electron given by

$$U' = -\mu \times \left(B - \frac{v}{c} \times E\right). \tag{82}$$

For a radial symmetric electric field, as the one originating from a nucleon, the electric field E is

$$E = -\frac{1}{e}\frac{r}{r}\frac{dV(r)}{dr}. \tag{83}$$

Insert the previous expression for the electric field into Eq. (82), the energy provided by the interaction with the spin of the electron yields

$$U' = -\frac{eg}{2mc} S \cdot B + \frac{g}{2m^2c^2} S \cdot L\left(\frac{1}{r}\frac{dV(r)}{dr}\right) \tag{84}$$

where $L = r \times mv$ denotes the orbital angular momentum of the electron. The spin-orbit coupling term is a factor of 2 off. The expression will nevertheless give the Zeeman effect correctly. The explanation of this factor of 2 was pointed out by Thomas [70]. The coordinate system is rotating, such that the equation of motion in Eq. (82) reads

$$\left(\frac{dS}{dt}\right)_{\text{nonrot}} = \left(\frac{dS}{dt}\right)_{\text{restframe}} + \omega_T \times S = S \times \left(\frac{egB'}{2mc} - \omega_T\right). \tag{85}$$

It then follows that the interaction energy is given by

$$U = U' + S \cdot \omega_T \tag{86}$$

where the angular velocity $\omega_T = -\frac{1}{2m^2c^2} L\left(\frac{r}{r}\frac{dV(r)}{dr}\right)$ is known as the Thomas angular velocity. The resulting coupling energy is then reduced by a factor of

1/2, known as the Thomas factor, which is necessary to obtain the correct result. Finally, the spin-orbit coupling is then given by

$$H_{SO} = \frac{1}{2m^2c^2}\mathbf{S}\cdot\mathbf{L}\left(\frac{1}{r}\frac{dV(\mathbf{r}}{dr}\right). \tag{87}$$

Pay attention to the form of the spin-orbit Hamiltonian which provides a shift in the energy of the electron.

A time-reversal invariant system requires that the energy of an electron obeys the relation $E(\mathbf{k},\uparrow) = E(-\mathbf{k},\downarrow)$ since $\mathbf{k} \to -\mathbf{k}$ and $\sigma \to -\sigma$ upon time reversal, according to Kramer's theorem [71]. Therefore, a state corresponding to spin-up and wave vector $\mathbf{k}$ degenerates with a spin-down state of wave vector $-\mathbf{k}$. Spin-orbit coupling preserves the time-reversal symmetry. As a result, if there is an inversion symmetry of the system, Kramer's theorem gives a degeneracy spin state for any wave vector $\mathbf{k}$ as $E(\mathbf{k},\uparrow) = E(\mathbf{k},\downarrow)$. In a crystal with inversion asymmetry, the spin-splitting is determined by Rashba spin-orbit coupling.

3.1.1 *Rashba spin-orbit coupling*

In this thesis, we will only consider a spin-orbit coupling of type Rashba, introduced by Bychov and Rashba in 1984 [72][73]. This type of spin-orbit coupling is caused by a broken inversion symmetry of the crystal, *i.e.* the crystal looks different in the two directions $\pm\mathbf{r}$. Such a broken inversion symmetry can give a potential difference along with the respective directions of $V(r) \neq V(r + \Delta r)$. The asymmetric potential provides a non-zero gradient, hence an electric field is given by the gradient of the crystal potential $\mathbf{E} = -\boldsymbol{\nabla}V$. This result enables the Rashba spin-orbit coupling to be controlled by an external electric field [74]. The Rashba spin-orbit Hamiltonian is given by

$$H_{SO} = \lambda\Big(\boldsymbol{\sigma}\times\mathbf{p}\Big)\cdot\hat{n} \tag{88}$$

where λ is a parameter describing the strength of the spin-orbit coupling, $\boldsymbol{\sigma}$ is the vector of Pauli matrices, $\mathbf{p}$ is the canonical momentum vector of the electron, and $\hat{n}$ is a unit vector along the axis with inversion symmetry breaking.

It is then clear that a Rashba spin-orbit coupling has both a strength and orientation. For simplicity, we will introduce a terminology that will appear in the following chapters. Firstly, we will refer to the spin-orbit coupling strength (λ) as spin-orbit magnitude. Secondly, the parameter determining the direction of the vector characterization to the spin-orbit coupling ($\hat{n}$) will be stated as spin-orbit orientation.

The electric field is related to the Hamiltonian as $\mathbf{E} = |E|\hat{n}$, such that $\mathbf{B} \propto \mathbf{k}\times\hat{n}$ where $\mathbf{B}$ is the magnetic field in the rest-frame of the electron. We can therefore

see that the Rashba spin-orbit coupling provides a Zeeman energy term $H_R \propto \boldsymbol{\sigma} \cdot \mathbf{B}$. Note that the displaced energy will be proportional to the component of $\mathbf{k}$ perpendicular to the direction of broken symmetry.

The magnitude of the Rashba spin-orbit coupling varies in a range of several orders of magnitude for different materials. For instance, a two-dimensional electron gas at a hybrid-interface is found to have $\lambda \simeq 0.05 eV\text{Å}$ [75], while heavy metals may provide much higher values like $\lambda \simeq 0.3 eV\text{Å}$ and $\lambda \simeq 0.6 eV\text{Å}$ for, respectively, surface states of $Au(111)$ and $Bi(111)$ [24][25]. An investigation of a surface alloy of Bi/Au showed Rashba spin-orbit magnitudes even stronger with $\lambda \simeq 3 eV\text{Å}$ [26].

3.2 FERROMAGNETISM

In the introduction of this thesis, we discussed that a magnetic Josephson junction (SC/F/SC) could create Cooper pairs with triplet symmetry. Moreover, we have pointed out how a spin-orbit coupling is analogous to an effective momentum-dependent magnetic field. Such a momentum-dependent magnetic field is not to be confused with the homogeneous magnetic field provided by a ferromagnet. However, a ferromagnet will provide a spin-dependent current. Therefore, let us make a brief summary of the behavior of a ferromagnetic SC/F/SC Josephson junction.

Ferromagnetism is characterized by the ability of the substance to exhibit a spontaneous magnetization [76]. Materials with ferromagnetic properties are strongly influenced by external magnetic fields, *e.g.* nickel and iron. The ferromagnetic property of a material is usually determined by a relative permeability much greater than one. Previous experiments show that the ferromagnetic character vanishes under heating, and the material receives paramagnetic properties [76].

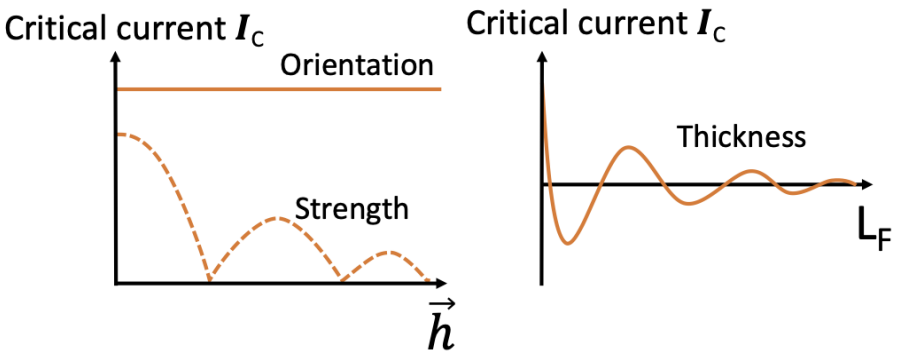

Figure 6: The current behavior of a ferromagnetic SC/F/SC Josephson junction. The left panel shows the current for varying orientation of the magnetic field and an increasing magnitude. The right panel shows the current as a function of the thickness of the ferromagnetic layer.

A mean-field approximation of the ferromagnetic order can be described as

$$H_h = -\mathbf{h} \cdot \boldsymbol{\sigma} \tag{89}$$

where $\mathbf{h}$ is the magnetic field, and $\boldsymbol{\sigma}$ is the vector of Pauli matrices. The interaction between the spin and the magnetic field gives rise to a Zeeman energy shift for particles with spin aligned parallel and anti-parallel to the magnetic field $\mathbf{h}$. As a result, the displaced energy bands for spin-up and spin-down particles will influence the Fermi surface of the ferromagnet. The importance of the displacement will be discussed further in chapter 4. For now, keep in mind that a displacement of the energy bands will provide Cooper pairs with a non-zero

center-of-mass momentum. Consequently, a singlet Cooper pair will acquire a momentum-dependent phase. This phase will give rise to a process called spin mixing [77], where the singlet pair oscillate into a spin-0 triplet pair. Thus, the current across an SC/F/SC junction will oscillate as a function of, among others, the length of the ferromagnetic material and the magnetic field strength [78][79][14]. Furthermore, since the magnetic field only couples to the particles spin, the current is invariant with respect to the orientation of the magnetic field [79]. The behavior is shown in Fig. 6.

4

DISPLACED ENERGY BANDS

When an Andreev reflection takes place, the generated Cooper pair is established around the superconductor's Fermi level. As a result, the size and shape of the Fermi surface to the material in proximity is urgent to avoid Fermi vector mismatch and scattering effects at the interface. This chapter will account for the phenomena that provide displaced energy bands and hereby unequal Fermi surfaces across the interface. In addition, this chapter will pay attention to the resulting Cooper pairs and their symmetry regarding different spin-dependent interactions.

The derivation of Cooper pairs through BCS theory presented in section 2.1, we have described how the probability amplitude of creating a Cooper pair depends on the spin, energy, and momentum of the two electrons involved. For Cooper pairs to be transferred back and forth inside a Josephson junction, we lean on Andreev reflections to occur. When an incoming electron travels inside the normal metal, it can interact with another electron close to the interface. It can then enter the superconductor's condensate as a Cooper pair. For this phenomenon to appear in a conventional superconductor, the two involved electrons need to have opposite spin (singlet symmetry), energy below the superconducting gap Δ, and opposite momentum.

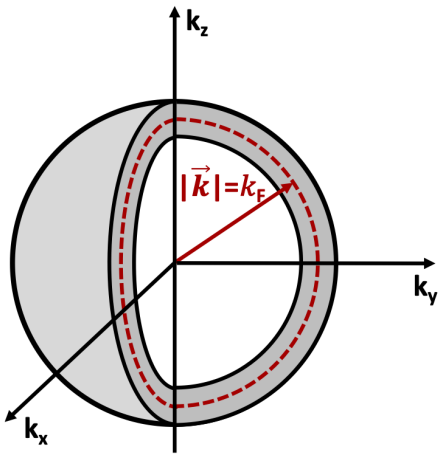

Figure 7: Fermi surface of a superconductor. The red line indicates the sphere of the Fermi surface, while the grey area includes a small displacement to k_F, which still provides a large probability amplitude of Cooper pairs.

Based on the existing theory, one could naively state that opposite momentum is sufficient to create a Cooper pair with singlet symmetry. However, the probability amplitudes of the creations of Cooper pairs depend on the absolute value of the momentum. In section 2.1, we derived that the probability amplitude of a Cooper pair to exist is determined by $|v_{\mathbf{k}}|^2$ which is greatest when $|\mathbf{k}| = k_F$. Thus, electrons living on the sphere shell of radius k_F, which defines the Fermi surface of a normal-state superconductor, have the highest probability of creating Cooper pairs. The surface is illustrated as a three-dimensional sphere shell with radius k_F in Fig. 7.

This thesis will only investigate systems that are invariant in y- and z-direction. Consequently, the momentum of the particles that travel across the interface between the normal metal and the superconductor are not able to change in the respective directions. However, since we have broken the translational symmetry in x-direction, the belonging k_x-modes are not conserved. Therefore, all incoming electrons can find an available state at the Fermi surface regardless of the value of k_x. Keep in mind that a Fermi vector mismatch in y- and z-direction do not make it impossible to create a Cooper pair, but the probability amplitude for such formation to take place is greatest at the Fermi surface.

4.1 SPIN-DEPENDENT FERMI SURFACE DUE TO SPIN-ORBIT COUPLING

This section will consider the Fermi surface of a heavy metal with Rashba spin-orbit coupling (HM) and the consequent effects in proximity with a superconductor (SC). Andreev reflections of electrons (holes) into holes (electrons) have to obey the inequality of the Fermi surfaces at the interface of an HM/SC bilayer. Therefore, the prevalence of the Fermi vector mismatch is essential to understand as we later will investigate an SC/HM/SC Josephson junction.

The Rashba spin-orbit coupling will favor a spin orientation relative to the momentum of the electrons. The spin degeneracy can be determined by the definition of the Hamiltonian in Eq. (88). A displacement in the energy bands is expected since the Hamiltonian of the Rashba spin-orbit coupling is equivalent to a momentum-dependent Zeeman-field, shown in section 3.1. In the following, we will study a spin-orbit coupling oriented parallel to the interface, $\hat{n} = \hat{z}$. This orientation will displace the Fermi surface in xy-plane illustrated in Fig 8. Notice how the orientation of the particles' spin is rotating at the Fermi surface. Moreover, the displacement of the energy bands depends on the spin-orbit orientation $\hat{n}$. Hence, it is possible to create both circular and elliptical Fermi surfaces in k-space.

Let us investigate the reflection and transmission across the interface of an HM/SC bilayer. The reflection of an incoming electron is illustrated in Fig. 9a.

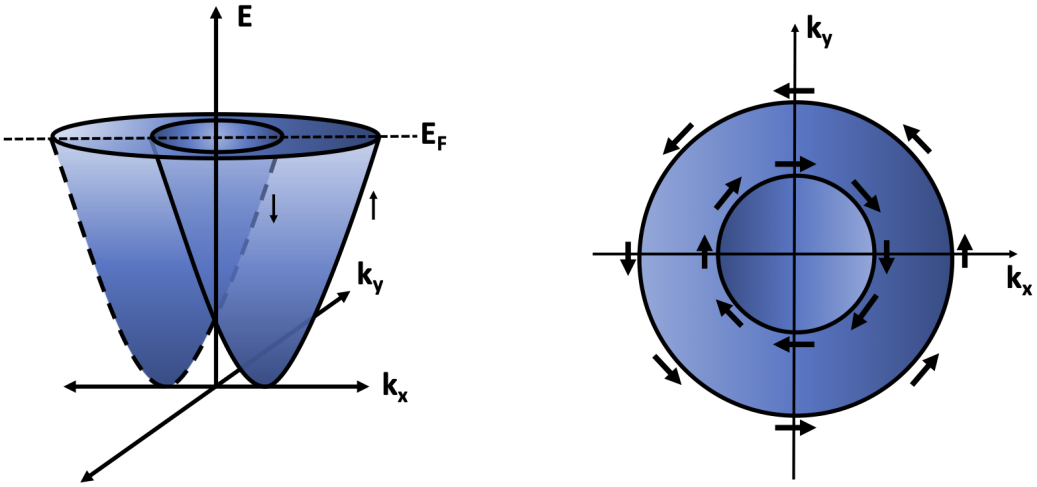

Figure 8: Illustration of the displaced energy band (left panel) and Fermi surface (right panel) in a heavy metal with Rashba spin-orbit orientation of $\hat{n} = \hat{z}$. Notice how the spin couples with the momentum, such that the Fermi surface creates a circle of rotating spin orientations.

The Andreev reflection will occur qualitatively as within an NC/SC bilayer. An incoming electron with energy just above Fermi level can find another electron just below Fermi level, and together enter the superconductor as a Cooper pair. Thus, the incoming electron will reflect as a hole generated by the electron below the Fermi level. However, the spin-orbit coupling can displace the Fermi surface and, consequently, the available states. Due to invariance in y- and z-direction, we require k_y and k_z to be conserved. The symmetry breaking along the x-direction allows for k_x to change when an electron travels through the interface. This is the key to understand the importance of the displaced energy bands and Fermi surface: spin-orbit coupling can provoke Fermi vector mismatch and displace the Fermi surface to perfectly coincide.

Furthermore, consider the formation of Andreev bound states in an SC/HM/SC Josephson junction due to the displaced energy band for spin-up and spin-down particles. First, recall how an Andreev bound state is established in an SC/NC/SC Josephson junction: An incoming electron, inside the normal metal, can Andreev reflected into a hole at the interface to the first superconductor. The reflected hole will then propagate away from the first superconductor. When the hole reaches the second superconductor, it can reflect into an electron through an Andreev reflection. Hence, electrons and holes can bounce back and forth between the sandwiched superconductors. If the reflected electron accumulates a phase by 2π after one round trip, we have the formation of an Andreev bound state. The process was discussed more thoroughly in section 2.4. Now, replace the normal conductor with a heavy metal with Rashba spin-orbit coupling. We have already explored that the spin degeneracy supports Andreev reflection of electron-hole conversation with singlet symmetry. As a result, the Andreev

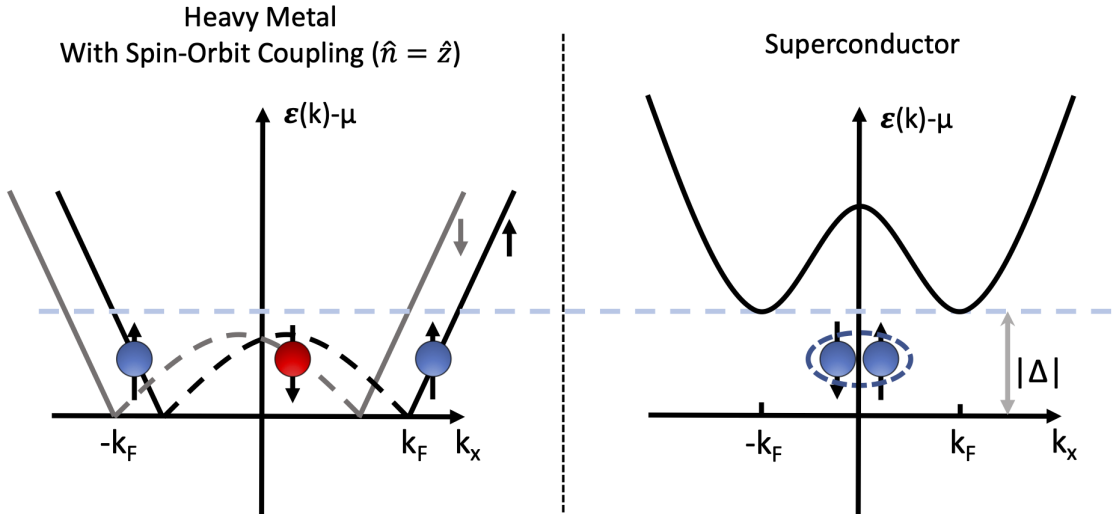

(a) Electron-hole conversion at the interface between a heavy metal with Rashba spin-orbit coupling and a superconductor. The incoming spin-up electron (blue circle) inside the heavy metal can reflect as a hole with spin down (red circle). The missing charge of 2e enters the superconductor as a Cooper pair in the ground state. The illustration also includes the event for the incoming electron to reflect as an electron.

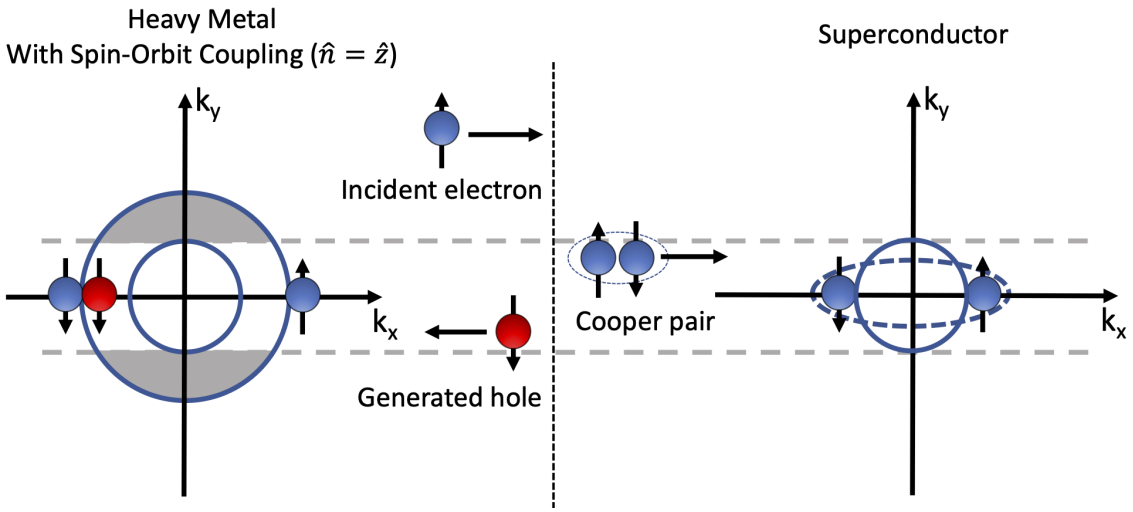

(b) Illustration of an Andreev reflection considered from the Fermi surface. The incoming electron has to conserve momenta in y-and z-direction. However, the momentum in the x-direction is not conserved due to broken symmetry. Hence, the incoming electron in the heavy metal can create a Cooper pair at the Fermi surface of the superconductor. The incident electron Andreev reflects like a hole, and the conserved charge of 2e enters the superconductor.

Figure 9: Andreev reflection at the interface of a HM/SC bi-layer

bound states will also support singlet symmetry. An illustration of the Andreev bound stated in an SC/HM/SC junction is described in Fig. 10.

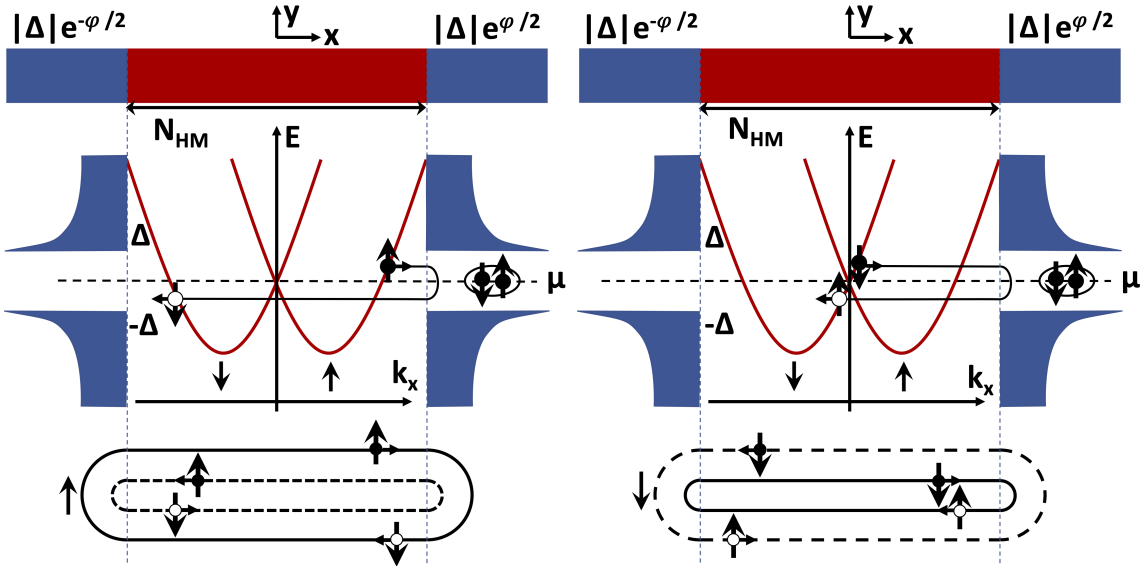

Figure 10: Illustration of the creation of Andreev bound states in a Josephson junction with a weak link of Rashba spin-orbit coupling. Electrons (black circles) and holes (white circles) can Andreev reflect back and forth between the two superconductors and establish Andreev bound states. The superconductor is characterized by a phase and a gap in the density of states. Rashba spin-orbit coupling lifts a spin degeneracy. However, it does not lift the degeneracy of the Andreev bound states since electrons with spin up and spin down have an equal velocity at Fermi surface and hence same effective length. Reproduced from Ref. [80]

4.2 ADJUSTED FERMI SURFACE DUE TO CHEMICAL POTENTIAL

We have now pointed out how spin-orbit coupling reshapes the Fermi surface of a heavy metal. Further, one could question if any other SC/HM/SC junction properties can deform the Fermi surface. Recall that the Fermi surface of a superconductor arises around the normal state Fermi surface. A property of the material which affects the normal state Fermi level is the chemical potential. Unlike the spin-orbit coupling, the chemical potential is momentum- and spin invariant. Therefore, the chemical potential will only affect the radius of the circular surface. The barrier which occurs from a different chemical potential in a HM/SC bilayer is understood by studying their normal state Fermi surface. That is analogous to an NC/NC system. In the normal state, without spin-orbit coupling, the energy bands take a parabola shape, $E \propto k^2$. The cut of the highest occupied energy state is defined from the chemical potential μ. Thus, the greater value of μ, a bigger circle will occur in the momentum space to include all occupied states for $E = \mu$. The different shapes of the energy bands is illustrated in Figure 11. As we require energy conservation, we know that an electron on the left has to find an available state on the right to tunnel across the interface

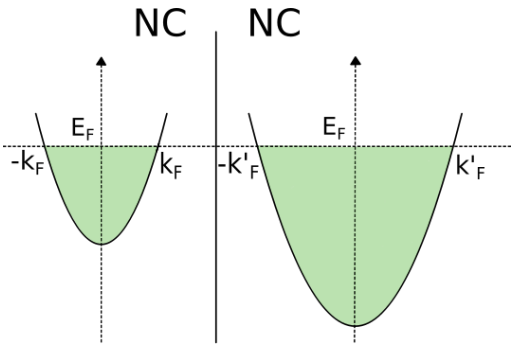

(a) Energy vs. momentum for the two normal conductors side by side. The green area is the occupied states. Note that the Fermi level will be equal when we have an equilibrium situation, but the associated Fermi wave vector, $\mathbf{k}$, is different.

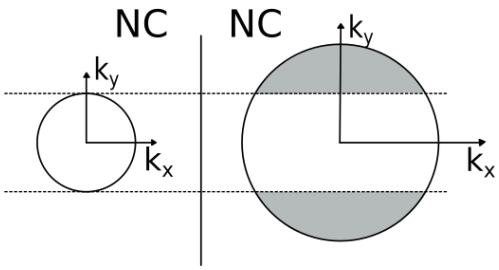

(b) The momentum plane at Fermi energy, $E = E_F$. We demonstrate how an electron that tries to tunnel across the interface experience a forbidden momentum barrier. The grey area represents the Fermi vector mismatch due to the conservation of energy and momentum.

Figure 11: Energy and momentum for a hybridstructure of a normal conductor(NC) to a normal conductor(NC). The left panel shows the energy as a function of the momentum wave vector k. We have indicated the Fermi level for the two states as the dashed, horizontal line.

or vice versa. Additionally, we require the momentum to be conserved along the y- and z-direction. As observed in Figure 11, there are less available states, which conserve momentum and energy, when the shape of the Fermi surface is unequal due to different chemical potential.

The conservation of energy will force the electrons inside the normal metal, which interact with the left superconductor, to reflect into holes around the superconductor's chemical potential. At the same time, the reflected hole has to conserve momentum in the y- and the z- direction due to symmetry, which provides a Fermi vector mismatch. As a result, a Fermi vector mismatch is interpreted as an effective momentum barrier. We will therefore include the barrier as a scattering potential in our analytical model in chapter 6. Consequently, absent barrier effects are expected in the event of a matching chemical potential across an SC/NC/SC junction. The resulting supercurrent is thus predicted to increase compared to a finite-barrier junction. Furusaki confirmed the tendency when he calculated the corresponding current to such a non-zero barrier junction [81].

4.3 SPIN-DEPENDENT FERMI SURFACE DUE TO MAGNETIC FIELD

A ferromagnet will displace the Fermi surface for spin-up and spin-down particles due to the coupling of spins parallel and anti-parallel to the magnetic field.The separation of energy bands is displayed in Fig. 12.

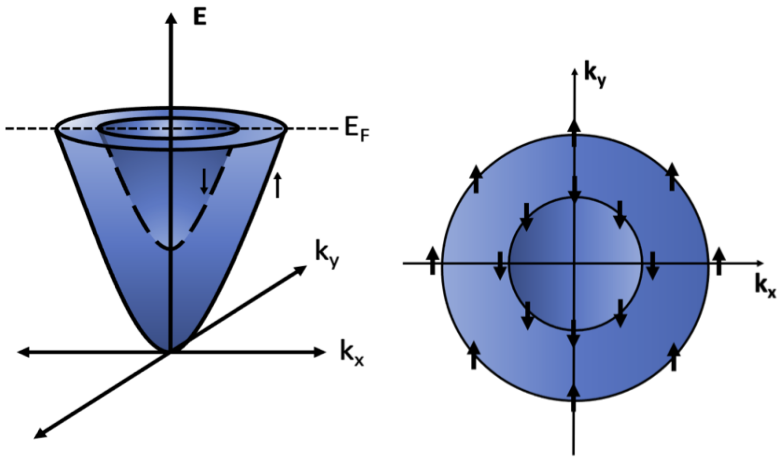

Figure 12: Displaced energy band (left panel) and Fermi surface (right panel) in a ferromagnet with $\mathbf{h} = z$. The energy favor spin-up, such that the Fermi surface displaces the shape for spin-up particles versus spin-down particles. This is unequal to the displaced Fermi surface rising from spin-orbit coupling where the spin orientation rotates.

The spin degeneracy will produce a Fermi surface of different sizes for spin-up and spin-down particles. Pay attention to the displaced Fermi surface which is different compared to the displaced Fermi surface due to spin-orbit coupling. In a ferromagnet, each surface has equal spin orientation, while spin-orbit coupling generates rotation spin orientations (Fig. 8).

The orientation of the spin plays an important role when studying Andreev reflections. If an incoming spin-up electron inside the ferromagnet wants to penetrate the superconductor, it must create a Cooper pair with a spin-down electron. As a result, an Andreev reflection involves both the spin-up and spin-down band of electrons. Therefore, a fully spin-polarized ferromagnetic SC/F/SC Josephson junction will suppress Andreev reflection due to the spin-dependent Fermi surface [14][82].

The spin-dependent Fermi surface will produce Cooper pairs with spin-triplet symmetry through a spin mixing process [77]. We can understand this transformation by following the treatment in Ref. [83]. Let the incoming spin-up electron inside the ferromagnet have a Fermi wave number k_F in the absence of magnetism. Accordingly, a finite magnetic field will lift the spin degeneracy, and the two interacting electrons of opposite spins have the Fermi wave numbers of $k_F + Q/2$ and $k_F - Q/2$, respectively. The resulting Cooper pair will then acquire a finite center-of-mass momentum Q. Thereupon, the momentum-dependent phase term will make a singlet Cooper pair which enters the ferromagnet to

oscillate between a singlet state $\left(\uparrow\downarrow - \downarrow\uparrow\right)$ and a spin-0 triplet state $\left(\uparrow\downarrow + \downarrow\uparrow\right)$. We can observe the oscillations as

$$\begin{aligned}\left(\uparrow\downarrow - \downarrow\uparrow\right) \rightarrow &\left(\uparrow\downarrow e^{iQ} - \downarrow\uparrow e^{-iQ}\right) \\ &= \left(\uparrow\downarrow - \downarrow\uparrow\right)\cos(Q) + i\left(\uparrow\downarrow + \downarrow\uparrow\right)\sin(Q).\end{aligned} \tag{90}$$

We have discussed the Cooper pairs with triplet symmetry further in Appendix A.2.

Keep in mind that Rashba spin-orbit coupling does not provide spin-singlet Cooper pairs that acquire center-of-mass momentum. The interaction couples the spin of the particle to its momentum, such that the spin orientations rotate around the Fermi surface. The spin-up and spin-down band for electrons under spin-orbit coupling will therefore have opposite momentum. Hence, the oscillations which follow from a non-zero center-of-mass momentum are expected to be absent.

5

NUMERICAL FRAMEWORK

I this chapter, we will derive the numerical framework used to investigate the supercurrent across a superconductor/heavy-metal/superconductor (SC/HM/SC) Josephson junction. We will consider a tight-binding approximation which treats the electrons to be tightly bound to the nucleons of the atoms in a tight-binding lattice following the Bogoliubov-de Gennes framework [8][38] [84][85] . In this theory, we neglect the potential from the neighboring nucleons and the overlap of the orbitals of two neighboring atoms. Hence, we can express the eigenfunctions of the crystal electron system as a linear combination of atomic orbitals [85][86] .

We will find it helpful to rewrite the Hamiltonian from a first quantization formalism into second quantization. Therefore, let us define the basis of the second quantization space as

$$\begin{aligned} |i\rangle &= \phi(\mathbf{r} - \mathbf{R}_i) \\ |j\rangle &= \phi(\mathbf{r} - \mathbf{R}_j) \\ |k\rangle &= \phi(\mathbf{r} - \mathbf{R}_k) \\ |l\rangle &= \phi(\mathbf{r} - \mathbf{R}_l) \end{aligned} \tag{91}$$

where $\mathbf{r}$ is the position of the electron and $\mathbf{R}_m$ is the position of the atom at lattice m. To solve the system in a self-consistent manner, we want the Hamiltonian of the system to be diagonalized. By adding different layers in the x-direction, we obtain a lattice where we can assume periodic boundary conditions along the y- and z-direction, *i.e.* translation invariance in the respective directions. This symmetry makes it possible to reduce the size of the problem by performing a Fourier transform. In order to achieve a diagonalized Hamiltonian, we define the following Fourier transform for the creation and annihilation operators [87]

$$\begin{aligned} \hat{c}^\dagger_{i,\sigma} &= \frac{1}{\sqrt{N_y N_z}} \sum_{k_y,k_z} \hat{c}^\dagger_{i_x,k_y,k_z,\sigma} e^{-i(k_y i_y + k_z i_z)} \\ \hat{c}_{i,\sigma} &= \frac{1}{\sqrt{N_y N_z}} \sum_{k_y,k_z} \hat{c}_{i_x,k_y,k_z,\sigma} e^{i(k_y i_y + k_z i_z)} \end{aligned} \tag{92}$$

where the sum over k_y and k_z are inside the first Brillouin zone, that is $k_y, k_z \in \langle -\pi, \pi]$. Subscript i represent the lattice site, and since we are studying a 3-dimensional lattice we have $i = \{i_x, i_y, i_z\}$. Subscript σ represents the spin for

the respective fermion, *i.e.* σ is either spin-up or spin-down represented by the notation $\uparrow$ and $\downarrow$, respectively. Later in this thesis, some terms are considering two fermionic creation and annihilation operators with individual spins, and we will utilize the subscripts α and β.

5.1 DIAGONALIZATION OF THE BDG EQUATIONS

In order to calculate the supercurrent, as well as other physical quantities, it will be helpful to diagonalize the Hamiltonian into a form including purely independent fermionic operators exclusively. We could then utilize the Fermi-Dirac distribution. *E.g.* when evaluating the combined quantum-mechanical expectation values and thermal averages of quasiparticle operators. This section will therefore provide the diagonalization of the BdG equations.

Starting from a general case with the three-dimensional Hamiltonian on the form

$$\hat{H} = \hat{H}_0 + \frac{1}{2}\sum_{k_y,k_z} W^\dagger_{k_y,k_z}\hat{H}_{k_y,k_z}W_{k_y,k_z}, \tag{93}$$

with

$$W_{k_y,k_z} = \begin{pmatrix} B_{1,k_y,k_z} \\ B_{2,k_y,k_z} \\ \cdots \\ B_{3,k_y,k_z} \end{pmatrix}, \quad B_{i_x,k_y,k_z} = \begin{pmatrix} \hat{c}_{i_x,k_y,k_z,\uparrow} \\ \hat{c}_{i_x,k_y,k_z,\downarrow} \\ \hat{c}^\dagger_{i_x,-k_y,-k_z,\uparrow} \\ \hat{c}^\dagger_{i_x,-k_y,-k_z,\downarrow} \end{pmatrix}, \quad \hat{H}_{k_y,k_z} = \begin{pmatrix} \hat{H}_{1,1,k_y,k_z} & \cdots & \hat{H}_{1,N_x,k_y,k_z} \\ \vdots & \ddots & \vdots \\ \hat{H}_{N_x,1,k_y,k_z} & \cdots & \hat{H}_{N_x,N_x,k_y,k_z} \end{pmatrix} \tag{94}$$

as in Ref. [87]. However, the diagonalization procedure of the Hamiltonian-operator presented in the respective reference is not providing independent operators. In particular, it does not take into account the degeneracy when $T \neq 0$, such that the number of degrees of freedom is not preserved. Therefore, we will now derive the correct diagonalization of the Hamiltonian-operator in the following, which will not overcount the number of independent operators.

Will will later show that the matrix $\hat{H}_{k_y,k_z}$ in the previous equation has the dimension $4N_x \times 4N_x$. Let us continue with an ansatz for an eigenvalue with belonging eigenvector to exist, which we can be written as

$$\sum_{j_x=1}^{N_x} \hat{H}_{i_x,j_x,k_y,k_z} \begin{pmatrix} u_{j_x,n,k_y,k_z,\uparrow} \\ u_{j_x,n,k_y,k_z,\downarrow} \\ v_{j_x,n,k_y,k_z,\uparrow} \\ v_{j_x,n,k_y,k_z,\downarrow} \end{pmatrix} = E_{i_x,n,k_y,k_z} \begin{pmatrix} u_{i_x,n,k_y,k_z,\uparrow} \\ u_{i_x,n,k_y,k_z,\uparrow} \\ v_{i_x,n,k_y,k_z,\downarrow} \\ v_{i_x,n,k_y,k_z,\downarrow} \end{pmatrix}. \tag{95}$$

Take Eq. (95), complex conjugate and let $k_y, k_z \to -k_y, -k_z$. We can then observe how the eigenvalue problem fulfill the two relations

$$\hat{H}_{k_y,k_z}\begin{pmatrix} u_{k_y,k_z,n,\uparrow} \\ u_{k_y,k_z,n,\downarrow} \\ v_{k_y,k_z,n,\uparrow} \\ v_{k_y,k_z,n,\downarrow} \end{pmatrix} = E_{k_y,k_z}\begin{pmatrix} u_{k_y,k_z,n,\uparrow} \\ u_{k_y,k_z,n,\downarrow} \\ v_{k_y,k_z,n,\uparrow} \\ v_{k_y,k_z,n,\downarrow} \end{pmatrix}, \quad \hat{H}_{-k_y,-k_z}\begin{pmatrix} v^*_{k_y,k_z,n,\uparrow} \\ v^*_{k_y,k_z,n,\downarrow} \\ u^*_{k_y,k_z,n,\uparrow} \\ u^*_{k_y,k_z,n,\downarrow} \end{pmatrix} = -E_{k_y,k_z}\begin{pmatrix} v^*_{k_y,k_z,n,\uparrow} \\ v^*_{k_y,k_z,n,\downarrow} \\ u^*_{k_y,k_z,n,\uparrow} \\ u^*_{k_y,k_z,n,\downarrow} \end{pmatrix}. \tag{96}$$

Utilize these symmetrical relations to diagonalize the Hamiltonian. First, define a new basis,

$$\Gamma_{k_y,k_z} = \begin{pmatrix} \hat{\gamma}_{k_y,k_z,1} \\ \hat{\gamma}_{k_y,k_z,2} \\ \cdots \\ \hat{\gamma}_{k_y,k_z,4N_x} \end{pmatrix} \tag{97}$$

with the belonging diagonalization matrix containing the eigenvectors of H_{k_y,k_z} as column vectors as

$$P_{k_y,k_z} = \begin{pmatrix} u_{1,1,k_y,k_z,\uparrow} & u_{1,2,k_y,k_z,\uparrow} & \cdots & u_{1,N_x,k_y,k_z,\uparrow} \\ u_{2,1,k_y,k_z,\downarrow} & \ddots & \ddots & \vdots \\ \vdots & \ddots & \ddots & \vdots \\ v_{N_x,1,k_y,k_z,\downarrow} & \cdots & \cdots & v_{N_x,N_x,k_y,k_z,\downarrow} \end{pmatrix}. \tag{98}$$

The relation of this new basis to the old one is originating from the Bogoliubov transformation given as [88]

$$\begin{aligned} \hat{c}_{i_x,k_y,k_z,\uparrow} &= \sum_n u_{i_x,n,k_y,k_z,\uparrow}\hat{\gamma}_{n,k_y,k_z} \\ \hat{c}_{i_x,k_y,k_z,\downarrow} &= \sum_n u_{i_x,n,k_y,k_z,\downarrow}\hat{\gamma}_{n,k_y,k_z} \\ \hat{c}^\dagger_{i_x,-k_y,-k_z,\uparrow} &= \sum_n v_{i_x,n,k_y,k_z,\uparrow}\hat{\gamma}_{n,k_y,k_z} \\ \hat{c}^\dagger_{i_x,-k_y,-k_z,\downarrow} &= \sum_n v_{i_x,n,k_y,k_z,\downarrow}\hat{\gamma}_{n,k_y,k_z} \end{aligned} \tag{99}$$

or in matrix form given as

$$\Gamma^\dagger_{k_y,k_z} = W^\dagger_{k_y,k_z}P_{k_y,k_z} \quad \Leftrightarrow \quad W_{-k_y,-k_z} = P_{-k_y,-k_z}\Gamma_{-k_y,-k_z}. \tag{100}$$

This new basis makes it possible to rewrite the Hamiltonian as

$$\hat{H} = \hat{H}_0 + \frac{1}{2}\sum_{k_y,k_z,n} E_{k_y,k_z,n}\hat{\gamma}^\dagger_{k_y,k_z,n}\hat{\gamma}_{k_y,k_z,n}. \tag{101}$$

Now, if we write out Eq. (100), the two expressions for $\hat{\gamma}_{k_y,k_z}$ is given by

$$\begin{aligned}\hat{\gamma}^\dagger_{k_y,k_z,n} = \sum_{i_x} \Big(&\hat{c}^\dagger_{i_x,k_y,k_z,\uparrow} u_{i_x,k_y,k_z,\uparrow} + \hat{c}^\dagger_{i_x,k_y,k_z,\downarrow} u_{i_x,k_y,k_z,\downarrow} \\ &+ \hat{c}_{i_x,-k_y,-k_z,\uparrow} v_{i_x,k_y,k_z,\uparrow} + \hat{c}_{i_x,-k_y,-k_z,\downarrow} v_{i_x,k_y,k_z,\downarrow} \Big) \\ \hat{\gamma}^\dagger_{-k_y,-k_z,n} = \sum_{i_x} \Big(&\hat{c}^\dagger_{i_x,-k_y,-k_z,\uparrow} v^*_{i_x,k_y,k_z,\uparrow} + \hat{c}^\dagger_{i_x,-k_y,-k_z,\downarrow} v^*_{i_x,k_y,k_z,\downarrow} \\ &+ \hat{c}_{i_x,k_y,k_z,\uparrow} u^*_{i_x,k_y,k_z,\uparrow} + \hat{c}_{i_x,k_y,k_z,\downarrow} u^*_{i_x,k_y,k_z,\downarrow} \Big).\end{aligned} \tag{102}$$

Comparing the two expressions in Eq. (102), it follows that

$$\hat{\gamma}^\dagger_{-k_y,-k_z,n} = \hat{\gamma}_{k_y,k_z,n}. \tag{103}$$

This previous equation shows that the spectra of $\gamma_{k_y,k_z,n}$ operators are indeed dependent on each other for all k-values. Furthermore, we can easily take care of the consequences by exploiting the symmetry of $\gamma_{k_y,k_z,n}$ with respect to k.

For concreteness, start from the Hamiltonian in Eq. (101) and split the sum into positive and negative k-values, exclusive $k = 0$ which we have to take care of separately. The Hamiltonian reads

$$\hat{H} = \hat{H}_0 + \frac{1}{2}\sum_{k>0,n} E_{k,n}\hat{\gamma}^\dagger_{k,n}\hat{\gamma}_{k,n}\frac{1}{2}\sum_{k<0,n} E_{k,n}\hat{\gamma}^\dagger_{k,n}\hat{\gamma}_{k,n}\frac{1}{2}\sum_{k=0,n} E_{k,n}\hat{\gamma}^\dagger_{k,n}\hat{\gamma}_{k,n} \tag{104}$$

where we have used the short-hand notation $\mathbf{k}$ for k_y, k_z. Before we continue with the evaluation, take a closer look at the Hamiltonian expression in the previous equation. We have divided the degenerated energy for positive and negative k-values, but the $k = 0$ mode is still degenerated. As mentioned earlier, we wish to obtain an expression where all operators are independent.

In our numerical calculations, we have discretized the allowed k-values with a periodic boundary condition as

$$k = \frac{2\pi n}{Na} \tag{105}$$

where the modeled material have a length $L = Na$ in a given direction with $n \in \mathbb{Z}$. To guarantee that all k-values has a $-k$ equivalent, we choose the number of lattice points N to be odd. Otherwise, we would have to handle the degeneration at the endpoint with the positive and negative k split. However, the $k = 0$ mode will always occur and need special treatment. Recall the already established relation by combining Eq. (93) and (101),

$$\sum_{\mathbf{k}} W^\dagger_{\mathbf{k}}\hat{H}_{\mathbf{k}}W_{\mathbf{k}} = \sum_{k,n} E_{k,n}\hat{\gamma}^\dagger_{k,n}\hat{\gamma}_{k,n}. \tag{106}$$

Realize that since $H_k = H_{-k}$ for $k = 0$, both $E_{n,k=0}$ and $-E_{n,k=0}$ are eigenvalues of $H_{k=0}$. If we now arrange the eigenvalues for the $k = 0$ mode such that the first $2N_x$ are positive and the last $2N_x$ are negative, it follows that

$$\gamma^\dagger_{k=0,2N_x+n} = \gamma_{k=0,n}. \tag{107}$$

It is now possible to rewrite the $k = 0$ term to only contain a sum over independent operators by dividing the sum into positive and negative n-values. With this in mind, we can manipulate the Hamiltonian into independent operators only,

$$\begin{aligned}
\hat{H} &= \hat{H}_0 + \frac{1}{2}\sum_{k>0,n} E_{k,n}\hat{\gamma}^\dagger_{k,n}\hat{\gamma}_{k,n} + \frac{1}{2}\sum_{k<0,n} E_{k,n}\hat{\gamma}^\dagger_{k,n}\hat{\gamma}_{k,n} \\
&\quad + \frac{1}{2}\sum_{0,n<2N_x} E_{0,n}\hat{\gamma}^\dagger_{0,n}\hat{\gamma}_{0,n} + \frac{1}{2}\sum_{0,n<2N_x} E_{0,2N_x+n}\hat{\gamma}^\dagger_{0,2N_x+n}\hat{\gamma}_{0,2N_x+n} \\
&= \hat{H}_0 + \frac{1}{2}\sum_{k>0,n} E_{k,n}\hat{\gamma}^\dagger_{k,n}\hat{\gamma}_{k,n} + \frac{1}{2}\sum_{k>0,n} E_{-k,n}\hat{\gamma}^\dagger_{-k,n}\hat{\gamma}_{-k,n} \\
&\quad + \frac{1}{2}\sum_{0,n<2N_x} E_{0,n}\hat{\gamma}^\dagger_{0,n}\hat{\gamma}_{0,n} - \frac{1}{2}\sum_{0,n<2N_x} E_{0,n}\hat{\gamma}_{0,n}\hat{\gamma}^\dagger_{0,n} \\
&= \hat{H}_0 + \frac{1}{2}\sum_{k>0,n} E_{k,n}\left(\hat{\gamma}^\dagger_{k,n}\hat{\gamma}_{k,n} - \hat{\gamma}_{k,n}\hat{\gamma}^\dagger_{k,n}\right) \\
&\quad + \frac{1}{2}\sum_{0,n<2N_x} E_{0,n}\left(\hat{\gamma}^\dagger_{0,n}\hat{\gamma}_{0,n} - \hat{\gamma}_{0,n}\hat{\gamma}^\dagger_{0,n}\right)
\end{aligned} \tag{108}$$

where we have used the derived relation $\hat{\gamma}^\dagger_{-k,n} = \hat{\gamma}_{k,n}$ and $E_{-k,n} = -E_{k,n}$. Since the creation- and annihilation operators anti-commute, we can demonstrate through a Bogoliubov transformation that the new quasioperators also anti-commute. The final Hamiltonian-operator is then

$$\begin{aligned}
\hat{H} &= \hat{H}_0 - \frac{1}{2}\sum_{k>0,n} E_{k,n} + \frac{1}{2}\sum_{k>0,n} E_{k,n}\hat{\gamma}^\dagger_{k,n}\hat{\gamma}_{k,n} \\
&\quad - \frac{1}{2}\sum_{0,n<2N_x} E_{0,n} + \frac{1}{2}\sum_{0,n<2N_x} E_{0,n}\hat{\gamma}^\dagger_{0,n}\hat{\gamma}_{0,n}
\end{aligned} \tag{109}$$

where all operators are independent of each other.

5.2 HAMILTONIAN MATRIX

The Hamiltonian that describes an SC/HM/SC Josephson junction of s-wave superconductors and heavy metal with Rashba spin-orbit coupling is, in the first quantization formalism, given by

$$\hat{H} = \sum_i \frac{\hat{p_i}^2}{2m} + \sum_i u(\mathbf{r_i}) + \frac{1}{2}\sum_{i,j\neq i} v(\mathbf{r_i} - \mathbf{r_j}) + \lambda(x)\big(\hat{n} \times \boldsymbol{\sigma}\big) \cdot \hat{p} - \mu N. \tag{110}$$

Here, the two first terms denote, respectively, the kinetic energy and the potential of the electrons relative to the lattice atoms. $\hat{p}_i$ is the canonical momentum and $\mathbf{r}_i$ is the position of electron i. The third term defines the electron-electron interaction through a Coulomb potential, where $\mathbf{r_i}, \mathbf{r_j}$ are the positions of electrons i, j, respectively. This interaction is only present in the superconductors, thus zero in the heavy metal. The fourth term considers the chemical potential μ, where N is the total number of particles. The last term is the Rashba spin-orbit coupling, where λ denotes the magnitude, $\boldsymbol{\sigma}$ is the vector of Pauli matrices, and $\hat{n}$ is a unit vector that aligns the electric field causing Rashba spin-orbit coupling. Keep in mind that this last term is only non-zero in the heavy metal.

Rewrite the previous Hamiltonian into second quantization formalism using the basis in Eq. (91). The result reads,

$$\begin{aligned}\hat{H} = &-t\sum_{\langle i,j\rangle,\sigma} \hat{c}^\dagger_{i,\sigma}\hat{c}_{j,\sigma} + U\sum_i \hat{c}^\dagger_{i,\uparrow}\hat{c}^\dagger_{i,\downarrow}\hat{c}_{i,\downarrow}\hat{c}_{i,\uparrow} - \mu\sum_{i,\sigma}\hat{c}^\dagger_{i,\sigma}\hat{c}_{i,\sigma} \\ &- \frac{i}{2}\sum_{\langle i,j\rangle,\alpha,\beta} \lambda\hat{c}^\dagger_{i,\alpha}\hat{n}\cdot\Big[\boldsymbol{\sigma}\times\frac{1}{2}\big(\mathbf{d}_{i,j}\big)_\perp + \boldsymbol{\sigma}\times\big(\mathbf{d}_{i,j}\big)_\parallel\Big]\hat{c}_{i,\beta}\end{aligned} \tag{111}$$

where t is the hopping integral, U is on-site electron-electron interaction which produce superconductivity, and $\mathbf{d_{i,j}}$ is the vector from lattice site $\mathbf{i}$ to site $\mathbf{j}$.

In section 5.1, we illustrated how to solve the system if we achieve a Hamiltonian given by

$$\hat{H} = H_0 + \frac{1}{2}\sum_{i_x,j_x,k_y,k_z} B^\dagger_{i_x,k_y,k_z}\hat{H}_{i_x,j_x,k_y,k_z}B_{j_x,k_y,k_z}. \tag{112}$$

Thus, Fourier transform Eq. (111) and rewrite the expression into a similar form as Eq. (112). A complete calculation is provided in Appendix A.1. It contains a careful computation of each term starting from the first quantization formalism. The arriving Hamiltonian satisfying to the form in Eq. (112) is found by com-

bining Eq. (A.1.13), Eq. (A.1.26), Eq. (A.1.31) and Eq. (A.1.68). The final result yields

$$\begin{aligned}
H_{i_x,j_x,k_y,k_z} &= \epsilon_{i_x,j_x,k_y,k_z}\hat{\tau}_3\hat{\sigma}_0 \\
&+ \left[\Delta^*_{i_x} i\hat{\tau}^- \hat{\sigma}_y - \Delta_{i_x} i\hat{\tau}^+\hat{\sigma}_y\right]\delta_{i_x,j_x} \\
&- \mu\hat{\tau}_3\hat{\sigma}_0\delta_{i_x,j_x} \\
&- \Big[\sin(k_y)\Lambda^x_{i_x}\hat{\tau}_0\hat{\sigma}_z \\
&- \Big(\sin(k_y)\Lambda^z_{i_x} - \sin(k_z)\Lambda^y_{i_x}\Big)\hat{\tau}_0\hat{\sigma}_x \\
&- \sin(k_z)\Lambda^x_{i_x}\hat{\tau}_3\hat{\sigma}_y\Big]\delta_{i_x,j_x} \\
&+ \frac{i}{4}\left[\Lambda^y_{i_x}\hat{\tau}_0\hat{\sigma}_z - \Lambda^z_{i_x}\hat{\tau}_3\hat{\sigma}_y\right](1+\xi)\delta_{i_x,j_x+1} \\
&- \frac{i}{4}\left[\Lambda^y_{i_x}\hat{\tau}_0\hat{\sigma}_z - \Lambda^z_{i_x}\hat{\tau}_3\hat{\sigma}_y\right](1+\xi)\delta_{i_x,j_x-1}
\end{aligned} \tag{113}$$

where we have defined

$$\begin{aligned}
\epsilon_{i_x,j_x,k_y,k_z} &= -t\Big(\delta_{i_x,j_x+1} + \delta_{i_x,j_x-1} + \delta_{i_x,j_x}2\Big[\cos k_y + \cos k_z\Big]\Big) \\
\Delta_{i_x} &= U\langle\hat{c}_{i_x,\uparrow}\hat{c}_{i_x,\downarrow}\rangle \\
\Lambda^x_{i_x} &= \lambda_{i_x} n_x = \lambda_{i_x}\cos(\phi_n)\sin(\theta_n) \\
\Lambda^y_{i_x} &= \lambda_{i_x} n_y = \lambda_{i_x}\sin(\phi_n)\sin(\theta_n) \\
\Lambda^z_{i_x} &= \lambda_{i_x} n_z = \lambda_{i_x}\cos(\theta_n) \\
\xi &= \begin{cases} 0 & \text{if } i,j \text{ are on opposite side of the interface} \\ 1 & \text{if } i,j \text{ are both in heavy metal} \end{cases}
\end{aligned} \tag{114}$$

and the constant term reads

$$\hat{H}_0 = N_y N_z \sum_{i_x} \frac{|\Delta_{i_x}|^2}{U_{i_x}}. \tag{115}$$

The Hamiltonian is an 4x4 block matrix given as

$$\begin{aligned}
H_{i_x,j_x,k_y,k_z} = &\begin{bmatrix} \epsilon_{i_x,j_x,k_y,k_z} - \mu & 0 & 0 & \Delta_{i_x} \\ 0 & \epsilon_{i_x,j_x,k_y,k_z} - \mu & -\Delta_{i_x} & 0 \\ 0 & -\Delta^*_{i_x} & -\epsilon_{i_x,j_x,k_y,k_z} + \mu & 0 \\ \Delta^*_{i_x} & 0 & 0 & -\epsilon_{i_x,j_x,k_y,k_z} + \mu \end{bmatrix} \\
&+ \delta_{i_x,j_x}\begin{bmatrix} \mathbf{A}_{2x2} & 0_{2x2} \\ 0_{2x2} & \mathbf{A}^*_{2x2} \end{bmatrix} + \delta_{i_x,j_x\pm1}(1+\xi)\begin{bmatrix} \mathbf{B}_{2x2} & 0_{2x2} \\ 0_{2x2} & -\mathbf{B}^*_{2x2} \end{bmatrix}
\end{aligned} \tag{116}$$

where we have defined

$$\begin{aligned}\mathbf{A}_{2x2} &= \begin{bmatrix} -\Lambda^x \sin(k_y) & \Lambda^z \sin(k_y) - \left(\Lambda^y + i\Lambda^x\right)\sin(k_z) \\ \Lambda^z \sin(k_y) - \left(\Lambda^y - i\Lambda^x\right)\sin(k_z) & \Lambda^x \sin(k_y) \end{bmatrix} \\ \mathbf{B}_{2x2} &= \frac{1}{4}\begin{bmatrix} \pm i\Lambda^y & \mp\Lambda^z \\ \pm\Lambda^z & \mp i\Lambda^y \end{bmatrix}\end{aligned} \tag{117}$$

to simplify the expression. The second term of Eq. (111) gives rise to the superconducting gap at site i given by

$$\Delta_i = U\langle \hat{c}_{i,\uparrow}\hat{c}_{i,\downarrow}\rangle. \tag{118}$$

Since this quantity depends on fermionic operators, we demand a self-consistent solution.

5.2.1 *Self-consistent solution of the superconducting gap Δ*

The superconducting gap Δ is proportional to the correlation function, also called the pairing field, as

$$\begin{aligned}\Delta_{i_x} &= U\langle \hat{c}_{i_x,\uparrow}\hat{c}_{i_x,\downarrow}\rangle \\ &= UF^{\uparrow\downarrow}_{i_x,i_x}.\end{aligned} \tag{119}$$

The pairing field, in addition to its complex conjugate, is defined as

$$F^{\uparrow\downarrow}_{i_x,i_x} = \langle \hat{c}_{i,\uparrow}\hat{c}_{i,\downarrow}\rangle, \qquad F^{\downarrow\uparrow *}_{i_x,i_x} = \langle \hat{c}^\dagger_{i,\uparrow}\hat{c}^\dagger_{i,\downarrow}\rangle. \tag{120}$$

Note that the pairing field satisfy $F^{\downarrow\uparrow}_{i_x,i_x} = -F^{\uparrow\downarrow}_{i_x,i_x}$. We can interpret the fields defined in Eq. (120) as the expectation value of a Cooper pairs to be created or destroyed, respectively. For the pairing field to get a larger magnitude, there opens up a gap in the continuous energy spectrum of electrons in the superconductor. It is convenient to calculate the paring field in reciprocal space due to the invariance in y- and z-direction. Using the transform in Eq. (92) we get

$$\begin{aligned}F^{\uparrow\downarrow}_{i_x,i_x} &= \langle \hat{c}_{i_x,\uparrow}\hat{c}_{i_x,\downarrow}\rangle \\ &= \frac{1}{N_y N_z}\sum_{k_y,k_z}\sum_{k'_y,k'_z}\langle \hat{c}_{ix,k_y,k_z,\uparrow}\hat{c}_{ix,k'_y,k'_z,\downarrow}\rangle e^{i(k_y i_y + k_z i_z)} e^{i(k'_y i_y + k'_z i_z)}.\end{aligned} \tag{121}$$

Since our system is invariant in y- and z-direction, we can take the average in the respective directions without changing the physics of the pairing field,

$$\begin{aligned} F^{\uparrow\downarrow}_{i_x,i_x} &= \frac{1}{N_y N_z} \sum_{k_y,k_z} \sum_{k'_y,k'_z} \langle \hat{c}_{ix,k_y,k_z,\uparrow} \hat{c}_{ix,k'_y,k'_z,\downarrow} \rangle e^{i(k_y i_y + k_z i_z)} e^{i(k'_y i_y + k'_z i_z)} \\ &= \frac{1}{N_y N_z} \sum_{i_y,i_z} \frac{1}{N_y N_z} \sum_{k_y,k_z} \sum_{k'_y,k'_z} \langle \hat{c}_{ix,k_y,k_z,\uparrow} \hat{c}_{ix,k'_y,k'_z,\downarrow} \rangle e^{i(k_y+k'_y)i_z} e^{i(k_z+k'_z)i_z} \\ &= \frac{1}{N_y N_z} \sum_{k_y,k_z} \langle \hat{c}_{ix,k_y,k_z,\uparrow} \hat{c}_{ix,-k_y,-k_z,\downarrow} \rangle. \end{aligned} \tag{122}$$

From the second to the last line, we have simplified the expression by using the identities

$$\begin{aligned} \frac{1}{N_y} \sum_{i_y} e^{i\left(k_y + k'_y\right) i_y} &= \delta_{k_y,-k'_y} \\ \frac{1}{N_z} \sum_{i_z} e^{i\left(k_z + k'_z\right) i_z} &= \delta_{k_z,-k'_z}. \end{aligned} \tag{123}$$

To calculate the expectation value of the pairing field, write out the creation and annihilation operators according to Eq. (99)

$$F^{\uparrow\downarrow}_{i_x,i_x} = \frac{1}{N_y N_z} \sum_{k_y,k_z} \sum_{n,n'} u_{ix,k_y,k_z,n,\uparrow} v^*_{ix,k_y,k_z,n',\downarrow} \langle \gamma_{k_y,k_z,n} \gamma^\dagger_{k_y,k_z,n'} \rangle. \tag{124}$$

At this point, we are still dealing with dependent quasioperators. Therefore, let us manipulate the sum in a similar manner as done when we diagonalized the BdG equations. As a result, we would achieve an expression consisting of independent operators exclusively. Recall that the procedure demands to split the sum into positive and negative k-values. However, special treatment of the $k = 0$ mode obligates an additional separation of positive and negative eigenvalues. Pay attention to how the expectation value of the quasioperators is only non-zero while treating equally n-modes. Thus, simplifying the sum over n, n' and the result yields

$$\begin{aligned} F^{\uparrow\downarrow}_{i_x,i_x} = &\frac{1}{N_y N_z} \sum_{\mathbf{k}>0,n} u_{ix,\mathbf{k},n,\uparrow} v^*_{ix,\mathbf{k},n,\downarrow} \langle \gamma_{\mathbf{k},n} \gamma^\dagger_{\mathbf{k},n} \rangle \\ &+ \frac{1}{N_y N_z} \sum_{\mathbf{k}<0,n} u_{ix,\mathbf{k},n,\uparrow} v^*_{ix,\mathbf{k},n,\downarrow} \langle \gamma_{\mathbf{k},n} \gamma^\dagger_{\mathbf{k},n} \rangle \\ &+ \frac{1}{N_y N_z} \sum_{\mathbf{k}=0,n} u_{ix,\mathbf{k}=0,n,\uparrow} v^*_{ix,\mathbf{k}=0,n,\downarrow} \langle \gamma_{\mathbf{k}=0,n} \gamma^\dagger_{\mathbf{k}=0,n} \rangle \end{aligned} \tag{125}$$

where we have used the short hand notation $\mathbf{k} \to k_y, k_z$.

Split the $k = 0$ term into positive and negative eigenvalues. Arrange the first $2N_x$ values to be positive, and the last $2N_x$ to be negative. This arrangement implies that

$$\begin{aligned} u_{i_x,k=0,2N_x+n,\uparrow} &= v^*_{i_x,k=0,n,\uparrow} \\ v_{i_x,k=0,2N_x+n,\downarrow} &= u^*_{i_x,k=0,n,\downarrow}. \end{aligned} \tag{126}$$

Inserting the previous relations into the correlation function in Eq. (125), together with the previous derived relations, $\hat{\gamma}^\dagger_{-k,n} = \hat{\gamma}_{k,n}$ and $E_{-k,n} = -E_{k,n}$, the result reads

$$\begin{aligned} F^{\uparrow\downarrow}_{i_x,i_x} &= \frac{1}{N_y N_z} \sum_{k>0,n} u_{ix,k,n,\uparrow} v^*_{ix,k,n,\downarrow} \langle \gamma_{k,n} \gamma^\dagger_{k,n} \rangle \\ &\quad + \frac{1}{N_y N_z} \sum_{k>0,n} u_{ix,-k,n,\uparrow} v^*_{ix,-k,n,\downarrow} \langle \gamma_{-k,n} \gamma^\dagger_{-k,n} \rangle \\ &\quad + \frac{1}{N_y N_z} \sum_{k=0,n<2N_x} u_{ix,0,n,\uparrow} v^*_{ix,0,n,\downarrow} \langle \gamma_{0,n} \gamma^\dagger_{0,n} \rangle \\ &\quad + \frac{1}{N_y N_z} \sum_{k=0,n<2N_x} u_{ix,0,2N_x+n,\uparrow} v^*_{ix,0,2N_x+n,\downarrow} \langle \gamma_{0,2N_x+n} \gamma^\dagger_{0,2N_x+n} \rangle \\ &= \frac{1}{N_y N_z} \sum_{k>0,n} u_{ix,k,n,\uparrow} v^*_{ix,k,n,\downarrow} \langle \gamma_{k,n} \gamma^\dagger_{k,n} \rangle \\ &\quad + \frac{1}{N_y N_z} \sum_{k>0,n} v^*_{ix,k,n,\uparrow} u_{ix,k,n,\downarrow} \langle \gamma^\dagger_{k,n} \gamma_{k,n} \rangle \\ &\quad + \frac{1}{N_y N_z} \sum_{k=0,n<2N_x} u_{ix,0,n,\uparrow} v^*_{ix,0,n,\downarrow} \langle \gamma_{0,n} \gamma^\dagger_{0,n} \rangle \\ &\quad + \frac{1}{N_y N_z} \sum_{0,n<2N_x} v^*_{ix,0,n,\uparrow} u_{ix,0,n,\downarrow} \langle \gamma^\dagger_{0,n} \gamma_{0,n} \rangle \\ &= \frac{1}{N_y N_z} \sum_{k>0,n} \left(u_{ix,k,n,\uparrow} v^*_{ix,k,n,\downarrow} \langle \gamma_{k,n} \gamma^\dagger_{k,n} \rangle + v^*_{ix,k,n,\uparrow} u_{ix,k,n,\downarrow} \langle \gamma^\dagger_{k,n} \gamma_{k,n} \rangle \right) \\ &\quad + \frac{1}{N_y N_z} \sum_{k=0,n<2N_x} \left(u_{ix,0,n,\uparrow} v^*_{ix,0,n,\downarrow} \langle \gamma_{0,n} \gamma^\dagger_{0,n} \rangle + v^*_{ix,0,n,\uparrow} u_{ix,0,n,\downarrow} \langle \gamma^\dagger_{0,n} \gamma_{0,n} \rangle \right) \end{aligned} \tag{127}$$

We have now derived an expression for the correlation function which only considers independent operators. Consequently, we can calculate the thermal average by the Fermi-Dirac distribution [87], *i.e.*

$$\begin{aligned} \langle \gamma^\dagger_{k,n} \gamma_{k,n} \rangle &= f(E_{k,n}) \\ \langle \gamma_{k,n} \gamma^\dagger_{k,n} \rangle &= 1 - f(E_{k,n}) \end{aligned} \tag{128}$$

where $f(E_{k,n})$ is the Fermi function. The arriving result for the superconducting gap with singlet symmetry is

$$\begin{aligned}\Delta_{i_x} &= U F^{\uparrow\downarrow}_{i_x,i_x} \\ &= \frac{U}{N_y N_z} \sum_{k>0,n} \left(u_{ix,k,n,\uparrow} v^*_{ix,k,n,\downarrow} + \left[v^*_{ix,k,n,\uparrow} u_{ix,k,n,\downarrow} - u_{ix,k,n,\uparrow} v^*_{ix,k,n,\downarrow} \right] f(E_{k,n}) \right) \\ &\quad + \frac{U}{N_y N_z} \sum_{k=0,n<2N_x} \left(u_{ix,0,n,\uparrow} v^*_{ix,0,n,\downarrow} + \left[v^*_{ix,0,n,\uparrow} u_{ix,0,n,\downarrow} - u_{ix,0,n,\uparrow} v^*_{ix,0,n,\downarrow} \right] f(E_{0,n}) \right)\end{aligned} \tag{129}$$

where we recognize the Fermi function as

$$f(E_{k,n}) = \frac{1}{1+e^{\beta E}} = \frac{1}{1+\frac{1+\tanh(\beta E/2)}{1-\tanh(\beta E/2)}} = \frac{1}{2}\left[1-\tanh\left(\frac{\beta E}{2}\right)\right]. \tag{130}$$

5.3 DERIVATION OF THE SUPPORTED SUPERCURRENT

To find an expression for the net current across a Josephson junction, we will use a procedure similar to the one in Ref. [83]. Begin the computation from the continuity equation

$$\partial_t \rho_i = -\nabla \cdot \mathbf{j}_i \tag{131}$$

where ρ_i and $\mathbf{j}_i$ are the charge density and current density at lattice site i, respectively. To calculate the supercurrent, integrate over the three-dimensional space. Starting with the left hand side of Eq. (131),

$$\int_\Omega d\mathbf{r} \partial_t \rho_i = \partial_t Q_i, \tag{132}$$

where Ω is the integration volume and Q_i is the total charge at lattice site i. For the right-hand side, we can use Green's theorem and get

$$-\int_\Omega d\mathbf{r}(\nabla \cdot \mathbf{j}_i) = -\int_{\partial\Omega} dS(\mathbf{j}_i \cdot \mathbf{n}) = -\sum_n \mathbf{j}_{i,n} a = \sum_n I_{i,n} \tag{133}$$

where a is the side length of the unit cube and $\mathbf{n}$ is the normal boundary vector pointing outwards. Index n runs over all the faces of the unit cube, providing $I_{i,n}$ to be the current out of each respective face. The result reads

$$\sum_n I_{i,n} = -\partial_t Q_i. \tag{134}$$

We can evaluate the right-hand side Eq. (134) using the Heisenberg equation of motion,

$$\partial_t Q_i = i[H, Q_i]. \tag{135}$$

Identify the charge at lattice site i as $Q_i = \sum_\sigma \hat{n}_{i,\sigma} = \sum_\sigma \hat{c}^\dagger_{i,\sigma}\hat{c}_{i,\sigma}$.

To continue, we have to evaluate the commutation relation of H and Q_i. The Hamiltonian H is a sum over several parts of the system, *e.g.* $H = H_t + H_U + H_\mu + H_\lambda + H_h$. The different parts of the Hamiltonian are derived in Appendix A.1. We will now evaluate the commutation of each part to Q separately.

5.3.1 *The hopping t term*

The hopping Hamiltonian in real-space is given in Eq. (A.1.5) as

$$\hat{H}_t = -t \sum_{\langle i,j\rangle,\sigma} \hat{c}^\dagger_{i,\sigma}\hat{c}_{j,\sigma}. \tag{136}$$

The commutation relation of $\hat{H}_t$ and Q_i is

$$\begin{aligned}\left[\hat{H}_t, Q_{i'}\right] &= -t\Big[\sum_{\langle i,j\rangle,\sigma} \hat{c}^\dagger_{i,\sigma}\hat{c}_{j,\sigma}, \sum_\sigma \hat{n}_{i',\sigma'}\Big] \\ &= -t \sum_{\langle i,j\rangle,\sigma,\sigma'} \Big(\hat{c}^\dagger_{i,\sigma}\hat{c}_{j,\sigma}\hat{n}_{i',\sigma'} - \hat{n}_{i',\sigma'}\hat{c}^\dagger_{i,\sigma}\hat{c}_{j,\sigma}\Big).\end{aligned} \tag{137}$$

Utilize the two commutation relations

$$\begin{aligned}\left[\hat{n}_\mu, \hat{c}^\dagger_\nu\right] &= \delta_{\mu,\nu}\hat{c}^\dagger_\mu \\ \left[\hat{n}_\mu, \hat{c}_\nu\right] &= -\delta_{\mu,\nu}\hat{c}_\mu\end{aligned} \tag{138}$$

and Eq. (137) reads

$$\begin{aligned}\left[\hat{H}_t, Q_{i'}\right] &= -t \sum_{\langle i,j\rangle,\sigma,\sigma'} \Big(\hat{c}^\dagger_{i,\sigma}\hat{c}_{j,\sigma}\hat{n}_{i',\sigma'} - \hat{n}_{i',\sigma'}\hat{c}^\dagger_{i,\sigma}\hat{c}_{j,\sigma}\Big) \\ &= -t \sum_{\langle i,j\rangle,\sigma,\sigma'} \Big(\delta_{j,i'}\delta_{\sigma,\sigma'}\hat{c}^\dagger_{i,\sigma}\hat{c}_{i',\sigma'} - \delta_{i,i'}\delta_{\sigma,\sigma'}\hat{c}^\dagger_{i',\sigma'}\hat{c}_{j,\sigma}\Big) \\ &= t \sum_{\langle i,j\rangle,\sigma} \Big(\delta_{i,i'}\hat{c}^\dagger_{i',\sigma}\hat{c}_{j,\sigma} - \delta_{j,i'}\hat{c}^\dagger_{i,\sigma}\hat{c}_{i',\sigma}\Big) \\ &= t \sum_{i,\delta,\sigma} \Big(\delta_{i,i'}\hat{c}^\dagger_{i',\sigma}\hat{c}_{i+\delta,\sigma} - \delta_{i+\delta,i'}\hat{c}^\dagger_{i,\sigma}\hat{c}_{i',\sigma}\Big) \\ &= t \sum_{\delta,\sigma} \Big(\hat{c}^\dagger_{i',\sigma}\hat{c}_{i'+\delta,\sigma} - \hat{c}^\dagger_{i'-\delta,\sigma}\hat{c}_{i',\sigma}\Big)\end{aligned} \tag{139}$$

where we have only considered nearest neighbors providing the substitution $j = i + \delta$. Thus, the quantity δ is a vector from lattice site i to its nearest neighbor lattice site.

5.3.2 *The Hubbard U term*

The real-space Hamiltonian that represents the electron-electron interaction inside the superconductors is given in Eq. (A.1.21) as

$$\hat{H}_U = \sum_i \left(\Delta_i \hat{c}^\dagger_{i,\uparrow} \hat{c}^\dagger_{i,\downarrow} + \Delta_i^* \hat{c}_{i,\downarrow} \hat{c}_{i,\uparrow} \right) + \sum_i \frac{|\Delta_i|^2}{U_i}. \tag{140}$$

To calculate the commutator of $\hat{H}_U$ and Q_i, we identify the commutator to be proportional to

$$\begin{aligned}
[\hat{H}_U, Q_{i'}] &\propto \left[\sum_i \left(\Delta_i \hat{c}^\dagger_{i,\uparrow} \hat{c}^\dagger_{i,\downarrow} + \Delta_i^* \hat{c}_{i,\downarrow} \hat{c}_{i,\uparrow} \right), \sum_\sigma \hat{n}_{i',\sigma'} \right] \\
&= \sum_{i,\sigma} \left(\Delta_i \hat{c}^\dagger_{i,\uparrow} \hat{c}^\dagger_{i,\downarrow} + \Delta_i^* \hat{c}_{i,\downarrow} \hat{c}_{i,\uparrow} \right) \hat{n}_{i',\sigma'} - \hat{n}_{i',\sigma'} \left(\Delta_i \hat{c}^\dagger_{i,\uparrow} \hat{c}^\dagger_{i,\downarrow} + \Delta_i^* \hat{c}_{i,\downarrow} \hat{c}_{i,\uparrow} \right) \\
&= \sum_{i,\sigma} \delta_{i,i'} \left(\Delta_i \delta_{i,i'} \delta_{\downarrow,\sigma'} \hat{c}^\dagger_{i',\uparrow} \hat{c}^\dagger_{i,\downarrow} + \Delta_i^* \delta_{i,i'} \delta_{\uparrow,\sigma'} \hat{c}_{i,\downarrow} \hat{c}_{i,\uparrow} \right) \\
&\quad - \left(\Delta_i \delta_{i,i'} \delta_{\uparrow,\sigma'} \hat{c}^\dagger_{i,\uparrow} \hat{c}^\dagger_{i,\downarrow} + \Delta_i^* \delta_{i,i'} \delta_{\downarrow,\sigma'} \hat{c}_{i,\downarrow} \hat{c}_{i,\uparrow} \right) \\
&= \sum_{i,\sigma} \delta_{i,i'} \left(\Delta_i^* \left[\delta_{\downarrow,\sigma'} + \delta_{\uparrow,\sigma'} \right] \hat{c}_{i,\downarrow} \hat{c}_{i,\uparrow} - \Delta_i \left[\delta_{\downarrow,\sigma'} + \delta_{\uparrow,\sigma'} \right] \hat{c}^\dagger_{i',\uparrow} \hat{c}^\dagger_{i,\downarrow} \right) \\
&= 2 \left(\Delta_{i'}^* \hat{c}_{i',\downarrow} \hat{c}_{i',\uparrow} - \Delta_{i'} \hat{c}^\dagger_{i',\uparrow} \hat{c}^\dagger_{i',\downarrow} \right)
\end{aligned} \tag{141}$$

where we have used the commutator relations in Eq. (138). To find the contribution of this term to the total current, we attempt to calculate the rate of charge generation from this commutator. That is the current from a flow of charges. Therefore, calculate the combined quantum-mechanical expectation value additional to the thermal average. The result reads

$$2 \left(\Delta_{i'}^* \langle \hat{c}_{i',\downarrow} \hat{c}_{i',\uparrow} \rangle - \Delta_{i'} \langle \hat{c}^\dagger_{i',\uparrow} \hat{c}^\dagger_{i',\downarrow} \rangle \right) = \frac{2}{U_{i'_x}} \left(\Delta^*_{i'_x} \Delta_{i'_x} - \Delta_{i'_x} \Delta^*_{i'_x} \right) = 0 \tag{142}$$

where we have used the definition of Δ from Eq. (118). This result confirms that the charged particle number has to be conserved, although the mean-field Hubbard term does not conserve the quasiparticle number. In other words, the Hubbard U Hamiltonian term will not contribute to the supercurrent.

5.3.3 *The chemical potential μ term*

The Hamiltonian corresponding to the chemical potential is given in Eq. (A.1.28) as

$$\hat{H}_\mu = -\mu \sum_{i,\sigma} \hat{c}^\dagger_{i,\sigma} \hat{c}_{i,\sigma}. \tag{143}$$

Since the commutator of two number operators commutes, $\left[n_\mu, n_\nu\right] = 0$, the chemical potential will not contribute to the flow of charges due to Eq. (135).

5.3.4 *The ferromagnetic h term*

The expression for $\hat{H}_h$ is found in Eq. (A.1.33) as

$$\hat{H}_h = \sum_{i,\alpha,\beta} \left(\mathbf{h}_i \cdot \boldsymbol{\sigma}\right)_{\alpha,\beta} \hat{c}^\dagger_{i,\alpha} \hat{c}_{i,\beta} \tag{144}$$

such that the commutator with Q_i is

$$\begin{aligned}
\left[\hat{H}_h, Q_{i'}\right] &= \left[\sum_{i,\alpha,\beta} \left(\mathbf{h}_i \cdot \boldsymbol{\sigma}\right)_{\alpha,\beta} \hat{c}^\dagger_{i,\alpha} \hat{c}_{i,\beta}, \sum_\sigma \hat{n}_{i,\sigma}\right] \\
&= \sum_{i,\alpha,\beta} \sum_\sigma \left(\mathbf{h}_i \cdot \boldsymbol{\sigma}\right)_{\alpha,\beta} \delta_{i',i} \Big(\delta_{\beta,\sigma} - \delta_{\alpha,\sigma}\Big) \hat{c}^\dagger_{i,\alpha} \hat{c}_{i,\beta} \\
&= \sum_{\gamma,\eta} \left(\mathbf{h}_i \cdot \boldsymbol{\sigma}\right)_{\gamma,\eta} \Big(\hat{c}^\dagger_{i',\gamma} \hat{c}_{i',\eta} - \hat{c}^\dagger_{i',\gamma} \hat{c}_{i',\eta}\Big) \\
&= 0.
\end{aligned} \tag{145}$$

after using the commutator relations in Eq. (138). This result shows that the commutator of Q and the ferromagnetic term will vanish. Consequently, the magnetic field inside a ferromagnet will not commit to any supercurrent.

5.3.5 *The Rashba λ term*

The second quantization expression for the Rashba spin-orbit Hamiltonian in real-space is found by combining Eq. (A.1.64) and Eq. (A.1.58). The resulting Hamiltonian reads

$$\hat{H}_\lambda = -\frac{i}{4} \sum_{\langle i,j\rangle,\alpha,\beta} \lambda \hat{c}^\dagger_{i,\alpha} \hat{n} \cdot \Big[(1+\xi)\boldsymbol{\sigma} \times \left(\mathbf{d}_{i,j}\right)_\perp + 2\boldsymbol{\sigma} \times \left(\mathbf{d}_{i,j}\right)_\parallel\Big] \hat{c}_{i,\beta} \tag{146}$$

where ξ is defined in Eq. (114). Recall the definition of $\mathbf{d}_{i,j}$ as a vector from lattice site i to j. We can thus introduce a new quantity $\boldsymbol{\delta} = \mathbf{d}_{i,j}$, since we only consider nearest neighbour interaction. The parameters $\hat{\mathbf{n}}$, $\boldsymbol{\sigma}$ and $\boldsymbol{\delta}$ have components in all directions in space, $\{\hat{x}, \hat{y}, \hat{z}\}$. Let us define

$$\begin{aligned}(\boldsymbol{\delta})_\perp &= \hat{x}\Big(\delta_{i,j+\hat{x}} - \delta_{i,j-\hat{x}}\Big) = \delta^x_\perp \hat{x} \equiv \delta^x \hat{x} \\ (\boldsymbol{\delta})_\parallel &= \hat{y}\Big(\delta_{i,j+\hat{y}} - \delta_{i,j-\hat{y}}\Big) + \hat{z}\Big(\delta_{i,j+\hat{z}} - \delta_{i,j-\hat{z}}\Big) = \delta^y_\parallel \hat{y} + \delta^z_\parallel \hat{z} \equiv \delta^y \hat{y} + \delta^z \hat{z}\end{aligned} \tag{147}$$

and substitute the new quantities into the Hamiltonian in Eq. (146). The result yields

$$\begin{aligned}\hat{H}_\lambda &= -\frac{i}{4} \sum_{i,\delta,\alpha,\beta} \lambda \hat{\mathbf{n}} \cdot \Big[(1+\xi)\boldsymbol{\sigma} \times (\boldsymbol{\delta})_\perp + 2\boldsymbol{\sigma} \times (\boldsymbol{\delta})_\parallel\Big] \hat{c}^\dagger_{i,\alpha} \hat{c}_{i+\delta,\beta} \\ &= -\frac{i}{4}\lambda \sum_{i,\delta,\alpha,\beta} \Big\{ (1+\xi)\Big[\sigma^z_{\alpha,\beta}\delta^x - \sigma^y_{\alpha,\beta}\delta^x\Big] \\ &\quad + 2\Big[\sigma^y_{\alpha,\beta}\delta^z - \sigma^z_{\alpha,\beta}\delta^y - \sigma^x_{\alpha,\beta}\delta^z + \sigma^x_{\alpha,\beta}\delta^y\Big]\Big\} \hat{c}^\dagger_{i,\alpha}\hat{c}_{i+\delta,\beta}\end{aligned} \tag{148}$$

Before we insert the previous equation into the commutator in Eq. (135), recognize that

$$\begin{aligned}\big[\hat{H}_\lambda, Q_{i'}\big] &\propto \Big[\sum_{i,\delta,\alpha,\beta} \hat{c}^\dagger_{i,\alpha}\hat{c}_{i+\delta,\beta}, \sum_\sigma \hat{n}_{i',\sigma}\Big] \\ &= \sum_{i,\delta,\alpha,\beta,\sigma} \Big(\delta_{i+\delta,i'}\delta_{\beta,\sigma}\hat{c}^\dagger_{i,\alpha}\hat{c}_{i+\delta,\beta} - \delta_{i,i'}\delta_{\alpha,\sigma}\hat{c}^\dagger_{i,\alpha}\hat{c}_{i+\delta,\beta}\Big) \\ &= \sum_{\delta,\alpha,\beta} \Big(\hat{c}^\dagger_{i'-\delta,\alpha}\hat{c}_{i',\beta} - \hat{c}^\dagger_{i',\alpha}\hat{c}_{i'+\delta,\beta}\Big),\end{aligned} \tag{149}$$

such that the complete commutator is

$$\begin{aligned}\big[\hat{H}_\lambda, Q_{i'}\big] &= -\frac{i}{4} \sum_{\delta,\alpha,\beta} \lambda \hat{\mathbf{n}} \cdot \Big[(1+\xi)\boldsymbol{\sigma} \times (\boldsymbol{\delta})_\perp + 2\boldsymbol{\sigma} \times (\boldsymbol{\delta})_\parallel\Big] \cdot \Big(\hat{c}^\dagger_{i'-\delta,\alpha}\hat{c}_{i',\beta} - \hat{c}^\dagger_{i',\alpha}\hat{c}_{i'+\delta,\beta}\Big) \\ &= -\frac{i}{4}\lambda \sum_{\delta,\alpha,\beta} \Big\{ (1+\xi)\Big[\sigma^z_{\alpha,\beta}\delta^x - \sigma^y_{\alpha,\beta}\delta^x\Big] + 2\Big[\sigma^y_{\alpha,\beta}\delta^z - \sigma^z_{\alpha,\beta}\delta^y - \sigma^x_{\alpha,\beta}\delta^z + \sigma^x_{\alpha,\beta}\delta^y\Big]\Big\} \\ &\quad \cdot \Big(\hat{c}^\dagger_{i'-\delta,\alpha}\hat{c}_{i',\beta} - \hat{c}^\dagger_{i',\alpha}\hat{c}_{i'+\delta,\beta}\Big).\end{aligned} \tag{150}$$

5.3.6 *Assemble the final current*

Combining the results from Eq. (150) and Eq. (139) into Eq. (135), we get an expression of the current through each of the faces of the unit cube. The result reads

$$\begin{aligned}\sum_n I_{i,n} &= -i\left[\hat{H}_t, Q_i\right] - i\left[\hat{H}_\lambda, Q_i\right] \\ &= -it\sum_{\delta,\sigma}\left[\hat{c}^\dagger_{i,\sigma}\hat{c}_{i+\delta,\sigma} - \hat{c}^\dagger_{i-\delta,\sigma}\hat{c}_{i,\sigma}\right] - \frac{1}{4}\lambda\sum_{\delta,\alpha,\beta}\Big\{(1+\xi)\left[\sigma^z_{\alpha,\beta}\delta^x - \sigma^y_{\alpha,\beta}\delta^x\right] \\ &\quad + 2\left[\sigma^y_{\alpha,\beta}\delta^z - \sigma^z_{\alpha,\beta}\delta^y - \sigma^x_{\alpha,\beta}\delta^z + \sigma^x_{\alpha,\beta}\delta^y\right]\Big\}\cdot\left(\hat{c}^\dagger_{i-\delta,\alpha}\hat{c}_{i,\beta} - \hat{c}^\dagger_{i,\alpha}\hat{c}_{i+\delta,\beta}\right).\end{aligned} \tag{151}$$

For further calculations, we are only investigating the current that flows along the x-direction. Thus, we will only consider terms that contains $\hat{c}^\dagger_{i\pm\delta_x,\alpha}\hat{c}_{i,\beta}$ or $\hat{c}^\dagger_{i,\alpha}\hat{c}_{i\pm\delta_x,\beta}$. Only including the previous terms, Eq. (151) reduces to

$$\begin{aligned}\sum_x I_{i,x} &= -it\sum_{\delta_x,\sigma}\left[\hat{c}^\dagger_{i,\sigma}\hat{c}_{i+\delta_x,\sigma} - \hat{c}^\dagger_{i-\delta_x,\sigma}\hat{c}_{i,\sigma}\right] \\ &\quad - \frac{1}{4}\lambda\sum_{\delta_x,\alpha,\beta}(1+\xi)\left[\sigma^z_{\alpha,\beta}\delta^x - \sigma^y_{\alpha,\beta}\delta^x\right]\cdot\left(\hat{c}^\dagger_{i-\delta_x,\alpha}\hat{c}_{i,\beta} - \hat{c}^\dagger_{i,\alpha}\hat{c}_{i+\delta_x,\beta}\right).\end{aligned} \tag{152}$$

Identify the current in positive and negative x-direction as

$$\begin{aligned}I^{x+}_i &= -it\sum_\sigma\left[\hat{c}^\dagger_{i,\sigma}\hat{c}_{i+1,\sigma} - \hat{c}^\dagger_{i+1,\sigma}\hat{c}_{i,\sigma}\right] \\ &\quad + \frac{1}{4}\lambda\sum_{\alpha,\beta}(1+\xi)\left[\sigma^z_{\alpha,\beta} - \sigma^y_{\alpha,\beta}\right]\cdot\left(\hat{c}^\dagger_{i+1,\alpha}\hat{c}_{i,\beta} + \hat{c}^\dagger_{i,\alpha}\hat{c}_{i+1,\beta}\right),\end{aligned} \tag{153}$$

$$\begin{aligned}I^{x-}_i &= -it\sum_\sigma\left[\hat{c}^\dagger_{i,\sigma}\hat{c}_{i-1,\sigma} - \hat{c}^\dagger_{i-1,\sigma}\hat{c}_{i,\sigma}\right] \\ &\quad - \frac{1}{4}\lambda\sum_{i,\alpha,\beta}(1+\xi)\left[\sigma^z_{\alpha,\beta} - \sigma^y_{\alpha,\beta}\right]\cdot\left(\hat{c}^\dagger_{i-1,\alpha}\hat{c}_{i,\beta} + \hat{c}^\dagger_{i,\alpha}\hat{c}_{i-1,\beta}\right).\end{aligned}$$

These two expressions determine the real space current. Perform a Fourier transform of the two expressions using the transformation defined in Eq. (92). The resulting current in reciprocal space is then

$$\begin{aligned}
I_i^{x+} &= -\frac{it}{N_y N_z}\sum_{k_y,k_z,\sigma}\left\{\hat{c}^\dagger_{i_x,k_y,k_z,\sigma}\hat{c}_{i_x+1,k_y,k_z,\sigma} - \hat{c}^\dagger_{i_x+1,k_y,k_z,\sigma}\hat{c}_{i_x,k_y,k_z,\sigma'}\right\} \\
&\quad + \frac{1}{N_y N_z}\sum_{k_y,k_z,\alpha,\beta}\left\{B_{\alpha,\beta,i_x,i_x+1}\hat{c}^\dagger_{i_x,k_y,k_z,\alpha}\hat{c}_{i_x+1,k_y,k_z,\beta} + B_{\alpha,\beta,i_x+1,i_x}\hat{c}^\dagger_{i_x+1,k_y,k_z,\alpha}\hat{c}_{i_x,k_y,k_z,\beta}\right\}, \\
I_i^{x-} &= -\frac{it}{N_y N_z}\sum_{k_y,k_z,\sigma}\left\{\hat{c}^\dagger_{i_x,k_y,k_z,\sigma}\hat{c}_{i_x-1,k_y,k_z,\sigma} - \hat{c}^\dagger_{i_x-1,k_y,k_z,\sigma}\hat{c}_{i_x,k_y,k_z,\sigma'}\right\} \\
&\quad - \frac{1}{N_y N_z}\sum_{k_y,k_z,\alpha,\beta}\left\{B_{\alpha,\beta,i_x,i_x-1}\hat{c}^\dagger_{i_x,k_y,k_z,\alpha}\hat{c}_{i_x-1,k_y,k_z,\beta} + B_{\alpha,\beta,i_x-1,i_x}\hat{c}^\dagger_{i_x-1,k_y,k_z,\alpha}\hat{c}_{i_x,k_y,k_z,\beta}\right\},
\end{aligned} \tag{154}$$

where we have introduced B as

$$B_{\alpha,\beta,i_x,j_x} \equiv \frac{\lambda_{i_x}}{4}\Big[\sin(\phi)\sin(\theta)(\hat{\sigma}_z)_{\alpha,\beta} - \cos(\theta)(\hat{\sigma}_y)_{\alpha,\beta}\Big](1+\xi) \tag{155}$$

with $\xi = 1$ if lattice site j_x is inside the spin-orbit layer, and zero otherwise. We can point out the total current along the x-direction at lattice site i, I_i^x, to be

$$I_i^x = I_i^{x+} - I_i^{x-}. \tag{156}$$

The physical current is recieved by taking the combined quantum-mechanical expectation values and thermal averages of this operator

$$\langle I_i^x\rangle = \langle I_i^{x+}\rangle - \langle I_i^{x-}\rangle. \tag{157}$$

First, consider the positive x-direction and use that $\langle\hat{c}^\dagger_\mu\hat{c}_\nu - \text{h.c.}\rangle = 2i\,\mathrm{Im}\langle\hat{c}^\dagger_\mu\hat{c}_\nu\rangle$,

$$\begin{aligned}
\langle I_i^{x+}\rangle &= \frac{2t}{N_y N_z}\sum_{k_y,k_z,\sigma}\mathrm{Im}\langle\hat{c}^\dagger_{i_x,k_y,k_z,\sigma}\hat{c}_{i_x+1,k_y,k_z,\sigma}\rangle \\
&\quad + \frac{1}{N_y N_z}\sum_{k_y,k_z,\alpha,\beta}\mathrm{Re}\left\{B_{\alpha,\beta,i_x,i_x+1}\langle\hat{c}^\dagger_{i_x,k_y,k_z,\alpha}\hat{c}_{i_x+1,k_y,k_z,\beta}\rangle + B_{\alpha,\beta,i_x+1,i_x}\langle\hat{c}^\dagger_{i_x+1,k_y,k_z,\alpha}\hat{c}_{i_x,k_y,k_z,\beta}\rangle\right\}.
\end{aligned} \tag{158}$$

Similar for the negative x-direction:

$$\begin{aligned}
\langle I_i^{x-}\rangle &= \frac{2t}{N_y N_z}\sum_{k_y,k_z,\sigma}\mathrm{Im}\langle\hat{c}^\dagger_{i_x,k_y,k_z,\sigma}\hat{c}_{i_x-1,k_y,k_z,\sigma}\rangle \\
&\quad - \frac{1}{N_y N_z}\sum_{k_y,k_z,\alpha,\beta}\mathrm{Re}\left\{B_{\alpha,\beta,i_x,i_x-1}\langle\hat{c}^\dagger_{i_x,k_y,k_z,\alpha}\hat{c}_{i_x-1,k_y,k_z,\beta}\rangle + B_{\alpha,\beta,i_x-1,i_x}\langle\hat{c}^\dagger_{i_x-1,k_y,k_z,\alpha}\hat{c}_{i_x,k_y,k_z,\beta}\rangle\right\}.
\end{aligned} \tag{159}$$

Insert Eq. (158) and Eq. (159) into Eq. (157) and collect the physical current given at lattice site i as

$$\begin{aligned}\langle I_i^x\rangle = \frac{2t}{N_y N_z}\sum_{k_y,k_z,\sigma}\mathrm{Im}\left[\langle \hat{c}^\dagger_{i_x,k_y,k_z,\sigma}\hat{c}_{i_x+1,k_y,k_z,\sigma}\rangle - \langle \hat{c}^\dagger_{i_x,k_y,k_z,\sigma}\hat{c}_{i_x-1,k_y,k_z,\sigma}\rangle\right]\\ + \frac{1}{N_y N_z}\sum_{k_y,k_z,\alpha,\beta}\mathrm{Re}\left\{B_{\alpha,\beta,i_x,i_x+1}\langle \hat{c}^\dagger_{i_x,k_y,k_z,\alpha}\hat{c}_{i_x+1,k_y,k_z,\beta}\rangle + B_{\alpha,\beta,i_x+1,i_x}\langle \hat{c}^\dagger_{i_x+1,k_y,k_z,\alpha}\hat{c}_{i_x,k_y,k_z,\beta}\rangle\right\}\\ + \frac{1}{N_y N_z}\sum_{k_y,k_z,\alpha,\beta}\mathrm{Re}\left\{B_{\alpha,\beta,i_x-1,i_x}\langle \hat{c}^\dagger_{i_x-1,k_y,k_z,\alpha}\hat{c}_{i_x,k_y,k_z,\beta}\rangle + B_{\alpha,\beta,i_x,i_x-1}\langle \hat{c}^\dagger_{i_x,k_y,k_z,\alpha}\hat{c}_{i_x-1,k_y,k_z,\beta}\rangle\right\}.\end{aligned} \tag{160}$$

To evaluate the expression, study the average over the creation and annihilation operators. Insert the Bogoliubov transformation given in Eq. (99), and utilize that the average of the quasiparticles is only non-zero for equal n-mode. The expectation value is then given as

$$\sum_{k,\alpha,\beta}\langle \hat{c}^\dagger_{i_x,k,\alpha}\hat{c}_{j_x,k,\beta}\rangle = \sum_{k,n,\alpha,\beta} u^*_{i_x,n,k_y,k_z,\alpha}u_{j_x,n,k_y,k_z,\beta}\langle \gamma^\dagger_{n,k_y,k_z}\gamma_{n,k_y,k_z}\rangle \tag{161}$$

where the operators are dependent on each other. To associate the expectation value of the quasioperators with the Fermi-Dirac distribution, we have to sum over independent quasioperators exclusively. Rewrite the previous expression to include independent operators following a similar procedure as for the correlations functions in section 5.2.1. For concreteness, separate the sum into positive k, negative k, positive energies for the $k = 0$ mode, and negative energies for the $k = 0$ mode,

$$\begin{aligned}&\sum_{k,\alpha,\beta}\langle \hat{c}^\dagger_{i_x,k,\alpha}\hat{c}_{j_x,k,\beta}\rangle\\ &= \sum_{k>0,n,\alpha,\beta} u^*_{i_x,n,k,\alpha}u_{j_x,n,k,\beta}\langle \gamma^\dagger_{n,k}\gamma_{n,k}\rangle + \sum_{k<0,n,\alpha,\beta} u^*_{i_x,n,k,\alpha}u_{j_x,n,k,\beta}\langle \gamma^\dagger_{n,k}\gamma_{n,k}\rangle\\ &\quad + \sum_{k=0,n<2N_x,\alpha,\beta} u^*_{i_x,n,k=0,\alpha}u_{j_x,n,k=0,\beta}\langle \gamma^\dagger_{n,k=0}\gamma_{n,k=0}\rangle\\ &\quad + \sum_{k=0,n<2N_x,\alpha,\beta} u^*_{i_x,2N_x+n,k=0,\alpha}u_{j_x,2N_x+n,k=0,\beta}\langle \gamma^\dagger_{2N_x+n,k=0}\gamma_{2N_x+n,k=0}\rangle\\ &= \sum_{k>0,n,\alpha,\beta}\left(u^*_{i_x,n,k,\alpha}u_{j_x,n,k,\beta}\langle \gamma^\dagger_{n,k}\gamma_{n,k}\rangle + u^*_{i_x,n,-k,\alpha}u_{j_x,n,-k,\beta}\langle \gamma^\dagger_{n,-k}\gamma_{n,-k}\rangle\right)\\ &\quad + \sum_{k=0,n<2N_x,\alpha,\beta}\left(u^*_{i_x,n,0,\alpha}u_{j_x,n,0,\beta}\langle \gamma^\dagger_{n,0}\gamma_{n,0}\rangle + u^*_{i_x,2N_x+n,0,\alpha}u_{j_x,2N_x+n,0,\beta}\langle \gamma^\dagger_{2N_x+n,0}\gamma_{2N_x+n,0}\rangle\right)\\ &= \sum_{k>0,n,\alpha,\beta}\left(u^*_{i_x,n,k,\alpha}u_{j_x,n,k,\beta}\langle \gamma^\dagger_{n,k}\gamma_{n,k}\rangle + v_{i_x,n,k,\alpha}v^*_{j_x,n,k,\beta}\langle \gamma_{n,k}\gamma^\dagger_{n,k}\rangle\right)\\ &\quad + \sum_{k=0,n<2N_x,\alpha,\beta}\left(u^*_{i_x,n,0,\alpha}u_{j_x,n,0,\beta}\langle \gamma^\dagger_{n,0}\gamma_{n,0}\rangle + v_{i_x,n,0,\alpha}v^*_{j_x,n,0,\beta}\langle \gamma_{n,0}\gamma^\dagger_{n,0}\rangle\right).\end{aligned} \tag{162}$$

We have now reduced the problem to only consist of independent operators, such that we can evaluate the thermal average as in terms of the Fermi Dirac distribution $\langle \gamma^\dagger_{k,n}\gamma_{k,n}\rangle = f(E_{k,n})$, where $f(E_{k,n})$ is the Fermi function.

The arriving result for the supported supercurrent is

$$\begin{aligned}\langle I^x_i\rangle = &\frac{2t}{N_y N_z}\sum_{k,\sigma}\mathrm{Im}\left[\langle \hat{c}^\dagger_{i_x,k,\sigma}\hat{c}_{i_x+1,k,\sigma}\rangle - \langle \hat{c}^\dagger_{i_x,k,\sigma}\hat{c}_{i_x-1,k,\sigma}\rangle\right]\\ &+\frac{1}{N_y N_z}\sum_{k,\alpha,\beta}\mathrm{Re}\left\{B_{\alpha,\beta,i_x,i_x+1}\langle \hat{c}^\dagger_{i_x,k,\alpha}\hat{c}_{i_x+1,k,\beta}\rangle + B_{\alpha,\beta,i_x+1,i_x}\langle \hat{c}^\dagger_{i_x+1,k,\alpha}\hat{c}_{i_x,k,\beta}\rangle\right\}\\ &+\frac{1}{N_y N_z}\sum_{k,\alpha,\beta}\mathrm{Re}\left\{B_{\alpha,\beta,i_x-1,i_x}\langle \hat{c}^\dagger_{i_x-1,k,\alpha}\hat{c}_{i_x,k,\beta}\rangle + B_{\alpha,\beta,i_x,i_x-1}\langle \hat{c}^\dagger_{i_x,k,\alpha}\hat{c}_{i_x-1,k,\beta}\rangle\right\}\end{aligned} \tag{163}$$

where

$$\begin{aligned}\sum_{k,\alpha,\beta}\langle \hat{c}^\dagger_{i_x,k,\alpha}\hat{c}_{j_x,k,\beta}\rangle = &\sum_{k>0,n,\alpha,\beta}\left(u^*_{i_x,n,k,\alpha}u_{j_x,n,k,\beta}f(E_{k,n}) + v_{i_x,n,k,\alpha}v^*_{j_x,n,k,\beta}(1-f(E_{k,n}))\right)\\ &+\sum_{k=0,n<2N_x,\alpha,\beta}\left(u^*_{i_x,n,0,\alpha}u_{j_x,n,0,\beta}f(E_{0,n}) + v_{i_x,n,0,\alpha}v^*_{j_x,n,0,\beta}(1-f(E_{0,n}))\right).\end{aligned} \tag{164}$$

Recall the Fermi function given in Eq. (130) as

$$f(E_{k,n}) = \frac{1}{2}\left[1-\tanh\left(\frac{\beta E}{2}\right)\right]. \tag{165}$$

6

ANALYTICAL FRAMEWORK

This chapter will use the BTK formalism to describe a superconductor/superconductor (SC/SC) Josephson junction, with Rashba spin-orbit coupling imposed to the boundary conditions. We will use this model to calculate the Andreev bound states and hereby the supported supercurrent which follows.

6.1 BTK WAVE FUNCTION

The solution of BdG-equations in Eq. (59) obeys the Schrödinger equation, $H\psi = \varepsilon\psi$, with a wave function on the form

$$\psi(x) = \left(u_\uparrow, u_\downarrow, v_\uparrow, v_\downarrow\right). \tag{166}$$

Under the quasiclassical Andreev approximation, *i.e.* $E_F \gg \varepsilon$, we may write the wave function as

$$\psi(x) = \begin{cases} a_e^\uparrow \begin{pmatrix} u \\ 0 \\ 0 \\ v \end{pmatrix} e^{-ik_x x} + a_e^\downarrow \begin{pmatrix} 0 \\ u \\ -v \\ 0 \end{pmatrix} e^{-ik_x x} + b_h^\uparrow \begin{pmatrix} v \\ 0 \\ 0 \\ u \end{pmatrix} e^{ik_x x} + b_h^\downarrow \begin{pmatrix} 0 \\ -v \\ u \\ 0 \end{pmatrix} e^{ik_x x} & x < 0 \\ c_e^\uparrow \begin{pmatrix} ue^{i\phi/2} \\ 0 \\ 0 \\ ve^{-i\phi/2} \end{pmatrix} e^{ik_x x} + c_e^\downarrow \begin{pmatrix} 0 \\ ue^{i\phi/2} \\ -ve^{-i\phi/2} \\ 0 \end{pmatrix} e^{ik_x x} + d_h^\uparrow \begin{pmatrix} ve^{i\phi/2} \\ 0 \\ 0 \\ ue^{-i\phi/2} \end{pmatrix} e^{-ik_x x} + d_h^\downarrow \begin{pmatrix} 0 \\ -ve^{i\phi/2} \\ ue^{-i\phi/2} \\ 0 \end{pmatrix} e^{-ik_x x} & x > 0 \end{cases} \tag{167}$$

where $u = \sqrt{\frac{\varepsilon+\sqrt{\varepsilon^2-\Delta_0^2}}{2\varepsilon}}$, $v = \sqrt{\frac{\varepsilon-\sqrt{\varepsilon^2-\Delta_0^2}}{2\varepsilon}}$, and $\phi = \phi_L - \phi_R$. Thus, ϕ denotes the relative difference of the superconducting phase between the left and right superconductor. The coefficients $a_e^{\uparrow,\downarrow}, b_h^{\uparrow,\downarrow}, c_e^{\uparrow,\downarrow}, d_h^{\uparrow,\downarrow}$ corresponds to the probability amplitude for, respectively, normal reflection as an electron-like quasiparticle, Andreev reflection as a hole-like quasiparticle, transmission to the right superconductor as an electron-like quasiparticle, and transmission to the right superconductor as a hole-like quasiparticle. In addition, the wave vector of the particles in the quasiclassical Andreev approximation is $\hbar k_F = \sqrt{2mE_F}$.

If $\psi = (u, v)^T$ is an eigenvector of H, it follows that $\psi = \text{constant} * (u, v)^T$ is an eigenvector of H. Therefore, let $\psi = (u, v)^T \Rightarrow \psi = v * (u/v, 1)^T$ and redefine the wave function by evaluating

$$\left.\frac{u}{v}\right|_{\varepsilon \geqslant \Delta_0} = \sqrt{\frac{\varepsilon + \sqrt{\varepsilon^2 - \Delta_0^2}}{\varepsilon - \sqrt{\varepsilon^2 - \Delta_0^2}}} = \sqrt{\frac{\varepsilon + \sqrt{\varepsilon - \Delta_0}\sqrt{\varepsilon + \Delta_0}}{\varepsilon - \sqrt{\varepsilon - \Delta_0}\sqrt{\varepsilon + \Delta_0}}} = \sqrt{\frac{\frac{\varepsilon}{\Delta_0} + \sqrt{\frac{\varepsilon}{\Delta_0} - 1}\sqrt{\frac{\varepsilon}{\Delta_0} + 1}}{\frac{\varepsilon}{\Delta_0} - \sqrt{\frac{\varepsilon}{\Delta_0} - 1}\sqrt{\frac{\varepsilon}{\Delta_0} + 1}}} = e^{\operatorname{arccosh}(\varepsilon/\Delta_0)}$$

$$\left.\frac{u}{v}\right|_{\varepsilon < \Delta_0} = \sqrt{\frac{\varepsilon + \sqrt{-(\Delta_0^2 - \varepsilon^2)}}{\varepsilon - \sqrt{-(\Delta_0^2 - \varepsilon^2)}}} = \sqrt{\frac{\varepsilon + i\sqrt{(\Delta_0 - \varepsilon)}\sqrt{\varepsilon + \Delta_0}}{\varepsilon - i\sqrt{(\Delta_0 - \varepsilon)}\sqrt{\varepsilon + \Delta_0}}} = \sqrt{\frac{\frac{\varepsilon}{\Delta_0} + i\sqrt{1 - \frac{\varepsilon}{\Delta_0}}\sqrt{\frac{\varepsilon}{\Delta_0} + 1}}{\frac{\varepsilon}{\Delta_0} - i\sqrt{1 - \frac{\varepsilon}{\Delta_0}}\sqrt{\frac{\varepsilon}{\Delta_0} + 1}}} = e^{i\arccos(\varepsilon/\Delta_0)}$$

where we have used the identities

$$e^{\pm \operatorname{arccosh}(A)} = A \pm \sqrt{A+1}\sqrt{A-1}, \qquad e^{\pm i \arccos(A)} = A \pm i\sqrt{A+1}\sqrt{1-A}.$$

Consequently, the explicit expression for u/v depends on whether we are inside or outside of the superconducting gap. Since v is a constant, we can rewrite the eigenvector in a simpler form given by $\psi = (u/v, 1)^T$. The simplified wave function reads

$$\psi(x) = \begin{cases} a_e^{\uparrow} \begin{pmatrix} e^{\beta} \\ 0 \\ 0 \\ 1 \end{pmatrix} e^{-ik_x x} + a_e^{\downarrow} \begin{pmatrix} 0 \\ e^{\beta} \\ -1 \\ 0 \end{pmatrix} e^{-ik_x x} + b_h^{\uparrow} \begin{pmatrix} 1 \\ 0 \\ 0 \\ e^{\beta} \end{pmatrix} e^{ik_x x} + b_h^{\downarrow} \begin{pmatrix} 0 \\ -1 \\ e^{\beta} \\ 0 \end{pmatrix} e^{ik_x x} & x < 0 \\ c_e^{\uparrow} \begin{pmatrix} e^{\beta} e^{i\phi/2} \\ 0 \\ 0 \\ e^{-i\phi/2} \end{pmatrix} e^{ik_x x} + c_e^{\downarrow} \begin{pmatrix} 0 \\ e^{\beta} e^{i\phi/2} \\ -e^{-i\phi/2} \\ 0 \end{pmatrix} e^{ik_x x} + d_h^{\uparrow} \begin{pmatrix} e^{i\phi/2} \\ 0 \\ 0 \\ e^{\beta} e^{-i\phi/2} \end{pmatrix} e^{-ik_x x} + d_h^{\downarrow} \begin{pmatrix} 0 \\ -e^{i\phi/2} \\ e^{\beta} e^{-i\phi/2} \\ 0 \end{pmatrix} e^{-ik_x x} & x > 0 \end{cases} \tag{168}$$

where we have defined

$$\beta = \begin{cases} \cosh^{-1}(\varepsilon/\Delta_0) & \text{if } \varepsilon \geqslant \Delta_0 \\ i\cos^{-1}(\varepsilon/\Delta_0) & \text{if } \varepsilon < \Delta_0 \end{cases}. \tag{169}$$

6.2 HAMILTONIAN MATRIX

The Hamiltonian of our system is, in terms of field operators, given as

$$\begin{aligned}\hat{H} &= \sum_{\alpha,\beta}\int d^3r\hat{\psi}^\dagger_\alpha(r)(H)_{\alpha\beta}\hat{\psi}_\beta(r)\\ &= \sum_{\alpha,\beta}\int d^3r\hat{\psi}^\dagger_\alpha(r)\left[-\frac{\hbar^2}{2m}\nabla^2\right]_{\alpha\beta}\hat{\psi}_\beta(r)\\ &\quad+\int d^3r\Big\{\Delta^*(\mathbf{r})\hat{\psi}_\downarrow(\mathbf{r})\hat{\psi}_\uparrow(\mathbf{r})+\Delta(\mathbf{r})\hat{\psi}^\dagger_\uparrow(\mathbf{r})\hat{\psi}^\dagger_\downarrow(\mathbf{r})\Big\}\\ &\quad+\sum_{\alpha,\beta}\int d^3r\hat{\psi}^\dagger_\alpha(r)(V_0)_{\alpha\beta}\hat{\psi}_\beta(r)\\ &\quad+\sum_{\alpha,\beta}\int d^3r\hat{\psi}^\dagger_\alpha(r)(H_\lambda)_{\alpha\beta}\hat{\psi}_\beta(r).\end{aligned} \tag{170}$$

Here, the different terms denote, respectively, the kinetic energy of the electrons, the attractive electron-electron interaction that gives rise to superconductivity, and a scattering- and a spin-orbit potential at the interface of the two superconducting elements. We want to express this Hamiltonian into a 4x4-matrix that correlates spin-space to charge-space. To derive the desired matrix, we will use the anti-commutation properties of the field operators to write out each term of the previous equation.

6.2.1 *The kinetic-energy term*

Write out the kinetic energy term by utilizing the anti-commutator relation of the fermionic field operators, $\{\hat{\psi}_\alpha,\hat{\psi}^\dagger_\beta\}=\delta_{\alpha,\beta}$. The result reads

$$\begin{aligned}&\sum_{\alpha,\beta}\int d^3r\hat{\psi}^\dagger_\alpha(r)\left[-\frac{\hbar^2}{2m}\nabla^2\right]_{\alpha\beta}\hat{\psi}_\beta(r)\\ &\quad=\frac{1}{2}\sum_{\alpha,\beta}\int d^3r\left\{\hat{\psi}^\dagger_\alpha(r)\left[-\frac{\hbar^2}{2m}\nabla^2\right]_{\alpha\beta}\hat{\psi}_\beta(r)-\hat{\psi}_\beta(r)\left[-\frac{\hbar^2}{2m}\nabla^2\right]_{\beta\alpha}\hat{\psi}^\dagger_\alpha(r)\right\}\\ &\quad=\frac{1}{2}\int d^3r\begin{pmatrix}\hat{\psi}^\dagger_\uparrow & \hat{\psi}^\dagger_\downarrow & \hat{\psi}_\uparrow & \hat{\psi}_\downarrow\end{pmatrix}\begin{pmatrix}-\frac{\hbar^2}{2m}\nabla^2 & 0 & 0 & 0\\ 0 & -\frac{\hbar^2}{2m}\nabla^2 & 0 & 0\\ 0 & 0 & \frac{\hbar^2}{2m}\nabla^2 & 0\\ 0 & 0 & 0 & \frac{\hbar^2}{2m}\nabla^2\end{pmatrix}\begin{pmatrix}\hat{\psi}_\uparrow\\ \hat{\psi}_\downarrow\\ \hat{\psi}^\dagger_\uparrow\\ \hat{\psi}^\dagger_\downarrow\end{pmatrix}\end{aligned} \tag{171}$$

where we have exploited that ∇^2 is diagonal in spin-space.

6.2.2 *The superconducting gap term*

The superconducting gap is straightforward with the anti-commute relation $\{\hat{\psi}_\alpha, \hat{\psi}_\beta\} = 0$. By writing out the Hamiltonian for the electron-electron interaction, the result yields

$$\begin{aligned}
&\int d^3r \Big\{ \Delta^*(\mathbf{r})\hat{\psi}_\downarrow(\mathbf{r})\hat{\psi}_\uparrow(\mathbf{r}) + \Delta(\mathbf{r})\hat{\psi}^\dagger_\uparrow(\mathbf{r})\hat{\psi}^\dagger_\downarrow(\mathbf{r}) \Big\} \\
&\quad = \frac{1}{2}\int d^3r \Big\{ \Delta^*(\mathbf{r})\hat{\psi}_\downarrow(\mathbf{r})\hat{\psi}_\uparrow(\mathbf{r}) - \Delta^*(\mathbf{r})\hat{\psi}_\uparrow(\mathbf{r})\hat{\psi}_\downarrow(\mathbf{r}) - \Delta(\mathbf{r})\hat{\psi}^\dagger_\downarrow(\mathbf{r})\hat{\psi}^\dagger_\uparrow(\mathbf{r}) + \Delta(\mathbf{r})\hat{\psi}^\dagger_\uparrow(\mathbf{r})\hat{\psi}^\dagger_\downarrow(\mathbf{r}) \Big\} \\
&\quad = \frac{1}{2}\int d^3r \begin{pmatrix} \hat{\psi}^\dagger_\uparrow & \hat{\psi}^\dagger_\downarrow & \hat{\psi}_\uparrow & \hat{\psi}_\downarrow \end{pmatrix} \begin{pmatrix} 0 & 0 & 0 & \Delta \\ 0 & 0 & -\Delta & 0 \\ 0 & -\Delta^* & 0 & 0 \\ \Delta^* & 0 & 0 & 0 \end{pmatrix} \begin{pmatrix} \hat{\psi}_\uparrow \\ \hat{\psi}_\downarrow \\ \hat{\psi}^\dagger_\uparrow \\ \hat{\psi}^\dagger_\downarrow \end{pmatrix}
\end{aligned} \tag{172}$$

where the superconducting gap is $\Delta = U\langle\hat{\psi}_\uparrow\hat{\psi}_\downarrow\rangle$.

6.2.3 *The scattering potential term*

The imposed scattering potential between the two superconducting elements is denoted by the parameter V_0. It follows that the scattering potential is diagonal in spin-space. Consequently, we can rewrite the scattering potential into a matrix form similar to the kinetic energy term,

$$\begin{aligned}
&\sum_{\alpha,\beta}\int d^3r \hat{\psi}^\dagger_\alpha(r)(V_0)_{\alpha\beta}\hat{\psi}_\beta(r) \\
&\quad = \frac{1}{2}\sum_{\alpha,\beta}\int d^3r \left\{ \hat{\psi}^\dagger_\alpha(r)(V_0)_{\alpha\beta}\hat{\psi}_\beta(r) - \hat{\psi}_\beta(r)(V_0)_{\beta\alpha}\hat{\psi}^\dagger_\alpha(r) \right\} \\
&\quad = \frac{1}{2}\int d^3r \begin{pmatrix} \hat{\psi}^\dagger_\uparrow & \hat{\psi}^\dagger_\downarrow & \hat{\psi}_\uparrow & \hat{\psi}_\downarrow \end{pmatrix} \begin{pmatrix} V_0 & 0 & 0 & 0 \\ 0 & V_0 & 0 & 0 \\ 0 & 0 & -V_0 & 0 \\ 0 & 0 & 0 & -V_0 \end{pmatrix} \begin{pmatrix} \hat{\psi}_\uparrow \\ \hat{\psi}_\downarrow \\ \hat{\psi}^\dagger_\uparrow \\ \hat{\psi}^\dagger_\downarrow \end{pmatrix}.
\end{aligned} \tag{173}$$

6.2.4 *The spin-orbit coupling term*

The Hermitian spin-orbit Hamiltonian is found in Appendix A.1 to fulfill the relation

$$H_\lambda = \frac{1}{2}(\hat{n} \times \boldsymbol{\sigma}) \cdot \{\lambda(x), \mathbf{p}\} \tag{174}$$

where the spin-orbit coupling is a boundary potential $\lambda(x) = \lambda\delta(x)$. In order to generalize the spin-orbit Hamiltonian in charge space, express the Hamiltonian in terms of field operators,

$$\begin{aligned}
\hat{H}_\lambda &= \sum_{\alpha,\beta} \int d^3r \hat{\psi}^\dagger_\alpha(r)(H_\lambda)_{\alpha\beta}\hat{\psi}_\beta(r) \\
&= \sum_{\alpha,\beta} \int d^3r \hat{\psi}^\dagger_\alpha(r) \left[\frac{1}{2}(\hat{n} \times \boldsymbol{\sigma}) \cdot \{\lambda(x), \mathbf{p}\}\right]_{\alpha\beta} \hat{\psi}_\beta(r) \\
&= \sum_{\alpha,\beta} \int d^3r \hat{\psi}^\dagger_\alpha(r) \left[\frac{-i\hbar}{2}(\hat{n} \times \boldsymbol{\sigma}_{\alpha\beta})\right] \cdot \lambda(x)\nabla\left[\hat{\psi}_\beta(r)\right] + \sum_{\alpha,\beta} \int d^3r \hat{\psi}^\dagger_\alpha(r) \left[\frac{-i\hbar}{2}(\hat{n} \times \boldsymbol{\sigma}_{\alpha\beta})\right] \cdot \nabla\left[\lambda(x)\hat{\psi}_\beta(r)\right]
\end{aligned} \tag{175}$$

where we have used $\mathbf{p} = -i\hbar\boldsymbol{\nabla}$. To diagonalize the previous equation, we want to manipulate the expression and achieve a term where the partial derivative acts on $\psi^\dagger$. Therefore, perform a partial integration

$$\begin{aligned}
\hat{H}_\lambda &= \sum_{\alpha,\beta} \cancel{\left\{\hat{\psi}^\dagger_\alpha(r) \left[\frac{-i\hbar}{2}(\hat{n} \times \boldsymbol{\sigma}_{\alpha\beta})\right] \lambda(x)\hat{\psi}_\beta(r)\right\}_{\text{boundary}}} - \sum_{\alpha,\beta} \int d^3r \nabla\left[\hat{\psi}^\dagger_\alpha(r)\lambda(x)\right] \cdot \left[\frac{-i\hbar}{2}(\hat{n} \times \boldsymbol{\sigma}_{\alpha\beta})\right] \hat{\psi}_\beta(r) \\
&\quad + \sum_{\alpha,\beta} \cancel{\left\{\hat{\psi}^\dagger_\alpha(r) \left[\frac{-i\hbar}{2}(\hat{n} \times \boldsymbol{\sigma}_{\alpha\beta})\right] \lambda(x)\hat{\psi}_\beta(r)\right\}_{\text{boundary}}} - \sum_{\alpha,\beta} \int d^3r \nabla\left[\hat{\psi}^\dagger_\alpha(r)\right] \cdot \left[\frac{-i\hbar}{2}(\hat{n} \times \boldsymbol{\sigma}_{\alpha\beta})\right] \lambda(x)\hat{\psi}_\beta(r) \\
&= \sum_{\alpha,\beta} \int d^3r \hat{\psi}_\beta(r) \left[\frac{1}{2}(\hat{n} \times \boldsymbol{\sigma}_{\alpha\beta})\right] \cdot \mathbf{p}\left[\lambda(x)\hat{\psi}^\dagger_\alpha(r)\right] + \sum_{\alpha,\beta} \int d^3r \hat{\psi}_\beta(r) \left[\frac{1}{2}(\hat{n} \times \boldsymbol{\sigma}_{\alpha\beta})\right] \cdot \lambda(x)\mathbf{p}\left[\hat{\psi}^\dagger_\alpha(r)\right] \\
&= \sum_{\alpha,\beta} \int d^3r \hat{\psi}_\beta(r) \left[\frac{1}{2}(\hat{n} \times \boldsymbol{\sigma}^*_{\beta\alpha}) \cdot \{\lambda(x), \mathbf{p}\}\right] \hat{\psi}^\dagger_\alpha(r)
\end{aligned} \tag{176}$$

where we have substituted back $\mathbf{p} = -i\hbar\boldsymbol{\nabla}$, and used that the field operators anti-commute. The boundary terms vanish because the field operators go to zero at infinity, $\psi(r \to \infty) = 0$.

Combining the results in Eq.(176) with the second line in Eq.(175), the result reads

$$\begin{aligned}
\hat{H}_\lambda = &\frac{1}{2} \sum_{\alpha,\beta} \int d^3r \hat{\psi}^\dagger_\alpha(r) \left[\frac{1}{2}(\hat{n} \times \boldsymbol{\sigma}_{\alpha\beta}) \cdot \{\lambda(x), \mathbf{p}\}\right] \hat{\psi}_\beta(r) \\
&+ \frac{1}{2} \sum_{\alpha,\beta} \int d^3r \hat{\psi}_\beta(r) \left[\frac{1}{2}(\hat{n} \times \boldsymbol{\sigma}^*_{\beta\alpha}) \cdot \{\lambda(x), \mathbf{p}\}\right] \hat{\psi}^\dagger_\alpha(r)\Big].
\end{aligned} \tag{177}$$

Here, the first line corresponds to the electron-like particles, and the last line considers hole-like particles.

6.3 BOUNDARY CONDITIONS

The Andreev bound states are constructed by combining the Hamiltonian and the wave functions, along with a set of boundary conditions. We require the wave function to be continuous everywhere. The equation to establish continuity at the boundary between the two superconductors at $x = 0$ is straightforward $\psi(x = 0^-) = \psi(x = 0^+)$. This boundary condition will provide four independent equations. However, we require a total of eight equations due to eight reflection/transmission coefficients. For that, utilize the conservation of energy to receive a set of boundary conditions for the discontinuous derivative. Furthermore, we need to do this calculation twice, one for the electron-like particles and another for the hole-like particles.

6.3.1 *Electron-like part*

Consider the Schrödinger equation for the electron-like particles,

$$-\frac{\hbar^2}{2m}\nabla^2\psi + \Delta\psi = \big[\varepsilon - V(x)\big]\psi \tag{178}$$

where $V(x) = H\delta(x) + \frac{1}{2}(\hat{n}\times\boldsymbol{\sigma})\cdot\{\lambda\delta(x), \mathbf{p}\}$ is the boundary potential. Here, H is the scattering strength. Integrate across the boundary, *i.e.* for x from $-\epsilon$ to ϵ, and let $\epsilon \to 0$. The integration gives

$$\begin{aligned}
-\frac{\hbar^2}{2m}\int_{-\epsilon}^{\epsilon}\nabla^2\psi\,dx - \frac{\hbar^2}{2m}\int_{-\epsilon}^{\epsilon}\Delta\psi\,dx &= \int_{-\epsilon}^{\epsilon}\varepsilon\,dx - \int_{-\epsilon}^{\epsilon}V(x)\psi\,dx \\
\int_{-\epsilon}^{\epsilon}\frac{\partial^2\psi}{\partial x^2}\,dx &= \frac{2m}{\hbar^2}\int_{-\epsilon}^{\epsilon}V(x)\psi\,dx \\
\int_{-\epsilon}^{\epsilon}\frac{\partial^2\psi}{\partial x^2}\,dx &= \frac{2m}{\hbar^2}\int_{-\epsilon}^{\epsilon}\frac{1}{2}(\hat{n}\times\boldsymbol{\sigma})\cdot\{\lambda(x), \hat{p}\}\psi\,dx + \frac{2m}{\hbar^2}\int_{-\epsilon}^{\epsilon}V_0(x)\psi\,dx\,.
\end{aligned} \tag{179}$$

Write out the last line in the previous equation and get

$$\begin{aligned}\int_{-\epsilon}^{\epsilon}\frac{\partial^2\psi}{\partial x^2}\,dx &= \frac{2m}{\hbar^2}\int_{-\epsilon}^{\epsilon}\lambda(x)(\hat{n}\times\boldsymbol{\sigma})\cdot\left(\hat{p_y}+\hat{p_z}\right)\psi\,dx\\ &+\frac{m}{\hbar^2}\int_{-\epsilon}^{\epsilon}\lambda(x)(\hat{n}\times\boldsymbol{\sigma})\cdot\hat{p_x}\psi\,dx\\ &+\frac{m}{\hbar^2}\int_{-\epsilon}^{\epsilon}(\hat{n}\times\boldsymbol{\sigma})\cdot\hat{p_x}\left[\lambda(x)\psi\,dx\right]\\ &+\frac{2m}{\hbar^2}\int_{-\epsilon}^{\epsilon}V_0(x)\psi\,dx\,.\end{aligned}\tag{180}$$

Insert for the two potentials, $\lambda(x) = \lambda\delta(x)$, $V_0(x) = H\delta(x)$, and use that $\mathbf{p} = -i\hbar\boldsymbol{\nabla}$. Perform the integration and get

$$\begin{aligned}\int_{-\epsilon}^{\epsilon}\frac{\partial^2\psi}{\partial x^2}\,dx &= -\frac{i2m\lambda}{\hbar}(\hat{n}\times\boldsymbol{\sigma})\cdot\int_{-\epsilon}^{\epsilon}\delta(x)\left(\partial_y\hat{y}+\partial_z\hat{z}\right)\psi\,dx\\ &-\frac{im\lambda}{\hbar}(\hat{n}\times\boldsymbol{\sigma})\cdot\int_{-\epsilon}^{\epsilon}\delta(x)\partial_x\psi\hat{x}\,dx\\ &-\frac{im\lambda}{\hbar}(\hat{n}\times\boldsymbol{\sigma})\cdot\int_{-\epsilon}^{\epsilon}\partial_x\hat{x}\left[\delta(x)\psi\right]dx\\ &+\frac{2mH}{\hbar^2}\int_{-\epsilon}^{\epsilon}\delta(x)\psi\,dx\\ \frac{d\psi}{dx}(0^+)-\frac{d\psi}{dx}(0^-) &= -\frac{i2m\lambda}{\hbar}(\hat{n}\times\boldsymbol{\sigma})\cdot\left(\partial_y\hat{y}+\partial_z\hat{z}\right)\psi(0)\\ &-\frac{im\lambda}{\hbar}(\hat{n}\times\boldsymbol{\sigma})\cdot\partial_x\psi(0)\hat{x}\\ &-\frac{im\lambda}{\hbar}(\hat{n}\times\boldsymbol{\sigma})\cdot\left\{\left[\delta(0^+)\psi(0^+)\right]-\left[\delta(0^-)\psi(0^-)\right]\right\}\\ &+\frac{2mH}{\hbar^2}\psi(0)\\ \frac{d\psi}{dx}(0^+)-\frac{d\psi}{dx}(0^-) &= -\frac{i2m\lambda}{\hbar}(\hat{n}\times\boldsymbol{\sigma})\cdot\left(\frac{\partial_x}{2}\hat{x}+\partial_y\hat{y}+\partial_z\hat{z}\right)\psi(0)\\ &+\frac{2mH}{\hbar^2}\psi(0)\\ \frac{d\psi}{dx}(0^+)-\frac{d\psi}{dx}(0^-) &= \hat{T}_e\psi(0)\end{aligned}\tag{181}$$

where we have defined the transmission matrix

$$\hat{T}_e = -iZ_{soc}(\hat{n} \times \boldsymbol{\sigma}) \cdot \left(\frac{\partial_x}{2}\hat{x} + \partial_y\hat{y} + \partial_z\hat{z}\right) + k_F Z_0 \cdot \sigma_0 \tag{182}$$

and introduced the dimensionless parameters $Z_{soc} = \frac{2m\lambda}{\hbar}$ and $Z_0 = \frac{2mH}{\hbar^2 k_F}$. This boundary condition holds for electron-like particles. The next step is to find the associated transmission matrix, $\hat{T}_h$, for the hole-like particles.

6.3.2 *Hole-like part*

To find the transmission matrix for the hole-like particles, start with the Schrödinger equation

$$\frac{\hbar^2}{2m}\nabla^2\psi + \Delta^*\psi = \left[\varepsilon - V(x)\right]\psi \tag{183}$$

where $V(x) = -H\delta(x) + \frac{1}{2}(\hat{n} \times \boldsymbol{\sigma}^*) \cdot \{\lambda\delta(x), \mathbf{p}\}$. Follow the similar procedure as we did for the electron-like particles and integrate across the boundary from $-\epsilon$ to ϵ. Let $\epsilon \to 0$, and get

$$\begin{aligned}
\frac{\hbar^2}{2m}\int_{-\epsilon}^{\epsilon}\nabla^2\psi\,dx + \int_{-\epsilon}^{\epsilon}\Delta^*\psi\,dx &= \int_{-\epsilon}^{\epsilon}\varepsilon\,dx - \int_{-\epsilon}^{\epsilon}V(x)\psi\,dx \\
\int_{-\epsilon}^{\epsilon}\frac{\partial^2\psi}{\partial x^2}\,dx &= -\frac{2m}{\hbar^2}\int_{-\epsilon}^{\epsilon}V(x)\psi\,dx \\
\int_{-\epsilon}^{\epsilon}\frac{\partial^2\psi}{\partial x^2}\,dx &= -\frac{2m}{\hbar^2}\int_{-\epsilon}^{\epsilon}\frac{1}{2}(\hat{n} \times \boldsymbol{\sigma}^*) \cdot \left\{\lambda(x), \hat{p}\right\}\psi\,dx + \frac{2m}{\hbar^2}\int_{-\epsilon}^{\epsilon}V_0(x)\psi\,dx \\
\int_{-\epsilon}^{\epsilon}\frac{\partial^2\psi}{\partial x^2}\,dx &= -\frac{2m}{\hbar^2}\int_{-\epsilon}^{\epsilon}\lambda(x)(\hat{n} \times \boldsymbol{\sigma}^*) \cdot \left(\hat{p_y} + \hat{p_z}\right)\psi\,dx \\
&\quad - \frac{m}{\hbar^2}\int_{-\epsilon}^{\epsilon}\lambda(x)(\hat{n} \times \boldsymbol{\sigma}^*) \cdot \hat{p_x}\psi\,dx \\
&\quad - \frac{m}{\hbar^2}\int_{-\epsilon}^{\epsilon}(\hat{n} \times \boldsymbol{\sigma}^*) \cdot \hat{p_x}\left[\lambda(x)\psi\,dx\right] \\
&\quad + \frac{2m}{\hbar^2}\int_{-\epsilon}^{\epsilon}V_0(x)\psi\,dx\,.
\end{aligned} \tag{184}$$

Insert for the two potentials, $\lambda(x) = \lambda\delta(x)$, $V_0(x) = H\delta(x)$, and use that $\mathbf{p} = -i\hbar\boldsymbol{\nabla}$. We will then obtain the transmission matrix for the hole-like particles by performing the integration

$$\begin{aligned}
\int_{-\epsilon}^{\epsilon} \frac{\partial^2\psi}{\partial x^2}\,dx &= \frac{i2m\lambda}{\hbar}(\hat{n}\times\boldsymbol{\sigma}^*)\cdot\int_{-\epsilon}^{\epsilon}\delta(x)\big(\partial_y\hat{y}+\partial_z\hat{z}\big)\psi\,dx \\
&\quad+\frac{im\lambda}{\hbar}(\hat{n}\times\boldsymbol{\sigma}^*)\cdot\int_{-\epsilon}^{\epsilon}\delta(x)\partial_x\psi\hat{x}\,dx \\
&\quad+\frac{im\lambda}{\hbar}(\hat{n}\times\boldsymbol{\sigma}^*)\cdot\int_{-\epsilon}^{\epsilon}\partial_x\hat{x}\big[\delta(x)\psi\big]\,dx \\
&\quad+\frac{2mH}{\hbar^2}\int_{-\epsilon}^{\epsilon}\delta(x)\psi\,dx \\
\frac{d\psi}{dx}(0^+)-\frac{d\psi}{dx}(0^-) &= \frac{i2m\lambda}{\hbar}(\hat{n}\times\boldsymbol{\sigma}^*)\cdot\big(\partial_y\hat{y}+\partial_z\hat{z}\big)\psi(0) \\
&\quad+\frac{im\lambda}{\hbar}(\hat{n}\times\boldsymbol{\sigma}^*)\cdot\partial_x\psi(0)\hat{x} \\
&\quad+\frac{im\lambda}{\hbar}(\hat{n}\times\boldsymbol{\sigma}^*)\cdot\Big\{\big[\delta(0^+)\psi(0^+)\big]-\big[\delta(0^-)\psi(0^-)\big]\Big\} \\
&\quad+\frac{2mH}{\hbar^2}\psi(0) \\
\frac{d\psi}{dx}(0^+)-\frac{d\psi}{dx}(0^-) &= \frac{i2m\lambda}{\hbar}(\hat{n}\times\boldsymbol{\sigma}^*)\cdot\big(\frac{\partial_x}{2}\hat{x}+\partial_y\hat{y}+\partial_z\hat{z}\big)\psi(0) \\
&\quad+\frac{2mH}{\hbar^2}\psi(0) \\
\frac{d\psi}{dx}(0^+)-\frac{d\psi}{dx}(0^-) &= \hat{T}_h\psi(0)
\end{aligned} \tag{185}$$

where we have defined the transmission matrix for the hole-like particles

$$\hat{T}_h = iZ_{soc}(\hat{n}\times\boldsymbol{\sigma}^*)\cdot\big(\frac{\partial_x}{2}\hat{x}+\partial_y\hat{y}+\partial_z\hat{z}\big)+k_F Z_0\cdot\sigma_0 \tag{186}$$

in terms of the dimensionless parameters for the scattering potential ($Z_0 = \frac{2mH}{\hbar^2 k_F}$) and spin-orbit potential ($Z_{soc} = \frac{2m\lambda}{\hbar}$).

6.3.3 *Assemble the effective barrier-matrix*

The effective barrier matrix for the complete system is achieved by the transmission matrix for the electron-like and hole-like particles given in Eq. (182) and (186) as

$$\begin{aligned}\hat{T}_e &= -iZ_{soc}(\hat{n}\times\boldsymbol{\sigma})\cdot\left(\frac{\partial_x}{2}\hat{x}+\partial_y\hat{y}+\partial_z\hat{z}\right)+k_F Z_0\cdot\sigma_0\\ &= Z_{soc}\left\{h^x_{soc}\sigma_x+h^y_{soc}\sigma_y+h^z_{soc}\sigma_z\right\}+k_F Z_0\cdot\sigma_0\\ \hat{T}_h &= iZ_{soc}(\hat{n}\times\boldsymbol{\sigma}^*)\cdot\left(\frac{\partial_x}{2}\hat{x}+\partial_y\hat{y}+\partial_z\hat{z}\right)+k_F Z_0\cdot\sigma_0\\ &= Z_{soc}\left\{-h^x_{soc}\sigma_x+h^y_{soc}\sigma_y-h^z_{soc}\sigma_z\right\}+k_F Z_0\cdot\sigma_0\end{aligned} \tag{187}$$

where we have defined

$$h^x_{soc}=i(n_y\partial_z-n_z\partial_y),\qquad h^y_{soc}=i(n_z\frac{\partial_x}{2}-n_x\partial_z),\qquad h^z_{soc}=i(n_x\partial_y-n_y\frac{\partial_x}{2}) \tag{188}$$

to simplify the expressions. The two transmission matrices, $\hat{T}_e$ and $\hat{T}_h$, are 2x2-matrices in spin-space. By combing them, we will receive a 4x4-transmission matrix in charge-space

$$\hat{T}_{4x4}=\begin{pmatrix}\hat{T}_e & 0\\ 0 & \hat{T}_h\end{pmatrix}. \tag{189}$$

The resulting boundary conditions for an SC/SC Josephson junction with Rashba spin-orbit coupling imposed to the boundary with an arbitrary direction of the spin-orbit orientation, $\hat{n}$, is

$$\begin{aligned}\psi(0^+)-\psi(0^-)&=0\\ \frac{d\psi}{dx}(0^+)-\frac{d\psi}{dx}(0^-)&=\hat{T}_{4x4}\psi(0)\end{aligned} \tag{190}$$

where the transmission matrix is given by

$$\hat{T}_{4x4}=Z_{soc}\left[h^x_{soc}\begin{pmatrix}\sigma_x & 0\\ 0 & -\sigma_x\end{pmatrix}+h^y_{soc}\begin{pmatrix}\sigma_y & 0\\ 0 & \sigma_y\end{pmatrix}+h^z_{soc}\begin{pmatrix}\sigma_z & 0\\ 0 & -\sigma_z\end{pmatrix}\right]+k_F Z_0\begin{bmatrix}\mathbb{1}_{2x2} & 0\\ 0 & \mathbb{1}_{2x2}\end{bmatrix}. \tag{191}$$

6.4 DERIVATION OF ANDREEV BOUND STATES AND SUPERCURRENT

This section will calculate the Andreev bound states and the supercurrent. We have found the wave functions and belonging boundary conditions in the two

previous sections. Insert the wave function in Eq. (168) into the set of boundary conditions in Eq. (190), and receive a system of eighth equations. The supercurrent is found by solving for quasiparticles inside the superconducting gap, *i.e.* $\varepsilon < \Delta_0$. To make the calculation easier, rewrite the set of equations in a matrix system of the form

$$\mathbf{A}\mathbf{x} = \mathbf{b} \tag{192}$$

where $\mathbf{A}$ is an 8x8-matrix and $\mathbf{x}$ is a vector of the reflection/transmission coefficients. In search for the Andreev bound states across the junction, we do not need to solve for the coefficients. Instead, we only require the system to be solvable in order to find an equation for the allowed energies. The key is to manipulate the system of equations such that $\mathbf{b} = 0$. From linear algebra, we know that a nontrivial solution to $\mathbf{A}\mathbf{x} = 0$ implies that

$$\det(\mathbf{A}) = 0. \tag{193}$$

The determinant of $\mathbf{A}$ is given by

$$\begin{aligned}\det(\mathbf{A}) &= a\cosh(2\beta)^2 + b\cosh(2\beta) + c \qquad \text{with} \quad \beta = -i\cos^{-1}(\varepsilon/\Delta_0) \\ &= 4a\left(\frac{\varepsilon}{\Delta_0}\right)^4 + (2b - 4a)\left(\frac{\varepsilon}{\Delta_0}\right)^2 + (a - b + c)\end{aligned} \tag{194}$$

where the coefficients a, b, c are functions of the superconducting phase ϕ, barrier strength Z_0, the spin-orbit magnitude Z_{soc}, the spin-orbit orientation $\hat{n}$ and the quasiparticle wave vector $\mathbf{k}$. The explicit form yields,

$$\begin{aligned} c &= B\cos^2(\phi) + \Big(A - B\Big)\cos(\phi) + C\Big(C + D\Big) \\ b &= -\Big(A + B\Big)\cos(\phi) - 2C\Big(C + D\Big) - A + B \\ a &= C\Big(C + D\Big) + A \end{aligned} \tag{195}$$

where

$$\begin{aligned} A &= 512k_x^2\Bigg[Z_{soc}^2\Bigg(k_y^2(n_x^2 + n_z^2) - k_y n_y(2k_z n_z + iZ_0 k_F n_x) \\ &\qquad + k_z^2(n_x^2 + n_y^2) - iZ_0 k_F k_z n_x n_z + \frac{k_x^2(n_y^2 + n_z^2)}{4}\Bigg) + Z_0^2 k_F^2 + 2k_x^2\Bigg] \\ B &= 256k_x^4\Bigg[4 + Z_{soc}^2(n_y^2 + n_z^2)\Bigg] \\ C &= 8Z_{soc}^2\Bigg[k_y^2(n_x^2 + n_z^2) - k_y n_y(k_x n_x + 2k_z n_z) + k_z^2(n_x^2 + n_y^2) \\ &\qquad - k_x k_z n_x n_z + \frac{k_x^2(n_y^2 + n_z^2)}{4}\Bigg] - 8Z_0^2 k_F^2 \\ D &= 16Z_{soc}^2 k_x n_x\Bigg[k_y n_y + k_z n_z\Bigg]. \end{aligned} \tag{196}$$

Use Eq. (194) and solve $\det(\mathbf{A}) = 0$ with respect to ε. We can find the energy modes given by $\varepsilon_i(\phi) = \pm\varepsilon_\sigma(\phi)$ with

$$\begin{aligned}\varepsilon_\sigma(\phi) &= \cos\left\{\frac{1}{2}\cos^{-1}\left(\frac{-\rho_\sigma b + \sqrt{b^2-4ac}}{2a}\right) - \left(\frac{\pi}{4} - \rho_\sigma\frac{\pi}{4}\right)\right\}\Delta \\ &= \cos\left\{\frac{1}{2}\cos^{-1}\left(\frac{\rho_\sigma\Big[\Big(A+B\Big)\cos(\phi) + 2C\Big(C+D\Big) + A - B\Big] + \sqrt{A^2+B^2-4C\big(C+D\big)-2A}\big(\cos(\phi)-1\big)}{2C\Big(C+D\Big)+2A}\right)\right. \\ &\quad \left. - \left(\frac{\pi}{4} - \rho_\sigma\frac{\pi}{4}\right)\right\}\Delta.\end{aligned} \tag{197}$$

Here, σ is a spin index such that $\rho_{\uparrow(\downarrow)} = 1(-1)$ for spin-up (spin-down) particles, and the $\pm$-sign in front of $\varepsilon_\sigma(\phi)$ indicated degenerated energy into a positive and negative mode. Thus, there are in total 4 possible energy modes for each parametric choice of Z_0, Z_{soc}, $\mathbf{k}$ and $\hat{\mathbf{n}}$.

This analytical BTK-like model is not capable of finding real energy modes for all combinations of the parameters Z_0, Z_{soc}, $\mathbf{k}$, and $\hat{\mathbf{n}}$. We can make a physical interpretation of this behavior; the analytical model cannot establish Andreev bound states for all parametric choices. However, chapter 7 demonstrates how the model nevertheless produces a similar current tendency as the numerical model through an sum over all k-modes for a specific spin-orbit orientation and barrier strength.

The Andreev bound energy states carry the supported supercurrent of the system. We can view this more clearly by the expression for the analytical current given by

$$I(\phi) = \frac{2e}{\hbar}\sum_i f(\varepsilon_i)\frac{d\varepsilon_i}{d\phi} \tag{198}$$

where i represents the sum over all energy modes and $f(\varepsilon)$ is the Fermi-Dirac distribution for the fermions. Since each energy mode is degenerated, we can rewrite the current into a sum over spin given by

$$I(\phi) = -\frac{2e}{\hbar}\sum_\sigma \tanh\left(\frac{\beta\varepsilon_\sigma}{2}\right)\frac{d\varepsilon_\sigma}{d\phi} \tag{199}$$

where we have used the Fermi-Dirac function defined in Eq. (130), and $\beta = \frac{1}{k_B T}$. Finally, the critical current is defined as

$$I_c = \max|I(\phi)|. \tag{200}$$

7

RESULTS

In chapter 5 and 6, we performed an explicit calculation of an analytical and a numerical model to describe an SC/HM/SC Josephson junction. We will use this chapter to present the supported supercurrent across the junction using these two independent models.

The analytical model considers an SC/SC junction with Rashba spin-orbit coupling imposed to the boundary conditions. The framework is approximating the heavy metal to be a thin film with a thickness of a few atomic distances, *i.e.* $\sim 1nm$. In general, any material that separates the two superconductors will provide a spin-orbit coupling with orientation perpendicular to the interface, $\hat{n} = \hat{x}$. This is regardless of the lattice structure of the respective material because the boundary layer between the material and the superconductors is independently breaking inversion symmetry. In order to obtain spin-orbit coupling for $\hat{n} \neq \hat{x}$, the material must have a non-centrosymmetric lattice structure.

Furthermore, the analytical model will try to provide bound states for a given k-mode. As discussed previously, it is not guaranteed that a bound state exists for every k-mode. The current is therefore calculated from a sum of distinct k-modes. In particular, for each $\mathbf{k}$ that corresponds to a real energy mode, the current has been calculated. The total current is then a summation of all sub-calculated current values for each real energy mode

$$I(\phi) = \sum_{\theta_k=0}^{\pi/2} \sum_{\phi_k=0}^{2\pi} I(\phi, \mathbf{k}) \tag{201}$$

where

$$\mathbf{k} = k_F \begin{bmatrix} \cos(\phi_k)\sin(\theta_k) & \sin(\phi_k)\sin(\theta_k) & \cos(\theta_k) \end{bmatrix}. \tag{202}$$

We have computed the current with a finite increment of $\delta\phi_k, \delta\theta_k = \frac{\pi}{4}$. All plots, provided by the analytical model, are normalized with respect to a constant normalization factor $I_0 = e\Delta/\hbar$. In our analysis, the parameters $\Delta = 3meV$, $E_F = 5eV$, and $T = 3meV$ are fixed. The scattering potential is present through the dimensionless parameter Z_0. This parameter is introduced to simulate a physical barrier, where $Z_0 = 0$ corresponds to an absent barrier that fully supports particles to tunneling across the interface. In the opposite regime, values of $Z_0 \gg 1$ result in a vanishing tunneling amplitude, and all particles are scattered

away at the interface. Hence, the parametric choices of $Z_0 \simeq 0 \rightarrow 10$ is reasonable values for the scattering potential [57]. We are assuming that a similar dimension would be beneficial to the spin-orbit potential, such that $Z_{soc} \simeq 1 \rightarrow 10$.

In the numerical model, the heavy metal has a finite length (thickness) of N_{HM}. The superconducting gap can be solved in a self-consistent manner, as described in section 5.2.1. Even though the calculation itself is easy, it turns out that the convergence process is time-consuming. A system with dimensions $N_x = 55$, and $N_y = N_z = 29$ needs about 2×10^3 iterations according to a convergence requirement of tolerance $= 10^{-4}$. In order to search across the superconducting phase ϕ, to find the critical current for every parametric choice of λ and $\hat{n}$, the number of iterations desired to investigate the current behavior has to be approximately $\sim 10^7$. As a result of this, it would be a great advantage to avoid a self-consistent solution.

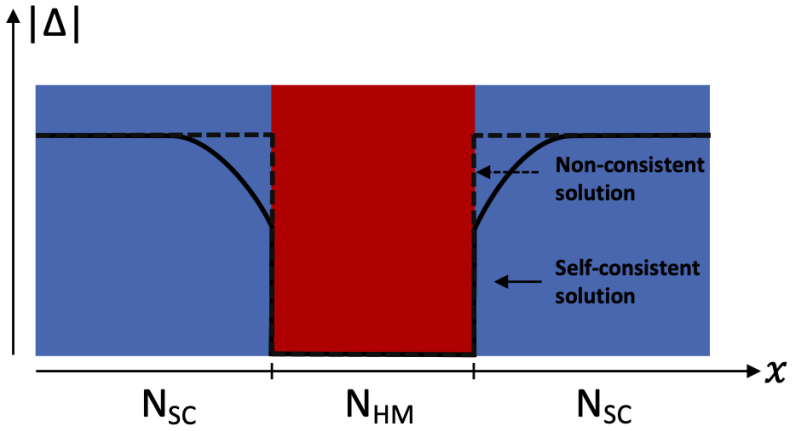

Figure 13: The superconducting gap $|\Delta|$ across the junction. We have illustrated a qualitative behavior of the self-consistent solution versus a non-consistent solution.

We tried solving the gap in a non-consistent manner, meaning we chose a constant value for Δ inside the superconductor and zero elsewhere. Such an approach will not provide the supercurrent an exact value, since the proximity effect will decrease Δ close to the interface. The different behaviors of $|\Delta|$ are illustrated in Fig. 13, which makes it clear that a non-consistent approach will deviate from a self-consistent solution. However, we will only investigate the supercurrent while adjusting properties of the weak link, *e.g.* spin-orbit magnitude λ, orientation $\hat{n}$, chemical potential μ_{HM}, and thickness N_{HM}. Thus, it is chosen a fixed non-consistent solution of $|\Delta|$ in all subsequent numerical results. The approach is justified because a static non-consistent solution will provide a stationary reference when studying the relative change in current magnitude. An exploration of the current behavior demonstrated that the relative change in the current magnitude is preserved through a non-consistent approach. The inspection was done for a spin-orbit orientation in the yz-plane, and the retained

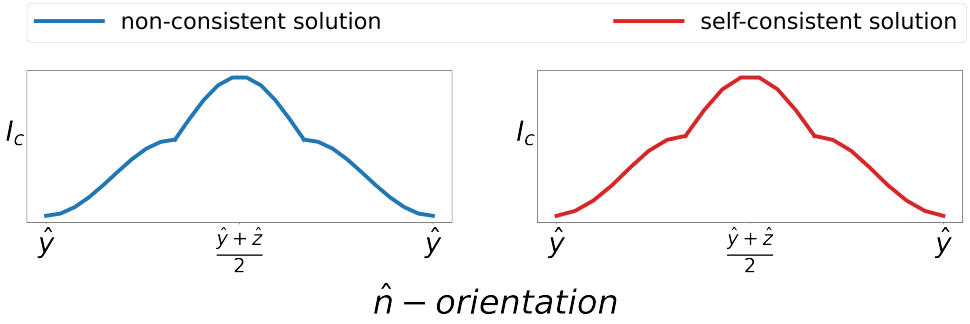

Figure 14: This is a qualitative comparison of the current behavior provided by a non-consistent (left panel) and a self-consistent solution (right panel) of the gap Δ. Both curves are produced with a spin-orbit magnitude $\lambda = 0.3t$. We have not included numbers representing the current magnitude on the y-axis, as we were interested in comparing the current's behavior while adjusting the spin-orbit coupling. Nevertheless, we can conclude that solving the superconducting gap in a non-consistent manner will produce a similar qualitative behavior as a self-consistent solution. We will elaborate further on the results in section 7.2.

behavior between the self-consistent and non-consistent solution is illustrated in Fig. 14. As a result, all numerical results in this thesis are solved in a non-consistent manner with $|\Delta| = 0.003t$ inside the superconductors and zero elsewhere. The geometry of the system is $N_{SC_L} = 25$, $N_{HM} = 5$, $N_{SC_R} = 25$, and $N_y = N_z = 29$ unless otherwise indicated. Other properties are $t = 1$, $T = 0.003$, and $\mu_{SC} = 0.0$, meaning that $\Delta\mu$ corresponds to an adjustment of the chemical potential of the heavy metal of unit t.

7.1 1D - SC/HM/SC JOSEPHSON JUNCTION

In this section, we will consider a one-dimensional SC/HM/SC junction. The limits of dimensions may arise in a Josephson junction nanowire. Consequently, the Cooper pairs can only travel along with the momentum mode $\mathbf{k} = k_F\hat{x}$, that is along the x-direction. We are not making any restrictions for the possible $\hat{n}$ orientations, meaning the spin-orbit coupling can be orientated in any spatial directions.

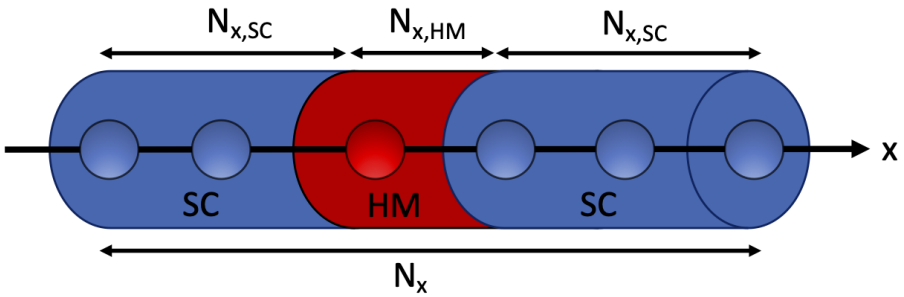

Figure 15: Suggested experimental setup of a 1D SC/HM/SC nanowire.

7.1.1 *Numerical approach*

To simulate a one-dimensional nanowire, we say that it consists of only one lattice point in y- and z-direction. We have implemented the restriction to the numerical system by choosing $N_y = N_z = 1$, implying $\mathbf{k} = k_F\hat{x}$. The only valid k-mode is therefore the one perpendicular to the interface. A demonstration of the supported supercurrent as a function of spin-orbit orientation is shown in Fig. 16. As expected from the geometry of the junction, there are several symmetry aspects in the current behavior.

First, the current is to be invariant for all $\hat{n} \in yz$-plane, *i.e.* the current is independent of the spin-orbit vector orientation as long as it is parallel to the interface. Recall the definition of spin-orbit coupling as $\hat{H} \propto \mathbf{k} \times \hat{n}$. From the definition, this behavior is expected since a spin-orbit orientation parallel to the interface ($\hat{n} \perp \hat{x}$) will influence all x-travelling particles equally in the absence of transverse propagating modes.

Second, when the spin-orbit vector is perpendicular to the interface, $\hat{n} = \hat{x}$, the spin-orbit coupling is not affecting the current. This is expected according to the definition of the spin-orbit Hamiltonian, where we consider a cross-product of the particles' momentum and the spin-orbit vector characterization. Note that this is only true for one dimension. The results can become more complicated in the three dimensions where k_y and k_z can influence the supercurrent.

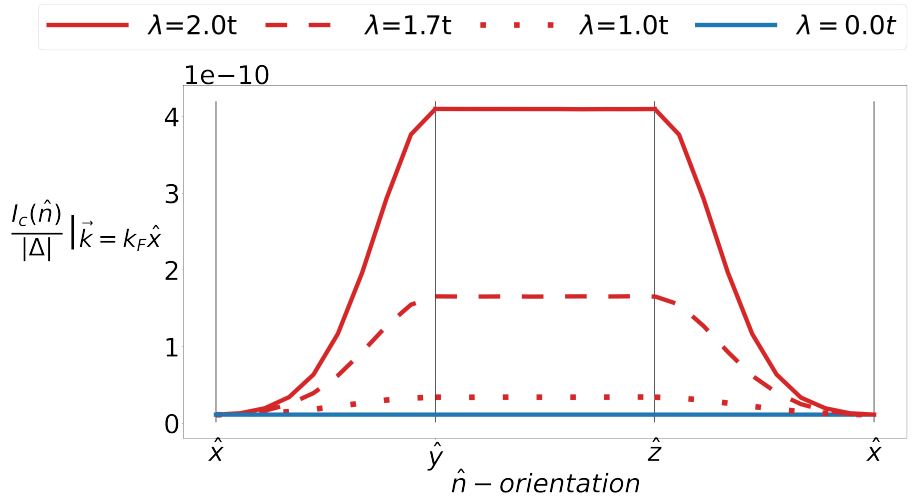

Figure 16: The supported supercurrent through an SC/HM/SC junction for different magnitude and vector orientation of the spin-orbit coupling imposed to the heavy metal. The blue line is the supported supercurrent without any spin-orbit coupling ($\lambda = 0$) and holds a current magnitude of 2.8% compared to the solid red line for $\lambda = 2$. The plots are created with our numerical model with a non-consistent solution of $\Delta = 0.003t$. Other parameters are $t = 1$, $\Delta\mu = 1$, $T = 0.003$, $N_{SC_L} = 25$, $N_{HM} = 5$, $N_{SC_R} = 25$, and $N_y = N_z = 1$.

Let us now consider the current behavior while varying the spin-orbit magnitude, shown in Fig. 17. First, note that the current exhibits three distinct peaks, before it stabilizes around a constant value. Second, a strong spin-orbit coupling will provide a current which is larger in magnitude compared to an SC/NC/SC junction with no spin-orbit coupling ($\lambda = 0$). This observation indicates that a strong spin-orbit coupling will increase the current in one dimension. Keep in mind that experimental values for spin-orbit magnitude are at maximum about $\lambda_{max} \sim 3eV\mathring{A}$, which in our framework with lattice spacing $a = 1$ corresponds to $\lambda_{max} \sim 3t$ [26]. The very large λ values are calculated with the intention to show a current tendency.

7.1.2 *Analytical approach*

We are now going to solve the one-dimensional system with our analytical BTK-like model. By choosing a spin-orbit orientation perpendicular to the interface, $\hat{n} = x$, the bound states are expected to be independent of the spin-orbit coupling. The analytical energy support this by reducing to

$$\varepsilon = \pm\cos\left\{\frac{1}{2}\cos^{-1}\left(\frac{Z_0^2 + 4\cos(\phi)}{Z_0^2 + 4}\right)\right\}\Delta. \tag{203}$$

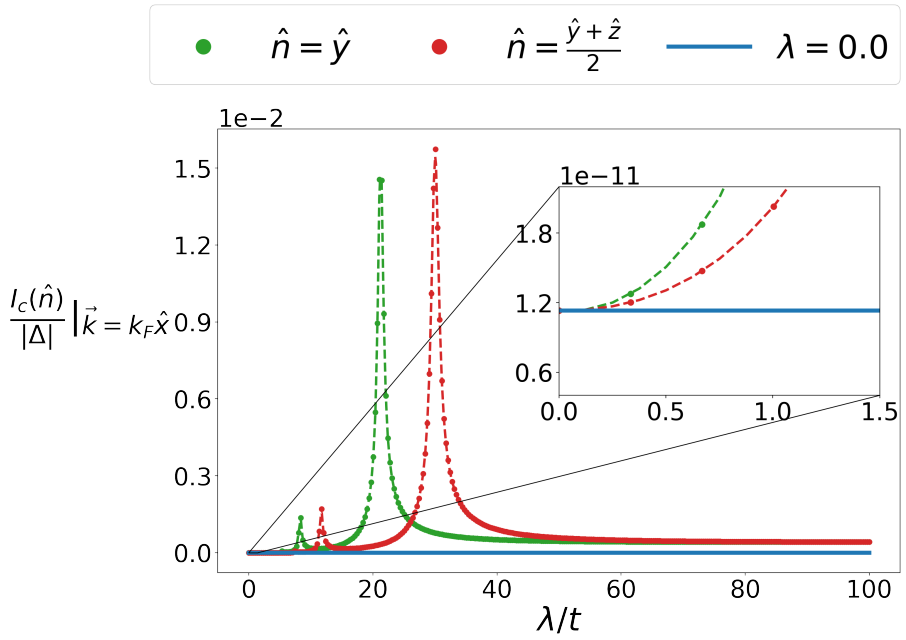

Figure 17: The supported supercurrent through an SC/HM/SC junction for different magnitude and vector orientation of the spin-orbit coupling imposed to the heavy metal. The blue line is the supported supercurrent without spin-orbit coupling, $\lambda = 0$. The plots are created with our numerical model with a non-consistent solution of $\Delta = 0.003t$. Other parameters are $t = 1$, $\Delta\mu = 1$, $T = 0.003$, $N_{SC_L} = 25$, $N_{HM} = 5$, $N_{SC_R} = 25$, and $N_y = N_z = 1$.

Consequently, a spin-orbit orientation of $\hat{n} = \hat{x}$ is not affecting the supported supercurrent across the junction. It is consistent with the numerical results and the definition of the spin-orbit coupling Hamiltonian which couples the spin and the momentum through a cross product.

We have now explored that an orthogonal spin-orbit orientation concerning the interface will remove the spin-orbit dependency. For the following, study the spin-orbit orientation, $\hat{n}$, to be aligned parallel to the interface. That is $n_x = 0, n_y \neq 0, n_z \neq 0$. The solutions of the respective bound states are then

$$\varepsilon_\sigma = \Delta \cos\left\{\frac{\pi}{4}\left(\rho_\sigma - 1\right) + \frac{1}{2}\cos^{-1}\left(\frac{\rho_\sigma 16 k_x^4\left[4Z_0^2 + 3Z_{soc}^2 + 16\right]\cos(\phi) + \rho_\sigma k_x^4\left[\left(Z_{soc}^2 - 4Z_0^2\right)^2 - 16\left(Z_{soc}^2 - 4Z_0^2\right)\right] + i8k_x^4 Z_{soc}\left(4Z_0^2 - Z_{soc}^2\right)(\cos(\phi) - 1)}{k_x^4\left[\left(Z_{soc}^2 - 4Z_0^2\right)^2 + 32\left(Z_{soc}^2 + 4Z_0^2 + 8\right)\right]}\right)\right\}. \tag{204}$$

Discover that these spin-dependent energy modes are independent of n_y and n_z. In other words, the energy modes are invariant for spin-orbit orientations parallel to the interface. This is consistent with the numerical result with an invariant current magnitude for $\hat{n} \in yz$-plane.

Furthermore, pay attention to the impact of the scattering potential Z_0 and the spin-orbit potential Z_{soc}. Observe how the choice of $Z_{soc} = 2Z_0$ will reduce the

expression of the energy modes into the well known SC/SC Josephson junction without any barrier potential given by

$$\varepsilon = \pm \cos(\phi/2)\Delta. \tag{205}$$

The result tells us that it is possible to make the effective barrier disappear for a specific relation of the scattering- and spin-orbit potential. This finding provides the effective barrier to be strongly related to the ratio of scattering- and spin-orbit potential. We have already observed a similar effect in the numerical results (Fig. 17) where we could detect the supercurrent peaking to distinct values of the spin-orbit magnitude. Unlike the analytical model, the numerical model does not have any parameters corresponding to a scattering potential (Z_0). However, section 4.2 argued that a different chemical potential between the superconductors and the heavy metal would contribute to a barrier. Consequently, this result from one dimension, where the effective barrier vanishes completely when the scattering- and spin-orbit potential takes a specific relationship, motivates an investigation of the supercurrent for different chemical potential. We will inspect this connection further when we extend to three dimensions in the next section by varying the chemical potential difference.

As mentioned previously, the analytical model cannot find Andreev bound states for all parametric choices. In this one-dimensional case where $\mathbf{k} = \hat{x}$, the model does not provide real energy values when $\hat{n} \in xy$-plane. However, the model can find real eigenvalues for the specific orientations of $\hat{n} = \hat{x}$ and $\hat{n} \in yz$-plane.

7.1.3 *Summary remarks*

Through both the analytical and the numerical model, we have demonstrated how the supercurrent is invariant when the spin-orbit coupling is orientated parallel to the interface. Furthermore, we have shown that the spin-orbit coupling does not affect the current for an orientation perpendicular to the interface. This is as expected according to a one-dimensional case where the particles only propagate perpendicular to the interface. In addition, Rashba spin-orbit coupling is a phenomenon that arises when particles travel across an electric field, shown in the Hamiltonian in Eq. (112), making this outcome reasonable.

The numerical model has given us insight into the spin-orbit coupling's ability to increase the supercurrent compared to a junction without spin-orbit coupling. The analytical model could not provide bound states for all spin-orbit magnitudes. However, we did prove that within a specific scattering- and spin-orbit potential relation, the analytical expression for the supported supercurrent reduces into an SC/SC junction with absent barrier effects. The discovery insinuates that the supercurrent is strongly related to the ratio of the chemical

potential and the spin-orbit coupling. We will continue the investigation in section 7.2 for a three-dimensional junction, aiming to understand the behavior in a physical manner.

7.2 3D - SC/HM/SC JOSEPHSON JUNCTION

After breaking down the problem in one dimension, as done in section 7.1, we can now extend the system to three dimensions. In the previous section, we confirmed that the k_x-modes were influenced by the spin-orbit coupling within the orientation $\hat{n} \in yz$-plane. This section will study the current where a three-dimensional junction allows for the transverse k-modes to be valid.

7.2.1 *Numerical approach*

The geometry of the junction investigated by the numerical model is shown in Fig. 18.

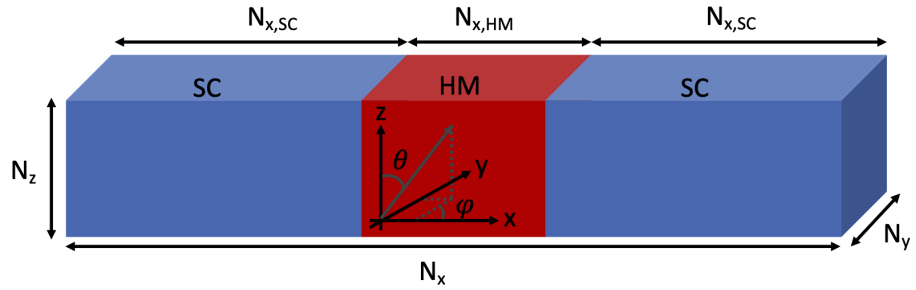

Figure 18: A numerical setup of a SC/HM/SC junction.

There are several interesting aspects to observe in order to keep track of all parameters that affect the supported supercurrent across an SC/HM/SC junction. We have in this section investigated the current related to the length of the incorporated heavy metal with Rashba spin-orbit coupling (L_{HM}), the spin-orbit magnitude (λ), spin-orbit orientation ($\hat{n}$), and the chemical potential difference between the superconductor and the heavy metal ($\Delta\mu$)

The calculated supercurrent across an SC/HM/SC junction as a function of the thickness of the heavy metal is shown in Fig. 19. The various lines in the respective figure represent different spin-orbit orientations indicated by color. Notice how the supercurrent decreases as a function of thickness. The reducing current magnitude is present without any superimposed oscillations, which we would get in a magnetic SC/F/SC junction [14] as discussed in section 3.2. Such oscillations are caused by a non-zero center-of-mass momentum which creates Cooper pairs with triplet symmetry. The current influenced by spin-orbit coupling acts in a similar manner as expected for a normal scattering potential which would be present in an SC/NC/SC junction. Consequently, the observation corroborates an understanding of spin-orbit coupling to provide

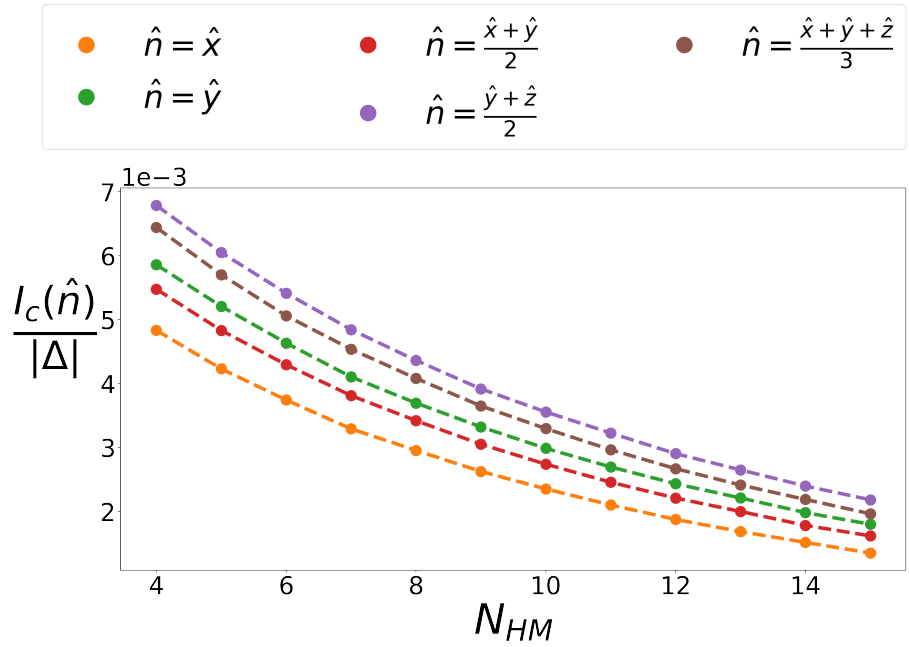

Figure 19: Supported supercurrent through a S/HM/S junction with spin-orbit coupling present in the heavy metal. The plot demonstrates the decreasing current as a function of the grid length of the heavy metal. The calculations have been done numerically with a non-consistent solution of $\Delta = 0.003t$. Each line represents a different orientation of the spin-orbit vector characterization. The spin-orbit magnitude is fixed to $\lambda = 1t$, and the chemical potential difference is $\Delta\mu = 0.7t$. Other parameters are $t = 1$, $T = 0.003$, $N_{SC_L} = 25$, $N_{SC_R} = 25$, and $N_y = N_z = 29$.

a supercurrent carried by normal Andreev reflection and Cooper pairs with singlet symmetry.

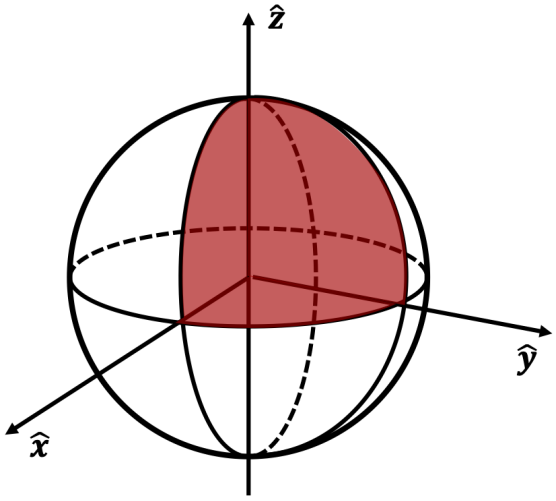

Figure 20: Three-dimensional unit sphere in real space. Due to symmetry, it is sufficient to only evaluate spin-orbit orientations on the red surface.

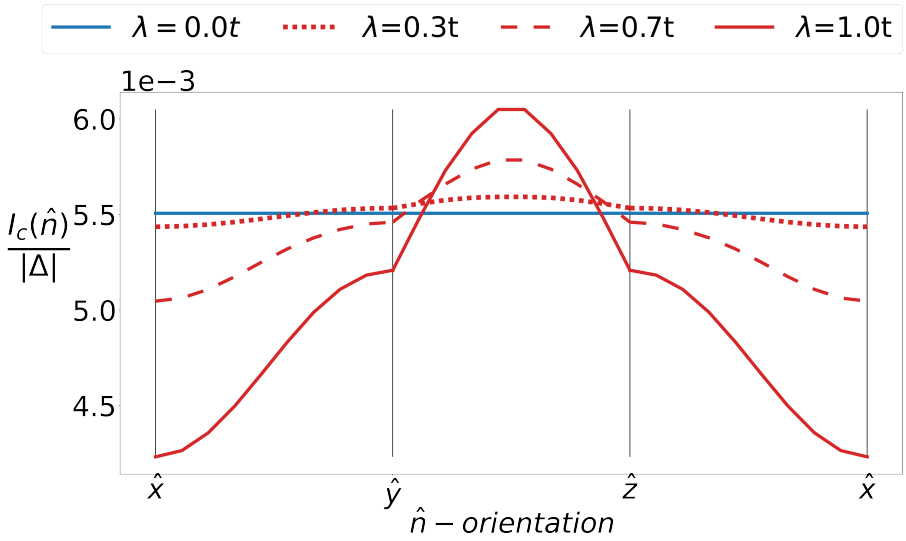

Figure 21: The supported supercurrent through an SC/HM/SC junction for different spin-orbit orientations. The blue lines in is the supported supercurrent in absence of spin-orbit coupling. The figure is created with our numerical model with a non-consistent solution of $\Delta = 0.003t$. The chemical potential is fixed at $\Delta\mu = 0.7t$. Other parameters are $t = 1$, $T = 0.003$, $N_{SC_L} = 25$, $N_{HM} = 5$, $N_{SC_R} = 25$, and $N_y = N_z = 29$.

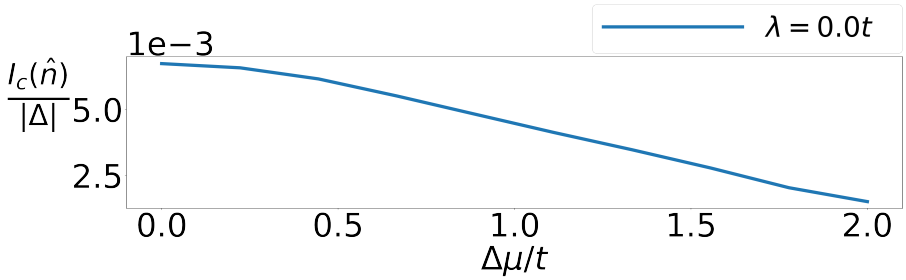

Figure 22: The supported supercurrent through an SC/NC/SC junction. Such a junction is similar to an SC/HM/SC junction with absent spin-orbit coupling ($\lambda = 0t$). The figure is created with our numerical model with a non-consistent solution of $\Delta = 0.003t$. $N_{NC} = 5$. Other parameters are $t = 1$, $T = 0.003$, $N_{SC_L} = 25$, $N_{SC_R} = 25$, and $N_y = N_z = 29$.

For further investigations of the spin-orbit coupling and its relation to supercurrent, utilize a fixed thickness of the heavy metal to $N_{HM} = 5$. The following will demonstrate the behavior of the current for different spin-orbit orientations $\hat{n}$. A geometrical symmetry of the junction makes it sufficient to only solve the system for $\hat{n}$ orientations on the red surface indicated in Fig. 20. We have used a fixed chemical potential difference ($\Delta\mu = 0.7t$) between the superconductors and the heavy metal. The supported supercurrent for the distinct $\hat{n}$ orientations are shown in Fig. 21, where the various lines present different spin-orbit magnitudes (λ). Notice that the current magnitude takes the lowest value when the spin-orbit orientation is pointing perpendicular to the interface, *i.e.*

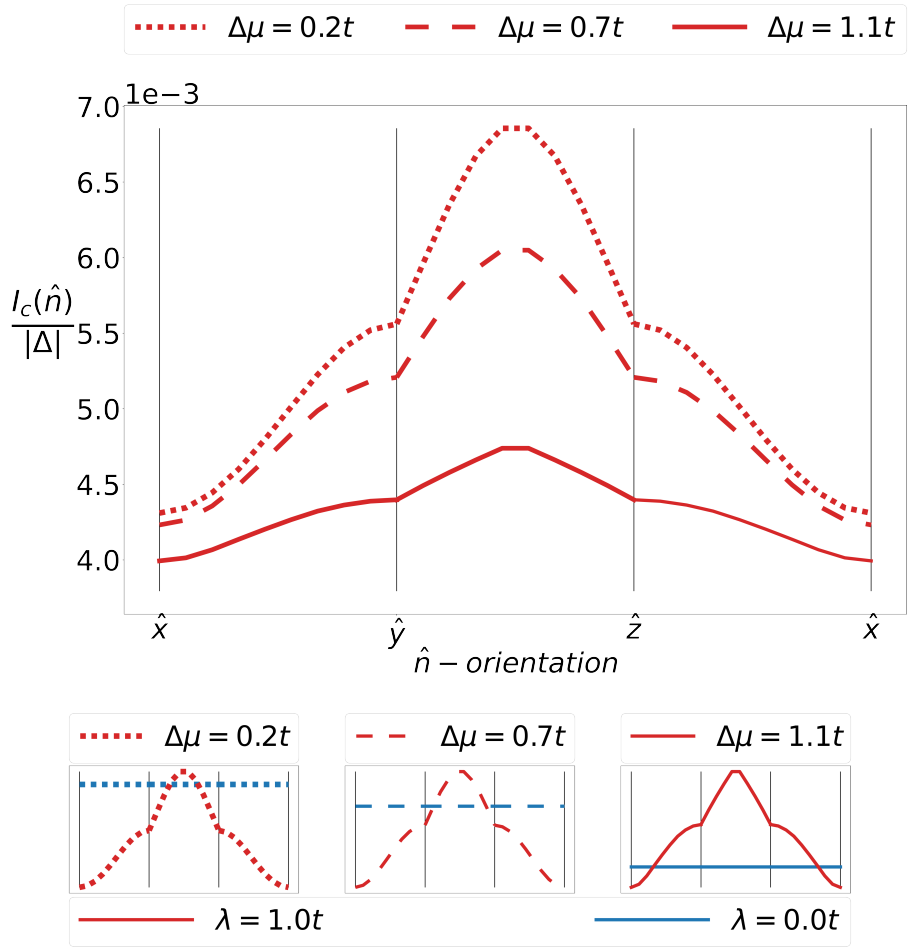

Figure 23: The supported supercurrent through an SC/HM/SC junction for different vector orientations of the spin-orbit coupling imposed to the heavy metal. The various lines (solid-dashed-dotted) demonstrated the impact of different chemical potential between the two superconductors and the heavy metal. The upper panel utilizes a fixed spin-orbit coupling magnitude of $\lambda = 1t$. The lower panel compares the current in the presence of a finite spin-orbit magnitude and the case without. That is $\lambda = 1t$ denoted by the red lines versus $\lambda = 0t$ denoted by the blue lines. The figure is created with our numerical model with a non-consistent solution of $\Delta = 0.003t$. Other parameters are $t = 1$, $T = 0.003$, $N_{SC_L} = 25$, $N_{HM} = 5$, $N_{SC_R} = 25$, and $N_y = N_z = 29$.

$\hat{n} = \hat{x}$, and increases as the orientation of the spin-orbit coupling reaches the yz-plane. This tendency is according to the one-dimensional outcomes. However, the current magnitude is not invariant for all spin-orbit orientations parallel to the interface, *i.e.* $\hat{n} \in yz$-plane. The supercurrent is greatest for a orientation $\hat{n} = \sqrt{\frac{1}{2}}(0,1,1) = \frac{\hat{y}+\hat{z}}{2}$. This is inconsistent with the one-dimensional results, thus the different behavior is explained by the contribution of particles with a parallel wave vector component.

Furthermore, we have calculated the supported supercurrent for different $\hat{n}$ orientations with a varying chemical potential difference ($\Delta\mu$). The red lines in Fig. 23 indicates the current for different chemical potential with a fixed spin-orbit magnitude ($\lambda = 1.0t$). The lower panel includes three blue lines included as a state of reference with no spin-orbit coupling present, *i.e.* $\lambda = 0$. The current magnitude is expected to decrease for large $\Delta\mu$. This is confirmed by Fig. 22 which shows the current for increasing chemical potential difference in the absence of spin-orbit coupling. Pay attention to Fig. 23 which provides the current as a function of the spin-orbit orientation with a varying chemical potential difference. Keep in mind that an increasing chemical potential difference provides a decreasing current magnitude. Consequently, the current with finite spin-orbit coupling will also increase as $\Delta\mu$ decreases. This is reasonable since $\Delta\mu$, alone, is a potential barrier. Thus, a significant barrier makes it hard for particles to propagate across the interface. Furthermore, observe how the red lines for finite spin-orbit coupling ($\lambda \neq 0$) are related to the blue lines with absent spin-orbit coupling ($\lambda = 0$). This relation is manifested in the lower panel: When $\Delta\mu = 0.2t$, all spin-orbit orientation with $\lambda = 1$ will correspond to a larger current magnitude compared to $\lambda = 0$. On the other hand, when $\Delta\mu = 1.1t$, the spin-orbit coupling will only provide a larger current magnitude when $\hat{n} \in yz$-plane. This finding states that the ratio of the spin-orbit coupling magnitude and chemical potential difference plays an important role. In addition, it is consistent with the result from one dimension where we noted that the effective barrier vanishes under a specific relation of the scattering- and spin-orbit coupling potential.

We will now investigate the current developed under an increasing spin-orbit magnitude, provided in Fig. 24. The plot shows different orientations of $\hat{n}$ indicated by color. The blue line denotes a state of reference in the absence of spin-orbit coupling. In general, regardless of the spin-orbit orientation, the current magnitude will increase until a critical value before it decreases. Some orientations have several critical points. The respective spin-orbit magnitude, where the critical point occurs, depends on the orientation of $\hat{n}$. We can observe that the greatest current magnitude corresponds to a orientation of $\hat{n} = \frac{1}{\sqrt{2}}(0, 1, 1) = \frac{\hat{y}+\hat{z}}{2}$. This is consistent with the previous result for current magnitude as a function of spin-orbit orientation in Fig. 21. Again, keep in mind that experimental values for spin-orbit magnitude are at maximum $\lambda_{max} \sim 3eV\text{Å} \sim 3t$ [26], such that the current for very large λ are calculated with the intention to show tendency.

7.2.2 *Analytical approach*

We will now provide the result from the analytical BTK-like model which investigates an SC/SC junction with scattering- and spin-orbit potential imposed to the boundary. A geometrical illustration of the junction is present in Fig. 25.

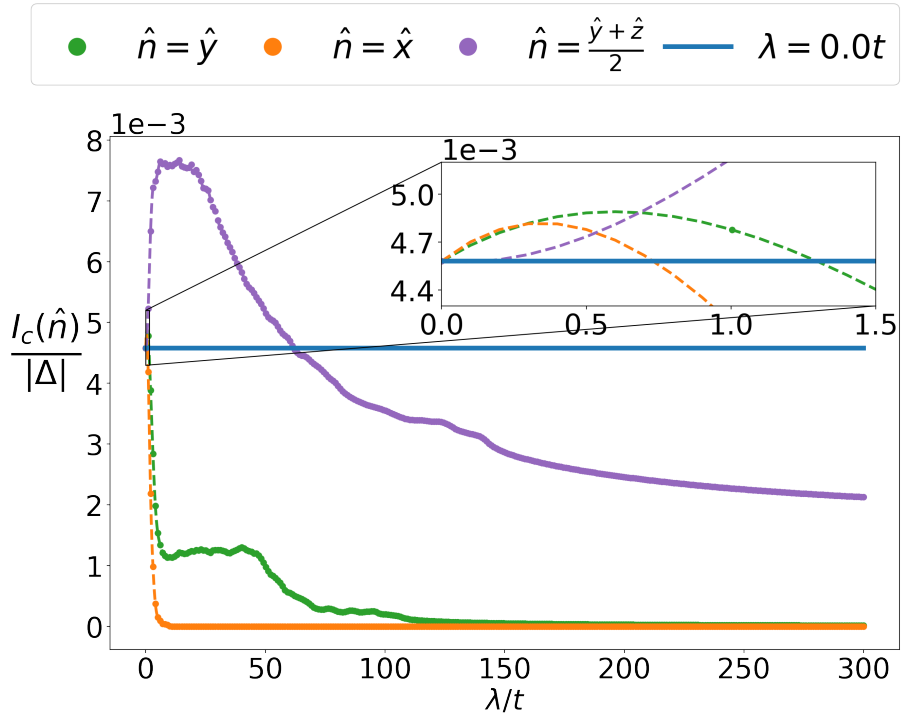

Figure 24: Supercurrent as a function of spin-orbit magnitude across an SC/HM/SC junction calculated by the numerical model utilizing a non-consistent solution of $\Delta = 0.003t$. The chemical potential difference is $\Delta\mu = 1t$. Other parameters are $t = 1$, $T = 0.003$, $N_{SC_L} = 25$, $N_{HM} = 5$, $N_{SC_R} = 25$, and $N_y = N_z = 29$.

Keep in mind that the analytical model treats the heavy metal as a boundary effect. Thus, the framework can not provide any relation to the thickness of the heavy metal. If we would like to solve for a finite thickness, the framework would need an extension requiring a set of wave functions inside the heavy metal, along with additional boundary conditions to treat the SC/HM- and HM/SC-interfaces.

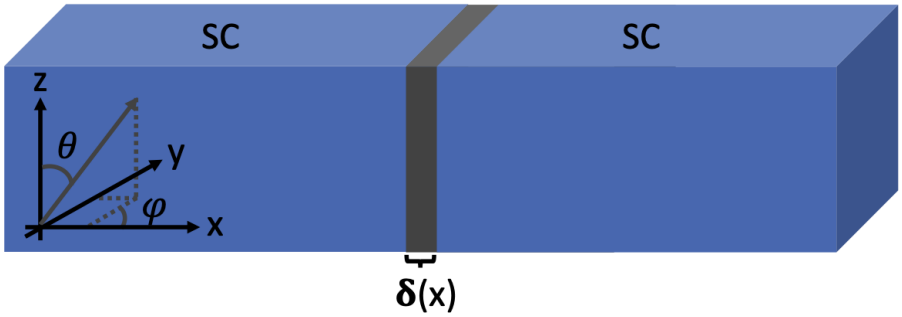

Figure 25: Analytical setup of a SC/SC Josephson junction divided by a δ-barrier

Begin by exploring the current as a function of the spin-orbit orientation $\hat{n}$, given in Fig. 26. We have calculated the current magnitude for different spin-

orbit potential (Z_{soc}) at a fixed scattering potential (Z_0). Notice that the analytical

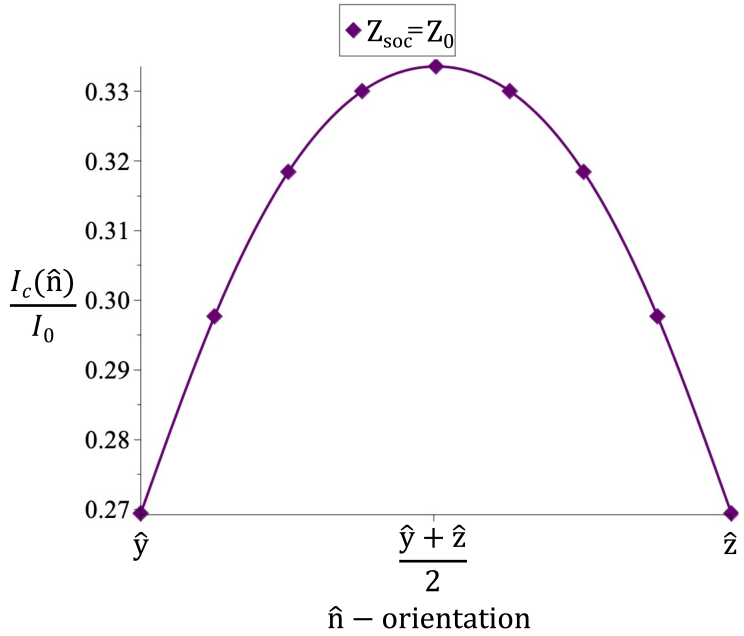

Figure 26: Critical current as function of spin-orbit coupling orientation parallel to the interface, i.e. $\hat{n} \in yz$-plane. The plot is produced by the analytical model with a static scattering- and spin-orbit potential $Z_{soc} = Z_0 = 2$. Other parameters are $\Delta = 3meV$ and $E_F = 5eV$. The normalization constant is $I_0 = \frac{e\Delta}{\hbar}$.

model provides a similar current behavior as produced by the numerical model: The current magnitude is most significant for a spin-orbit orientation $\hat{n} = \frac{\hat{y}+\hat{z}}{2}$ compared to $\hat{n} = \hat{y}(\hat{z})$.

Next, consider the current as a function of the effective barrier potential. The result from one dimension in section 7.1 suggests that the current depends on the relation between the scattering potential (Z_0) and the spin-orbit potential (Z_{soc}). In order to investigate this connection, the current has been calculated as a function of spin-orbit magnitude in Fig. 27 and as a function of scattering potential in Fig. 28.

The analytical model predicts a similar current trend as the numerical model. The left panel of Figures 27a and 28a demonstrated the current for a spin-orbit orientation $\hat{n} = \hat{y}$, where the current magnitude increases towards a critical point before decreasing. Furthermore, given a non-zero scattering- and spin-orbit potential, we can explore how the two potentials have an inverted impact on the supported supercurrent. The right panel of Figures 27 and 28 shows the current for a spin-orbit orientation $\hat{n} \in \{\hat{y}, \frac{\hat{y}+\hat{z}}{2}\}$. We have included this scope of $\hat{n}$-orientations based on the previous result for the current as a function of $\hat{n}$, where the calculation provided an asymmetric magnitude relation in the respective $\hat{n}$-region. Given these spin-orbit orientations, the current demonstrates that the two potential barriers are opposed to each other. We can observe this

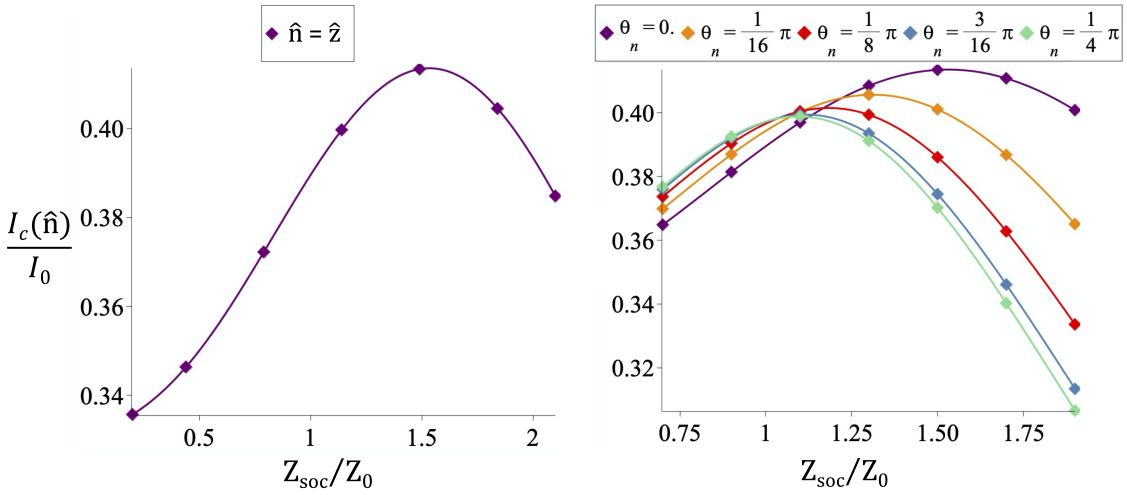

Figure 27: The two panels shows the supported supercurrent as a function of the spin-orbit coupling magnitude Z_{soc}. The plot is made with the analytical model with a static scattering potential of $Z_0 = 1$. Other parameters are $\Delta = 3meV$ and $E_F = 5eV$. The normalization constant is $I_0 = \frac{e\Delta}{\hbar}$. The left panel shows the current for $\hat{n} = \hat{z}$. The right panel shows the current for different orientation of the spin-orbit coupling. The different lines represent an orientation parallel to the interface. That is $\hat{n} = (0, \sin(\theta_n), \cos(\theta_n))$, where θ_n is indicated in the figure legend. In particular, the purple one is $\hat{n} = \hat{z}$ while the green one is $\hat{n} = \frac{\hat{y}+\hat{z}}{2}$.

by looking at the different lines representing various spin-orbit orientations of $\hat{n} \in \{\hat{y}, \frac{\hat{y}+\hat{z}}{2}\}$ which are crossing in an inverted order in Fig. 27b versus Fig. 28b. Once more, this outcome strengthens the suspicion that the current magnitude is strongly related to the ratio of scattering- and spin-orbit potential. This is analogous to the ratio between the chemical potential and the spin-orbit potential regarding the numerical model.

7.2.3 *Summary remarks*

Before we discuss the underlying physics behind these results, let us briefly summarize the main observations related to three dimension. First, we have observed that the supercurrent depends on the spin-orbit orientation $\hat{n}$, expected since the interaction couples spin and momentum. This behavior is different from the currents dependency on the magnetic field orientation in a ferromagnetic Josephson junction. Second, we have demonstrated that a $\hat{n}$ parallel to the interface provides the most significant changes in the magnitude of the supercurrent compared to a junction without spin-orbit coupling. Moreover, this observation was predicted according to the definition of spin-orbit coupling,

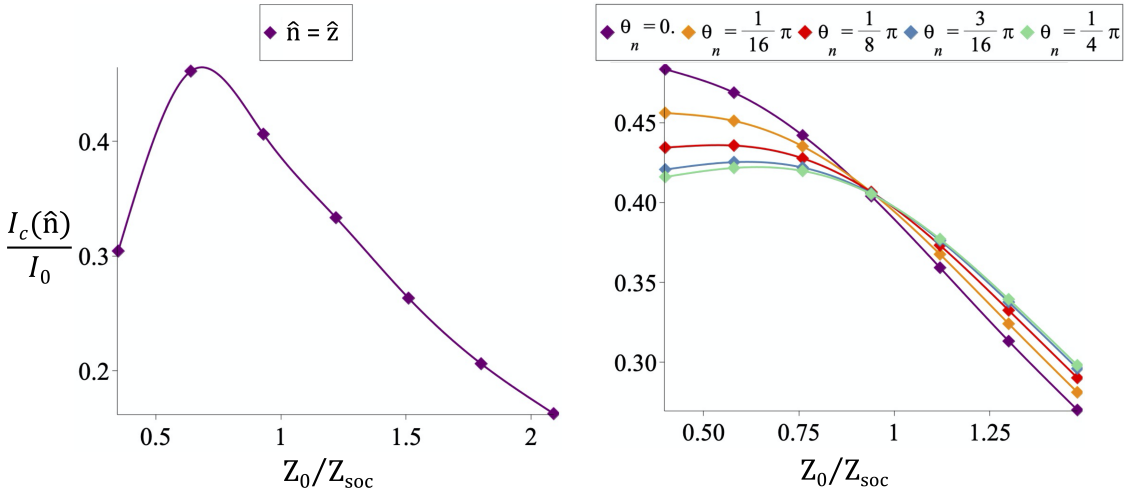

Figure 28: The two panels shows the supported supercurrent as a function of the scattering potential Z_0. The plot is made with the analytical model with a spin-orbit magnitude of $Z_{soc} = 1$. Other parameters are $\Delta = 3meV$ and $E_F = 5eV$. The normalization constant is $I_0 = \frac{e\Delta}{\hbar}$. The left panel shows the current for $\hat{n} = \hat{z}$. The right panel shows the current for different orientation of the spin-orbit coupling. The different lines represent an orientation parallel to the interface. That is $\hat{n} = (0, \sin(\theta_n), \cos(\theta_n))$, where θ_n is indicated in the figure legend. In particular, the purple one is $\hat{n} = \hat{z}$ while the green one is $\hat{n} = \frac{\hat{y}+\hat{z}}{2}$.

which includes a cross-product between the particle's momentum and spin-orbit orientation.

We have previously argued that the system is invariant along the y- and z-direction. Therefore, it is expected to obtain an equal magnitude of the supercurrent for a spin-orbit orientation along those two axes. Both the numerical and analytical models confirm this. However, if the two directions were purely equal, we could suppose the current to be invariant for all spin-orbit orientations with the basis $\hat{n} = n_y\hat{y} + n_z\hat{z}$. An increased current magnitude for a spin-orbit orientation in between those two axes, $\hat{n} = \frac{\hat{y}+\hat{z}}{2}$, was therefore not expected at first glance. Nevertheless, the symmetry between $\hat{n} = \hat{y}$ and $\hat{n} = \hat{z}$ only provides invariant physical observables, *e.g.* supercurrent. Two invariant states can therefore deviate by a local phase. Recall that a spin-orbit interaction couples the spin and the momentum of a particle. Hence, we believe the two spin-orbit orientations of $\hat{n} = \hat{y}$ and $\hat{n} = \hat{z}$ to have an underlying inverted spin/momentum symmetry which we will investigate further in the following chapter. Furthermore, to understand how the spin-orbit coupling influences the current, we can use the barrier matrix to the analytical SC/SC junction. In the next chapter, we will do this and also discuss how the change in the Fermi surface, induced by the spin-orbit coupling, influences the supercurrent.

8

DISCUSSION OF RESULTS

The results' after investigating the supercurrent with the numerical and analytical framework show three significant findings regarding the supercurrent across an SC/HM/SC junction with spin-orbit coupling:

1. The length (thickness) of the incorporated material with spin-orbit coupling is demonstrated to affect the supported supercurrent. Its influence to the supercurrent is present in a similar manner as for a normal material without spin-orbit coupling; as the length of the weak link gets longer, the current decrease. This is expected from the superconducting proximity and superconducting coherence length. In addition, the current magnitude does not oscillate in our results in comparison to a magnetic SC/F/SC junction.

2. The strength of the spin-orbit coupling influences the supercurrent. There is a critical region for the spin-orbit magnitude where the supported supercurrent is increasing towards a critical point. As a result, we can predict a greater current compared to a junction with normal metal without spin-orbit coupling. The numerical calculations have demonstrated that the supported supercurrent will decrease towards zero for sufficiently strong interactions. This is consistent with an infinitely strong barrier.

3. The maximum magnitude of the supported supercurrent is determined, not only by the magnitude of the spin-orbit coupling, but also by the direction of the vector $\hat{n}$ characterizing the inversion symmetry breaking. Interestingly, this is in stark contrast to magnetic SC/F/SC junctions, where the supercurrent is independent of the direction of the spin-splitting field. The spin-orbit orientation also affects which spin-orbit magnitude that reflects the maximal current value.

Symmetry provides the argument that the two directions $\hat{y}$ and $\hat{z}$ are invariant and, consequently, follow the same physical interpretation. This is confirmed by both the numerical and analytical results where $\hat{n} = \hat{y}$ gives equal current magnitude as for $\hat{n} = \hat{z}$. As a result, we can observe three distinguish orientations of the spin-orbit orientation: $\hat{n} = \left\{\hat{x}, \hat{y}(\hat{z}), \frac{\hat{y}+\hat{z}}{2}\right\}$.

8.1 SPIN-ORBIT ORIENTATION SIGNIFICANCE TO DISPLACE FERMI SURFACE

In chapter 4, we accounted for the Fermi surface of the superconductor and the consequence related to the conservation of k_y and k_z. To understand how spin-orbit coupling enhances Josephson effect, we begin by studying the prevalence of the Fermi vector mismatch. For that sake, we will establish an overview of the Fermi surfaces of the heavy metal for different spin-orbit orientations.

According to the spin-orbit coupling Hamiltonian defined in Eq. (88), the sign is inverted by flipping the particle's spin regarding a given k-mode and $\hat{n}$ orientation. Hence, the energy band will split for a given spin orientation and a given k-mode.

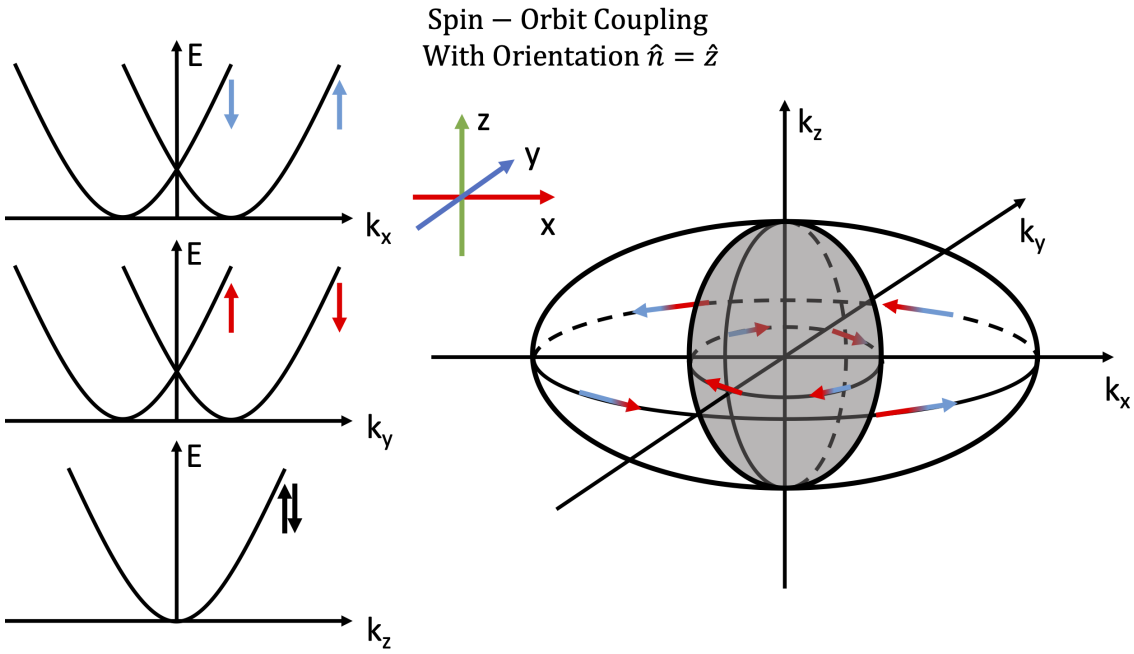

Figure 29: Displaced energy bands (left panel) and Fermi surface (right panel) due to Rashba spin-orbit coupling of orientation $\hat{n} = \hat{z}$. The spins of the particles are aligned in the same spatial direction as denoted by the color. Thus, the green arrow indicates that the spins are oriented along the z-direction, the blue arrow indicates that the spins are oriented along the y-direction, while the red arrow indicates that the spins are oriented along the x-direction. The black arrow indicates a combination of all possible spin orientations, meaning no band splitting due to spin-orbit coupling.

Fig. 29 illustrates an example of the displaced Fermi surface in three dimensions according to a spin-orbit coupling along the z-axis. Symmetry will split the energy bands similarly for x- and y-direction where spin alignment is favored, respectively, along $-\hat{y}$ and $\hat{x}$. The spin-orbit coupling will not cause an energy shift in the z-direction due to the cross-product in the definition.

A question to arise is whether the elliptical shape of the Fermi Surface has a consequence on the supercurrent. Recall that the Fermi surface of the normal-state of a conventional superconductor (Fig. 7) is isotropic, and thus takes the shape of a perfect circular sphere. Since the spin-orbit orientation of $\hat{n} = \hat{z}$ displaces the Fermi surface of the heavy metal away from a perfectly circular shape, we can no longer achieve a situation where the Fermi vectors are symmetric in all directions across the boundary simultaneously for $\lambda \neq 0$. However, symmetry only requires conservation of momenta in y- and z-direction, and we will not need to consider the Fermi vector mismatch for the k_x-modes. As a consequence, we will only investigate the Fermi surface in xy- and xz-plane, as illustrated in Fig. 30b.

Section 4.1 demonstrated the importance of the shape of the Fermi surface with respect to Andreev reflection. The consequences will be pointed out more thoroughly. But first, find the shape of the Fermi surfaces of all spin-orbit orientations. Due to symmetry, all possible configurations of the spin-orbit orientation are covered on the red surface in Fig. 20. The corners of the red triangle-like surface are located at $\hat{n} = \{\hat{x}, \hat{y}, \hat{z}\}$. The displaced energy bands of the specific spin orientations are shown in Figures 30a, 30c and 30e, while the corresponding Fermi surfaces are illustrated in Figures 30b, 30d and 30f.

After having settled the shape of the Fermi surface for all the spin-orbit orientations of interest, return to the spin-orbit orientation $\hat{n} = \hat{z}$. Compare the Fermi surfaces established for $\hat{n} = \hat{y}$ and $\hat{n} = \hat{z}$ in Figures 30d and 30f. Notice a symmetry where the surface is a perfect circle in one plane, while it takes an elliptical form in the orthogonal one. Moreover, the various orientations of the spins are indicated by color. The orientations of the spins with the displaced energy bands are different for k_y/k_z-mode for the two respective n-orientations. An unequal spin-degeneracy is achieved due to the cross-product in the Hamiltonian definition. However, the impact of the Fermi surface on the supported supercurrent is not dependent on whether the spin is aligned parallel to y- or z-axis since the two directions are invariant. Hence, the illustrated Fermi surfaces rising for $\hat{n} = \hat{y}$ and $\hat{n} = \hat{z}$ are equal in a physical manner. We can therefore continue to consider $\hat{n} = \hat{y}$ while keeping in mind that similar physics would regard $\hat{n} = \hat{z}$.

8.2 INTERPRETATION OF ALTERED JOSEPHSON EFFECT FOR $\hat{n} = \hat{y}(\hat{z})$

Consider a spin-orbit orientation parallel to the interface with $\hat{n} = \hat{y}$. Fig. 31 illustrates how the spin-orbit coupling gives rise to a Fermi vector mismatch at the intersection of a heavy metal and a superconductor. This is due to conservation of k_y and k_z. Furthermore, a spin-orbit orientation of $\hat{n} = \hat{y}$ will displace the

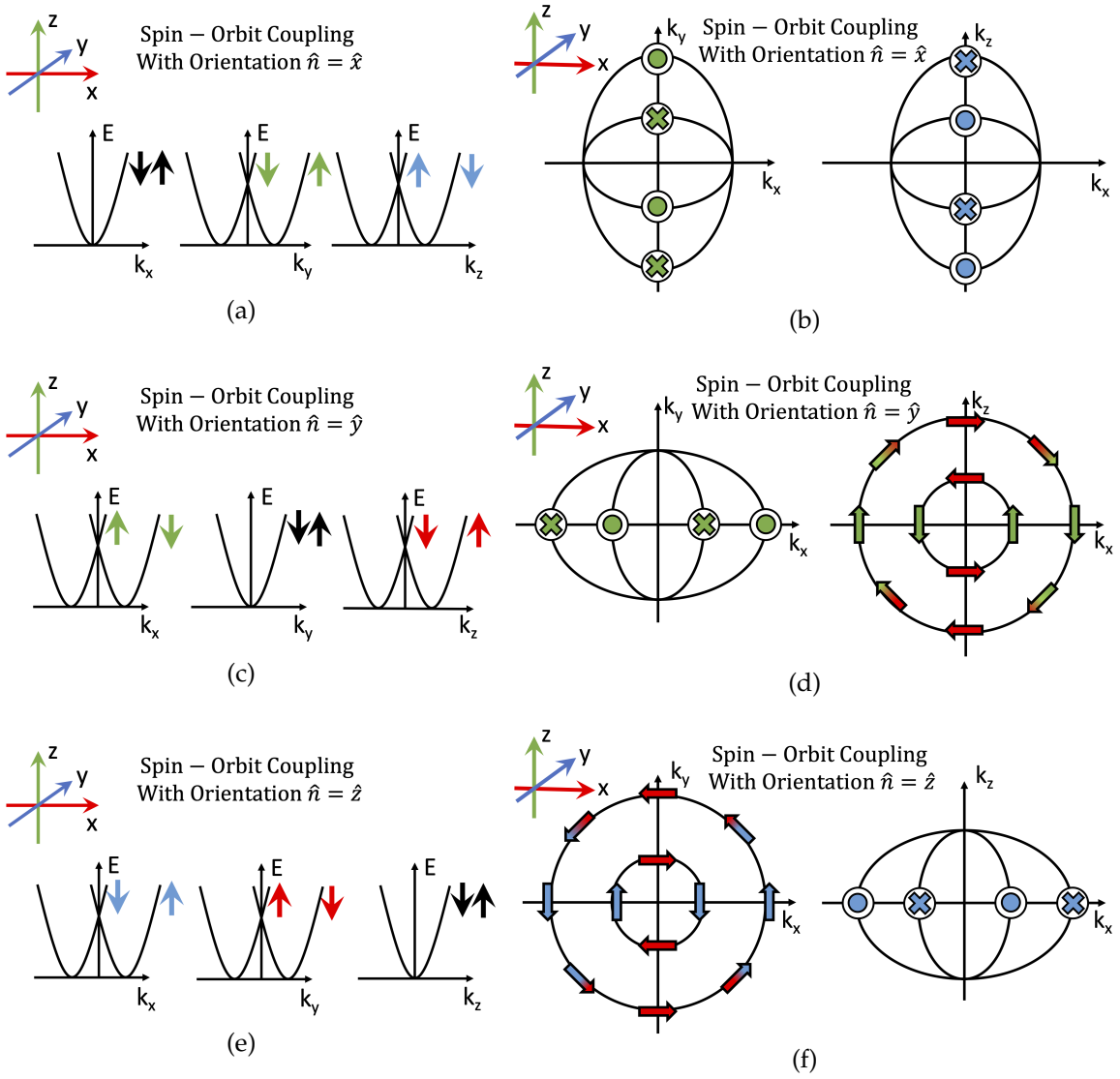

Figure 30: Displaced energy bands and thereby Fermi surface rising from the spin-orbit coupling. The left panel shows how the energies according to spin orientation will deviate from a normal state. The right panel illustrates the two-dimensional Fermi surfaces for the concrete energy band split indicated to the left. The spins of the particles are aligned in the same spatial direction as denoted by the color. Thus, the green arrow indicates that the spins are oriented along the z-direction, the blue arrow indicates that the spins are oriented along the y-direction, while the red arrow indicates that the spins are oriented along the x-direction. The black arrow indicates a combination of all possible spin orientations, meaning no band splitting due to spin-orbit coupling.

energy bands in the z-direction. Thus, by modifying the radius of the Fermi surface, we can make the Fermi surface of the superconductor coincide with one of the co-centered surfaces of the heavy metal in the xz-plane. We have previously

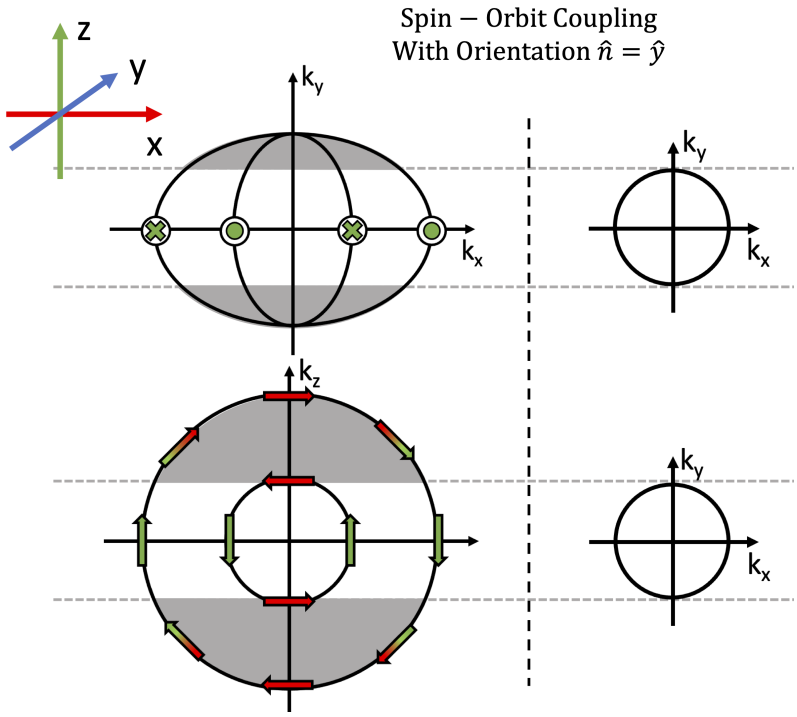

Figure 31: Demonstration of Fermi vector mismatch between a heavy metal with Rashba spin-orbit coupling of orientation $\hat{n} = \hat{y}$ (left panel) and s-wave superconductor (right panel). The grey region of the Fermi surface to the heavy metal indicated the scope of the Fermi vector mismatch in comparison with the Fermi surface of the superconductor. This is due to the conservation of momentum in k_y and k_z. The spins of the particles are aligned in the same spatial direction as denoted by the color. Thus, the green arrow indicates that the spins are oriented along the z-direction, the blue arrow indicates that the spins are oriented along the y-direction, while the red arrow indicates that the spins are oriented along the x-direction.

accounted that we can adjust the Fermi surfaces' radius by either changing the chemical potential or the spin-orbit magnitude. As a result, we could suspect that there would be a higher probability of Andreev reflections for particles living on the surface. Keep in mind the established support for Cooper pairs with singlet symmetry due to spin-orbit coupling (sec. 4.1). However, a Fermi vector match is not enough for a Cooper pair to form. Additionally, we require the incoming electron to observe a weak barrier at the interface to not increase the scattering probability. In order to answer our suspicion, we will explore the transmission probability of electrons across the interface by composing the effective barrier matrix.

The already derived boundary conditions to the analytical model provides the effective barrier in Eq. (190) given by

$$\hat{T}_{4x4} = Z_{soc}\left[h^x_{soc}\begin{pmatrix}0&1&0&0\\1&0&0&0\\0&0&0&-1\\0&0&-1&0\end{pmatrix} + h^y_{soc}\begin{pmatrix}0&-i&0&0\\i&0&0&0\\0&0&0&-i\\0&0&i&0\end{pmatrix} + h^z_{soc}\begin{pmatrix}1&0&0&0\\0&-1&0&0\\0&0&-1&0\\0&0&0&1\end{pmatrix}\right] + k_F Z_0\begin{bmatrix}1&0&0&0\\0&1&0&0\\0&0&1&0\\0&0&0&1\end{bmatrix} \tag{206}$$

where we have defined the dimensionless parameters $Z_0 = \frac{2mH}{\hbar^2 k_F}$ and $Z_{soc} = \frac{2m\lambda}{\hbar k_F}$ in addition to the coefficients

$$h^x_{soc} = n_z k_y - n_y k_z, \quad h^y_{soc} = n_x k_z - n_z \frac{k_x}{2}, \quad h^z_{soc} = n_y \frac{k_x}{2} - n_x k_y \tag{207}$$

for one specific particle momentum $\mathbf{k} = \left[k_x, k_y, k_z\right]$. To compute the matrix for a spin-orbit orientation parallel to the interface between the two superconducting elements, continue the calculation by choosing $n_x = 0$. The effective barrier-matrix reduces to

$$\hat{T}_{4x4} = Z_{soc}\begin{bmatrix} n_y\frac{k_x}{2} & -(n_y k_z - n_z k_y) + i n_z \frac{k_x}{2} & 0 & 0 \\ -(n_y k_z - n_z k_y) - i n_z \frac{k_x}{2} & -n_y \frac{k_x}{2} & 0 & 0 \\ 0 & 0 & -n_y \frac{k_x}{2} & (n_y k_z - n_z k_y) + i n_z \frac{k_x}{2} \\ 0 & 0 & (n_y k_z - n_z k_y) + i n_z \frac{k_x}{2} & -n_y \frac{k_x}{2} \end{bmatrix} + k_F Z_0 \begin{bmatrix}1&0&0&0\\0&1&0&0\\0&0&1&0\\0&0&0&1\end{bmatrix}. \tag{208}$$

The matrix T_{4x4} is interpreted as the transmission matrix for propagating particles. Thus, it is beneficial to consider a transmission matrix with only non-zero elements on the diagonal. This specific kind of matrix provides an analogy to the barrier effects for different spin-up and spin-down particles. Recognize that all

off-diagonal elements are zero if $\mathbf{k} = k_F\hat{x}$. Therefore, illustrate a one-dimensional junction as in section 7.1, and the effective barrier reads

$$\begin{aligned}\hat{T}_{4x4}\Big|_{\mathbf{k}=k_F\hat{x}} &= \frac{k_F}{2}Z_{soc}\begin{bmatrix} n_y & in_z & 0 & 0 \\ -in_z & -n_y & 0 & 0 \\ 0 & 0 & -n_y & in_z \\ 0 & 0 & -in_z & n_y \end{bmatrix} + k_F Z_0 \begin{bmatrix} 1 & 0 & 0 & 0 \\ 0 & 1 & 0 & 0 \\ 0 & 0 & 1 & 0 \\ 0 & 0 & 0 & 1 \end{bmatrix} \\ &= \frac{k_F}{2}\begin{bmatrix} 2Z_0 + n_y Z_{soc} & in_z Z_{soc} & 0 & 0 \\ -in_z Z_{soc} & 2Z_0 - n_y Z_{soc} & 0 & 0 \\ 0 & 0 & 2Z_0 - n_y Z_{soc} & in_z Z_{soc} \\ 0 & 0 & -in_z Z_{soc} & 2Z_0 + n_y Z_{soc} \end{bmatrix}.\end{aligned} \tag{209}$$

Choose a spin-orbit orientation in y-direction, $\hat{n} = \hat{y}$, and the previous matrix yields

$$\hat{T}_{4x4}\Big|_{\mathbf{k}=k_F\hat{x},\hat{n}=\hat{y}} = \frac{k_F}{2}\begin{bmatrix} 2Z_0 + Z_{soc} & 0 & 0 & 0 \\ 0 & 2Z_0 - Z_{soc} & 0 & 0 \\ 0 & 0 & 2Z_0 - Z_{soc} & 0 \\ 0 & 0 & 0 & 2Z_0 + Z_{soc} \end{bmatrix}. \tag{210}$$

This is the final effective barrier matrix for a one-dimensional junction with spin-orbit orientation $\hat{n} = \hat{y}$. The barrier will appear differently for the three cases of $Z_{soc} \ll 2Z_0$, $2Z_{soc} = 2Z_0$ and $Z_{soc} \gg 2Z_0$.

When $Z_{soc} \ll 2Z_0$, the effective barrier is equal for all types of particles. Moreover, if we increase the spin-orbit magnitude to reach the particular case of $2Z_0 = Z_{soc}$, the effective barrier will disappear for spin-up electron reflected into spin-down holes. However, this is only true for right traveling electrons. If the electron were traveling towards the left, $\hat{k} = -\hat{x}$, we would obtain the opposite barrier matrix where the barrier effect vanishes for a spin-down electron reflected into a spin-up hole. We can point this more clearly by writing out the two matrices

$\rightarrow Z_{soc} = 2Z_0$	
$\hat{T}_{4x4}\Big\|_{\mathbf{k}=k_F\hat{x},\hat{n}=\hat{y}} = 2k_F Z_0 \begin{bmatrix} 1 & 0 & 0 & 0 \\ 0 & 0 & 0 & 0 \\ 0 & 0 & 0 & 0 \\ 0 & 0 & 0 & 1 \end{bmatrix}$	$\hat{T}_{4x4}\Big\|_{\mathbf{k}=-k_F\hat{x},\hat{n}=\hat{y}} = 2k_F Z_0 \begin{bmatrix} 0 & 0 & 0 & 0 \\ 0 & 1 & 0 & 0 \\ 0 & 0 & 1 & 0 \\ 0 & 0 & 0 & 0 \end{bmatrix}$

(211)

The cancellation of barrier effects for particles with a specific spin orientation is consistent with the illustration of Fermi surfaces in Fig. 31: the Fermi surface of the superconductor can only simultaneously coincide with *one* of the two displaced spin-rotating Fermi surfaces of the heavy metal. Pay attention to Eq. (210), and observe that the spin-orbit coupling magnitude and the scattering potential are oppose to each other. This is consistent with the observation of the current in section 7.2.2.

Modes with small transverse momentum (k_y, k_z) are the main carriers of current along the x-direction. Even though the choice of momentum $\mathbf{k} = k_x\hat{x}$ simulates a one-dimensional junction, it will also be apparent for a three-dimensional junction. Recall that y- and z-direction are invariant, meaning that similar spin cancellation is present when the spin-orbit orientation is parallel to z-axis as well.

8.3 INTERPRETATION OF ALTERED JOSEPHSON EFFECT FOR $\hat{n} = \frac{\hat{y}+\hat{z}}{2}$

In section 7.2, the current acquires its strongest magnitude for a spin-orbit orientation parallel to the interface, more concrete in the middle of the y- and z-axis. The Fermi surface for this orientation, $\hat{n} = \frac{\hat{y}+\hat{z}}{2}$, is illustrated in Fig. 32. The orientation is a superposition of the previously reviewed $\hat{n} = \hat{y}$ and $\hat{n} = \hat{z}$. However, the Fermi surface is no longer asymmetric. The spin-orbit orientation will displace the energy band in y- and z-direction, both bands regarding spin aligned along x-axis. Pay attention to Fig. 32 and discover that that spin orientation is inverted between the yx- and zx-plane. This effect is crucial for the Fermi vector mismatch. We can now make the effective barrier for particles with spin-up and spin-down to disappear simultaneously! Symmetrical aspects can be used to understand the vanishing barrier. We have derived the transmission matrix for $\hat{n} = \hat{y}$. The matrix demonstrated how a spin-orbit orientation, aligned along the y-axis, could make spin-down electrons transmit across the interface with a given momentum because of an absent barrier. By symmetry, a similar effect rise for spin-orbit coupling orientated along z-axis. Regarding an electron with equal momentum, the spin will be inverted due to the coupling of spin and momentum in H_{SO}. Thus, a spin-orbit orientation where we combine the outcome of y- and z-orientation provides a disappearing barrier for both spin-up and spin-down particles. This superposition is mirrored in the Fermi surfaces for the spin-orbit orientation $\hat{n} = \frac{\hat{y}+\hat{z}}{2}$ illustrated in Fig. 32. The red arrows, which indicate a spin orientation along x-axis, are reversed for $k_y = k_z$.

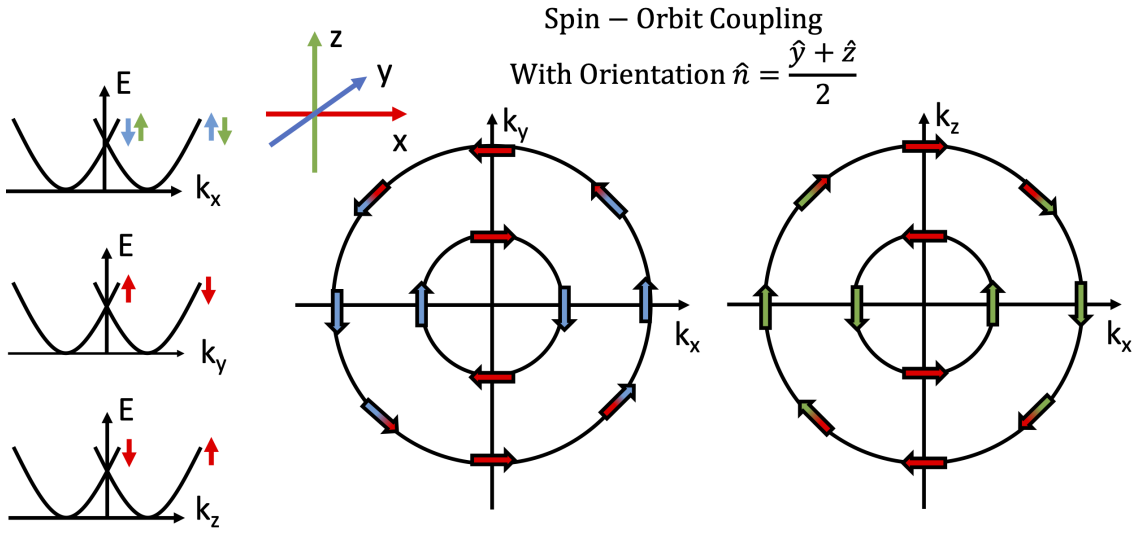

Figure 32: Illustration of the symmetric Fermi surfaces of a heavy metal with Rashba spin-orbit coupling with orientation $\hat{n} = \frac{\hat{y}+\hat{z}}{2}$. The spins of the particles are aligned in the same spatial direction as denoted by the color. Thus, the green arrow indicates that the spins are oriented along the z-direction, the blue arrow indicates that the spins are oriented along the y-direction, while the red arrow indicates that the spins are oriented along the x-direction.

8.4 INTERPRETATION OF ALTERED JOSEPHSON EFFECT FOR $\hat{n} = \hat{x}$

Study a spin-orbit orientation perpendicular to the interface, $\hat{n} = \hat{x}$. The energy bands will then be displaced in both y- and z-direction due to spin-orbit coupling. We can explore the physics behind the current through a similar procedure as in the previous sections: matching Fermi surfaces and utilize the analytical barrier matrix. First, recognize the Fermi vector mismatch illustrated in Fig. 33. Notice that the displacement for k_y and k_z can be modified by the spin-orbit magnitude, while k_x is unaffected. Additionally, we only require a conserved wave vector in the y- and z- direction. Based on the displacement of the Fermi surface, we could presume for the Andreev reflections to increase dramatically when the radius of the Fermi surface of the superconductor coincides with one of the co-centered elliptical Fermi surfaces of the heavy metal. Since the spin-orbit coupling affects the two directions equally, a Fermi vector match would occur at the same time. Nevertheless, chapter 7 showed the current to being much weaker compared to parallel orientation of the spin-orbit coupling, $\hat{n} = \hat{y}$. Therefore, we understand that the possibility of vanishing Fermi vector mismatch is not sufficient to enhance the Josephson effect. The particles require an absent barrier in the direction of propagation and a large transmission probability.

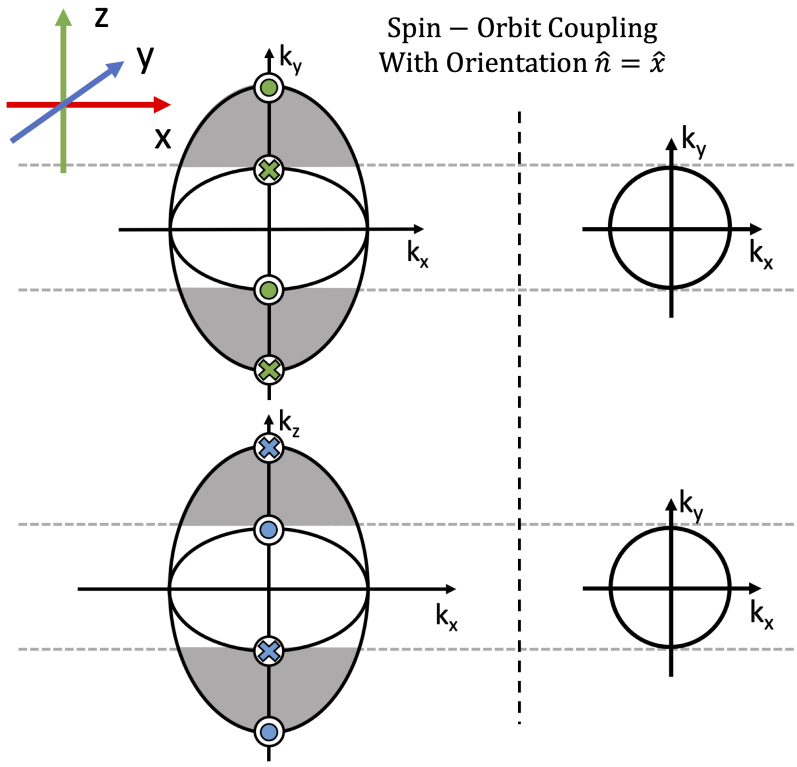

Figure 33: Demonstration of Fermi vector mismatch between a heavy metal with Rashba spin-orbit coupling with orientation $\hat{n} = \hat{x}$ (left panel) and an s-wave superconductor (right panel). The grey region on the left, indicating the Fermi surface to the heavy metal, compared to the lack thereof on the right, demonstrates the Fermi vector mismatch between the two materials. This is due to the conservation of momentum in k_y and k_z The spins of the particles are aligned in the same spatial direction as denoted by the color. Thus, the green arrow indicates that the spins are oriented along the z-direction, the blue arrow indicates that the spins are oriented along the y-direction, while the red arrow indicates that the spins are oriented along the x-direction.

Moreover, the effective barrier from the analytical framework can provide the transmission probability as described previously. For $\hat{n} = \hat{x}$, the effective barrier reads

$$\hat{T}_{4x4}\Big|_{\hat{n}=\hat{x}} = Z_{soc}\begin{bmatrix} -k_y & -ik_z & 0 & 0 \\ ik_z & k_y & 0 & 0 \\ 0 & 0 & k_y & -ik_z \\ 0 & 0 & ik_z & -k_y \end{bmatrix} + k_F Z_0 \begin{bmatrix} 1 & 0 & 0 & 0 \\ 0 & 1 & 0 & 0 \\ 0 & 0 & 1 & 0 \\ 0 & 0 & 0 & 1 \end{bmatrix}. \tag{212}$$

In order to rewrite the effective barrier matrix to include non-zero elements along the diagonal exclusively, we have chosen $\mathbf{k} = k_F\hat{y}$. The effective barrier will, consequently, only disappear for particles moving parallel to the interface. Unfortunately, this traveling mode does not support supercurrent, since the current flows across the junction along the x-direction. This is the explanation for the low current magnitude.

Furthermore, the parallel wave-vector components of the propagating particles can indeed experience a vanishing barrier. This effect explains the current plot for $\hat{n} = \hat{x}$ in section 7.2.1. The supported supercurrent increases when the parallel component experiences a zero barrier effect. Simultaneously, the perpendicular component will acquire an increased barrier due to greater effective potential. As a result, the removed barrier in y-and z-direction will contrast with the increasing barrier in the x-direction. The calculated current substantiates the understanding that the increased barrier, for particles traveling in the x-direction, defeats the removed barrier for transverse traveling particles. We can point out the tendency in Figures 17 and 24 present with a small peak for low spin-orbit magnitudes before the current reduces dramatically for large spin-orbit magnitudes.

9

SUMMARY AND OUTLOOK

In this thesis, we have investigated the supercurrent across a Josephson junction comprised of two conventional s-wave superconductors (SC) separated by a heavy metal with Rashba spin-orbit coupling (HM). The results show that the supercurrent will respond to the strength of the spin-orbit coupling (λ) and orientation ($\hat{n}$). We have interpreted the underlying physics through a vanishing barrier potential due to an interplay between the scattering- and spin-orbit potential. The spin-orbit coupling gives rise to a momentum-dependent magnetic field that will couple the spin of the particles to its momentum. Consequently, a displacement of the energy bands and the Fermi surface of the heavy metal will appear. The displaced energy bands will occur such that the electrons have a rotating spin orientation along the two co-centered Fermi surfaces. A rotating spin orientation supports normal Andreev reflection with zero center-of-mass momentum. Thus, the generated Cooper pairs will have a singlet symmetry. We have demonstrated this through a supercurrent without superimposed oscillations. It is neither current oscillations as a function of the spin-orbit coupling strength nor as a function of the thickness to the heavy metal. This is in contrast to a ferromagnetic SC/F/SC junction where we can observe an oscillating supercurrent magnitude. We have explained the differing behavior by the displaced energy bands in the presence of a magnetic field compared to spin-orbit coupling. The energy bands are displaced for spin-up and spin-down electrons in a ferromagnetic material regardless of the electrons' momentum. Therefore, the generated Cooper pairs under a magnetic field will acquire center-of-mass momentum and fluctuate between a singlet and triplet state.

Furthermore, the displaced Fermi surface in the presence of spin-orbit coupling can remove the barrier effect between the superconductor and the heavy metal. Consequently, the supercurrent can increase to a more significant value compared to a case without spin-orbit coupling. The interplay between the normal scattering and the spin-orbit scattering at the SC/HM interface is explained in the following fashion: The scattering potential will make the normal-state Fermi surfaces take different sizes across the SC/HM interface. However, the spin-orbit coupling will displace the Fermi surface of the heavy metal into two co-centered surfaces. Hence, the Fermi surface of the superconductor can coincide with one of those of the heavy metal. The amount of coincidence depends on the relation between the scattering potential and the spin-orbit potential. A perfect coincidence will provide a vanishing barrier of the particles living on the surface. We

have predicted how such a barrier cancellation can provide a supercurrent larger than without spin-orbit coupling. This was done for different directions of $\hat{n}$ in combination with specific ratios of the scattering- and spin-orbit potential.

We have shown that all spin-orbit orientations can remove the barrier for particles with specific spin and momentum. However, we are investigating a supercurrent that flows along the x-direction. Thus, the greatest impact of the supercurrent will take place when the effective barrier vanishes for particles traveling along the respective axis. The various spin-orbit orientations will therefore have different effects on the supercurrent. In particular, an orientation parallel to the interface will provide the most significant magnitude of the supercurrent, with the largest enhancement when $\hat{n} = \frac{\hat{y}+\hat{z}}{2}$. On the other hand, a spin-orbit orientation perpendicular to the interface $\hat{n} = \hat{x}$ will produce the smallest change compared to an absent spin-orbit coupling. Additionally, we have demonstrated that this cancellation effect will only be present within a specific scattering- and spin-orbit potential ratio. As a result, a strong spin-orbit magnitude will eventually decrease the supercurrent due to a strong effective barrier potential.

The possibility to control the supercurrent by the spin-orbit orientation, in addition to the ability for the supercurrent to be made larger in the presence of spin-orbit coupling, are in stark contrast with a ferromagnetic SC/F/SC junction. The supercurrent across an SC/F/SC junction is invariant of the magnetic orientation, and the magnetization always suppresses the supercurrent compared to the case without magnetization.

This research project was motivated by the possibility of controlling the supercurrent without the need for an external magnetic field. We have confirmed the action in a theoretical manner, using *one* spin-orbit layer incorporated between two superconductors. We have mainly focused on exploring the theoretical possibility of controlling the supercurrent. An experimental investigation of the spin-obit coupling enhancing Josephson effect would be attractive for further applications. In addition, the interpretation of the underlying physics has, in this thesis, focused on the spin-singlet Cooper pairs. Thus, there are yet to investigate whether the spin-triplet Cooper pairs arise in an SC/HM/SC Josephson junction. In particular, an investigation of a Josephson junction where the two superconducting elements are separated by *two* spin-orbit coupling materials could be interesting.

A

APPENDIX

A.1 DERIVING THE NUMERICAL SUB-MATRICES HAMILTONIAN

In section 5.1, we assumed an Hamiltonian given on a general from in Eq. (93). We will now derive the complete expression necessary to describe an SC/H-M/SC junction. The following will also consider the Hamiltonian of the magnetic field provided by a ferromagnet. This term is included to establish a numerical framework where one could simulate a magnetic SC/F/SC junction for comparison reasons.

A.1.1 *The hopping t term*

In the tight-binding model, we often start with a simple model consisting of the electrons' kinetic energy and potential relative to the lattice atoms. In first quantization formalism, this has the following expression

$$\begin{aligned}\hat{H}_t &= \sum_i \frac{\hat{p_i}^2}{2m} + \sum_i u(\mathbf{r}_i) \\ &= \sum_i \left[\frac{\hat{p_i}^2}{2m} + u(\mathbf{r}_i)\right]\end{aligned} \tag{A.1.1}$$

where $\hat{p}_i$ is the canonical momentum and $\mathbf{r}_i$ is the position of electron i. Using the basis in Eq. (91) we can rewrite Eq. (A.1.1) to the second quantization formalism by recognize the two terms as single-particle operators [89]. The resulting equation is

$$\hat{H}_t = \sum_{i,j,\sigma} \langle i| \left[\frac{\hat{p_i}^2}{2m} + u(\mathbf{r}_i)\right] |j\rangle \, \hat{c}^\dagger_{i,\sigma}\hat{c}_{j,\sigma}. \tag{A.1.2}$$

Define the parameter

$$t_{ij} \equiv \int \phi^*(\mathbf{r} - \mathbf{R_i})\left[-\frac{\nabla^2}{2m} + u(\mathbf{r})\right]\phi(\mathbf{r} - \mathbf{R_j})d\mathbf{r}. \tag{A.1.3}$$

Notice that this matrix element $t_{i,j}$ will appear in combination with a creation operator, which creates an electron at lattice site i, and an annihilation operator

that destroys an electron at lattice site j. Consequently, $t_{i,j}$ is called the hopping amplitude and represents the probability of an electron to move from lattice site j to lattice site i. The tight-binding approximation neglects the overlap of the nucleons' orbitals. However, there would still be a slight overlap of the orbitals between the electrons and the neighboring atoms. As a result, it would be a small probability of tunneling, or hopping, as we will refer to later. For simplicity, we assume this hopping amplitude to be constant for all lattice sites, i.e. $t_{i,j} = -t$. Thus, Eq. (A.1.1) takes the form [90],

$$\hat{H}_t = \sum_{i,j,\sigma} t_{i,j} \hat{c}^\dagger_{i,\sigma} \hat{c}_{j,\sigma} \tag{A.1.4}$$

$$\simeq -t \sum_{\langle i,j\rangle,\sigma} \hat{c}^\dagger_{i,\sigma} \hat{c}_{j,\sigma} \tag{A.1.5}$$

where we in the transition from Eq. (A.1.4) to Eq. (A.1.5) have introduced $\sum_{\langle i,j\rangle}$ to indicate sum over nearest neighbours, i.e. only nonzero when $i = j \pm 1$ or $i = j$, since we neglect hopping to next-nearest neighbours and further away. To diagonalize the hopping term, we use the Fourier transform defined as Eq. (92) such that Eq. (A.1.5) reads

$$\begin{aligned}\hat{H}_t = -\frac{t}{N_y N_z} \sum_{\sigma} \sum_{\langle i_x,i_y,i_z,j_x,j_y,j_z\rangle} \sum_{k_y,k_z} \sum_{k'_y,k'_z} \Big[&\hat{c}^\dagger_{i_x,k_y,k_z,\sigma} \hat{c}_{j_x,k'_y,k'_z,\sigma} \\ &\cdot e^{-i(k_y\hat{y}+k_z\hat{z})\cdot(i_x\hat{x}+i_y\hat{y}+i_z\hat{z})} e^{i(k'_y\hat{y}+k'_z\hat{z})\cdot(j_x\hat{x}+j_y\hat{y}+j_z\hat{z})}\Big].\end{aligned} \tag{A.1.6}$$

To simplify the previous equation, utilize that we are only considering nearest neighbors. The summation is thus only nonzero when

$$\begin{aligned}j_x\hat{x} + j_y\hat{y} + j_z\hat{z} \in \Big\{ &(i_x \pm \delta_{j_x})\hat{x} + i_y\hat{y} + i_z\hat{z}, \\ &i_x\hat{x} + (i_y \pm \delta_{j_y})\hat{y} + i_z\hat{z}, \\ &i_x\hat{x} + i_y\hat{y} + (i_z \pm \delta_{j_z})\hat{z}\Big\}\end{aligned} \tag{A.1.7}$$

where $\delta_{j_m}\hat{m}$ is a vector from the lattice site i to its nearest neighbour in $\hat{m}$-direction for $m = \{x, y, z\}$. Combining Eq. (A.1.7) and Eq. (A.1.6) gives

$$\begin{aligned}\hat{H}_t = -\frac{t}{N_y N_z} \sum_{\sigma} \sum_{\langle i_x,i_y,i_z,j_x,j_y,j_z\rangle} \sum_{k_y,k_z} \sum_{k'_y,k'_z} \Bigg[&\hat{c}^\dagger_{i_x,k_y,k_z,\sigma} \hat{c}_{i_x+\delta_{j_x},k'_y,k'_z,\sigma} \\ &\cdot e^{-i\left(k_y-k'_y\right)i_y} e^{-i\left(k_z-k'_z\right)i_z} e^{i(k'_y\hat{y}+k'_z\hat{z})} e^{\delta_{j_x}\hat{x}+\delta_{j_y}\hat{y}+\delta_{j_z}\hat{z}}\Bigg].\end{aligned} \tag{A.1.8}$$

Take taking advantage of the identities [88]

$$\begin{aligned}\frac{1}{N_y} \sum_{i_y} e^{-i\left(k_y-k'_y\right)i_y} &= \delta_{k_y,k'_y} \\ \frac{1}{N_z} \sum_{i_y z} e^{-i\left(k_z-k'_z\right)i_z} &= \delta_{k_z,k'_z}\end{aligned} \tag{A.1.9}$$

and write out Eq. (A.1.8) with respect to j_x, j_y and j_z. The result yields

$$\begin{aligned}
\hat{H}_t &= -t \sum_{i_x,k_y,k_z,\sigma} \hat{c}^\dagger_{i_x,k_y,k_z,\sigma}\hat{c}_{i_x+\delta_{j_x},k_y,k_z,\sigma} e^{i(k_y\hat{y}+k_z\hat{z})} e^{\delta_{j_x}\hat{x}+\delta_{j_y}\hat{y}+\delta_{j_z}\hat{z}} \\
&= -t \sum_{i_x,k_y,k_z,\sigma} \hat{c}^\dagger_{i_x,k_y,k_z,\sigma}\hat{c}_{i_x+1,k_y,k_z,\sigma} e^{i(k_y\hat{y}+k_z\hat{z})\cdot(\hat{x})} + \hat{c}^\dagger_{i_x,k_y,k_z,\sigma}\hat{c}_{i_x-1,k_y,k_z,\sigma} e^{i(k_y\hat{y}+k_z\hat{z})\cdot(-\hat{x})} \\
&\quad + \hat{c}^\dagger_{i_x,k_y,k_z,\sigma}\hat{c}_{i_x,k_y,k_z,\sigma} e^{i(k_y\hat{y}+k_z\hat{z})\cdot(\hat{y})} + \hat{c}^\dagger_{i_x,k_y,k_z,\sigma}\hat{c}_{i_x,k_y,k_z,\sigma} e^{i(k_y\hat{y}+k_z\hat{z})\cdot(-\hat{y})} \\
&\quad + \hat{c}^\dagger_{i_x,k_y,k_z,\sigma}\hat{c}_{i_x,k_y,k_z,\sigma} e^{i(k_y\hat{y}+k_z\hat{z})\cdot(\hat{z})} + \hat{c}^\dagger_{i_x,k_y,k_z,\sigma}\hat{c}_{i_x,k_y,k_z,\sigma} e^{i(k_y\hat{y}+k_z\hat{z})\cdot(-\hat{z})} \\
&= -t \sum_{i_x,k_y,k_z,\sigma} \hat{c}^\dagger_{i_x,k_y,k_z,\sigma}\hat{c}_{i_x+1,k_y,k_z,\sigma} + \hat{c}^\dagger_{i_x,k_y,k_z,\sigma}\hat{c}_{i_x-1,k_y,k_z,\sigma} \\
&\quad + \hat{c}^\dagger_{i_x,k_y,k_z,\sigma}\hat{c}_{i_x,k_y,k_z,\sigma}\left(e^{ik_y} + e^{-ik_y} + e^{ik_z} + e^{-ik_z}\right) \\
&= -t \sum_{i_x,j_x,k_y,k_z,\sigma} \hat{c}^\dagger_{i_x,k_y,k_z,\sigma}\hat{c}_{j_x,k_y,k_z,\sigma}\left(\delta_{i_x,j_x+1} + \delta_{i_x,j_x-1} + \delta_{i_x,j_x}\left[e^{ik_y} + e^{-ik_y} + e^{ik_z} + e^{-ik_z}\right]\right) \\
&= -t \sum_{i_x,j_x,k_y,k_z,\sigma} \hat{c}^\dagger_{i_x,k_y,k_z,\sigma}\hat{c}_{j_x,k_y,k_z,\sigma}\left(\delta_{i_x,j_x+1} + \delta_{i_x,j_x-1} + \delta_{i_x,j_x} 2\left[\cos k_y + \cos k_z\right]\right) \\
&= \sum_{i_x,j_x,k_y,k_z} \epsilon_{i_x,j_x,k_y,k_z,\sigma}\hat{c}^\dagger_{i_x,k_y,k_z,\sigma}\hat{c}_{j_x,k_y,k_z,\sigma}
\end{aligned} \tag{A.1.10}$$

where we in the last line introduced

$$\epsilon_{i_x,j_x,k_y,k_z} = -t\left(\delta_{i_x,j_x+1} + \delta_{i_x,j_x-1} + \delta_{i_x,j_x} 2\left[\cos k_y + \cos k_z\right]\right). \tag{A.1.11}$$

To diagonalize the Hamiltonian, we want to rewrite Eq. (A.1.10) into a form of

$$\hat{H}_t = \frac{1}{2} \sum_{i_x,j_x,k_y,k_z} B^\dagger_{i_x,k_y,k_z} \hat{H}^t_{i_x,j_x,k_y,k_z} B_{j_x,k_y,k_z}. \tag{A.1.12}$$

The hopping Hamiltonian will thus provide the sub-matrix

$$H^t_{i_x,j_x,k_y,k_z} = \epsilon_{i_x,j_x,k_y,k_z}\hat{\tau}_3\hat{\sigma}_0. \tag{A.1.13}$$

Expressing Eq. (A.1.13) in matrix notation reads

$$H^t_{i_x,j_x,k_y,k_z} = \begin{bmatrix} \epsilon_{i_x,j_x,k_y,k_z} & 0 & 0 & 0 \\ 0 & \epsilon_{i_x,j_x,k_y,k_z} & 0 & 0 \\ 0 & 0 & -\epsilon_{i_x,j_x,k_y,k_z} & 0 \\ 0 & 0 & 0 & -\epsilon_{i_x,j_x,k_y,k_z} \end{bmatrix}.$$

A.1.2 *The Hubbard U term*

To include the electron-electron interaction in a superconductor, we can do this through the well-known Coulomb potential [91]. In first quantization formalism, this is

$$\hat{H}_U = \frac{1}{2}\sum_{i,j\neq i} v(\mathbf{r}_i - \mathbf{r}_j) \tag{A.1.14}$$

where $\mathbf{r}_i, \mathbf{r}_j$ are the positions of electron i, j, respectively. Note how this is a two-particle operator. In order to diagonalize the Hamiltonian, rewrite Eq. (A.1.14) utilizing the basis defined in Eq. (91). We will then achieve a Hamiltonian within the second quantization formalism given as

$$\hat{H}_U = \frac{1}{2}\sum_{i,j,k,l,\sigma,\sigma'} \langle i,j|\, v(\mathbf{r}-\mathbf{r}')\, |k,l\rangle\, \hat{c}^\dagger_{i,\sigma}\hat{c}^\dagger_{j,\sigma}\hat{c}_{l,\sigma}\hat{c}_{k,\sigma}. \tag{A.1.15}$$

To simplify the expression of $\hat{H}_U$, introduce

$$v_{i,j,k,l} \equiv \iint \phi^*(\mathbf{r}-\mathbf{R}_i)\phi^*(\mathbf{r}-\mathbf{R}_j)\Big[v(\mathbf{r}-\mathbf{R}_i)\Big]\phi^*(\mathbf{r}-\mathbf{R}_k)\phi^*(\mathbf{r}-\mathbf{R}_l). \tag{A.1.16}$$

By studying the on-site electron-electron interactions term, we observe that $i = j = k = l$ gives $v_{i,j,k,l} \neq 0$, and $v_{i,j,k,l} = 0$ otherwise [90]. Thus,

$$\begin{aligned} v_{i,i,i,i} &= \iint \phi^*(\mathbf{r}-\mathbf{R}_i)\phi^*(\mathbf{r}-\mathbf{R}_i)\Big[v(\mathbf{r}-\mathbf{R}_i)\Big]\phi^*(\mathbf{r}-\mathbf{R}_i)\phi^*(\mathbf{r}-\mathbf{R}_i) \\ &= 2U \end{aligned} \tag{A.1.17}$$

where we have introduced the energy amount of U, representing Coulomb interactions, for each pair of electrons occupying the same lattice site. This simplification results in

$$\begin{aligned} \hat{H}_U &= \frac{1}{2}\sum_{i,j,k,l,\alpha,\beta} v_{i,j,k,l}\hat{c}^\dagger_{i,\alpha}\hat{c}^\dagger_{j,\beta}\hat{c}_{l,\beta}\hat{c}_{k,\alpha} \\ &= U\sum_i \hat{c}^\dagger_{i,\uparrow}\hat{c}^\dagger_{i,\downarrow}\hat{c}_{i,\downarrow}\hat{c}_{i,\uparrow} \end{aligned} \tag{A.1.18}$$

The fermonic particle operator is defined as $\hat{n}_{i,\sigma} = \hat{c}^\dagger_{i,\sigma}\hat{c}_{i,\sigma}$, and it follows that Eq. (A.1.18) can be written as $\hat{H}_U = U\sum_i \hat{n}^\dagger_{i,\uparrow}\hat{n}_{i,\downarrow}$. We can now clearly point out how this term respects the Pauli exclusion principle: the two on-site electrons have to hold opposite spin. We can interpret this term as an energy cost, since two electrons with opposite spins increases the energy of the system by U.

Notice that $\hat{H}_U$ includes a quadratic dependence in the fermionic creation and annihilation operators. Such a problem is challenging to solve, and does often

fail in providing an exact solution. According to BCS-theory, a mean-field approximation is a good approach for a system with many particles involved [50].

Perform a mean-field approximation where

$$\begin{aligned}\hat{c}_{i,\uparrow}\hat{c}_{i,\downarrow} &= \langle \hat{c}_{i,\uparrow}\hat{c}_{i,\downarrow}\rangle + \delta_i \\ \hat{c}^\dagger_{i,\uparrow}\hat{c}^\dagger_{i,\downarrow} &= \langle \hat{c}^\dagger_{i,\uparrow}\hat{c}^\dagger_{i,\downarrow}\rangle - \delta^\dagger_i.\end{aligned} \tag{A.1.19}$$

Assume δ_i and $\delta_i^\dagger$ to be small, thus neglect terms of second-order and higher. We will now introduce a new quantity defined as [87]

$$\Delta_i = U\langle \hat{c}_{i,\uparrow}\hat{c}_{i,\downarrow}\rangle. \tag{A.1.20}$$

This property is the superconducting gap, also known as the ordering parameter, for a conventional s-wave superconductor [50].

Combining Eq. (A.1.18), Eq. (A.1.19) and Eq. (A.1.20), we get a mean-field Hubbard Hamiltonian term given as

$$\hat{H}_U = \sum_i \left[\Delta_i \hat{c}^\dagger_{i,\uparrow}\hat{c}^\dagger_{i,\downarrow} + \Delta_i^* \hat{c}_{i,\downarrow}\hat{c}_{i,\uparrow}\right] + \sum_i \frac{|\Delta_i|^2}{U_i}. \tag{A.1.21}$$

Notice that the second term is the Hermitian conjugate of the first term.

Similar to the hopping term, perform the Fourier transform defined in Eq. (92). Thus, the Hubbard Hamiltonian reads

$$\begin{aligned}\hat{H}_U &= \frac{1}{N_y N_z}\sum_{i_x,i_y,i_z,\sigma}\sum_{k_y,k_z}\sum_{k'_y,k'_z}\Bigg[\Delta_{i_x}\hat{c}^\dagger_{i_x,k_y,k_z,\sigma}\hat{c}^\dagger_{i_x,k'_y,k'_z,\sigma} \\ &\qquad \cdot e^{-i(k_y i_y + k_z i_z)} e^{-i(k'_y i_y + k'_z i_z)} + \textbf{h.c.}\Bigg] + N_y N_z \sum_{i_x}\frac{|\Delta_{i_x}|^2}{U_{i_x}} \\ &= \frac{1}{N_y N_z}\sum_{i_x,i_y,i_z,\sigma}\sum_{k_y,k_z}\sum_{k'_y,k'_z}\Bigg[\Delta_{i_x}\hat{c}^\dagger_{i_x,k_y,k_z,\sigma}\hat{c}^\dagger_{i_x,k'_y,k'_z,\sigma} \\ &\qquad \cdot e^{-i\left(k_y+k'_y\right)i_y} e^{-i\left(k_z+k'_z\right)i_z} + \textbf{h.c.}\Bigg] + N_y N_z \sum_{i_x}\frac{|\Delta_{i_x}|^2}{U_{i_x}}\end{aligned} \tag{A.1.22}$$

where h.c is short for the Hermitian conjugate. Utilize the following identities to simplify the previous expression,

$$\begin{aligned}\frac{1}{N_y}\sum_{i_y} e^{-i\left(k_y+k'_y\right)i_y} &= \delta_{k_y,-k'_y} \\ \frac{1}{N_z}\sum_{i_y z} e^{-i\left(k_z+k'_z\right)i_z} &= \delta_{k_z,-k'_z}.\end{aligned} \tag{A.1.23}$$

Finally, the resulting expression for $\hat{H}_U$ is

$$\hat{H}_U = \hat{H}_0 + \sum_{i_x,k_y,k_z} \left[\Delta_{i_x} \hat{c}^\dagger_{i_x,k_y,k_z,\uparrow} \hat{c}^\dagger_{i_x,-k_y,-k_z,\downarrow} + \Delta^*_i \hat{c}_{i_x,-k_y,-k_z,\downarrow} \hat{c}_{i_x,k_y,k_z,\uparrow} \right] \tag{A.1.24}$$

where we have defined the constant term $\hat{H}_0 = N_y N_z \sum_{i_x} \frac{|\Delta_{i_x}|^2}{U_{i_x}}$. To rewrite Eq. (A.1.24) on the form

$$\hat{H}_U = \hat{H}_0 + \frac{1}{2} \sum_{i_x,j_x,k_y,k_z} B^\dagger_{i_x,k_y,k_z} \hat{H}^U_{i_x,j_x,k_y,k_z} B_{j_x,k_y,k_z}. \tag{A.1.25}$$

we receive an expression of the sub-matrix as

$$\hat{H}^U_{i_x,j_x,k_y,k_z} = \delta_{i_x,j_x} \left[\Delta^*_{i_x} i\hat{\tau}^- \hat{\sigma}_y - \Delta_{i_x} i\hat{\tau}^+ \hat{\sigma}_y \right]. \tag{A.1.26}$$

Writing out the matrix notation gives

$$H^U_{i_x,j_x,k_y,k_z} = \delta_{i_x,j_x} \begin{bmatrix} 0 & 0 & 0 & \Delta_{i_x} \\ 0 & 0 & -\Delta_{i_x} & 0 \\ 0 & -\Delta^*_{i_x} & 0 & 0 \\ \Delta^*_{i_x} & 0 & 0 & 0 \end{bmatrix}$$

for $\Delta_{i_x} = U\langle \hat{c}_{i,\uparrow} \hat{c}_{i,\downarrow} \rangle$.

A.1.3 *The chemical potential μ term*

The chemical potential is, in thermodynamics, the energy which can be absorbed or released due to a change in the particle number. According to the grand canonical ensemble, the equivalent Hamiltonian is [92]

$$H_\mu = -\mu N \tag{A.1.27}$$

where N is the total number of particles. Assume the chemical potential μ to be constant for all lattice sites, and use that the particle number can be expressed in terms of the fermionic creation and annihilation operators as $\hat{n}_\mu = \hat{c}^\dagger_\mu \hat{c}_\mu$. Thus, the chemical potential in second quantization formalism is

$$\hat{H}_\mu = -\mu \sum_{i,\sigma} \hat{c}^\dagger_{i,\sigma} \hat{c}_{i,\sigma}. \tag{A.1.28}$$

After a Fourier transform according to the definition in Eq. (92) we get

$$\begin{aligned}\hat{H}_\mu &= -\mu \sum_{i_x,i_y,i_z,\sigma} \sum_{k_y,k_z,k_y',k_z'} \hat{c}^\dagger_{i_x,k_y,k_z,\sigma} \hat{c}_{i_x,k_y',k_z',\sigma} e^{-i(k_y i_y - k_y' i_y)} e^{-i(k_z i_z - k_z' i_z)} \\ &= -\mu \sum_{i_x,k_y,k_z,\sigma} \hat{c}^\dagger_{i_x,k_y,k_z,\sigma} \hat{c}_{i_x,k_y,k_z,\sigma} \\ &= -\mu \sum_{i_x,k_y,k_z} \left[\hat{c}^\dagger_{i_x,k_y,k_z,\uparrow} \hat{c}_{i_x,k_y,k_z,\uparrow} + \hat{c}^\dagger_{i_x,k_y,k_z,\downarrow} \hat{c}_{i_x,k_y,k_z,\downarrow} \right]\end{aligned} \tag{A.1.29}$$

where we have inserted the identities in Eq. (A.1.9). Next, rewrite Eq. (A.1.29) into the form

$$H_\mu = \frac{1}{2} \sum_{i_x,j_x,k_y,k_z} B^\dagger_{i_x,k_y,k_z} \hat{H}^\mu_{i_x,j_x,k_y,k_z} B_{j_x,k_y,k_z} \tag{A.1.30}$$

and we get the sub-matrix

$$H^\mu_{i_x,j_x,k_y,k_z} = -\mu \delta_{i_x,j_x} \hat{\tau}_3 \hat{\sigma}_0. \tag{A.1.31}$$

In explicit matrix given in Eq. (A.1.31) is

$$H^\mu_{i_x,j_x,k_y,k_z} = \delta_{i_x,j_x} \begin{bmatrix} -\mu & 0 & 0 & 0 \\ 0 & -\mu & 0 & 0 \\ 0 & 0 & \mu & 0 \\ 0 & 0 & 0 & \mu \end{bmatrix}.$$

A.1.4 *The ferromagnetic h term*

In a ferromagnet, the energetically favorable state is when the spins of the electrons are oriented along the magnetic field. The local magnetic exchange field will interact with the spins of the electrons and contribute to the Hamiltonian as

$$\hat{H}_h = \sum_i \mathbf{h}_i \cdot \mathbf{S}_i. \tag{A.1.32}$$

Here, $\mathbf{h}_i$ is the local magnetic exchange field and $\mathbf{S}_i$ is the spin operator at lattice site i. Insert for the spin operator $\mathbf{S}_i = \sum_{\alpha,\beta} \hat{c}^\dagger_{i,\alpha} \boldsymbol{\sigma}_{\alpha,\beta} \hat{c}_{i,\beta}$ where $\boldsymbol{\sigma}_{\alpha,\beta}$ is the (α,β) element of the vector of Pauli matrices $\boldsymbol{\sigma}$, and the result yields

$$\begin{aligned}\hat{H}_h &= \sum_i \mathbf{h}_i \cdot \sum_{\alpha,\beta} \hat{c}^\dagger_{i,\alpha} \boldsymbol{\sigma}_{\alpha,\beta} \hat{c}_{i,\beta} \\ &= \sum_{i,\alpha,\beta} \left(\mathbf{h}_i \cdot \boldsymbol{\sigma} \right)_{\alpha,\beta} \hat{c}^\dagger_{i,\alpha} \hat{c}_{i,\beta}.\end{aligned} \tag{A.1.33}$$

Fourier transform the previous expression for $\hat{H}_h$ according to the definition in Eq. (92), and use the identities defined in Eq. (A.1.9). The Hamiltonian will then reduces to

$$\begin{aligned}\hat{H}_h &= \sum_{i_x,k_y,k_z,\alpha,\beta} \left(\mathbf{h}_{i_x}\cdot\boldsymbol{\sigma}\right)_{\alpha,\beta} \hat{c}^{\dagger}_{i_x,k_y,k_z,\alpha}\hat{c}_{i_x,k_y,k_z,\beta} \\ &= \sum_{i_x,k_y,k_z}\Big[\left(\mathbf{h}_{i_x}\cdot\boldsymbol{\sigma}\right)_{\uparrow,\uparrow}\hat{c}^{\dagger}_{i_x,k_y,k_z,\uparrow}\hat{c}_{i_x,k_y,k_z,\uparrow} \\ &\quad + \left(\mathbf{h}_{i_x}\cdot\boldsymbol{\sigma}\right)_{\uparrow,\downarrow}\hat{c}^{\dagger}_{i_x,k_y,k_z,\uparrow}\hat{c}_{i_x,k_y,k_z,\downarrow} \\ &\quad + \left(\mathbf{h}_{i_x}\cdot\boldsymbol{\sigma}\right)_{\downarrow,\uparrow}\hat{c}^{\dagger}_{i_x,k_y,k_z,\downarrow}\hat{c}_{i_x,k_y,k_z,\uparrow} \\ &\quad + \left(\mathbf{h}_{i_x}\cdot\boldsymbol{\sigma}\right)_{\downarrow,\downarrow}\hat{c}^{\dagger}_{i_x,k_y,k_z,\downarrow}\hat{c}_{i_x,k_y,k_z,\downarrow}\Big].\end{aligned} \tag{A.1.34}$$

To diagonalize the Hamiltonian, make the expression satisfy

$$H_h = \frac{1}{2}\sum_{i_x,j_x,k_y,k_z} B^{\dagger}_{i_x,k_y,k_z}\hat{H}^{h}_{i_x,j_x,k_y,k_z}B_{j_x,k_y,k_z} \tag{A.1.35}$$

such that we get the sub-matrix

$$H^{h}_{i_x,j_x,k_y,k_z} = \delta_{i_x,j_x}\left[h^{x}_{i_x}\hat{\tau}_3\hat{\sigma}_x + h^{y}_{i_x}\hat{\tau}_0\hat{\sigma}_y + h^{z}_{i_x}\hat{\tau}_3\hat{\sigma}_z\right] \tag{A.1.36}$$

In matrix form this reads

$$H^{h}_{i_x,j_x,k_y,k_z} = \delta_{i_x,j_x}\begin{bmatrix} h^{z}_{i_x} & h^{x}_{i_x}-ih^{y}_{i_x} & 0 & 0 \\ h^{x}_{i_x}+ih^{y}_{i_x} & -h^{z}_{i_x} & 0 & 0 \\ 0 & 0 & -h^{z}_{i_x} & -h^{x}_{i_x}-ih^{y}_{i_x} \\ 0 & 0 & -h^{x}_{i_x}+ih^{y}_{i_x} & h^{z}_{i_x}\end{bmatrix}.$$

A.1.5 *The Rashba λ term*

By introducing a heavy metal to our junction, we give rise to the existence of spin-orbit coupling. Since we assume a tight-binding model, the spin-orbit coupling is of a type called Rashba discovered by Rashba and Sheka in 1959 [93] [73].

The spin-orbit coupling is a relativistic effect that appears in the Dirac equation by expanding and include terms up to the order of $1/c^2$ [94]. The field is due to the relative motion of particles with a spin that travels across an electric field. The particle will then feel an effective magnetic field that couples the particles' spin to their momentum. As a result, the spin can align itself in a favorable

direction to minimize energy. The name spin-orbit coupling is connected to the ability to couple the electron's spin to its orbital motion.

As discussed in section 3.1, an electron moving under an external electric field $\mathbf{E}$, has a relativistic spin-orbit coupling given, in first quantization formalism, as

$$\hat{H} = -\frac{e\hbar}{(2mc)^2}\boldsymbol{\sigma}\cdot(\mathbf{E}(\mathbf{r})\times\mathbf{p}). \tag{A.1.37}$$

We can recognize the effective magnetic field by rewriting

$$\frac{e\hbar}{2mc}\boldsymbol{\sigma}\cdot(\mathbf{E}(\mathbf{r})\times\mathbf{p}) = \frac{e\hbar}{4mc}\boldsymbol{\sigma}\cdot\mathbf{B}_0. \tag{A.1.38}$$

which has a similar form as the Zeeman energy.

We can derive the diagonal Hamiltonian in a similar fashion as done in Ref. [95]. Start by using that $\mathbf{E} = E\hat{n}$ and collect all constant pre-factors into the parameter λ. The spin-orbit field has both a magnitude and orientation, which we will treat as uniform in the heavy metal. The Rashba spin-orbit coupling Hamiltonian in first quantization formalism for a single band model is then given by [72]

$$\hat{H}_\lambda = (\hat{n}\times\boldsymbol{\sigma})\cdot\lambda(x)\hat{p} \tag{A.1.39}$$

where $\hat{n} = \left[\cos(\phi_n)\sin(\theta_n), \sin(\phi_n)\sin(\theta_n), \cos(\theta_n)\right]$ is the unit vector along the spin-orbit field orientation which can be orientated in any direction in space, λ is the Rashba spin-orbit coupling magnitude, $\hat{p} = (\hat{p}_x, \hat{p}_y, \hat{p}_z) = -i\hbar\nabla$ is the momentum operator, and σ is the vector of Pauli matrices. The magnitude of the electric field is included in the spin-orbit magnitude $\lambda \propto |\mathbf{E}|$, and the orientation is parallel to the unit vector $\hat{n}$ [94].

We will only consider heavy metals where the spin-orbit coupling magnitude is uniform. Furthermore, since the system is translation invariant in y- or z-direction, λ will not depend on the respective directions. For x-direction, the situation is not that simple. Since we want to add different materials in the x-direction, we break down the translational invariance. The variance will be significant at the intersection of the heavy metal and the superconductor. In particular, when we are coupling two electrons appearing on different sides of the HM/SC interface. Thus, let the magnitude quantity have x-dependence, hence $\lambda = \lambda(x)$.

To transform the first quantization expression to second quantization formalism, we have to evaluate

$$\hat{H}_\lambda = \sum_{\langle i,j\rangle,\alpha,\beta} \hat{c}^\dagger_{i,\alpha}\langle i|\left[(\hat{n}\times\boldsymbol{\sigma})\cdot\lambda(x)\hat{p}\right]|j\rangle\,\hat{c}_{i,\beta} \equiv \sum_{\langle i,j\rangle,\alpha,\beta} \hat{c}^\dagger_{i,\alpha}\langle i|\,\hat{h}\,|j\rangle\,\hat{c}_{i,\beta} \tag{A.1.40}$$

where we have defined $\hat{h} \equiv (\hat{n} \times \boldsymbol{\sigma}) \cdot \lambda(x)\hat{p}$ as the first quantization formalism in Eq. (A.1.39).

In order to solve the Hamiltonian in a self-consistent manner, we need the spin-orbit coupling operator to be Hermitian. This is not the case since $\hat{h} \neq \hat{h}^\dagger$. We can observe this explicitly by

$$\begin{aligned} \hat{h}^\dagger = \Big[(\hat{n} \times \boldsymbol{\sigma}) \cdot \lambda(x)\hat{p}\Big]^\dagger &= \hat{p}^\dagger \lambda(x)^\dagger \cdot (\hat{n} \times \boldsymbol{\sigma})^\dagger \\ &= (\hat{n} \times \boldsymbol{\sigma}) \cdot \hat{p}\lambda(x) \\ &\neq (\hat{n} \times \boldsymbol{\sigma}) \cdot \lambda(x)\hat{p} = \hat{h} \end{aligned} \tag{A.1.41}$$

since $\hat{p}$ and $\lambda(x)$ do not commute. Note that this non-Hermitian operator is nor symmetric. In order to make $\hat{h}$ Hermitian and symmetric, we can use the anti-commutator,

$$\hat{h} = \frac{1}{2}(\hat{n} \times \boldsymbol{\sigma}) \cdot \{\lambda(x), \hat{p}\}. \tag{A.1.42}$$

This operator is Hermitian proven by

$$\begin{aligned} \hat{h}^\dagger = \Big[\frac{1}{2}(\hat{n} \times \boldsymbol{\sigma}) \cdot \{\lambda(x), \hat{p}\}\Big]^\dagger &= \frac{1}{2}(\hat{n} \times \boldsymbol{\sigma}) \cdot \{\hat{p}, \lambda(x)\} \\ &= \frac{1}{2}(\hat{n} \times \boldsymbol{\sigma}) \cdot \{\lambda(x), \hat{p}\} = \hat{h}. \end{aligned} \tag{A.1.43}$$

When evaluating the previous Hamiltonian, the anti-commutator is straightforward regarding y-, z-direction since $\lambda(x)$ commutes with the respective momentum operators, i.e. $\{\lambda(x), \hat{p}_y\} = 2\lambda(x)\hat{p}_y$ and $\{\lambda(x), \hat{p}_z\} = 2\lambda(x)\hat{p}_z$. The anti-commutator of λ and $\hat{p}_x$ has to be calculated more carefully,

$$\begin{aligned} \Big[\lambda(x)\hat{p}_x + \hat{p}_x\lambda(x)\Big] f(x) &= \lambda(x)\hat{p}_x f(x) + \Big[\hat{p}_x\lambda(x)\Big] f(x) + \lambda(x)\Big[\hat{p}_x f(x)\Big] \\ &= \Big[2\lambda(x)\hat{p}_x + \hat{p}_x\lambda(x)\Big] f(x) \end{aligned} \tag{A.1.44}$$

where we have used the chain rule since $\hat{p}_x$ is a derivative operator with respect to x. Using the anti-commutator relation in Eq. (A.1.44), we can write out the operator in Eq. (A.1.42) as

$$\begin{aligned} \hat{h} &= \frac{1}{2}(\hat{n} \times \boldsymbol{\sigma}) \cdot \{\lambda(x), \hat{p}\} \\ &= (\hat{n} \times \boldsymbol{\sigma}) \cdot \Big\{\lambda(x)\hat{p}_x + \frac{1}{2}\Big[\hat{p}_x\lambda(x)\Big]\Big\} + \lambda(x)(\hat{n} \times \boldsymbol{\sigma}) \cdot \hat{p}_y + \lambda(x)(\hat{n} \times \boldsymbol{\sigma}) \cdot \hat{p}_z. \end{aligned} \tag{A.1.45}$$

Next, we need to evaluate the overlap integral from Eq. (A.1.40) which, after making the operator Hermitian, is

$$\begin{aligned} \langle i|\,\hat{h}\,|j\rangle = \langle i|\,(\hat{n} \times \boldsymbol{\sigma}) \cdot \Big\{\lambda(x)\hat{p}_x + \frac{1}{2}\Big[\hat{p}_x\lambda(x)\Big]\Big\}\,|j\rangle \\ + \langle i|\,\lambda(x)(\hat{n} \times \boldsymbol{\sigma}) \cdot \hat{p}_y\,|j\rangle \\ + \langle i|\,\lambda(x)(\hat{n} \times \boldsymbol{\sigma}) \cdot \hat{p}_z\,|j\rangle \end{aligned} \tag{A.1.46}$$

Start with the first term in Eq. (A.1.46),

$$\begin{aligned}\langle i|\left(\hat{n}\times\boldsymbol{\sigma}\right)\cdot\left\{\lambda(x)\hat{p}_x+\frac{1}{2}\left[\hat{p}_x\lambda(x)\right]\right\}|j\rangle \\ =\left(\hat{n}\times\boldsymbol{\sigma}\right)\cdot\hat{x}\int d\mathbf{r}\phi_i^*(\mathbf{r})\left\{\lambda(x)p_x+\frac{1}{2}\left[p_x\lambda(x)\right]\right\}\phi_j(\mathbf{r}).\end{aligned} \tag{A.1.47}$$

By partially integrating half of the first term, the second term cancels and we recieve

$$\langle i|\left(\hat{n}\times\boldsymbol{\sigma}\right)\cdot\left\{\lambda(x)\hat{p}_x+\tfrac{1}{2}\left[\hat{p}_x\lambda(x)\right]\right\}|j\rangle=\tfrac{1}{2}\left(\hat{n}\times\boldsymbol{\sigma}\right)\cdot\hat{x}\left[\langle i|\lambda(x)p_x|j\rangle+\langle j|\lambda(x)p_x|i\rangle^*\right]. \tag{A.1.48}$$

Insert Eq. (A.1.48) into Eq. (A.1.46) and calculate the overlap integral given as

$$\begin{aligned}\langle i|\hat{h}|j\rangle=&\frac{1}{2}\left(\hat{n}\times\boldsymbol{\sigma}\right)\cdot\hat{x}\left[\langle i|\lambda(x)p_x|j\rangle+\langle j|\lambda(x)p_x|i\rangle^*\right] \\ &+\left(\hat{n}\times\boldsymbol{\sigma}\right)\cdot\hat{y}\,\langle i|\lambda(x)p_y|j\rangle \\ &+\left(\hat{n}\times\boldsymbol{\sigma}\right)\cdot\hat{z}\,\langle i|\lambda(x)p_z|j\rangle\,.\end{aligned} \tag{A.1.49}$$

Realize how all terms in the overlap integral have been reduced to depend on integrals like

$$\int d\mathbf{r}\phi_i^*(\mathbf{r})\lambda(x)\hat{p}_m\phi_j=-i\int d\mathbf{r}\phi_i^*(\mathbf{r})\lambda(x)\partial_m\phi_j \tag{A.1.50}$$

where $m=\{x,y,z\}$. By writing out the derivative in discretize terms as $\partial_m\phi_j(\mathbf{r})=\frac{1}{2}\left[\phi_{j-\hat{m}}(\mathbf{r})-\phi_{j+\hat{m}}(\mathbf{r})\right]$ where $\phi_{j\pm\hat{m}}(\mathbf{r})=\phi(\mathbf{r}-\mathbf{R}_j\pm\hat{m})$ and $\mathbf{R}_j$ is a vector to the position of lattice site j, Eq. (A.1.50) takes the form

$$\int d\mathbf{r}\phi_i^*(\mathbf{r})\lambda(x)\hat{p}_m\phi_j=-\frac{i}{2}\int d\mathbf{r}\phi_i^*(\mathbf{r})\lambda(x)\left[\phi_{j-\hat{m}}(\mathbf{r})-\phi_{j+\hat{m}}(\mathbf{r})\right]. \tag{A.1.51}$$

If we assume each ϕ_i to be highly localized, meaning the probability distributions to atoms at lattice site i has small overlap to the neighbouring atoms, we can evaluate the integrals $\int d\mathbf{r}\phi_i^*(\mathbf{r})\phi_j(\mathbf{r})=\delta_{i,j}$.

The spin-orbit magnitude $\lambda(x)$ is constant when both electrons are inside the heavy metal. At the intersection, $\lambda(x)$ will act like a step-function, meaning $\lambda(x)=0$ when both electrons are in another material. First, consider the case of both electrons inside the heavy metal, i.e. both $j+\hat{m}$, $j-\hat{m}$ and i inside the heavy metal. For this specific case, we can use $\lambda(x)=\lambda$, i.e. constant in all directions. Applying the discussed requirements to Eq. (A.1.51), we get

$$\int d\mathbf{r}\phi_i^*(\mathbf{r})\lambda(x)\hat{p}_m\phi_j=\frac{i}{2}\lambda\Big(\delta_{i,j+\hat{m}}-\delta_{i,j-\hat{m}}\Big). \tag{A.1.52}$$

Use this result, and note that the last term in Eq. (A.1.48) gives

$$\begin{aligned}\left[\int d\mathbf{r}\phi_i^*(\mathbf{r})\lambda(x)\hat{p}_x\phi_j\right]^* &= i\int d\mathbf{r}\left[\frac{\partial}{\partial x}\phi_i(\mathbf{r})\right]^*\lambda(x)\phi_j \\ &= i\int d\mathbf{r}\left[\phi^*_{j-\hat{x}}(\mathbf{r})-\phi^*_{j+\hat{x}}(\mathbf{r})\right]^*\lambda(x)\phi_j \\ &\overset{\lambda(x)=\lambda}{=} \frac{i}{2}\lambda\left(\delta_{i,j+\hat{x}}-\delta_{i,j-\hat{x}}\right).\end{aligned} \tag{A.1.53}$$

Combining the result from Eq. (A.1.53) and Eq. (A.1.52) we arrive at

$$\frac{1}{2}(\hat{n}\times\boldsymbol{\sigma})\cdot\hat{x}\left[\langle i|\,\lambda(x)p_x\,|j\rangle+\langle j|\,\lambda(x)p_x\,|i\rangle^*\right]=\langle i|\,\lambda(x)\hat{p}_x\,|j\rangle\,. \tag{A.1.54}$$

Eq. (A.1.49) will thus equal

$$\begin{aligned}\langle i|\,\hat{h}\,|j\rangle = \frac{1}{2}(\hat{n}\times\boldsymbol{\sigma})\cdot\Big[&\hat{x}\left(\delta_{i,j+\hat{x}}-\delta_{i,j-\hat{x}}\right) \\ &+\hat{y}\left(\delta_{i,j+\hat{y}}-\delta_{i,j-\hat{y}}\right) \\ &+\hat{z}\left(\delta_{i,j+\hat{z}}-\delta_{i,j-\hat{z}}\right)\Big].\end{aligned} \tag{A.1.55}$$

To the substitution

$$\mathbf{d}_{i,j}=\hat{x}\left(\delta_{i,j+\hat{x}}-\delta_{i,j-\hat{x}}\right)+\hat{y}\left(\delta_{i,j+\hat{y}}-\delta_{i,j-\hat{y}}\right)+\hat{z}\left(\delta_{i,j+\hat{z}}-\delta_{i,j-\hat{z}}\right) \tag{A.1.56}$$

which represent the vector from lattice site i to site j. Through a circular shift $(\hat{n}\times\boldsymbol{\sigma})\cdot\mathbf{d}_{i,j}=\hat{n}\cdot(\boldsymbol{\sigma}\times\mathbf{d}_{i,j})$, we can simplify the overlap integral in Eq. (A.1.55) as

$$\langle i|\,\hat{h}\,|j\rangle=-\frac{i}{2}\lambda\hat{n}\cdot(\boldsymbol{\sigma}\times\mathbf{d}_{i,j}). \tag{A.1.57}$$

In short, if both lattice site i and j are inside the heavy metal, and neither is the lattice site closest to the interface, the Hamiltonian for the respective system is

$$\hat{H}_\lambda=-\frac{i}{2}\sum_{\langle i,j\rangle,\alpha,\beta}\lambda\hat{c}^\dagger_{i,\alpha}\hat{n}\cdot(\boldsymbol{\sigma}\times\mathbf{d}_{i,j})_{\alpha,\beta}\hat{c}_{i,\beta}. \tag{A.1.58}$$

Preform the Fourier transform defined in Eq. (92) due to translation invariance in y- and z-direction. By utilizing the identities provided in Eq. (A.1.9) the result is

$$\begin{aligned}\hat{H}_\lambda=\sum_{i_x,j_x,k_y,k_x,\alpha,\beta}\lambda\hat{n}\cdot\Big[&\frac{i}{2}(\sigma_z\hat{y}-\sigma_y\hat{z})_{\alpha,\beta}(\delta_{i_x,j_x+1}-\delta_{i_x,j_x-1}) \\ &+(\sigma_x\hat{z}-\sigma_z\hat{x})_{\alpha,\beta}(\sin(k_y)\delta_{i_x,j_x}) \\ &+(\sigma_y\hat{x}-\sigma_x\hat{y})_{\alpha,\beta}\sin(k_z)\delta_{i_x,j_x})\Big]\hat{c}^\dagger_{i_x,k_y,k_z,\alpha}\hat{c}_{j_x,k_y,k_z,\beta}.\end{aligned} \tag{A.1.59}$$

Rewrite Eq. (A.1.59) as

$$\hat{H}_\lambda = \frac{1}{2} \sum_{i_x,j_x,k_y,k_z} B^\dagger_{i_x,k_y,k_z} H^\lambda_{i_x,j_x,k_y,k_z} B_{j_x,k_y,k_z} \tag{A.1.60}$$

which gives the sub-matrix

$$\begin{aligned}
\hat{H}^\lambda_{i_x,j_x,k_y,k_z} = &- \Big[\sin(k_y)\cos(\phi)\sin(\theta)\hat{\tau}_0\hat{\sigma}_z \\
&- (\sin(k_y)\cos(\theta) - \sin(k_z)\sin(\phi)\sin(\theta))\hat{\tau}_0\hat{\sigma}_x \\
&- \sin(k_z)\cos(\phi)\sin(\theta)\hat{\tau}_3\hat{\sigma}_y \Big] \lambda_{i_x}\delta_{i_x,j_x} \\
&+ \Big[\frac{i}{2}\sin(\phi)\sin(\theta)\hat{\tau}_0\hat{\sigma}_z - \frac{i}{2}\cos(\theta)\hat{\tau}_3\hat{\sigma}_y \Big] \lambda_{i_x}\delta_{i_x,j_x+1} \\
&- \Big[\frac{i}{2}\sin(\phi)\sin(\theta)\hat{\tau}_0\hat{\sigma}_z - \frac{i}{2}\cos(\theta)\hat{\tau}_3\hat{\sigma}_y \Big] \lambda_{i_x}\delta_{i_x,j_x-1}.
\end{aligned} \tag{A.1.61}$$

This is the sub-matrix for coupling between two particles inside the heavy metal, where neither site i or j is the lattice site closest to the HM/SC interface.

Second, derive the corresponding sub-matrix assuming lattice sites j and i are on opposite sides of the interface, i.e. one inside the heavy metal and the other one in another material. For this situation, first term in Eq. (A.1.49) cannot be evaluated as we did in Eq. (A.1.53). Therefore, calculate the overlap integral in a different manner. Begin by using discretize terms according to Eq. (A.1.51), and obtain

$$\begin{aligned}
\frac{1}{2}\left[\langle i|\lambda(x)p_x|j\rangle + \langle j|\lambda(x)p_x|i\rangle^*\right] = -\frac{i}{4}\Bigg[&\int d\mathbf{r}\phi^*_i(\mathbf{r})\lambda(x)\phi_{j+\hat{x}}(\mathbf{r}) \\
&- \int d\mathbf{r}\phi^*_i(\mathbf{r})\lambda(x)\phi_{j-\hat{x}}(\mathbf{r}) \\
&- \left(\int d\mathbf{r}\phi^*_j(\mathbf{r})\lambda(x)\phi_{i+\hat{x}}(\mathbf{r})\right)^* \\
&+ \left(\int d\mathbf{r}\phi^*_j(\mathbf{r})\lambda(x)\phi_{i-\hat{x}}(\mathbf{r})\right)^* \Bigg]
\end{aligned} \tag{A.1.62}$$

Notice how the two first terms in Eq. (A.1.62) represent the overlap at lattice site i, and similar the two last terms are considering the overlap at lattice site j.

There are two different scenarios. Firstly, when j is inside the heavy metal, and site i is not. For this situation, the overlap at site i gives $\lambda(x) = 0$, and the two first terms vanish. On the other hand, the overlap at lattice site j, which is inside the heavy metal, provides $\lambda(x) = \lambda$. For the opposite scenario, when lattice site i is inside the heavy metal and site j is in another material, the two first terms of Eq. (A.1.62) will contribute with $\lambda(x) = \lambda$, and the two last terms will vanish as $\lambda(x) = 0$. Therefore, the two first terms are equal to the two last terms

comparing the two scenarios. If lattice site i or j is inside the heavy metal, which we showed in Eq. (A.1.53) and Eq. (A.1.52), we get exactly half contribution for the intersection case. The overlap integral is then

$$\begin{aligned}\langle i|\,\hat{h}\,|j\rangle &= \frac{i}{2}\lambda(\hat{n}\times\boldsymbol{\sigma})\cdot\Big[\frac{1}{2}\hat{x}\Big[\Big(\delta_{i,j+\hat{x}}-\delta_{i,j-\hat{x}}\Big)\\ &\qquad+\hat{y}\Big(\delta_{i,j+\hat{y}}-\delta_{i,j-\hat{y}}\Big)+\hat{z}\Big(\delta_{i,j+\hat{z}}-\delta_{i,j-\hat{z}}\Big)\Big]\\ &= -\frac{i}{2}\lambda(\hat{n}\times\boldsymbol{\sigma})\cdot\Big[\frac{1}{2}(\mathbf{d}_{i,j})_{\perp}+(\mathbf{d}_{i,j})_{\parallel}\Big]\\ &= -\frac{i}{2}\lambda\hat{n}\cdot\Big[\boldsymbol{\sigma}\times\frac{1}{2}(\mathbf{d}_{i,j})_{\perp}+\boldsymbol{\sigma}\times(\mathbf{d}_{i,j})_{\parallel}\Big]\end{aligned} \tag{A.1.63}$$

where we have used the identity defined in Eq. (A.1.56) to simplify the expression, and decomposed $\mathbf{d}_{i,j}$ into a part perpendicular to the interface ($(\mathbf{d}_{i,j})_{\perp}$), and one parallel ($(\mathbf{d}_{i,j})_{\parallel}$). Inserting the overlap integral from Eq. (A.1.63) into Eq. (A.1.40) we get

$$\hat{H}_{\lambda} = -\frac{i}{2}\sum_{\langle i,j\rangle,\alpha,\beta}\lambda\hat{c}^{\dagger}_{i,\alpha}\hat{n}\cdot\Big[\boldsymbol{\sigma}\times\frac{1}{2}(\mathbf{d}_{i,j})_{\perp}+\boldsymbol{\sigma}\times(\mathbf{d}_{i,j})_{\parallel}\Big]\hat{c}_{i,\beta}. \tag{A.1.64}$$

If we compare the expression for $\hat{H}_{\lambda}$ when lattice sites i and j are inside the heavy metal and the situation when they are on opposite side of the interface, i.e. Eq. (A.1.58) and Eq. (A.1.64), we realize that the only difference is a factor $\frac{1}{2}$ in front of $(\mathbf{d}_{i,j})_x$. Therefore, generalize the expression in Eq. (A.1.61) and the final result for the sub-matrix Hamiltonian yields

$$\begin{aligned}H^{\lambda}_{i_x,j_x,k_y,k_z} = -\Big[&\sin(k_y)\cos(\phi)\sin(\theta)\hat{\tau}_0\hat{\sigma}_z\\ &-(\sin(k_y)\cos(\theta)-\sin(k_z)\sin(\phi)\sin(\theta))\hat{\tau}_0\hat{\sigma}_x\\ &-\sin(k_z)\cos(\phi)\sin(\theta)\hat{\tau}_3\hat{\sigma}_y\Big]\lambda_{i_x}\delta_{i_x,j_x}\\ &+\Big[\frac{i}{4}\sin(\phi)\sin(\theta)\hat{\tau}_0\hat{\sigma}_z-\frac{i}{4}\cos(\theta)\hat{\tau}_3\hat{\sigma}_y\Big]\lambda_{i_x}(1+\xi)\delta_{i_x,j_x+1}\\ &-\Big[\frac{i}{4}\sin(\phi)\sin(\theta)\hat{\tau}_0\hat{\sigma}_z-\frac{i}{4}\cos(\theta)\hat{\tau}_3\hat{\sigma}_y\Big]\lambda_{i_x}(1+\xi)\delta_{i_x,j_x-1}\end{aligned} \tag{A.1.65}$$

where

$$\xi = \begin{cases}0 & \text{if } i,j \text{ are on opposite side of the interface}\\ 1 & \text{if } i,j \text{ are both in heavy metal}\end{cases} \tag{A.1.66}$$

We would obtain the same result through an alternative procedure by Fourier transforming Eq. (A.1.64) and combining it with Eq. (A.1.61).

Define the vector

$$\begin{aligned}\boldsymbol{\Lambda}_{i_x} &= \begin{bmatrix}\lambda_{i_x}\cos(\phi)\sin(\theta) & \lambda_{i_x}\sin(\phi)\sin(\theta) & \lambda_{i_x}\cos(\theta)\end{bmatrix}\\ &= \Lambda^{x}_{i_x}\hat{x}+\Lambda^{y}_{i_x}\hat{y}+\Lambda^{z}_{i_x}\hat{z}\end{aligned} \tag{A.1.67}$$

just to simplify the expression. Finally, the arriving Hamiltonian is given as

$$\begin{aligned} H^{\lambda}_{i_x,j_x,k_y,k_z} =& -\left[\sin(k_y)\Lambda^x_{i_x}\hat{\tau}_0\hat{\sigma}_z - (\sin(k_y)\Lambda^z_{i_x} - \sin(k_z)\Lambda^y_{i_x})\hat{\tau}_0\hat{\sigma}_x - \sin(k_z)\Lambda^x_{i_x}\hat{\tau}_3\hat{\sigma}_y\right]\delta_{i_x,j_x} \\ &+ \left[\frac{i}{4}\Lambda^y_{i_x}\hat{\tau}_0\hat{\sigma}_z - \frac{i}{4}\Lambda^z_{i_x}\hat{\tau}_3\hat{\sigma}_y\right](1+\xi)\delta_{i_x,j_x+1} \\ &- \left[\frac{i}{4}\Lambda^y_{i_x}\hat{\tau}_0\hat{\sigma}_z - \frac{i}{4}\Lambda^z_{i_x}\hat{\tau}_3\hat{\sigma}_y\right](1+\xi)\delta_{i_x,j_x-1}. \end{aligned} \tag{A.1.68}$$

Written in matrix form, Eq. (A.1.68) reads

$$H^{\lambda}_{i_x,j_x,k_y,k_z} = \delta_{i_x,j_x}\begin{bmatrix}\mathbf{A}_{2x2} & 0_{2x2}\\ 0_{2x2} & \mathbf{A}^*_{2x2}\end{bmatrix} + \delta_{i_x,j_x\pm1}(1+\xi)\begin{bmatrix}\mathbf{B}_{2x2} & 0_{2x2}\\ 0_{2x2} & -\mathbf{B}^*_{2x2}\end{bmatrix}$$

where we have introduced the 2x2-matrices $\mathbf{A}_{2x2}$ and $\mathbf{B}^m_{2x2}$ to simply shorten the equation,

$$\mathbf{A}_{2x2} = \begin{bmatrix} -\Lambda^x\sin(k_y) & \Lambda^z\sin(k_y) - (\Lambda^y + i\Lambda^x)\sin(k_z) \\ \Lambda^z\sin(k_y) - (\Lambda^y - i\Lambda^x)\sin(k_z) & \Lambda^x\sin(k_y)\end{bmatrix}, \mathbf{B}_{2x2} = \frac{1}{4}\begin{bmatrix}\pm i\Lambda^y & \mp\Lambda^z \\ \pm\Lambda^z & \mp i\Lambda^y\end{bmatrix}. \tag{A.1.69}$$

A.2 CORRELATION FUNCTIONS OF SPIN-TRIPLET SYMMETRY

The condensate of conventional s-wave superconductors consists of bound electron pairs with opposite spin and momentum. These states are called Cooper pairs and have singlet symmetry. In section 2.1, we demonstrated that the bound states are formed regardless of the strength of the interaction as long as it is attractive[53]. However, the Pauli exclusion principle permits other types of pairing as well. These types of pairing could be beneficial to produce under magnetic fields; since fermions tend to align their spin along an external magnetic field. As a result, the field is detrimental to the existence of spin-singlet Cooper pairs.

We can indeed observe an anti-symmetric property of the superconducting gap $\Delta_i = UF_{ii}^{\uparrow\downarrow}$. The pairing function corresponding to an exchange of the spins,

$$F_{ii}^{\uparrow\downarrow} = \langle \hat{c}_{i,\uparrow} \hat{c}_{i,\downarrow} \rangle = -\langle \hat{c}_{i,\downarrow} \hat{c}_{i,\uparrow} \rangle = -F_{ii}^{\downarrow\uparrow}. \tag{A.2.1}$$

This correlation of two electrons is a spin-singlet state. This symmetry is established because it creates a favorable energetic state of the two interacting electrons with opposite spin and momentum. An experimental observation at the beginning of 1970 investigated the phases of the superfluid ^3He at very low temperatures. The result opened up the idea for the order parameter, Δ, to depend on the momentum [88]. To describe a momentum-dependent bound state, we have to allow for pairing between fermions with equal spin, in addition to a pairing of fermions with opposite spin. Consequently, there can exist Cooper pairs with both singlet- and triplet symmetry.

Furthermore, we can interpret the enabling of Cooper pairs of triplet symmetry by studying the crystal symmetry. Begin with the spin-singlet states. By assuming an isotropic system, it follows that Δ is independent of the wave number $\mathbf{k}$ due to the spherical symmetry inside the crystal. The corresponding correlation as an s-wave pairing [50], and has spin-singlet symmetry. In addition, the spin-state is anti-symmetric under spin exchanges. The conventional BCS-theory is based on materials of this s-wave type. A question that arises is if it exists other forms of pairing, hereby the spin-triplet symmetry. Conventional superconductor has an order parameter that is independent of the momentum, i.e. $\Delta_{k_y,k_z} = \Delta$. However, if we happen to have anisotropic materials, we would expect an associated anisotropic order parameter $\Delta_{k_y,k_z} \neq \Delta$ since it depends on the wave number $\mathbf{k}$, which reflects the underlying symmetry of the crystal. An example of such system is a tetragonal crystal where the length of the three primitive lattice vector is nonequal, i.e. $|\mathbf{a}| = |\mathbf{b}| \neq |\mathbf{c}|$. Consequently, we expect the gap related to the momentum along $\mathbf{c}$ to be different than for the gap related to the momentum along $\mathbf{a}$ and $\mathbf{b}$. Although the conventional s-wave pairing is the basis for superconductivity, it is important to note how BCS-theory only

requires an attractive interaction. Therefore, there might be different paring interactions responsible for the superconductivity in some superconductors.

With this in mind, correlation functions can have both spin-singlet symmetry(S) and spin-triplet symmetry(T). The four different pairing functions is defined as

$$\begin{aligned}
&\text{Singlet state: } \begin{cases} F_{ii}^{\uparrow\downarrow(S)} &= \frac{F_{ii}^{\uparrow\downarrow} - F_{ii}^{\downarrow\uparrow}}{2} = \frac{\langle \hat{c}_{i,\uparrow}\hat{c}_{i,\downarrow}\rangle - \langle \hat{c}_{i,\downarrow}\hat{c}_{i,\uparrow}\rangle}{2} \end{cases} \\
&\text{Triplet state: } \begin{cases} F_{ij}^{\uparrow\uparrow(T)} &= \langle \hat{c}_{i,\uparrow}\hat{c}_{j,\uparrow}\rangle \\ F_{ij}^{\downarrow\downarrow(T)} &= \langle \hat{c}_{i,\downarrow}\hat{c}_{j,\downarrow}\rangle \\ F_{ij}^{\uparrow\downarrow(T)} &= \frac{F_{ij}^{\uparrow\downarrow} + F_{ij}^{\downarrow\uparrow}}{2} = \frac{\langle \hat{c}_{i,\uparrow}\hat{c}_{j,\downarrow}\rangle + \langle \hat{c}_{i,\downarrow}\hat{c}_{j,\uparrow}\rangle}{2}. \end{cases}
\end{aligned} \tag{A.2.2}$$

The spin-singlet symmetry is symmetric under coordinate exchange, while spin-triplet symmetry is anti-symmetric. The singlet state is trivial under the respective exchange since the definition in Eq. (A.2.2) considers equal lattice point for the two fermionic operators. On the other hand, the spin-triplet states have an unequal index of the lattice sites. This is due to the commutation relation of the fermionic operator, which forces the spin-triplet pairing of two electrons at equal lattice site to vanish. We can demonstrate this anti-symmetric symmetry of the spin-triplet states with respect to a coordinate exchange as

$$\begin{aligned}
F_{ij}^{\uparrow\uparrow(T)} &= \langle \hat{c}_{i,\uparrow}\hat{c}_{j,\uparrow}\rangle = -\langle \hat{c}_{j,\uparrow}\hat{c}_{i,\uparrow}\rangle = -F_{ji}^{\uparrow\uparrow(T)} \\
F_{ij}^{\downarrow\downarrow(T)} &= \langle \hat{c}_{i,\downarrow}\hat{c}_{j,\downarrow}\rangle = -\langle \hat{c}_{j,\downarrow}\hat{c}_{i,\downarrow}\rangle = -F_{ji}^{\downarrow\downarrow(T)} \\
F_{ij}^{\uparrow\downarrow(T)} &= \frac{F_{ij}^{\uparrow\downarrow} + F_{ij}^{\downarrow\uparrow}}{2} = \frac{\langle \hat{c}_{i,\uparrow}\hat{c}_{j,\downarrow}\rangle + \langle \hat{c}_{i,\downarrow}\hat{c}_{j,\uparrow}\rangle}{2} = -\frac{\langle \hat{c}_{j,\downarrow}\hat{c}_{i,\uparrow}\rangle + \langle \hat{c}_{j,\uparrow}\hat{c}_{i,\downarrow}\rangle}{2} = -F_{ji}^{\uparrow\downarrow(T)}.
\end{aligned} \tag{A.2.3}$$

Regarding the spin-exchange, the spin-singlet state is anti-symmetric, while the spin-triplet is symmetry. We can demonstrate this symmetries as

$$\begin{aligned}
F_{ii}^{\uparrow\downarrow(S)} &= \frac{F_{ii}^{\uparrow\downarrow} - F_{ii}^{\downarrow\uparrow}}{2} = \frac{\langle \hat{c}_{i,\uparrow}\hat{c}_{i,\downarrow}\rangle - \langle \hat{c}_{i,\downarrow}\hat{c}_{i,\uparrow}\rangle}{2} = -\frac{\langle \hat{c}_{i,\downarrow}\hat{c}_{i,\uparrow}\rangle - \langle \hat{c}_{i,\uparrow}\hat{c}_{i,\downarrow}\rangle}{2} = -F_{ii}^{\downarrow\uparrow(S)} \\
F_{ij}^{\uparrow\downarrow(T)} &= \frac{F_{ij}^{\uparrow\downarrow} + F_{ij}^{\downarrow\uparrow}}{2} = \frac{\langle \hat{c}_{i,\uparrow}\hat{c}_{j,\downarrow}\rangle + \langle \hat{c}_{i,\downarrow}\hat{c}_{j,\uparrow}\rangle}{2} = \frac{\langle \hat{c}_{i,\downarrow}\hat{c}_{i,\uparrow}\rangle + \langle \hat{c}_{i,\uparrow}\hat{c}_{i,\downarrow}\rangle}{2} = F_{ij}^{\downarrow\uparrow(T)}.
\end{aligned} \tag{A.2.4}$$

We have now pointed out the symmetries of the singlet- and triplet states. Next is to investigate whether our system allows for the different pairing to arise.

Taking a closer look at the Hamiltonian of our system, notice how $\hat{H}_\lambda$ and $\hat{H}_F$ enable for correlation functions with spin-triplet symmetry.

Begin with a brief exploration of spin-triplets states due to ferromagnetism. As discussed in section 4.3, the energy bands in a ferromagnetic material will displace themselves according to spin-up and spin-down particles. The established Cooper pairs will therefore acquire a finite momentum. As a consequence, the correlation function will oscillate in space. Thus, the conventional singlets ($|\uparrow\downarrow\rangle - |\downarrow\uparrow\rangle$) will generate spin-0 triplets ($|\uparrow\downarrow\rangle + |\downarrow\uparrow\rangle$) through a spin-mixing process [77]. However, the spin of the electrons tends to align themselves with the direction of an external magnetic field. In other words, a magnetic field has a pair-breaking effect on the alternating spin states. The correlation function will therefore decay rapidly into the magnet, even more rapidly than in a disordered SC/NC bilayer [14]. The generated spin-0 triplet states are thus referred to as short-ranged triplet states.

Suppose the spins were aligned parallel to the exchange field ($|\uparrow\uparrow\rangle$, $|\downarrow\downarrow\rangle$), the Cooper pairs would then not scattered off due to the magnetic interaction. Hence, the equal-projected spin states are called long-ranged triplets and would be valuable to transfer superconducting correlations over a larger distance. However, we can convince ourselves that the alternating spin-projection of the spin-0 triplet state ($|\uparrow\downarrow\rangle - |\downarrow\uparrow\rangle$) can be rewritten into equal spin-projection ($|\uparrow\uparrow\rangle + |\downarrow\downarrow\rangle$) by rotating the frame. We can show this conceptually. First, assume the spin-0 triplet state to be quantized along the z-axis. Now, perform a quantum mechanical rotation to quantize the spin along the y-axis.

$$
\begin{aligned}
&R(z \to y)_1 R(z \to y)_2 \Big(|\uparrow_1\downarrow_2\rangle + |\downarrow_1\uparrow_2\rangle\Big)_z \\
&\qquad = \frac{1}{\sqrt{2}}\begin{pmatrix} 1 & i \\ i & 1 \end{pmatrix}_1 \frac{1}{\sqrt{2}}\begin{pmatrix} 1 & i \\ i & 1 \end{pmatrix}_2 \left(\begin{bmatrix} 1 \\ 0 \end{bmatrix}_1 \begin{bmatrix} 0 \\ 1 \end{bmatrix}_2 + \begin{bmatrix} 0 \\ 1 \end{bmatrix}_1 \begin{bmatrix} 1 \\ 0 \end{bmatrix}_2\right) \\
&\qquad = i\left(\frac{1}{\sqrt{2}}\begin{bmatrix} 1 \\ i \end{bmatrix}_1 \frac{1}{\sqrt{2}}\begin{bmatrix} i \\ 1 \end{bmatrix}_2 + \frac{1}{\sqrt{2}}\begin{bmatrix} i \\ 1 \end{bmatrix}_1 \frac{1}{\sqrt{2}}\begin{bmatrix} 1 \\ i \end{bmatrix}_2\right) \\
&\qquad = i\Big(|\uparrow_1\uparrow_2\rangle + |\downarrow_1\downarrow_2\rangle\Big)_y .
\end{aligned}
\tag{A.2.5}
$$

As a result fo this, we can obtain the equal-spin triplets from a homogeneous magnetic field where the magnetization field goes from $y \to z$ at the SC/F interface [13][16][17].

If we replace the ferromagnet with a spin-orbit material, previous research are suggesting for spin-triplet states to nevertheless occur [19]. This is due to the spin-orbit interaction to couple the spin of the electron to its momentum. Moreover, Rashba spin-orbit coupling can be the source of Cooper pairs with spin-triplet symmetry because it provides a spin-dependent potential[19][21][22][23]. By considering the spin-orbit Hamiltonian, $\hat{H}_\lambda$, we can point out this singlet to

triplet pairing by combining Eq. (A.1.64) and Eq. (A.1.58). We will then achieve a spin-orbit Hamiltonian term as

$$\hat{H}_\lambda = -\frac{i}{4} \sum_{\langle i,j\rangle,\alpha,\beta} \lambda \hat{c}^\dagger_{i,\alpha} \hat{n} \cdot \left[(1+\xi)\boldsymbol{\sigma} \times \left(\mathbf{d}_{i,j}\right)_\perp + 2\boldsymbol{\sigma} \times \left(\mathbf{d}_{i,j}\right)_\parallel \right] \hat{c}_{i,\beta} \tag{A.2.6}$$

where ξ are defined in Eq. (A.1.66), and $\hat{n}$, $\boldsymbol{\sigma}$ and $\boldsymbol{\delta}$ have components in all the direction in space, $\{\hat{x}, \hat{y}, \hat{z}\}$. The quantity $\mathbf{d}_{i,j}$ is a vector from lattice site i to site j which ensures nearest neighbour interaction, as defined in Eq. (A.1.56).

Since the sum runs over α and β, which represent the spin orientation, there are four different combinations of creation-annihilation rising,

$$\hat{H}_\lambda \propto \{\hat{c}^\dagger_\uparrow \hat{c}_\downarrow, \quad \hat{c}^\dagger_\downarrow \hat{c}_\uparrow, \quad \hat{c}^\dagger_\uparrow \hat{c}_\uparrow, \quad \hat{c}^\dagger_\downarrow \hat{c}_\downarrow\}. \tag{A.2.7}$$

The two last terms are just the number operator, $\hat{c}^\dagger_\sigma \hat{c}_\sigma = \hat{n}_\sigma$. The two first terms have another interpretation. Note how the spin of the creation and annihilation operator is opposite. As a result, the two terms attempt to flip the spin. In other words, the spin-orbit term attempt effectively to flip the spin of one of the electrons in a Cooper pair. These new Cooper pairs with equal spin orientation have triplet symmetry. We can thus obtain spin-triplet correlation due to spin-orbit coupling.

A.2.1 *Numerical expression of correlation functions of any spin orientation*

We can calculate the correlation function related to Cooper pairs of spin-triplet symmetry. Therefore, define correlations functions with all combinations of spin directions, $F^{\alpha\beta}_{i_x,j_x}$ where $\{\alpha, \beta\}$ can take all spin combinations of $\{\uparrow, \downarrow\}$. Following the same procedure as done for $F^{\uparrow\downarrow}_{i_x,i_x}$ the final expression yields

$$\begin{aligned} F^{\alpha\beta}_{i,j} = {} & \frac{1}{L_y L_z} \sum_{k>0,n} \left(v^*_{ix,k,n,\alpha} u_{jx,k,n,\beta} f(E_{0,n}) e^{ik\delta} + u_{ix,k,n,\alpha} v^*_{jx,k,n,\beta} (1 - f(E_{k,n})) e^{-ik\delta} \right) \\ & + \frac{1}{L_y L_z} \sum_{0,n<2N_x} \left(v^*_{ix,0,n,\alpha} u_{jx,0,n,\beta} f(E_{0,n}) + u_{ix,0,n,\alpha} v^*_{jx,0,n,\beta} (1 - f(E_{0,n})) \right). \end{aligned} \tag{A.2.8}$$

BIBLIOGRAPHY

[1] I. Žutić, J. Fabian, and S. Das Sarma, "Spintronics: Fundamentals and applications," *Reviews of Modern Physics*, vol. 76, no. 2, pp. 323–410, 2004, DOI: 10.1103/RevModPhys.76.323.

[2] S. H. Jacobsen, J. A. Ouassou, and J. Linder, "Superconducting Order in Magnetic Heterostructures," in *Advanced Magnetic and Optical Materials*, Hoboken, NJ, USA: John Wiley & Sons, Inc., 2016, pp. 1–46, DOI: 10.1002/9781119241966.ch1.

[3] M. N. Baibich, J. M. Broto, A. Fert, F. N. Van Dau, F. Petroff, P. Etienne, G. Creuzet, A. Friederich, and J. Chazelas, "Giant Magnetoresistance of (001)Fe/(001)Cr Magnetic Superlattices," *Physical Review Letters*, vol. 61, no. 21, pp. 2472–2475, 1988, DOI: 10.1103/PhysRevLett.61.2472.

[4] C. Chappert, A. Fert, and F. N. Van Dau, "The emergence of spin electronics in data storage," *Nature Materials*, vol. 6, no. 11, pp. 813–823, 2007, DOI: 10.1038/nmat2024.

[5] S. Bhatti, R. Sbiaa, A. Hirohata, H. Ohno, S. Fukami, and S. Piramanayagam, "Spintronics based random access memory: a review," *Materials Today*, vol. 20, no. 9, pp. 530–548, 2017, DOI: 10.1016/j.mattod.2017.07.007.

[6] J. Linder and J. W. Robinson, "Superconducting spintronics," *Nature Physics*, vol. 11, no. 4, pp. 307–315, 2015, DOI: 10.1038/nphys3242, arXiv: 1510.00713.

[7] P. De Gennes and E. Guyon, "Superconductivity in "normal" metals," *Physics Letters*, vol. 3, no. 4, pp. 168–169, 1963, DOI: 10.1016/0031-9163(63)90401-3.

[8] P. G. de Gennes, "Boundary Effects in Superconductors," *Reviews of Modern Physics*, vol. 36, no. 1, pp. 225–237, 1964, DOI: 10.1103/RevModPhys.36.225.

[9] R. Holm and W. Meissner, "Messungen mit Hilfe von flüssigem Helium. XIII," *Zeitschrift für Physik*, vol. 74, no. 11-12, pp. 715–735, 1932, DOI: 10.1007/BF01340420.

[10] J. J. Hauser, H. C. Theuerer, and N. R. Werthamer, "Superconductivity in Cu and Pt by Means of Superimposed Films with Lead," *Physical Review*, vol. 136, no. 3A, A637–A641, 1964, DOI: 10.1103/PhysRev.136.A637.

[11] N. R. Werthamer, "Theory of the Superconducting Transition Temperature and Energy Gap Function of Superposed Metal Films," *Physical Review*, vol. 132, no. 6, pp. 2440–2445, 1963, DOI: 10.1103/PhysRev.132.2440.

[12] G. Deutscher, J. Hurault, and P. van Dalen, "Electrodynamical properties of superconducting contacts," *Journal of Physics and Chemistry of Solids*, vol. 30, no. 3, pp. 509–520, 1969, DOI: 10.1016/0022-3697(69)90007-9.

[13] F. S. Bergeret, A. F. Volkov, and K. B. Efetov, "Odd triplet superconductivity and related phenomena in superconductor-ferromagnet structures," *Reviews of Modern Physics*, vol. 77, no. 4, pp. 1321–1373, 2005, DOI: 10.1103/RevModPhys.77.1321.

[14] A. I. Buzdin, "Proximity effects in superconductor-ferromagnet heterostructures," *Reviews of Modern Physics*, vol. 77, no. 3, pp. 935–976, 2005, DOI: 10.1103/RevModPhys.77.935.

[15] I. F. Lyuksyutov and V. L. Pokrovsky, "Ferromagnet–superconductor hybrids," *Advances in Physics*, vol. 54, no. 1, pp. 67–136, 2005, DOI: 10.1080/00018730500057536.

[16] F. S. Bergeret, A. F. Volkov, and K. B. Efetov, "Josephson current in superconductor-ferromagnet structures with a nonhomogeneous magnetization," *Physical Review B*, vol. 64, no. 13, p. 134 506, 2001, DOI: 10.1103/PhysRevB.64.134506.

[17] ——, "Long-Range Proximity Effects in Superconductor-Ferromagnet Structures," *Physical Review Letters*, vol. 86, no. 18, pp. 4096–4099, 2001, DOI: 10.1103/PhysRevLett.86.4096.

[18] M. Houzet, "Ferromagnetic Josephson Junction with Precessing Magnetization," *Physical Review Letters*, vol. 101, no. 5, p. 057 009, 2008, DOI: 10.1103/PhysRevLett.101.057009.

[19] F. S. Bergeret and I. V. Tokatly, "Spin-orbit coupling as a source of long-range triplet proximity effect in superconductor-ferromagnet hybrid structures," *Physical Review B*, vol. 89, no. 13, p. 134 517, 2014, DOI: 10.1103/PhysRevB.89.134517, arXiv: 1402.1025.

[20] M. Houzet and A. I. Buzdin, "Long range triplet Josephson effect through a ferromagnetic trilayer," *Physical Review B*, vol. 76, no. 6, p. 060 504, 2007, DOI: 10.1103/PhysRevB.76.060504.

[21] V. M. Edelstein, "Triplet superconductivity and magnetoelectric effect near the s -wave-superconductor– normal-metal interface caused by local breaking of mirror symmetry," *Physical Review B*, vol. 67, no. 2, p. 020 505, 2003, DOI: 10.1103/PhysRevB.67.020505.

[22] M. Duckheim and P. W. Brouwer, "Andreev reflection from noncentrosymmetric superconductors and Majorana bound-state generation in half-metallic ferromagnets," *Physical Review B*, vol. 83, no. 5, p. 054 513, 2011, DOI: 10.1103/PhysRevB.83.054513.

[23] S. Takei and V. Galitski, "Microscopic theory for a ferromagnetic nanowire/-superconductor heterostructure: Transport, fluctuations, and topological superconductivity," *Physical Review B*, vol. 86, no. 5, p. 054 521, 2012, DOI: 10.1103/PhysRevB.86.054521.

[24] S. LaShell, B. A. McDougall, and E. Jensen, "Spin Splitting of an Au(111) Surface State Band Observed with Angle Resolved Photoelectron Spectroscopy," *Physical Review Letters*, vol. 77, no. 16, pp. 3419–3422, 1996, DOI: 10.1103/PhysRevLett.77.3419.

[25] Y. M. Koroteev, G. Bihlmayer, J. E. Gayone, E. V. Chulkov, S. Blügel, P. M. Echenique, and P. Hofmann, "Strong Spin-Orbit Splitting on Bi Surfaces," *Physical Review Letters*, vol. 93, no. 4, p. 046 403, 2004, DOI: 10.1103/PhysRevLett.93.046403.

[26] C. R. Ast, J. Henk, A. Ernst, L. Moreschini, M. C. Falub, D. Pacilé, P. Bruno, K. Kern, and M. Grioni, "Giant Spin Splitting through Surface Alloying," *Physical Review Letters*, vol. 98, no. 18, p. 186 807, 2007, DOI: 10.1103/PhysRevLett.98.186807.

[27] O. Darrigol, *Electrodynamics from Ampère to Einstein*, 2. Oxford University Press, 2000, vol. 55, pp. 3–36, ISBN: 0198505949, DOI: 10.1063/1.1461329.

[28] B. N. Dwivedi, "James Clerk Maxwell and his equations," *Resonance*, vol. 8, no. 5, pp. 4–16, 2003, DOI: 10.1007/BF02867125.

[29] F. Weinert, "Stern—Gerlach Experiment," in *Compendium of Quantum Physics*, Berlin, Heidelberg: Springer Berlin Heidelberg, 2009, pp. 746–750, DOI: 10.1007/978-3-540-70626-7_214.

[30] M. Massimi, "Pauli Exclusion Principle," in *Compendium of Quantum Physics*, D. Greenberger, K. Hentschel, and F. Weinert, Eds., Berlin, Heidelberg: Springer Berlin Heidelberg, 2009, ch. Exclusion, pp. 220–222, DOI: 10.1007/978-3-540-70626-7_141.

[31] C. Timm, "Theory of magnetism," in *Theory of magnetism*, 2015, ch. 4,10, pp. 23,89–91, [Online]. Available: https://www.physik.tu-dresden.de/$\sim$timm/personal/teaching/thmag_w09/lecturenotes.pdf.

[32] D. van Delft and P. Kes, "The discovery of superconductivity," *Physics Today*, vol. 63, no. 9, pp. 38–43, 2010, DOI: 10.1063/1.3490499.

[33] A. M. Forrest, "Meissner and Ochsenfeld revisited," *European Journal of Physics*, vol. 4, no. 2, pp. 117–120, 1983, DOI: 10.1088/0143-0807/4/2/011.

[34] K. Fossheim and A. Sudbø, *Superconductivity Physics and Applications*. John Wiley & Sons, Ltd, 2004, ISBN: 0-470-84452-3.

[35] V. L. Ginzburg and L. D. Landau, "On the Theory of Superconductivity," in *On Superconductivity and Superfluidity*, Berlin, Heidelberg: Springer Berlin Heidelberg, pp. 113–137, DOI: 10.1007/978-3-540-68008-6_4.

[36] J. Bardeen, L. N. Cooper, and J. R. Schrieffer, "Theory of Superconductivity," *Physical Review*, vol. 108, no. 5, pp. 1175–1204, 1957, DOI: 10.1103/PhysRev.108.1175.

[37] G. W. Webb, F. Marsiglio, and J. E. Hirsch, "Superconductivity in the elements, alloys and simple compounds," *Physica C: Superconductivity and its Applications*, vol. 514, pp. 17–27, 2015, DOI: 10.1016/j.physc.2015.02.037, arXiv: 1502.04724.

[38] N. N. Bogoljubov, "On a new method in the theory of superconductivity," *Il Nuovo Cimento*, vol. 7, no. 6, pp. 794–805, 1958, DOI: 10.1007/BF02745585.

[39] J. G. Bednorz, "Perovskite-Type Oxides - The New Approach to High-Tc Superconductivity," pp. 424–455, 1987, [Online]. Available: https://www.nobelprize.org/uploads/2018/06/bednorz-muller-lecture.pdf.

[40] J. G. Bednorz and K. A. Müller, "Possible high Tc superconductivity in the Ba-La-Cu-O system," *Zeitschrift für Physik B Condensed Matter*, vol. 64, no. 2, pp. 189–193, 1986, DOI: 10.1007/BF01303701.

[41] M. K. Wu, J. R. Ashburn, C. J. Torng, P. H. Hor, R. L. Meng, L. Gao, Z. J. Huang, Y. Q. Wang, and C. W. Chu, "Superconductivity at 93 K in a new mixed-phase Yb-Ba-Cu-O compound system at ambient pressure," *Physical Review Letters*, vol. 58, no. 9, pp. 908–910, 1987, DOI: 10.1103/PhysRevLett.58.908.

[42] A. P. Drozdov, P. P. Kong, V. S. Minkov, S. P. Besedin, M. A. Kuzovnikov, S. Mozaffari, L. Balicas, F. F. Balakirev, D. E. Graf, V. B. Prakapenka, E. Greenberg, D. A. Knyazev, M. Tkacz, and M. I. Eremets, "Superconductivity at 250 K in lanthanum hydride under high pressures," *Nature*, vol. 569, no. 7757, pp. 528–531, 2019, DOI: 10.1038/s41586-019-1201-8, arXiv: 1812.01561.

[43] G. R. Stewart, "Unconventional superconductivity," *Advances in Physics*, vol. 66, no. 2, pp. 75–196, 2017, DOI: 10.1080/00018732.2017.1331615.

[44] M. D. Hansen, "Superconducting proximity effect with spin-orbit interactions," Specialization project - Unpublished, NTNU, 2020.

[45] J. O. Fjaerestad, "Second quantization (the occupation-number representation)," *Norwegian University of Science and Technology*, vol. 2, pp. 1–16, 2013, [Online]. Available: http://www.nt.ntnu.no/users/johnof/TFY4210-2013.html.

[46] A. L. Fetter and J. D. Walecka, *Quantum Theory of Many-Particle Systems*. Dover Publications, 2013, pp. 7–19, ISBN: 0-486-42827-3.

[47] H. Onnes, "Further experiments with liquid helium. C. On the change of electric resistance of pure metals at very low temperatures etc. IV. The resistance of pure mercury at helium temperatures.," *KNAW, Proceedings*, vol. 13 II, pp. 1274–1276, 1911.

[48] H. K. Onnes, "Further Experiments with Liquid Helium. D. On the Change of the Electrical Resistance of Pure Metals at very low Temperatures, etc. V. The Disappearance of the resistance of mercury," in *KNAW, Proceedings*, vol. 14 I, 1991, pp. 113–115.

[49] W. Meissner and R. Ochsenfeld, "Ein neuer Effekt bei Eintritt der Supraleitfühigkeit," *Die Naturwissenschaften*, vol. 21, no. 44, pp. 787–788, 1933, DOI: 10.1007/BF01504252.

[50] M. Tinkham, *Introduction to Superconductivity*. Dover Publications, 2004, ISBN: 9780486435039.

[51] P. G. de Gennes, *Superconductivity of Metals and Alloys*. W. A. Benjamin, New York, 1966.

[52] J. Bardeen, L. N. Cooper, and J. R. Schrieffer, "Microscopic Theory of Superconductivity," *Physical Review*, vol. 106, no. 1, pp. 162–164, 1957, DOI: 10.1103/PhysRev.106.162.

[53] L. N. Cooper, "Bound Electron Pairs in a Degenerate Fermi Gas," *Physical Review*, vol. 104, no. 4, pp. 1189–1190, 1956, DOI: 10.1103/PhysRev.104.1189.

[54] A. F. Andreev, "The thermal conductivity of the intermadiate state in superconductors," *Soviet Physics JETP*, vol. 19, no. 5, p. 1228, 1964, [Online]. Available: http://www.jetp.ac.ru/cgi-bin/dn/e_019_05_1228.pdf%0Ahttp://www.jetp.ac.ru/cgi-bin/e/index/e/19/5/p1228?a=list.

[55] B. Pannetier and H. Courtois, "Andreev Reflection and Proximity effect," *Journal of Low Temperature Physics*, vol. 118, no. 5-6, pp. 599–615, 2000, DOI: 10.1023/a:1004635226825, arXiv: 9912024 [cond-mat].

[56] T. M. Klapwijk, "Proximity effect from an Andreev perspective," *Journal of Superconductivity and Novel Magnetism*, vol. 17, no. 5, pp. 593–611, 2004, DOI: 10.1007/s10948-004-0773-0.

[57] G. E. Blonder, M. Tinkham, and T. M. Klapwijk, "Transition from metallic to tunneling regimes in superconducting microconstrictions: Excess current, charge imbalance, and supercurrent conversion," *Physical Review B*, vol. 25, no. 7, pp. 4515–4532, 1982, DOI: 10.1103/PhysRevB.25.4515.

[58] J. Bass and W. P. Pratt, "Spin-diffusion lengths in metals and alloys, and spin-flipping at metal/metal interfaces: an experimentalist's critical review," *Journal of Physics: Condensed Matter*, vol. 19, no. 18, p. 183 201, 2007, DOI: 10.1088/0953-8984/19/18/183201.

[59] B. Pannetier and H. Courtois, "Andreev Reflection and Proximity effect," 1999, arXiv: 9912024 [cond-mat], [Online]. Available: http://arxiv.org/abs/cond-mat/9912024.

[60] B. Josephson, "Possible new effects in superconductive tunnelling," *Physics Letters*, vol. 1, no. 7, pp. 251–253, 1962, DOI: 10.1016/0031-9163(62)91369-0.

[61] P. W. Anderson and J. M. Rowell, "Probable Observation of the Josephson Superconducting Tunneling Effect," *Physical Review Letters*, vol. 10, no. 6, pp. 230–232, 1963, DOI: 10.1103/PhysRevLett.10.230.

[62] R. Feynman, R. Leighton, and M. Sands, *The Feynman lectures on physics, vol. 3*. Addison-Wesley, 1965, ISBN: 0465023827.

[63] K. K. Likharev, "Superconducting weak links," *Reviews of Modern Physics*, vol. 51, no. 1, pp. 101–159, 1979, DOI: 10.1103/RevModPhys.51.101, arXiv: arXiv:1011.1669v3.

[64] M. Eschrig, "Spin-polarized supercurrents for spintronics: A review of current progress," *Reports on Progress in Physics*, vol. 78, no. 10, 2015, DOI: 10.1088/0034-4885/78/10/104501, arXiv: 1509.02242.

[65] S. Datta, *Electronic transport in mesoscopic systems*. Cambridge University Press, 1995, ISBN: 0521416043, [Online]. Available: http://macbeth.if.usp.br/$\sim$gusev/Datta.pdf.

[66] T. Heinzel, *Mesoscopic Electronics in Solid State Nanostructures*. Wiley-vch Verlag GmbH, 2006, ISBN: 978-3-527-40638-8, [Online]. Available: http://www.fulviofrisone.com/attachments/article/403/Heinzel,MesoscopicElectronicsinSolidStateNanostructures.pdf.

[67] T. Klapwijk, G. Blonder, and M. Tinkham, "Explanation of subharmonic energy gap structure in superconducting contacts," *Physica B+C*, vol. 109-110, no. C, pp. 1657–1664, 1982, DOI: 10.1016/0378-4363(82)90189-9.

[68] J. D. Jackson, *Classical Electrodynamics*. New York, NY: John Wiley & Sons, 1998.

[69] M. Catapano, "Interface Effects In Superconducting Heterostructures," Doctoral thesis, Universita' Degli Studi Di Salerno, 2016, [Online]. Available: http://hdl.handle.net/10556/2196.

[70] L. H. THOMAS, "The Motion of the Spinning Electron," *Nature*, vol. 117, no. 2945, pp. 514–514, 1926, DOI: 10.1038/117514a0.

[71] H. A. Kramers, "Théorie générale de la rotation paramagnétique dans les cristaux," *Proceedings Koninklijke Akademie van Wetenschappen*, vol. 33, pp. 959–972, 1930.

[72] Y. A. Bychkov and E. I. Rashba, "Oscillatory effects and the magnetic susceptibility of carriers in inversion layers," *Journal of Physics C: Solid State Physics*, vol. 17, no. 33, pp. 6039–6045, 1984, DOI: 10.1088/0022-3719/17/33/015.

[73] E. I. Rashba and V. I. Sheka, "Symmetry of Energy Bands in Crystals of Wurtzite Type II . Symmetry of Bands with Spin-Orbit Interaction Included Construction of double-valued irreducible repre- sentations," *Deutsche Physikalische Gesellschaft*, vol. 2, pp. 162–176, 1959.

[74] G. Engels, J. Lange, T. Schäpers, and H. Lüth, "Experimental and theoretical approach to spin splitting in modulation-doped In_x $Ga_{1-x}As$/InP quantum wells for B→0," *Physical Review B*, vol. 55, no. 4, R1958–R1961, 1997, DOI: 10.1103/PhysRevB.55.R1958.

[75] A. D. Caviglia, M. Gabay, S. Gariglio, N. Reyren, C. Cancellieri, and J.-M. Triscone, "Tunable Rashba Spin-Orbit Interaction at Oxide Interfaces," *Physical Review Letters*, vol. 104, no. 12, p. 126 803, 2010, DOI: 10.1103/PhysRevLett.104.126803.

[76] C. Kittel, *Introduction to Solid State Physics, 8th edition*, 2004.

[77] M. Eschrig, J. Kopu, J. C. Cuevas, and G. Schön, "Theory of Half-Metal/Superconductor Heterostructures," *Physical Review Letters*, vol. 90, no. 13, p. 137 003, 2003, DOI: 10.1103/PhysRevLett.90.137003.

[78] B. Kastening, D. K. Morr, L. Alff, and K. Bennemann, "Charge Transport and Quantum Phase Transitions in Singlet Superconductor - Ferromagnet - Singlet Superconductor Junctions," 2006, arXiv: 0610283 [cond-mat], [Online]. Available: http://arxiv.org/abs/cond-mat/0610283.

[79] N. G. Pugach, E. Goldobin, R. Kleiner, and D. Koelle, "Method for reliable realization of a ϕ Josephson junction," *Physical Review B*, vol. 81, no. 10, p. 104 513, 2010, DOI: 10.1103/PhysRevB.81.104513.

[80] L. Tosi, *MASSS-Building Andreev States*, [Online]. Available: http://iramis.cea.fr/drecam/spec/Pres/Quantro/static/projects/josephson-effects-in-weak-links/manipulation-of-a-single-spin-in-a-superconductor/masss-building-andreev-states/index.html (visited on 05/28/2021).

[81] A. Furusaki, "Josephson current carried by Andreev levels in superconducting quantum point contacts," *Superlattices and Microstructures*, vol. 25, no. 5-6, pp. 809–818, 1999, DOI: 10.1006/spmi.1999.0730.

[82] M. J. M. de Jong and C. W. J. Beenakker, "Andreev Reflection in Ferromagnet-Superconductor Junctions," *Physical Review Letters*, vol. 74, no. 9, pp. 1657–1660, 1995, DOI: 10.1103/PhysRevLett.74.1657.

[83] V. K. Risinggård, "Spin currents and torques via magnons, electrons, and Cooper pairs," Doctoral thesis, NTNU, 2019, [Online]. Available: http://hdl.handle.net/11250/2609915.

[84] F. Bloch, "Über die Quantenmechanik der Elektronen in Kristallgittern," *Zeitschrift für Physik*, vol. 52, no. 7-8, pp. 555–600, 1929, DOI: 10.1007/BF01339455.

[85] J. C. Slater and G. F. Koster, "Simplified LCAO method for the periodic potential problem," *Physical Review*, vol. 94, no. 6, pp. 1498–1524, 1954, DOI: 10.1103/PhysRev.94.1498.

[86] W. E. Pickett, ""Tight Binding" Method : Linear Combination of Atomic Orbitals (LCAO)," pp. 1–9, 2014, [Online]. Available: http://yclept.ucdavis.edu/course/240A.F17/supple/TightBindingPrimer.pdf.

[87] J. Linder, M. Amundsen, and V. Risinggård, "Intrinsic superspin Hall current," *Physical Review B*, vol. 96, no. 9, pp. 1–8, 2017, DOI: 10.1103/PhysRevB.96.094512, arXiv: 1704.07381.

[88] D. Terrade, "Proximity Effects and Josephson Currents in Ferromagnet - Spin-Triplet Superconductors Junctions," Doctorial thesis, 2015, [Online]. Available: https://pdfs.semanticscholar.org/485e/d43c1bdc98994a9d2f88e04d308f5af2eabe.pdf.

[89] W. M. C. Foulkes, "Tight-Binding Models and Coulomb Interactions for s, p, and d Electrons," in *Quantum Material: Experiments and Theory*, E. Pavarini, Ed., vol. 6, 2016, ch. 4, pp. 29–32, ISBN: 9783958061590.

[90] W. Nolting and A. Ramakanth, "Hubbard Model," in *Quantum Theory of Magnetism*, Berlin, Heidelberg: Springer Berlin Heidelberg, 2009, ch. 8, pp. 388–409, ISBN: 978-3-540-85415-9, DOI: 10.1007/978-3-540-85416-6.

[91] J. Hubbard and B. H. Flowers, "Electron correlations in narrow energy bands," *Proceedings of the Royal Society of London. Series A. Mathematical and Physical Sciences*, vol. 276, no. 1365, pp. 238–257, 1963, DOI: 10.1098/rspa.1963.0204.

[92] D. Tong, *Statistical Physics*. 2012, pp. 27–32, [Online]. Available: http://www.damtp.cam.ac.uk/user/tong/statphys/sp.pdf.

[93] G. Bihlmayer, O. Rader, and R. Winkler, "Focus on the Rashba effect," *New Journal of Physics*, vol. 17, no. 5, p. 050 202, 2015, DOI: 10.1088/1367-2630/17/5/050202.

[94] G Bihlmayer, "A10 Relativistic effects in solids," in *Computing Solids: Models, ab-initio methods and supercomputing*, Forschungszentrum Jülich GmbH, 2014, ISBN: 978-3-89336-912-6.

[95] L. G. Johnsen, "Controllable Superconducting Phase Transition and Magnetization Reorientation due to Spin-Orbit Interactions," Master thesis, NTNU, 2019, [Online]. Available: http://hdl.handle.net/11250/2610772.

The design of this thesis is based on the LaTeX classic thesis template originally developed by André Miede.

Martine Dyring Hansen

Master's thesis

NTNU
Norwegian University of
Science and Technology